Numerical Treatment of Imprecise Random Fields in Non-Linear Solid Mechanics

Von der Fakultät für Bauingenieurwesen und Geodäsie
der Gottfried Willhelm Leibniz Universität Hannover
zur Erlanung des Grades

Doktor-Ingenieurin (Dr.-Ing.)

genehmigte Dissertation von

Mona Madlen Dannert, M.Sc.

2023

Hauptreferent:

Prof. Dr.-Ing. Udo Nackenhorst

Korreferent:

Prof. dr. ir. David Moens

Tag der Promotion:

30. November 2022

Typeset in FreeSerif with LaTeX

"Ich weiß vieles ungefähr und sehr weniges genau."

Danger Dan

Acknowledgements

My personal thanks

...go to everyone who contributed directly or indirectly to this work, starting with all of my friends who took a lot of load off me, especially during the last year. If it wasn't for you and your cooking now and then, I would have depended entirely on chocolate last summer. Thank you for all the empowering talks, for some time off and for celebrating this great day with me. The same holds for my sisters and my brother, thank you so much!

I was lucky to have some engaged students participating in this research during their assistant jobs and/or student theses. Fynn, Ammar, Esther and Johannes, it was really fun to work with you and I am glad that most of you are my colleagues now. Which brings me to many (former) colleagues, not only at IBNM but also at IRZ and within the SPP group. Many thanks for the fruitful discussions, paper cooperations, general advise, all the coffee breaks and some Friday evenings at Kuriosum. A special thanks to my office mates, first Tine, then Paula, for all the help, advise, comfort and chats. And many props for enduring to share the office with a person as chaotic as me.

Besides uncertainty quantification, I learned so many - more and less research and academia related - things from my mentors and friends Amélie, Rodolfo, Matteo and Matthias. Thank you for a great time in Hanover, Seoul and Leuven. Additionally, I want to thank Michael for pushing me to conferences, which I first had to learn to enjoy. Many thanks also to David for the fruitful cooperation that started at one of these occasions.

At last, I want to appreciate my doctorate supervisor. Udo, thank you so much for all the understanding, the patience and the trust you had in me. Thank you for letting me try out things at my own, enabling me to work very independently and encouraging me to do some things less perfectionist. I grew so much during the last years!

<div align="center">

Vielen Dank!

Thank you very much!

Merci beaucoup!

Grazie mille!

Muito obrigada!

Dank je wel!

شكرا جزيلا!

¡Muchas gracias!

非常感谢!

Děkuju moc!

</div>

Abstract

The quantification and propagation of mixed uncertain material parameters in the context of solid mechanical finite element simulations is studied. While aleatory uncertainties appear in terms of spatial varying parameters, i.e. random fields, the epistemic character is induced by a lack of knowledge regarding the correlation length, which is therefore described by interval values. The concept and description of the resulting imprecise random fields is introduced in detail. The challenges occurring from interval valued correlation lengths are clarified. These include mainly the stochastic dimension, which can become very high under some circumstances, as well as the comparability of different correlation length scenarios with regard to the underlying truncation error of the applied Karhunen-Loève expansion.

Additionally, the computation time can increase drastically, if the straightforward and robust double loop approach is applied. Sparse stochastic collocation method and sparse polynomial chaos expansion are studied to reduce the number of required sample evaluations, i.e. the computational cost. To keep the stochastic dimension as low as possible, the random fields are described by Karhunen-Loève expansion, using a modified exponential correlation kernel, which is advantageous in terms of a fast convergence while providing an analytic solution. Still, for small correlation lengths, the investigated approaches are limited by the curse of dimensionality. Furthermore, they turn out to be not suited for non-linear material models.

As a straightforward alternative, a decoupled interpolation approach is proposed, offering a practical engineering estimate. For this purpose, the uncertain quantities only need to be propagated as a random variable and deterministically in terms of the mean values. From these results, the so-called *absolutely no idea probability box (ani-p-box)* can be obtained, bounding the results of the interval valued correlation length being between zero and infinity. The idea is, to interpolate the result of any arbitrary correlation length within this ani-p-box, exploiting prior knowledge about the statistical behaviour of the input random field corresponding to the correlation length.

The new approach is studied for one- and two-dimensional random fields. Furthermore, linear and non-linear finite element models are used in terms of linear-elastic or elasto-plastic material laws, the latter including linear hardening. It appears that the approach only works satisfyingly for sufficiently smooth responses but an improvement by considering also higher order statistics is motivated for future research.

Keywords   uncertainty quantification and propagation, aleatory and epistemic uncertainties, imprecise random fields, probability boxes, stochastic finite element simulation, elasto-plasticity

Zusammenfassung

Es wird die Quantifizierung und die Berücksichtigung von gemischt ungewissen Materialparametern im Rahmen von Finite-Elemente-Simulationen in der Festkörpermechanik untersucht. Während aleatorische Ungewissheiten in Form von räumlich variierenden Parametern, d.h. Zufallsfeldern, auftreten, fließt der epistemische Charakter durch die Unwissenheit über die Korrelationslänge ein, die daher durch Intervallwerte beschrieben wird. Das Konzept und die Beschreibung der entstehenden unpräzisen Zufallsfelder wird im Detail vorgestellt. Die Herausforderungen, die sich aus intervallbasierten Korrelationslängen ergeben, werden verdeutlicht. Dazu gehören vor allem die stochastische Dimension, die unter Umständen sehr hoch werden kann, sowie die Vergleichbarkeit verschiedener Korrelationslängenszenarien im Hinblick auf den zugrundeliegenden Abbruchfehler der verwendeten Karhunen-Loève-Entwicklung.

Außerdem kann die Rechendauer drastisch ansteigen, wenn der einfache und robuste Doppelschleifenansatz verwendet wird. Die spärliche stochastische Kollokationsmethode und die spärliche polynomiale Chaos-Entwicklung werden untersucht, um die Anzahl der erforderlichen Stichproben-Evaluierungen, d.h. die Rechenkosten, zu reduzieren. Um die stochastische Dimension so gering wie möglich zu halten, werden die Zufallsfelder durch die Karhunen-Loève-Entwicklung beschrieben, wobei ein modifizierter exponentieller Korrelationskern verwendet wird, der hinsichtlich seiner schnellen Konvergenz von Vorteil ist und gleichzeitig eine analytische Lösung ermöglicht. Für kleine Korrelationslängen sind die untersuchten Ansätze jedoch durch den Fluch der Dimensionalität begrenzt. Außerdem erweisen sie sich als ungeeignet für nichtlineare Materialmodelle.

Als einfache Alternative wird ein entkoppelter Interpolationsansatz vorgeschlagen, der eine ingenieurpraktische Abschätzung ermöglicht. Zu diesem Zweck müssen die ungewissen Größen lediglich als Zufallsvariable und deterministisch unter Annahme der Mittelwerte simuliert werden. Aus diesen Ergebnissen lässt sich die so genannte *"absolut keine Ahnung Wahrscheinlichkeitsbox"* (absolutely no idea probability box: ani-p-box) bestimmen, die die Ergebnisse begrenzt, die aus einer intervalbasierten Korrelationslänge zwischen Null und Unendlich resultieren. Die Idee besteht darin, das Ergebnis einer beliebigen Korrelationslänge innerhalb dieser ani-p-box zu interpolieren, wobei das Vorwissen über das statistische Verhalten des zugrundeliegenden Zufallsfeldes der entsprechenden Korrelationslänge genutzt wird.

Der neue Ansatz wird für ein- und zweidimensionale Zufallsfelder untersucht. Außerdem werden lineare und nichtlineare Finite-Elemente-Modelle in Form von linear-elastischen oder elasto-plastischen Materialgesetzen verwendet, wobei letztere eine lineare Verfestigung beinhalten. Es zeigt sich, dass der Ansatz nur für hinreichend glatte Systemantworten zufriedenstellend funktioniert, es wird jedoch eine Verbesserung durch die Berücksichtigung statistischer Werte höherer Ordnung für eine zukünftige Erforschung angeregt.

Stichworte   Quantifizierung und Berücksichtigung von Ungewissheiten, Aleatorische und Epistemische Ungewissheiten, Impräzise Zufallsfelder, Wahrscheinlichkeitsboxen, Stochastische Finite Elemente Simulation, Elasto-Plastizität

Contents

List of Figures

List of Tables

List of Algorithms

Glossary

$\mathcal{L}$	linear or non-linear differential operator
$\mathcal{B}$	operator of boundary conditions
E	expected value $E\{\cdot\}$
Var	variance $Var\{\cdot\}$
Std	standard deviation $Std\{\cdot\}$
Cov	covariance $Cov\{\cdot, \cdot\}$
Corr	correlation coefficient $Corr\{\cdot, \cdot\}$
$\boldsymbol{\beta}$	unobservable state variable variable (internal variable)
$\dot{\gamma}$	plastic multiplier
$\boldsymbol{\varepsilon}$	strain tensor
$\tilde{\boldsymbol{\varepsilon}}$	deviatoric part of the strain tensor
ε	one-dimensional strain (component)
$\boldsymbol{\varepsilon}^{\mathrm{e}}$	elastic part of the strain tensor
$\boldsymbol{\varepsilon}^{\mathrm{p}}$	plastic part of the strain tensor
$\dot{\boldsymbol{\varepsilon}}^{\mathrm{p}}$	plastic strain rate
$\bar{\varepsilon}^{\mathrm{p}}$	equivalent plastic strain
$\dot{\bar{\varepsilon}}^{\mathrm{p}}$	equivalent plastic strain rate
ϑ	temperature
κ	bulk modulus
ν	Poisson's ratio
ρ	mass density
$\boldsymbol{\sigma}$	stress tensor
$\tilde{\boldsymbol{\sigma}}$	deviatoric part of the stress tensor
σ	one-dimensional stress (component)
σ_{y}	yield stress
σ_{vM}	equivalent von Mises stress
$\boldsymbol{\tau}$	back stress tensor
ψ	free energy function
$\boldsymbol{t}$	tension
$\boldsymbol{b}$	body forces
$\mathbf{B}$	matrix containing the spatial derivations of the shape functions

$\mathbb{C}$	fourth order linear-elastic material tensor
$\mathbf{C}$	linear-elastic material matrix (Voigt notation)
C	one-dimensional linear-elastic material tensor (component)
$\mathcal{D}$	physical domain
$\partial\mathcal{D}$	surface of a physical domain
$\mathcal{D}_{\mathrm{e}}$	element domain
$\mathcal{D}_{\square}$	reference element domain
D	dissipation
D^{in}	internal dissipation
D^{th}	thermal dissipation
d	spatial dimension
$\boldsymbol{d}$	strain velocity tensor
$\mathrm{d}z$	infinitesimal small length
$\mathrm{d}a$	infinitesimal small area
$\mathrm{d}v$	infinitesimal small volume
E	Young's modulus
e	internal energy
$\boldsymbol{f}$	force vector
$\hat{\mathbf{f}}$	external forces at finite element nodes
F	single load
f	flow rule
G	shear modulus
H	hardening parameter
h	shape function
$\mathbf{H}$	matrix containing the shape functions
$\mathbf{J}$	Jacobian matrix
$\mathbf{K}$	stiffness matrix
l	domain length
m	mass
n_{el}	number of elements
n_{n}	number of nodes
p	hydrostatic pressure
$\boldsymbol{q}$	heat flux vector
q	line load
r	radiant heat
s	specific entropy
t	time
$\boldsymbol{u}$	displacement vector
u	one-dimensional displacement (component)
$\hat{\mathbf{u}}$	displacement of finite element nodes
u_{max}	maximum deflection of a tensioned rod

$\boldsymbol{v}$	velocity
v	volume dilatation
w_{max}	maximum deflection of a bending beam
$\boldsymbol{z}$	location in physical space
z	location in a one-dimensional physical domain
$\hat{\mathbf{z}}$	location of finite element nodes
α	multi-index $\boldsymbol{\alpha} = (\alpha_1, \ldots, \alpha_N) \in \mathbb{N}^N$
Γ	autocorrelation function of a random field
$\bar{\Gamma}$	approximated autocorrelation function of a truncated random field
γ	skewness
$\epsilon_{\bar{\Gamma}}$	local truncation error of the truncated correlation function
$\bar{\epsilon}_{\bar{\Gamma}}$	mean truncation error of the truncated correlation function
ϵ_{σ^2}	local error variance
$\bar{\epsilon}_{\sigma^2}$	mean error variance
ϵ_k	relative error of the current Smolyak level
ϵ_{LOO}	leave one out error
ϵ_{val}	validation error
ϵ_{ref}	reference error
θ	membership function
κ	kurtosis
λ	eigenvalue, where λ_i is the ith eigenvalue with $\lambda_1 > \lambda_2 > \cdots$
μ	mean value
$\hat{\mu}$	individual mean value of a truncated random field realisation
ν	smoothness parameter of Whittle-Matérn correlation kernel family
ξ	standard normal distributed random variable
σ^2	variance
σ	standard deviation
ϕ	eigenfunction, with ϕ_i corresponding to the ith eigenvalue λ_i
φ	base function
Ψ	orthonormal polynomial basis
Ω	sample space
ω	element of the sample space
$\mathcal{A}$	index set
A	event
$\hat{a}$	polynomial chaos coefficients
$\mathcal{B}$	Borel σ-field
B	Borel set
C	autocovariance function of a random field
$\bar{C}$	approximated autocovariance function of a truncated random field

c	scenario of discretised epistemic parameter (combinations)
$\mathcal{F}$	σ-field
F	cumulative distribution function
$\overline{F}$	left bound of a probability box
$\underline{F}$	right bound of a probability box
f	probability density function
H	Lagrange polynoials
$\mathcal{I}$	interpolant
I	interval
$I^\times$	vertex combinations
k	Smolyak level
L	correlation length
L^*	intermediate correlation length value
$\mathcal{M}$	model
N	stochastic dimension
n_s	number of samples
n_MC	number of Monte Carlo samples
n_SC	number of collocation points
n_PC	number of polynomial chaos samples
n_RV	number of random variables
n_RF	number of random fields
$\mathfrak{P}$	power set
$\mathcal{P}$	probability box
P	probability measure
p	polynomial degree
R	reliability function
S	standard normal distributed random quantity (variable, field or process)
T	truncation order
X	(epistemic/aleatory/mixed) uncertain input quantity (variable/field/process)
x	realisation of a random quantity
X^I	interval valued uncertain quantity
$\underline{X}$	left bound of an interval valued quantity
$\overline{X}$	right bound of an interval valued quantity
$X(\omega)$	random variable
$X^I(\boldsymbol{z})$	interval field
$X(\omega, \boldsymbol{z})$	random field
$\bar{X}(\omega, \boldsymbol{z})$	random field approximation described by a truncated series expansion
$[X](\omega)$	imprecise random variable
$[X](\omega, \boldsymbol{z})$	imprecise random field
$\mathcal{X}$	set of collocation points or experimental designs
$\boldsymbol{Y}$	vector of uncertain model responses

Y uncertain model response

$\boldsymbol{y}$ realisation of a vector of uncertain model responses

y realisation of an uncertain model response

Abbreviations

1D	one-dimensional
2D	two-dimensional
3D	three-dimensional
ani-p-box	absolutely no idea probability box
BN	binary noise
CDF	cumulative distribution function
FE	finite element
FEM	finite element method
IRF	imprecise random field
KL	Karhunen-Loève
MC	Monte Carlo
ME	modified exponential
p-box	probability box
PC	polynomial chaos
PDE	partial differential equation
PDF	probability density function
QE	squared exponential
QoI	quantity of interest
RF	random field
RV	random variable
SC	stochastic collocation
SE	single exponential

SFEM	stochastic finite element method
SPDE	stochastic partial differential equation
UP	uncertainty propagation
UQ	uncertainty quantification
WM	Whittle-Matérn
WN	white noise

1. Introduction

In any engineering design and building processes uncertainties are not avoidable. To judge the risk of failure, unforeseen events must be considered within the whole process of planning, building and using. For that purpose, codes (e.g. Eurocodes in civil engineering) are used in conventional engineering design. The listed knockdown and safety factors result from experiments and analytic expertise and may depend on environmental or regional conditions (e.g. snow load). Still, to be generally applicable in different scenarios, they lead to conservative designs to the expense of economical and ecological costs. However, not only regarding climate change but also with respect to efficiency in general, more sustainable and resource saving approaches are desired. For this purpose, quantifying and considering uncertainties within the engineering design process can help to reduce both, ecological and economical costs.

Instead of the conservative safety and knockdown factors, a finite element (FE) analysis considering individual uncertainties may enable an optimised design. While deterministic finite element method (FEM) is well established in engineering application to solve partial differential equations (PDEs), computational techniques to treat stochastic partial differential equations (SPDEs) are intensively discussed in the scientific community but not yet established in engineering design. Quantifying all (critical) uncertainties involved within the design, simulation and building process is the crucial point. Their appearance may have different reasons and can formally be categorised into three source types [Der Kiureghian and Ditlevsen, 2009]: *(i) uncertainty in basic variables* such as load or material data, *(ii) model uncertainty* considering both, the physical and the probabilistic/possibilistic model and *(iii) parameter uncertainty* regarding the parameters used within a model. Especially in civil engineering, building prototypes (as e.g. crash test dummies in car manufacturing) is usually not possible and environmental impacts are barely predictable for several decades for which the building is planned to be used.

In this work, it is distinguished into uncertainty quantification (UQ) and uncertainty propagation (UP). The fist term is understood as the description and modelling of uncertain input parameters, while the second means a general analysis including uncertain input parameters to describe the stochastic response at the outcome of a model. The quantity of interest (QoI) obtained by UP can then again be described in terms of UQ. In the following section, different terms and concepts in the context of UQ are introduced before briefly summarising the most important developments regarding UP in structural mechanics Section 1.2 and motivating the aim of this work. An outlook on the following chapters is given in Section 1.3.

1.1. Uncertainty quantification

Uncertainties can be distinguished into two types, *epistemic* and *aleatory* [Der Kiureghian and Ditlevsen, 2009] but can also be described of *mixed type*. Appropriate approaches to model different kind of uncertain variables are exemplified in Figure 1.1. Note that they can be extended to uncertain fields or processes, which include additionally a spatial or temporal dependency. For the sake of clarity, only scalar valued uncertain variables are depicted and discussed here but uncertain fields will be addressed as well in the course of this thesis.

A *deterministic* value can be found in Figure 1.1 (a) as the special case of a certain variable $X = x_0$ (i.e. the probability density function $f_X(x) = 1$) in the context of aleatory uncertainty. Regarding epistemic uncertainty, the deterministic value X does not contain imprecision and is therefore defined as a crisp number in terms of set theory, i.e. the membership function is exactly equal to one at this very value, $\theta(x) = 1$. The UQ models depicted in Figure 1.1 (b) to (h), assigned to aleatory, epistemic or mixed uncertainty, are further explained in the following corresponding subsections.

1.1.1. Aleatory uncertainty

The intrinsic randomness of a phenomena itself can be characterised as aleatory (or stochastic) uncertainty, arising from the Latin word *alea* meaning dice or gambling [Der Kiureghian and Ditlevsen, 2009]. These include for example the material behaviour which is varying from sample to sample. Furthermore, imperfections during the manufacturing process are usually not avoidable and future loading conditions can only be estimated. Aleatory uncertainties are therefore not reducible, i.e. the material property of a next sample or real building cannot be predicted for sure but only estimated with a certain probability. The same holds true regarding the geometry of the object or loading conditions resulting from natural phenomenons. Aleatory uncertain parameters can be classified into random variables (or vectors of random variables), as exemplified in Figure 1.1 (b) and (c), random fields and random processes, depending on their (in)dependency on space and time.

Aleatory uncertainties are described in terms of stochastic theory, composed by two main branches, statistics and probability theory [Georgii, 2004]. Experiments can be performed to describe parameters statistically, e.g. in terms of mean value, standard deviation, higher stochastic moments or even a probability family. This information can then be used to model aleatory uncertainties mathematically by probability theory. Afterwards, the stochastic model can again be verified by statistics.

Depending on the assumed sample space Ω being countable or uncountable, a random quantity X is distinguished into *discrete* variables x_i and *continuous* variables x. The first is described by *finite probability theory* given in the left column of the probability theory block. It is a special case of the more general *infinite probability theory* [Grigoriu, 2002] depicted on the right. The corresponding probability densities f_{X_i} and $f_X(x)$ as well as the distribution functions $F_{X_i} = \sum_i f_{X_i}$ and $F_X(x) = \int_x f_X(x)\,\mathrm{d}x$, are exemplified in Figure 1.1 (b) and (c). Infinite probability theory will be briefly introduced in Section 2.1.

UQ ⟶ **aleatory**

probabilistic concept

| parameter | finite | infinite |

(a) deterministic value
$\theta(x), f(x)$
1
x_0
x
h

$\Theta(x), F(x)$
1
x

(b) discrete random variable
f_{X_i}
1
$x_1 \quad x_2 \quad x_3$
x_i
h_i

F_{X_i}
1
x_i

(c) continuous random variable
$f_X(x)$
1
μ_X
x
$h(x)$

$F_X(x)$
1
x

epistemic

classical set theory

number

interval

(d) interval variable
$\theta^I(x)$
1
$\underline{x} \quad \overline{x}$
x
h

$\Theta^I(x)$
1
x

(e) Dempster-Shafer structure
$f_{X_i}\,\theta^I(x)$
1
$x_1^I \quad x_2^I \quad x_3^I$
x_i
h_i

$F_{X_i}\,\Theta^I(x)$
1
x_i

(f) probability box
$f_X(x)\,\theta^I(x)$
1
μ_X^I
x
$h(x)$

$F_X(x)\,\Theta^I(x)$
1
x

possibilistic concept

fuzzy set theory

fuzzy number

(g) fuzzy variable
$\tilde{\theta}(x)$
1
$\underline{x} \quad x_m \quad \overline{x}$
x
h

$\tilde{\Theta}(x)$
1
x

(h) fuzzy probability box
$f_{X_i}\,\tilde{\theta}(x)$
1
$\tilde{x}_1 \quad \tilde{x}_2 \quad \tilde{x}_3$
x_i
h_i

$F_{X_i}\,\tilde{\Theta}(x)$
1
x_i

$f_X(x)\,\tilde{\theta}(x)$
1
$\tilde{\mu}_X$
x
$h(x)$

$F_X(x)\,\tilde{\Theta}(x)$
1
x

fuzzy interval

$\tilde{\theta}^I(x)$
1
$\underline{x} \quad \underline{x}_m \quad \overline{x}_m \quad \overline{x}$
x
h

$\tilde{\Theta}^I(x)$
1
x

$f_{X_i}\,\tilde{\theta}^I(x)$
1
$\tilde{x}_1^I \quad \tilde{x}_2^I$
x_i
h_i

$F_{X_i}\,\tilde{\Theta}^I(x)$
1
x_i

$f_X(x)\,\tilde{\theta}^I(x)$
1
$\tilde{\mu}_X^I$
x
$h(x)$

$F_X(x)\,\tilde{\Theta}^I(x)$
1
x

imprecise probabilities

| height: | $h = 1$ | $\sum h_i = 1$ | $\int h(x)\,\mathrm{d}x = 1$ |

Figure 1.1: Overviews of probabilistic concepts to model aleatory, possibilistic concepts to model epistemic and imprecise probability concepts to model mixed uncertain variables.

1.1.2.   Epistemic uncertainty

Uncertainties resulting from a lack of knowledge or data are defined as epistemic uncertainties, originating from the Greek term $\varepsilon\pi\iota\sigma\tau\eta\mu\eta$ (episteme) meaning knowledge [Der Kiureghian and Ditlevsen, 2009]. These imprecisions - also referred to incertitudes [Ferson and Troy Tucker, 2006] - are traced back, e.g. to a small sample size or a poor measurement accuracy and can (theoretically) be reduced by collecting more information, for example choosing a more precise model or improving the measurement equipment.

Epistemic uncertainties can be observed by possibilistic theories, e.g. in terms of *intervals* [Moore et al., 2009] or *fuzzy parameters* [Zadeh, 1965, 1978, Hanss, 2005], both of which visualised in the left block of Figure 1.1 depicting the models to describe purely epistemic uncertainty. Note that both concepts can be extended towards interval fields and fuzzy fields, respectively, in order to model spatial/temporal variability [Faes and Moens, 2020b].

Defining a membership function $\theta(x)$, an epistemic uncertain parameter X which is described by an interval $X^I = [\underline{x}, \overline{x}]$ is clearly defined to be either within ($\theta^I(x) = 1$ if $x \in X^I$) or outside ($\theta^I(x) = 0$ else) of the interval, see Figure 1.1 (d). Regarding a fuzzy number $\tilde{X}$ or a fuzzy interval $\tilde{X}^I$ as depicted in (g), the membership function $\tilde{\theta}(x) \in [0, 1]$ assigns a weighted membership of x towards the fuzzy number $\tilde{X}$ or fuzzy interval $\tilde{X}^I$. As fuzzy parameters require further assumptions on $\tilde{\theta}(x)$, epistemic uncertain parameters are limited to an interval valued description within this thesis. The underlying interval theory is therefore further introduced in Section 2.2. A detailed introduction to the given and further theories to model epistemic uncertainties can be found, e.g. in the book by Klir and Wierman [1999].

Note that probabilistic concepts are not appropriate to model epistemic uncertainties. Even when assuming a uniform distribution instead of an interval, an arbitrary assumption of an - actually unknown - probability family is made [Beer et al., 2013]. The following example illustrates the different meaning of a uniform distribution and an interval. Imagine two discrete, uniformly distributed values $A \sim \mathcal{U}(1,3)$ and $B \sim \mathcal{U}(2,5)$, the possible results of $C = A + B$ are

$$C = \{1+2;\ 1+3;\ 1+4;\ 1+5;\ 2+2;\ 2+3;\ 2+4;\ 2+5;\ 3+2;\ 3+3;\ 3+4;\ 3+5\}$$
$$= \{3;\ 4;\ 5;\ 6;\ 4;\ 5;\ 6;\ 7;\ 5;\ 6;\ 7;\ 8\}$$

and the corresponding probability $f_C(c_i)$ results in

$$f_C(c = 3) = {}^1\!/\!{}_{12}, \quad f_C(c = 4) = {}^2\!/\!{}_{12}, \quad f_C(c = 5) = {}^3\!/\!{}_{12},$$
$$f_C(c = 6) = {}^3\!/\!{}_{12}, \quad f_C(c = 7) = {}^2\!/\!{}_{12}, \quad f_C(c = 8) = {}^1\!/\!{}_{12}.$$

Then, the probability of gaining for example $f_C(c = 5)$ is three times higher than to gain $f_C(c = 3)$. On the contrary, modelling $A^I = [1, 3]$ and $B^I = [3, 5]$ as intervals without any distribution assumed, the result is

$$C^I = A^I + B^I = [\min(A) + \min(B);\ \max(A) + \max(B)] = [3;\ 8]$$

and the only information about C is that its value lays somewhere between $C = 3$ and $C = 8$ without dedicating any probability or weighting to the possible values.

1.1.3. Mixed uncertainty

If one or more parameters contain a mixed, aleatory and epistemic uncertainty, both probabilistic and possibilistic theories can be combined in terms of imprecise probabilities [Beer et al., 2013], as exemplified in Figure 1.1. Such mixed uncertainties are also referred to *polymorphic uncertainty* [Götz, 2017, Fina, 2020].

Using interval valued parameters within discrete probability theory, the cumulative density function is not given by a crisp step function anymore but by two step function bounds, describing the lower and upper bound of each quantity. This concept is visualised in Figure 1.1 (e) and referred to as *evidence theory* or *Dempster-Shafer structure* [Dempster, 1967, Shafer, 1976, Ferson et al., 2003]. Equivalently, *probability boxes* [Ferson et al., 2003, Faes et al., 2021] provide the more general case regarding interval valued parameters within infinite probability theory. For example, the mean value μ_X^I of a parameter could be described by an interval, see Figure 1.1 (f). The information on the distribution function can then be given by a left and right bound of $F_X(x)$, the so-called probability box (p-box). It may also be interpreted as the combination of an interval valued variable x^I (i.e. a Dempster-Shafer structure) and an interval valued probability $f_X^I(x)$ [Beer et al., 2013]. Finally, *fuzzy probabilities* [Kwakernaak, 1978, 1979, Zadeh, 1984, Gil et al., 2006] as depicted in Figure 1.1 (h) cover both, finite or infinite theories combined with any kind of fuzzy parameters, i.e fuzzy numbers and/or fuzzy intervals. This can be interpreted as a more general case of a p-box where additional information on the membership weighting is available. A sound overview on the discussed and further concepts to describe imprecise probabilities can be found in the review by Beer et al. [2013] or the dissertation by Schöbi [2019].

The focus of this contribution is on the description of continuous random quantities including interval valued parameters leading to a classical p-box. For this purpose, the construction of p-boxes is introduced more profound in Section 2.3. Furthermore, the theory of p-box valued variables is extended to the concept of *imprecise random fields* in Chapter 3, in order to describe also a spatial variability of mixed uncertain parameters.

1.2. Uncertainty propagation

The different theories to describe uncertainties require appropriate methods to propagate them through a given model, e.g. an FE simulation. It is distinguished into *forward* and *inverse approaches* [Faes and Moens, 2020b]. The first describes a model response given a set of uncertain parameters in the model input [Moens and Vandepitte, 2006] and will be the main focus of this work. On the contrary, inverse methods enable to draw conclusions about the input parameters from a response, e.g. in terms of updating approaches [Faes et al., 2019]. There exist *intrusive* and *non-intrusive methods* [Le Maître and Knio, 2010], meaning that the model solver is or is not affected by the approach. In the latter case, the model does not change and can be used as a black box within the UQ/UP framework. In this contribution, only non-intrusive methods are applied. Furthermore, FEM is used to solve the (stochastic) PDEs. Therefore, the focus is on propagation methods using FE analysis.

While aleatory uncertainties are usually propagated by probabilistic approaches, epistemic uncertainties require possibilistic approaches, which are also referred to non-probabilistic approaches. Both methods are briefly reviewed in Subsection 1.2.1 and Subsection 1.2.2, respectively. Afterwards, an overview about general hybrid approaches to propagate mixed (or polymorphic) uncertainties is given in Subsection 1.2.3, before motivating and reviewing the idea of imprecise random field propagation in more detail. A profound introduction into and a comparison of both, probabilistic and non-probablistic approaches can be found by Moens and Vandepitte [2006].

1.2.1.   Probabilistic approaches

Regarding probabilistic approaches to propagate uncertainties, it can be distinguished into sampling approaches and approximation approaches. The latter comprise for instance *perturbation methods* [Stefanou, 2009], such as the first or second order reliability methods [Der Kiureghian et al., 1987], and *reliability methods* based on limit state functions [Sudret and Der Kiureghian, 2000]. They are not further addressed in this work. Instead, the focus lays on stochastic finite element method (SFEM) using sampling approaches.

Before aleatory uncertain input parameters can be propagated through a model, they must be parameterised based on a set of independent random variables. Regarding random fields, i.e. spatially varying random parameters, a discretisation is necessary. For that purpose, a spectral representation - e.g. by Karhunen-Loève (KL) or polynomial chaos (PC) decomposition - becomes usefull to reduce the number of random variables within the approximation [Le Maître and Knio, 2010]. In this work, KL expansion is used with this regard and is therefore described and investigated more detailed in Section 3.1.

Aiming to propagate uncertainties, an early development to solve SPDEs is the (intrusive) spectral SFEM using Galerkin approach [Ghanem and Spanos, 1991], also referred to as *stochastic Galerkin method* [Xiu, 2009]. The advantage of intrusive methods is given by the fact that only one linear equation system needs to be solved, while non-intrusive sampling methods are based on the repetitive solution of many deterministic equation systems. For the latter purpose, a set of input parameters is sampled pseudo-randomly or chosen artificially, leading to straightforward methods using the model as a black box. The equation system of intrusive approaches requires to discretise the random space and therefore may become very large. Furthermore, only linear problems are applicable [Stefanou, 2009]. For this reason, intrusive methods are not further considered in this work.

Three sampling techniques are discussed in more detail in Chapter 5. The brute force *Monte Carlo (MC) simulation* [Le Maître and Knio, 2010] is based on pseudo-random sampling and a statistical evaluation. On the contrary, the idea of *stochastic collocation (SC) method* [Xiu and Hesthaven, 2005] is to interpolate within the probability space, discretiesed by a grid of pre-defined samples. The *PC expansion* [Sudret, 2015] aims to find a surrogate model based on a pseudo-randomly sampled experimental design.

An overview on well-established SFEM can be found in the reviews by Stefanou [2009] and Xiu [2009]. Additionally, Le Maître and Knio [2010] provide in their book a sound introduction to various spectral expansion methods, non-intrusive sampling as well as (intrusive) stochastic Galerkin methods, including many examples and applications. A sound overview on SFEM including comprehensive instructions on the implementation in Matlab are provided by Sudret and Der Kiureghian [2000].

1.2.2. Possibilistic approaches

Interval FEM provides a broad range of approaches to propagate interval variables. For instance, based on interval arithmetic [Moore et al., 2009], the FE problem can be solved in terms of interval valued stiffness or mass matrices [Muhanna and Mullen, 2001, Sofi and Romeo, 2016], which is however an intrusive approach. Alternatively, different optimisation strategies are available, aiming to find the smallest conservative hypercube [Moens and Hanss, 2011, Faes and Moens, 2020b]. A survey on interval FEM including different implementation strategies can be found by Moens and Vandepitte [2005]. Extending the epistemic uncertainty towards fuzzy valued variables, these are propagated by fuzzy FEM, accordingly, e.g. in terms of α-cut discretisation or α-cut optimisation [Möller et al., 2000]. Moens and Hanss [2011] provide a sound review on interval and fuzzy FEM regarding interval or fuzzy variable input parameters. A more recent review by Faes and Moens [2020b] additionally covers interval and fuzzy FEM in terms of interval fields and fuzzy fields, respectively.

1.2.3. Hybrid approaches

Acknowledging a mixture of both types of uncertainties in hybrid approaches while maintaining efficiency and accuracy has become an important field of research. The German Research Foundation currently grants an own priority program regarding "Polymorphic uncertainty modelling for the numerical design of structures - SPP 1886", advancing this topic as recently published in a special issue [Kaliske and Graf, 2019].

Several approaches are available to propagate imprecise probabilities as given in Figure 1.1. In analogy to interval valued quantities as applied in Dempster-Shafer theory, also the assigned probability [Weichselberger, 2000] or reliability [Qiu et al., 2008] can be defined to be interval valued. A very general approach is the *probability bounds analysis* [Faes et al., 2021], which can be used to propagate mixed uncertain input parameters described by a p-box, but also Dempster-Shafer structures as the discrete case of a p-box. For this purpose, the p-box can either be considered within a double loop approach, decoupled approaches or in terms of surrogate models, as recently reviewed by Faes et al. [2021]. The double loop approach will be introduced in more detail in Section 3.3 in order to propagate imprecise random fields. Probability bounds analysis can be extended to *fuzzy probability bounds analysis* [Schietzold et al., 2021], to propagate all kind of fuzzy probabilities, e.g. in terms of fuzzy SFEM [Möller, 2004].

In this work, mixed uncertain and spatially varying parameters are considered as imprecise random fields. In the following, this concept is motivated and existing experience regarding the propagation of imprecise random fields as well as their application in engineering is reviewed.

Imprecise random fields in engineering application: Mixed uncertain parameters which also include a spatial dependency are described by imprecise random fields. While classical random fields are purely aleatory, imprecise random fields may include interval and/or fuzzy valued hyper parameters, i.e. parameters that are required to describe the random field, e.g. the mean value or the standard deviation. Random fields do not only imply a dependence on chance (such as random variables) but also on space (and/or time, which is then usually referred to as random process). On the contrary to white noise, where the data at two arbitrary points within the field are completely uncorrelated, a random field implies a certain correlation within the field. For instance, it is realistic that the material data of a steel specimen are relatively similar (i.e. more correlated) while soil can be much more inhomogeneous and therefore might be less correlated. There are different (auto[1])correlation functions available to model the correlation within the random field in terms of a so called (auto)correlation length. This material parameter is a measure for how fast the correlation decreases with increasing distance. Regarding its limit representation, the random field converges towards white noise for a correlation length converging to zero and towards a random variable (i.e. the field is constant) if the correlation length converges towards infinity.

Concerning material data, their statistical parameters such as the mean value and the standard deviation can often be determined experimentally. However, the correlation function, can usually only be assumed by engineering reasoning. The same holds for the correlation length. As described above, it might be estimated as large or small depending on the underlying problem but is difficult or even impossible to measure. On the other hand, regarding large engineering structures, the correlation model can become highly important. Due to mistakes, imperfections or separated steps in the manufacturing or building process, it is unlikely that the material is everywhere the same best, worst or any inbetween case, as it would be assumed describing the parameter by a random variable. Acknowledging a spatial variation in the material data can therefore be of high value regarding an ecological and economical design.

For this reason, it seems natural to model material data by imprecise random fields, e.g. occurring from an imprecise correlation length. They have been investigated in several engineering contexts during the last years. Götz [2017] applied random and fuzzy fields for a numerical design of a reinforced concrete frame structure. Interval probability based random fields are described as a special case of fuzzy probability based random fields by Schietzold et al. [2019]. Both are applied to different engineering problems, i.e. for a concrete damage simulation, in terms of a hydromechanical problem involving auto- and crosscorrelation of different random fields and considering a structural dependent autocorrelation in case of a timber structure. Furthermore, Schietzold et al. [2021] use the latter case to simulate a purlin part of timber roof construction describing the auto- and crosscorrelation of random fields by fuzzy parameters. Imprecise random fields induced by fuzzy valued autocorrelation lengths are applied by Schmidt et al. [2019] within a multiphasic and hydro-mechanical coupled FE analysis. Fina [2020], Fina et al. [2020] use fuzzy random fields and processes to model the geometric imperfections in the context of shell buckling analysis.

---

[1]Note that some application consider a correlation between several random field parameters as well. In such cases, it is distinguished into autocorrelation, i.e. within the field, and crosscorrelation, i.e. between fields.

Interval valued induced imprecise random fields can be interpreted as a special case of fuzzy random fields. There are two main advantages of using interval instead of fuzzy valued parameters. First, no further assumptions on the membership function need to be done. Second, the computational cost is not as high as if there was a α-level discretisation or -optimisation necessary. Imprecise random fields obtained by an interval valued correlation length have been applied to concrete damage simulation by Dannert et al. [2019] using interval discretisation and by Dannert et al. [2021a] using an a-priori optimisation to obtain the relevant interval values. The latter approach has been introduced by Faes and Moens [2019b] and studied in the context of transient dynamics. Gao et al. [2022] apply imprecise random field for different continuum structures, performing a topology optimisation.

Concerning the propagation of imprecise random fields in the context of engineering structures including many degrees of freedom, the computational effort becomes challenging, even if only interval valued epistemic parameters are considered. This is even more compounded in terms of non-linear problems, requiring often many load or time steps. Therefore, two different sophisticated sampling techniques, sparse SC method and sparse PC expansion, are studied within this contribution. The aim is to reduce the computational cost by requiring less samples as an MC simulation. It is shown that both methods are limited in terms of non-linear problems. An additional challenge lays the discretisation of the random fields corresponding to different correlation length values. The underlying KL series expansion requires different truncation orders to obtain a comparable truncation error, which depends on the correlation length. Therefore, different stochastic dimensions are induced for the different correlation length scenarios. Especially for small correlation length values, this may lead the SC and PC method to suffer from the curse of dimensionality.

This thesis provides a sound description of the challenges that have to be solved or at least approached when dealing with imprecise random fields. Many attempts to overcome these challenges are described and studied. It is shown under which model assumptions some of them are fruitful. For the other cases, suggestions on further improvements or alternative methods are provided.

1.3. Outline

This dissertation is structured as following. The next two chapters follow the structure provided in this introduction to overview the uncertainty quantification and uncertainty propagation of (1) aleatory, (2) epistemic and (3) mixed uncertainties and corresponding theories. For this purpose, (1) probability theory, (2) interval theory and (3) imprecise probability theory are introduced in Chapter 2 and fundamental definitions are provided. Afterwards, the propagation of imprecise random fields by the double loop approach is presented in Chapter 3. For that purpose, (1) the discretisation of aleatory random fields by Karhunen-Loève expansion is described, before providing (2) a brief overview on interval analysis. Both concepts are combined to the probability bounds analysis, which is introduced and investigated in part (3) of the chapter.

Before focusing on different sampling based stochastic finite element method to propagate aleatory random fields through high-dimensional and/or non-linear models in Chapter 5, a short excursus on the fundamentals of solid mechanics is provided in Chapter 4, in order to clarify the used notation and material models.

Imprecise random fields are then carefully studied with regard to the influence of the correlation length in Chapter 6. Based on the findings, a decoupled interpolation approach is proposed and studied intensively concerning one- and two-dimensional (imprecise) random fields regarding linear and non-linear model propagations.

Finally, the main challenges of propagating imprecise random fields as well as all findings of this thesis are summarised in Chapter 7, providing also further perspectives and future steps of research.

2. Describing Uncertain Parameters

Uncertainties can appear in all forms of parameters, as *(a) uncertain variable* meaning a constant but uncertain value in the system, as an *(b) uncertain field* implying a spatial variability and as an *(c) uncertain process* when the parameter is time dependent. Furthermore, uncertain parameters depending on space and time are referred to as *space-time uncertain process*. Depending on the classification of uncertainties, *(i) aleatory*, *(ii) epistemic* or *(iii) mixed*, (a) can be classified into random variables, interval variables or imprecise random variables. Analogously, (b) and (c) are classified as random field or stochastic process, respectively, interval field/process and imprecise random field/process. The different classifications are given in Table 2.1.

Table 2.1: Overviews of theories to model (i) aleatory, (ii) epistemic or (iii) mixed uncertain parameters p depending on the physical dependency, (a) no dependency, (b) spatial dependency and (c) temporal dependency.

physical dependency	(i) probability theory	(ii) interval theory	(iii) imprecise probability theory
(a) non $p = p_0$	random variable $p = X(\omega)$	interval variable $p = X^I$	imprecise random variable $p = [X](\omega)$
(b) spatial $p = p(\boldsymbol{z})$	random field $p = X(\omega, \boldsymbol{z})$	interval field $p = X^I(\boldsymbol{z})$	imprecise random field $p = [X](\omega, \boldsymbol{z})$
(c) temporal $p = p(t)$	random process $p = X(\omega, t)$	interval process $p = X^I(t)$	imprecise random process $p = [X](\omega, t)$

The definitions of random variables, random fields, stochastic processes and space-time dependent processes in the framework of probability theory can be found, e.g. in the book on Stochastic Calculus by Grigoriu [2002]. An Introduction to Interval Analysis can be found by Moore et al. [2009]. Furthermore, Beer et al. [2013] provide a sound review on different concepts of imprecise probabilities such as evidence theory, probability bound analysis and fuzzy probabilities.

In the following sections the fundamentals of probability theory, interval theory and imprecise probability theory are introduced. Regarding the physical dependency of the uncertain parameters the focus is on constant variables as well as spatially dependent fields. Despite some minor differences in definition[1], processes can be interpreted as fields where the spatial parameter $\boldsymbol{z}$ is replaced by the time t and will not be discussed further within this work, as only static problems are considered.

---

[1]e.g. the concept of past and future in the context of uncertain processes [Grigoriu, 2002]

Model assumptions: The theoretical descriptions in the following chapter are limited towards uncertain parameters for which the following model assumptions are given.

- All uncertain parameters are considered to be *continuous*.

- Epistemic uncertainties are modelled by *intervals*, there are no fuzzy parameters considered and therefore not further introduced.

- All aleatory uncertainties are assumed to be *Gaussian distributed*. For this reason, no other distribution families are introduced and no transformation strategies are discussed.

- Random variables are considered *independent*, i.e. a joint probability density function (PDF) can be obtained by the product of the individual PDFs.

- There is *no crosscorrelation* between several random field parameters assumed.

The focus of this chapter is to state fundamental definitions and terms which are required for this thesis as well as to introduce the used notation. For further extensions and definitions as well as derivations and proofs, please refer to the literature provided accordingly.

2.1.   Probability theory for aleatory uncertain parameters

Probability theory provides mathematical models to describe random phenomena by abstraction or idealisation. The parameters needed to describe a model can be obtained by statistical evaluation of experiments. Furthermore, statistics can be used to validate probabilistic models. Together, probability theory and statistics form each one component of stochastic theory [Georgii, 2004].

Within this section, the main fundamentals of probability theory are briefly summarised. In the following paragraphs, some general definitions based on Grigoriu [2002] are given, which are required in terms of probability theory. Afterwards, the concepts of random variables and vectors are described in Subsection 2.1.1, before introducing random fields in Subsection 2.1.2.

Probability space: The triple $(\Omega, \mathcal{F}, P)$ is called probability space and is defined by the following components.

- The set of all possible events of interest is called *sample space* Ω and every possible outcome $\omega \in \Omega$ is called an element of the sample space. The sample space might be finite, countable or uncountable. If Ω is finite or countable, $(\Omega, \mathcal{F}, P)$ is called discrete while it is called continuous if Ω is uncountable.

- A non-empty collection of subsets of Ω is denoted by $\mathcal{F}$ and called *set of events*. It contains all relevant subsets, meaning that it is chosen according to the outcome of interest. It is called *σ-field* if the following holds true

    i) $\emptyset \in \mathcal{F}$,
    ii) $A \in \mathcal{F} \implies A^c \in \mathcal{F}$,
    iii) $A_i \in \mathcal{F} \implies \bigcup_{i \in \mathcal{I}} A_i \in \mathcal{F}$,

where A is called event or $\mathcal{F}$-measurable subset, $A^{\mathrm{c}} := \Omega \backslash A$ is the complement of A and $\mathcal{I}$ is a countable set of indices.

For countable sample spaces Ω the σ-field can be chosen as $\mathcal{F} = \mathfrak{P}(\Omega)$, where $\mathfrak{P}(\Omega)$ is the power set of Ω containing all its subsets. If the sample space is uncountable, however, $\mathcal{F}$ needs to be chosen as a subset of $\mathfrak{P}(\Omega)$. For example, if $\Omega \subset \mathbb{R}^N$ it is $\mathcal{F} = \mathcal{B}_\Omega^N$, where $\mathcal{B}_\Omega^N$ is a Borel σ-field on Ω. The latter is a σ-field obtained by sets of a topological space, so-called Borel sets B_i. If it is generated on $\mathbb{R}^N$, where $N \geq 1$ is the dimension, the Borel σ-field is written as $\mathcal{B}(\mathbb{R}^N) = \mathcal{B}^N$.

- The *probability measure* $P : \mathcal{F} \to [0,1]$ assigns a probability of occurrence $P(A)$ to the event A and needs to fulfil the following properties

    i) non-negativity: $P(A) \geq 0, \quad \forall A \in \mathcal{F}$,

    ii) normalisation: $P(\Omega) = 1$

    iii) σ-additivity: $P\left(\bigcup_{i=1}^\infty A_i\right) = \sum_{i=1}^\infty P(A_i), \quad A_i \in \mathcal{F}, \quad A_i \cap A_j = \emptyset, \; i \neq j$

    With $P(A) = 1 - P(A^{\mathrm{c}})$ it follows from ii) that the probability of an impossible event $\emptyset$ is zero, $P(\emptyset) = 1 - P(\Omega) = 0$. Furthermore, it is $P(A_i) \leq P(A_j)$ if $A_i \subseteq A_j$ and $P(A_i \cup A_j) = P(A_i) + P(A_j) - P(A_i \cap A_j)$.

Independence: The sub-σ-fields $\mathcal{F}_i$ of $\mathcal{F}$ given in the probability space $(\Omega, \mathcal{F}, P)$ are independent if

$$P\left(\bigcap_{i \in \mathcal{I}} A_i\right) = \prod_{i \in \mathcal{I}} P(A_i), \quad \forall A_i \in \mathcal{F}_i. \tag{2.1}$$

Two events A_i and A_j being independent means that the outcome of A_i is independent of the outcome of A_j, $P(A_i | A_j) = P(A_i)$, and vice versa. If the σ-fields $\sigma(A_i)$ generated from the events $A_i \in \mathcal{F}$ are independent, the events A_i are independent as well and Eq. (2.1) holds.

Measurable functions: The pair $(\Omega, \mathcal{F})$ is called measurable space. A function $h : \Omega \mapsto \Psi$ is called measurable from $(\Omega, \mathcal{F})$ to a second measurable space $(\Psi, \mathcal{G})$ if

$$h^{-1}(B) = \{\omega : h(\omega) \in B\} \in \mathcal{F}, \quad \forall B \in \mathcal{G}. \tag{2.2}$$

Random variables and vectors are measurable functions when a probability measure P is assigned to the measurable space $(\Omega, \mathcal{F})$.

2.1.1.   Random variables

A random variable is a parameter depending on chance and assigns a real number to each result of an experiment. The mathematical definition of a random variable, its properties and applicable measures is briefly summarised in this subsection. If not indicated differently, all descriptions are based on the definitions and derivations given by Grigoriu [2002].

Consider a measurable space $(\Omega, \mathcal{F})$, a random variable $X = X(\omega)$ is a measurable function $X : (\Omega, \mathcal{F}) \mapsto (\mathbb{R}, \mathcal{B})$, with $\mathcal{B} = \mathcal{B}^1$ denoting a one-dimensional (1D) Borel σ-field. To be defined as a random variable, X must hold

$$X^{-1}\left((-\infty, x]\right) \in \mathcal{F}, \quad x \in \mathbb{R}. \tag{2.3}$$

As visualised in Figure 2.1, $X(\omega)$ assigns a real value $x \in \mathbb{R}$ to the result $\omega \in \Omega$. A certain observation $x_j = X(\omega_j)$ is called realisation. Depending on the likelihood of occurrence of ω_j, a probability measure $P(X \leq x_j)$ is assigned to the corresponding value x_j. With an N-dimensional Borel σ-field $\mathcal{B}^N$, the concept of random variables can be extended to a random vector $\boldsymbol{X} : (\Omega, \mathcal{F}) \mapsto (\mathbb{R}^N, \mathcal{B}^N), N > 1$. With $\boldsymbol{X}^{-1}(B) \in \mathcal{F}$ for every Borel set $B \in \mathcal{B}^N$, the assigned probability measure is $P(\boldsymbol{X} \in B) = P(\boldsymbol{X}^{-1}(B))$ on the measurable space $(\mathbb{R}^N, \mathcal{B}^N)$. Each coordinate of a random vector is a random variable which needs to hold Eq. (2.3).
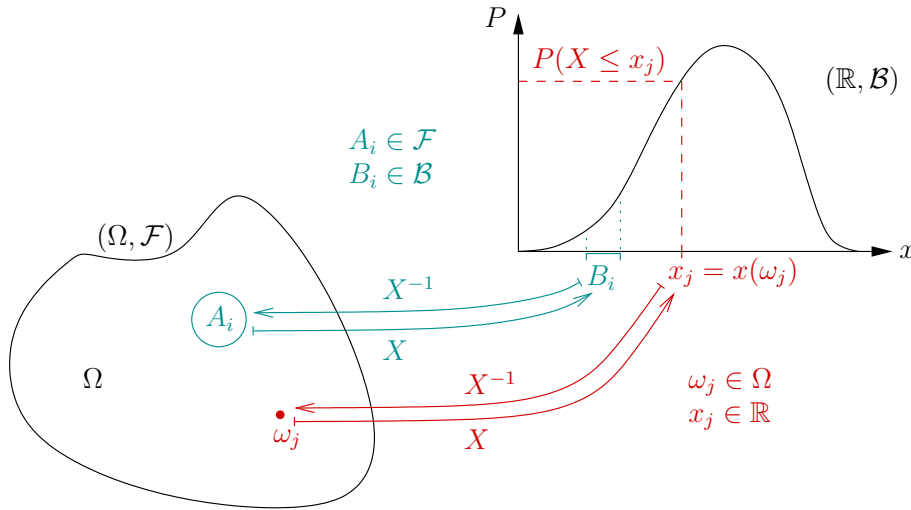
Figure 2.1: A random variable $X(\omega)$ defined as a mapping between the measurable spaces $(\Omega, \mathcal{F})$ and $(\mathbb{R}, \mathcal{B})$.

Depending on the probability space $(\Omega, \mathcal{F}, P)$ being discrete or continuous, a random variable or vector defined within this probability space is distinguished into discrete or continuous as well. In this work, only continuous probability theory is further described. The discrete case is a special case of the continuous one and can be obtained from it by discretisation.

Two random variables $X_i := X_i(\omega)$ and $X_j := X_j(\omega)$ are independent, if their corresponding σ-fields $\mathcal{F}(X_i)$ and $\mathcal{F}(X_j)$ are independent according to Eq. (2.1). Then, the joint probability measure of both random variables is

$$P(X_i, X_j) = P(X_i)P(X_j). \tag{2.4}$$

The linear relationship between X_i and X_j is quantified by their covariance $\mathrm{Cov}\{X_i, X_j\}$,

$$\mathrm{Cov}\{X_i, X_j\} = \mathrm{E}\{\,(X_i - \mathrm{E}\{X_i\})\,(X_j - \mathrm{E}\{X_j\})\,\}, \tag{2.5}$$

with $\text{Cov}\{X_i, X_i\} = \text{Var}\{X_i\}$ for $i = j$ and $\text{Var}\{X_i\}$ the variance of the random variable X_i. Normalising the covariance by the standard deviation $\text{Std}\{X\}$ yields the correlation coefficient

$$\text{Corr}\{X_i, X_j\} = \frac{\text{Cov}\{X_i, X_j\}}{\text{Std}\{X_i\}\text{Std}\{X_j\}}, \quad -1 \leq \text{Corr}\{X_i, X_j\} \leq 1. \tag{2.6}$$

If $\text{Corr}\{X_i, X_j\} = 0$, X_i and X_j are uncorrelated. Note that X_i and X_j being independent implies them to be uncorrelated but vice versa two uncorrelated random variables are not necessary independent.

In the following paragraphs, important functions and measures of random variables and vectors are introduced.

Cumulative distribution function (CDF): If only real numbers are contained in Ω, the probability $P(X \leq x)$ of a random variable $X(\omega) : \Omega \mapsto \mathbb{R}$ can be described by the cumulative distribution function (CDF) $F_X(x) : \mathbb{R} \mapsto [0, 1]$ depending on x,

$$F_X(x) = P\left(X^{-1}\left((-\infty, x]\right)\right) = P\left(\{A : X(\omega) \leq x\}\right) = P(X \leq x). \tag{2.7}$$

A CDF is monotonically increasing, right continuous and follows an asymptotic behaviour,

$$\lim_{x \to -\infty} F_X(x) = 0, \tag{2.8}$$

$$\lim_{x \to +\infty} F_X(x) = 1. \tag{2.9}$$

The reliability of a system is given by $R_X(x) = 1 - F_X(x)$. The joint CDF of a random vector $\boldsymbol{X}(\omega)$ is obtained from the probability measure of its individual random variables $X_i(\omega)$,

$$F_{\boldsymbol{X}}(\boldsymbol{x}) = P\left(\bigcap_{i=1}^{N}\{X_i \leq x_i\}\right), \quad \boldsymbol{x} = (x_1, \ldots, x_N) \in \mathbb{R}^N. \tag{2.10}$$

If the random vector consists of independent random variables $X_i(\omega), i = 1, \ldots, N$, the joint CDF is given by

$$F_{\boldsymbol{X}}(\boldsymbol{x}) = \prod_{i=1}^{N} F_{X_i}(x_i). \tag{2.11}$$

Probability density function (PDF): The function $f_X(x) \geq 0$ with $\int_{-\infty}^{\infty} f_X(x)\,\mathrm{d}x = 1$ is called probability density function if it fulfils

$$P(a \leq X \leq b) = F_X(b) - F_X(a) = \int_a^b f_X(x)\,\mathrm{d}x, \quad a \leq b. \tag{2.12}$$

Given $f_X(x)$ to be integrable, the CDF $F_X(x)$ is determined by

$$F_X(x) = \int_{-\infty}^{x} f_X(s)\,\mathrm{d}s. \tag{2.13}$$

The function $f_{\boldsymbol{X}}(\boldsymbol{x})$ fulfilling

$$f_{\boldsymbol{X}}(\boldsymbol{x}) = \frac{\partial^N F_{\boldsymbol{X}}(\boldsymbol{x})}{\partial x_1 \cdots \partial x_N}, \quad \boldsymbol{x} = (x_1, \ldots, x_N) \in \mathbb{R}^N \tag{2.14}$$

is the joint PDF of the random vector $\boldsymbol{X}(\omega)$ and can be obtained by

$$f_{\boldsymbol{X}}(\boldsymbol{x}) = \prod_{i=1}^{N} f_{X_i}(x_i), \tag{2.15}$$

if the coordinates $X_i(\omega)$ of the random vector are independent.

Stochastic moments: For real-valued random variables $X(\omega) : \Omega \mapsto \mathbb{R}$, the moment of n-th order is given as

$$\mathrm{E}\{X^n\} = \int_{-\infty}^{\infty} x^n f_X(x) \, \mathrm{d}x. \tag{2.16}$$

The moment of first order $\mathrm{E}\{X\}$ is called expected value and can be estimated statistically by the mean value μ_X of the random parameter to be modelled. The central moment of n-th order is defined by

$$\mathrm{E}\{[X - \mathrm{E}\{X\}]^n\} = \int_{-\infty}^{\infty} [x - \mathrm{E}\{X\}]^n \, f_X(x) \, \mathrm{d}x. \tag{2.17}$$

The second central moment $\mathrm{Var}\{X\} = \mathrm{E}\{[X - \mathrm{E}\{X\}]^2\}$ results in the variance, the central moment of third order in the skewness and the one of fourth order in the kurtosis of the distribution of X. Furthermore, $\mathrm{Std}\{X\} = \sqrt{\mathrm{Var}\{X\}}$ is the standard deviation of X. These operators on the mathematical model of the distribution can be estimated statistically by the variance σ_X^2, the skewness γ_X, the kurtosis κ_X and the standard deviation σ_X, respectively.

In case of a random vector $\boldsymbol{X}(\omega)$, the expected value and the variance are a vector containing the expected values and variances of the individual random variable coordinates X_i, i.e. $\mathrm{E}\{\boldsymbol{X}\} = \mathrm{E}\{X_i\}$ and $\mathrm{Var}\{\boldsymbol{X}\} = \mathrm{Var}\{X_i\}$. Furthermore, the covariance and correlation coefficient of each combination i, j are included in the covariance matrix $\mathrm{Cov}\{\boldsymbol{X}\} = \mathrm{Cov}\{X_i, X_j\}$ and the correlation coefficient matrix $\mathrm{Corr}\{\boldsymbol{X}\} = \mathrm{Corr}\{X_i, X_j\}$, respectively.

Gaussian random variable: A random variable $X(\omega) \sim \mathcal{N}(\mu_X, \sigma_X)$ with mean value μ_X and standard deviation σ_X is called Gaussian or normal distributed if its PDF is given by

$$f_X(x) = \frac{1}{\sqrt{2\pi}\sigma_X} \exp\left\{ -\frac{1}{2}\left(\frac{x - \mu_X}{\sigma_X} \right)^2 \right\}, \quad x \in \mathbb{R}. \tag{2.18}$$

Due to the symmetry of $f_X(x)$ about $x = \mu_X$, the skewness is zero, $\gamma_X = 0$. Furthermore, it is $\kappa_X = 3$. The PDF and the CDF of a Gaussian random variable are depicted in Figure 2.2. Note that $99.73\,\%$ of the samples following a Gaussian distribution are located in the range $\mu_X \pm 3\,\sigma_X$, which is visualised in dash-dotted lines. A special case of the Gaussian random variable is the standard normal distributed random variable $S(\omega) \sim \mathcal{N}(0, 1)$ with zero mean and unified standard deviation.
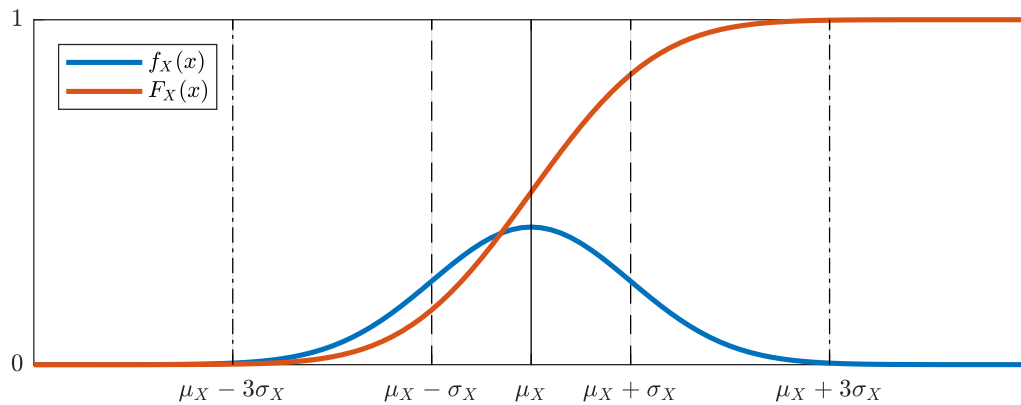
Figure 2.2: Probability density function $f_X(x)$ and cumulative distribution function $F_X(x)$ of a Gaussian distributed random variable $X(\omega) \sim \mathcal{N}(\mu_X, \sigma_X)$.

Note that due to the fact of being unbounded, Gaussian random variables are not appropriate from the physical point of view to model parameters that are only defined for positive values, e.g. material data. However, depending on the relative standard deviation $\sigma_X = r \cdot \mu_X$ with $r < 1$ a certain percentage of the mean value $\mu_X > 0$, the appearance of negative values is unlikely. Therefore, Gaussian distribution is often used nevertheless for convenience, as also done within this thesis. In this case, a sufficiently small likelihood of obtaining negative values should be quantified and it should be assured during all studies that no negative values occur in the sampling process. Although this is mathematically not correct as the probability does not integrate exactly to be one, this error can be neglected from the engineering point of view.

2.1.2. Random fields

Random fields are parameters depending spatially on chance. They assign a real function depending on the spatial variable to each result of an experiment. In this subsection, random fields are defined from the mathematical point of view. If no other literature is referred to, all definitions follow the book on random fields by Vanmarcke [2010].

On the contrary to random variables, which are only a function $X(\omega)$ of chance, $\omega \in \Omega$, a random field $X(\omega, \boldsymbol{z}) : \mathcal{D} \times \Omega \mapsto \mathbb{R}$ depends additionally on space $\boldsymbol{z} \in \mathcal{D}$ within the domain $\mathcal{D} \subset \mathbb{R}^d, d = 1, 2, 3$. For a fixed value ω_j, the deterministic function $x_j(\boldsymbol{z}) = X(\omega_j, \boldsymbol{z})$ is called *realisation*. On the other hand, for a fixed location $\boldsymbol{z}_J$, the resulting random variable $X_J(\omega) = X(\omega, \boldsymbol{z}_J)$ is called *state* of the random field.

The autocovariance $C_X(\boldsymbol{z}, \boldsymbol{z}') =: \text{Cov}\{X(\omega, \boldsymbol{z}), X(\omega, \boldsymbol{z}')\}$ of two arbitrary values $X(\omega, \boldsymbol{z})$ and $X(\omega, \boldsymbol{z}')$ within the random field is described by the autocovariance function. Alternatively, the dependency of two values within the field can also be expressed in terms of the standard deviation $\sigma_X(\boldsymbol{z})$ and the autocorrelation function $\Gamma_X(\boldsymbol{z}, \boldsymbol{z}') : \mathcal{D} \times \mathcal{D} \mapsto [0, 1]$,

$$C_X(\boldsymbol{z}, \boldsymbol{z}') = \sigma_X(\boldsymbol{z})\sigma_X(\boldsymbol{z}')\Gamma_X(\boldsymbol{z}, \boldsymbol{z}'), \tag{2.19}$$

with $\Gamma_X(\boldsymbol{z}, \boldsymbol{z}') =: \text{Corr}\{X(\omega, \boldsymbol{z}), X(\omega, \boldsymbol{z}')\}$ as defined in Eq. (2.6). If its autocovariance or autocorrelation function is a function only of the distance $\boldsymbol{z} - \boldsymbol{z}'$, a random field is called

homogeneous. Moreover, if the function is even only depending on $|\boldsymbol{z} - \boldsymbol{z}'|$, the random field is called *isotropic*, i.e. the autocorrelation structure is the same in any direction. In this case, the autocorrelation length L_X is a measure describing how fast the autocorrelation between two values $X(\omega, \boldsymbol{z})$ and $X(\omega, \boldsymbol{z}')$ decreases with respect to their distance $\boldsymbol{z} - \boldsymbol{z}'$. The autocorrelation function is then usually described by a function of $(\boldsymbol{z} - \boldsymbol{z}')/L_X$. If two or more random fields are defined on the same domain, the dependency of the corresponding parameters between each other is described by the crosscovariance or crosscorrelation function [Vořechovský, 2008]. However, crosscorrelation is not further discussed and applied in this work. For this reason, the short terms "covariance", "correlation" and "correlation length" are used for convenience whenever autocovariance, autocorrelation or autocorrelation length are meant.

Random fields can be extended to random vector fields $\boldsymbol{X}(\omega, \boldsymbol{z}) : \mathcal{D} \times \Omega \mapsto \mathbb{R}^N, N > 1$. Then, the realisation $\boldsymbol{x}_j(\boldsymbol{z})$ is a deterministic vector function and the state $\boldsymbol{X}_J(\omega)$ is a random vector. In engineering application, $X(\omega, \boldsymbol{z})$ is often referred to as *univariate*, $\boldsymbol{X}(\omega, \boldsymbol{z})$ as *multivariate* random field, while it is called *one-dimensional* ($d = 1$) or *multi-dimensional* ($d > 1$), depending on the dimension d of the domain $\mathcal{D} \in \mathbb{R}^d$ [Sudret and Der Kiureghian, 2000].

Gaussian random fields: A random field with any vector $(X(\omega, \boldsymbol{z}_1), X(\omega, \boldsymbol{z}_2), ...)$ being jointly Gaussian distributed $\forall \boldsymbol{z} \in \Omega$ is called Gaussian random field. It then is completely described by its mean function $\mu_X(\boldsymbol{z}) : \Omega \mapsto \mathbb{R}$ and its covariance function $C_X(\boldsymbol{z}, \boldsymbol{z}') : \mathcal{D} \times \mathcal{D} \mapsto \mathbb{R}$ [Sudret and Der Kiureghian, 2000]. Regarding the physical aspect of some parameters, also for Gaussian random fields the same constraints hold as for Gaussian random variables.

In Figure 2.3, five realisations $x_j(z) = X(\omega_j, z)$, $j = 1, \ldots, 5$, of a Gaussian distributed 1D random field are exemplified as red solid lines, each describing a deterministic function resulting for ω_j. Their value at z_J is depicted as a red circle, representing the state $X_J(\omega_j) = X(\omega_j, z_J)$ of the individual realisation j. For an infinite amount of realisations, the corresponding states $X_J(\omega) = X(\omega, z_J)$ of the random field $X(\omega, z)$ are Gaussian distributed at any location z_J. Furthermore, the mean value and standard deviation of $X_J(\omega)$ are equal to the values of the random field $X(\omega, \boldsymbol{z})$, i.e. $\mu_{X_J} = \mu_X(\boldsymbol{z}_J)$ and $\sigma_{X_J} = \sigma_X(\boldsymbol{z}_J)$. If all states of a random field are standard normal distributed, i.e. $\mu_X(\boldsymbol{z}) = 0$ and $\sigma_X(\boldsymbol{z}) = 1$, the random field is called *standard normal distributed random field* $S(\omega, \boldsymbol{z})$.

Random field discretisation: To use a random field $X(\omega, \boldsymbol{z})$ for stochastic simulation it needs to be discretised in both manners, in terms of the physical domain (i.e. spatial domain in terms of random fields) as well as the stochastic domain. The spatial domain is usually discretised already in order to solve a given problem deterministically, e.g. by finite element method (FEM). Discretisation methods for random fields can be categorised into three groups [Sudret and Der Kiureghian, 2000]:

- The most straightforward way is to select the values of $X(\omega, \boldsymbol{z}_i)$ at given points $\boldsymbol{z}_i$ as random variables $\{X_i(\omega)\}$ as it is done by *point discretisation methods*. For example, this can be the centroid of each element (midpoint method), the Gauss points of each element (integration point method) or a linear function of nodal values (optimal linear estimation method).

- Regarding *average discretisation methods*, the random variables $\{X_i(\omega)\}$ are chosen by weighted integrals over the element domain, e.g. in terms of a constant value at each element (spatial average method).

- A spectral representation of a random field is theoretically exact and given by several *series expansion methods*. They decouple the dependency on chance and space by describing the first in terms of random variables and the second by deterministic spatial functions within an infinite series. To be used within a stochastic simulation, the expanded random field is discretised within the stochastic space by truncating the series after a certain truncation term T. The stochastic dimension of the approximated random field $\bar{X}(\omega, z)$ is then given by $N = T$. Among other methods, as e.g. the expansion optimal linear estimation method or the orthogonal series expansion method, a commonly used method of this category is the Karhunen-Loève (KL) expansion. The latter will also be used within this work and is therefore introduced comprehensively in Section 3.1.

The first and second method connect the stochastic discretisation directly to the spatial discretisation and are therefore mesh-dependent. For more details on the given examples as well as further methods of these categories, the reader is referred to the state of the art report by Sudret and Der Kiureghian [2000] and the literature provided therein.
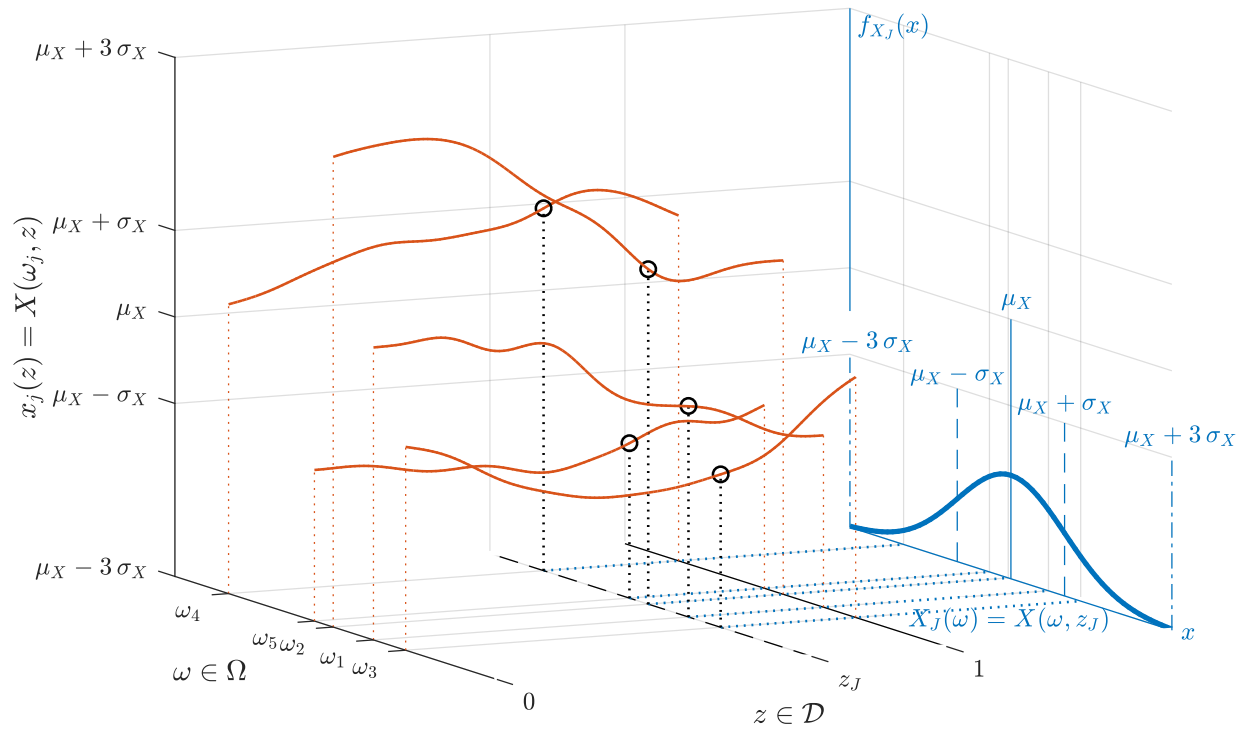
Figure 2.3: Five one-dimensional random field realisations $x_j(z) = X(\omega_j, z)$, $j = 1, \ldots, 5$, $z \in [0, 1]$ (red) as well as the probability density function $f_{X_J}(x)$ (blue) corresponding to a random field state $X_J(\omega) = X(\omega, z_J)$.

2.2. Interval theory for epistemic uncertain parameters

An intuitive way to describe imprecision is given by intervals. The interval bounds can be estimated by expert opinion or - if available, e.g. when the measuring inaccuracy of a machine is known - defined by available information. An interval $I = [a, b]$, $I \subseteq \mathbb{R}$, is defined as a real-numbered set containing all elements x between two bounding elements and can be described explicitly by [Moore et al., 2009]

$$[a, b] = \{x \in \mathbb{R} : a \leq x \leq b\}. \tag{2.20}$$

The interval definition of Eq. (2.20), i.e. including both interval bounds, is called *closed*. On the contrary, an *open* interval does not include its bounds,

$$(a, b) = \{x \in \mathbb{R} : a < x < b\}. \tag{2.21}$$

The combination of both in either way is called *semi-open*, i.e. semi-left-open $(a, b]$ and semi-right-open if $[a, b)$.

In the following subsection, interval variables and vectors are introduced, which are a straightforward method to describe epistemically uncertain variables. Afterwards, the concept of interval fields is briefly introduced in Subsection 2.2.2, which extends interval variables towards a spatial dependency.

2.2.1. Interval variables

Interval variables are uncertain parameters described by an interval. They are handled by arithmetic operations or, regarding more sophisticated problems, can be propagated by discretisation or sampling and simulation, as described in Section 3.2. Within this subsection, the basic definitions of interval variables are summarised based on the book by Moore et al. [2009]. Additional literature is adduced as cited accordingly.

Regarding a closed interval, an interval variable X^I is given by a lower bound $\underline{X}$ and an upper bound $\overline{X}$ as

$$X^I = [\underline{X}, \overline{X}], \quad \{x \in \mathbb{R} : \underline{X} \leq x \leq \overline{X}\}. \tag{2.22}$$

Otherwise, it is defined accordingly to the definitions of open or semi-open intervals. In order to not repeat all the interval types all the time, the notation of closed intervals is used in this work whenever intervals in general are meant. A crisp number can be interpreted as a special case of an interval variable with $x = \underline{X} = \overline{X}$.

Interval variables can be extended to interval vectors $\boldsymbol{X}^I$ containing an ordered n-tuple of intervals,

$$\boldsymbol{X}^I = \left(X_1^I, \ldots, X_n^I\right) \tag{2.23}$$
$$= \left([\underline{X}_1, \overline{X}_1], \ldots, [\underline{X}_n, \overline{X}_n]\right). \tag{2.24}$$

An interval vector represents an n-dimensional hyper-rectangular domain, which can be represented by the Cartesian product $\boldsymbol{X}^I = [\underline{X}_1, \overline{X}_1] \times \cdots \times [\underline{X}_n, \overline{X}_n]$. Note that the individual interval variables are independent by definition [Faes and Moens, 2020b]. A vector $\boldsymbol{x} = (x_1, \ldots, x_n)$, $x_i \in \mathbb{R}$ is included in an n-dimensional interval vector, $\boldsymbol{x} \in \boldsymbol{X}^I$, if

$$x_i \in X_i^I \quad \text{for} \quad i = 1, ..., n. \tag{2.25}$$

In the following paragraphs, some characteristic values of an interval variable or vector as well as relations, operations and arithmetics for two or more interval variables are briefly summarised.

Characteristic values: An interval variable X^I (or an interval vector $\boldsymbol{X}^I$) has the following properties.

- The *width* $w(X^I)$ is the range of the interval variable, i.e.

$$w(X^I) = \overline{X} - \underline{X}. \tag{2.26}$$

  In case of an interval vector, the width is defined to be the largest component range,

$$w(\boldsymbol{X}^I) = \max_i w(X_i^I), \tag{2.27}$$

  i.e. the longest edge of the hyper cuboid.

- The central point within an interval variable is called *midpoint* and given by

$$m(X^I) = \frac{1}{2} \left(\underline{X} + \overline{X} \right), \tag{2.28}$$

  or, in case of an interval vector, by the vector

$$m(\boldsymbol{X}^I) = \left(m(X_1^I), \ldots, m(X_n^I) \right). \tag{2.29}$$

- The *absolute value* can be interpreted as the Chebyshev distance, which is

$$|X^I| = \max\{|\underline{X}, \overline{X}|\} \tag{2.30}$$

  in case of an interval variable and extended to interval vectors by

$$\|\boldsymbol{X}^I\| = \max_i |X_i^I|, \tag{2.31}$$

  which is then called the *norm* of the interval vector.

- The *interval radius* is defined by

$$\Delta X^I = \frac{1}{2} \left(\overline{X} - \underline{X} \right). \tag{2.32}$$

Interval relations and operations: For two interval variables X_1^I and X_2^I - or two n-dimensional interval vectors $\boldsymbol{X}_1^I = \left(X_{1,1}^I, \ldots, X_{1,n}^I\right)$ and $\boldsymbol{X}_2^I = \left(X_{2,1}^I, \ldots, X_{2,n}^I\right)$ - the following relations and operations are applicable.

- There are several useful *order relations*. An interval variable is called *positive*, $X^I > 0$, if $x > 0$ for all $x \in X^I$ and *negative*, $X^I < 0$, if $x < 0$ for all $x \in X^I$. Furthermore, it is

$$X_1^I < X_2^I \quad \text{if} \quad \overline{X}_1 < \underline{X}_2. \tag{2.33}$$

An interval variable is included in another,

$$X_1^I \subseteq X_2^I, \quad \text{if and only if} \quad \underline{X}_2 \leq \underline{X}_1 \quad \text{and} \quad \overline{X}_1 \leq \overline{X}_2. \tag{2.34}$$

Consequently, for interval vectors it is

$$\boldsymbol{X}_1^I \subseteq \boldsymbol{X}_2^I \quad \text{if} \quad X_{1,i}^I \subseteq X_{2,i}^I \quad \text{for} \quad i = 1, \ldots, n. \tag{2.35}$$

- If the *intersection* is not empty, i.e. $X_1^I \cap X_2^I = \emptyset$ if either $\overline{X}_1 < \underline{X}_2$ or $\overline{X}_2 < \underline{X}_1$ meaning that both intervals have no points in common, the intersection is defined as an interval value resulting from

$$X_1^I \cap X_2^I = [\max(\underline{X}_1, \underline{X}_2), \ \min(\overline{X}_1, \overline{X}_2)]. \tag{2.36}$$

Furthermore, it is $\boldsymbol{X}_1^I \cap \boldsymbol{X}_2^I$ if any $X_{1,i}^I \cap X_{2,i}^I$. Otherwise, the operation leads to an interval vector given by

$$\boldsymbol{X}_1^I \cap \boldsymbol{X}_2^I = \left(X_{1,1}^I \cap X_{2,1}^I, \ldots, X_{1,n}^I \cap X_{2,n}^I\right). \tag{2.37}$$

- The *union* $X_1^I \cup X_2^I$ of two interval variables does not necessarily result in an interval and has no particular relevance in interval analysis. More precisely, the union of two interval variables lead to an interval only if $X_1^I \cap X_2^I \neq \emptyset$.

- The *interval hull* is defined as

$$X_1^I \underline{\cup} X_2^I = [\min(\underline{X}_1, \underline{X}_2), \ \max(\overline{X}_1, \overline{X}_2)] \tag{2.38}$$

and is of higher importance for interval computations than the union, as it always leads to an interval. The interval hull includes the union, i.e. $X_1^I \cup X_2^I \subseteq X_1^I \underline{\cup} X_2^I$. It is the smallest interval containing both intervals, X_1^I and X_2^I. Analogously, the interval hull of two interval vectors is the smallest interval vector containing both interval vectors, $\boldsymbol{X}_1^I$ and $\boldsymbol{X}_2^I$.

Interval arithmetic: The addition, subtraction, multiplication or division of two interval variables X_1^I and X_2^I is explicitly defined by

$$X_1^I \odot X_2^I = \{x_1 \odot x_2 : x_1 \in X_1^I,\ x_2 \in X_2^I\}, \tag{2.39}$$

with $\odot$ being any of the operators $+$, $-$, $\cdot$ or $/$. Note that the division of two intervals is only defined for $0 \notin X_2^I$. The calculation can also be performed straightforwardly by the following endpoint formulas

$$X_1^I + X_2^I = [\underline{X}_1 + \underline{X}_2,\ \overline{X}_1 + \overline{X}_2], \tag{2.40}$$

$$X_1^I - X_2^I = [\underline{X}_1 - \overline{X}_2,\ \overline{X}_1 - \underline{X}_2], \tag{2.41}$$

$$X_1^I \cdot X_2^I = [\min(S),\ \max(S)]; \tag{2.42}$$
$$S = \{\underline{X}_1\underline{X}_2,\ \underline{X}_1\overline{X}_2,\ \overline{X}_1 \cdot \underline{X}_2,\ \overline{X}_1\overline{X}_2\},$$

$$X_1^I / X_2^I = X_1^I \left[\frac{1}{\overline{X}_2},\ \frac{1}{\underline{X}_2}\right] \quad \text{if } 0 \notin X_2^I, \quad \text{undefined else.} \tag{2.43}$$

2.2.2. Interval fields

Assuming interval valued parameters often leads to a conservative estimate as each parameter is assumed to be either best case or worst case at the whole domain and a dependency between several interval parameters cannot be modelled. In order to acknowledge a spatial dependence of an interval, Moens et al. [2011] introduced the concept of explicit interval fields as a non-probabilistic equivalent to random fields. Note that there exist also other methods to model dependency, e.g. ellipsoid approaches [Elishakoff and Elettro, 2014] or admissible set decomposition [Faes and Moens, 2020a].

The idea of interval fields is to superpose a number n of deterministic base functions $\varphi_i(\boldsymbol{z}) : \mathcal{D} \mapsto [0,1]$, i.e. a set of patterns describing the spatial dependency, scaled by interval valued factors $a_i \in \mathbb{IR}$. The latter describe the magnitude of the epistemic uncertainty, with $\mathbb{IR}$ being the space of real valued intervals. The interval field $X^I(\boldsymbol{z}) : \mathcal{D} \times \mathbb{IR}^n \mapsto \mathbb{IR}$ is then described by the sum of weighted base functions

$$X^I(\boldsymbol{z}) = \sum_{i=1}^{n} \varphi_i(\boldsymbol{z}) a_i. \tag{2.44}$$

With a_i being independent, interval fields can be considered as input parameters by common methods to propagate interval uncertainties [Faes and Moens, 2020b]. Alternatively, an interval field can be defined implicitly by

$$X^I(\boldsymbol{z}) = \{\boldsymbol{\varphi}_X(\boldsymbol{a}_X),\ \boldsymbol{a}_X \in \boldsymbol{a}_X^I\}, \tag{2.45}$$

with $\boldsymbol{\varphi}_X(\boldsymbol{a}_X) = (\varphi_{X,1}(\boldsymbol{a}_X), \ldots, \varphi_{X,n}(\boldsymbol{a}_X))$ being implicit functions of predefined interval factors $\boldsymbol{a}_X^I$ [Verhaeghe et al., 2013].

In general, the base functions are not orthogonal by construction, i.e. for the inner product $\langle \cdot, \cdot \rangle$ it is

$$\langle \varphi_i(\boldsymbol{z}), \varphi_j(\boldsymbol{z}) \rangle = \int_{\mathcal{D}} \varphi_i(\boldsymbol{z}) \varphi_j(\boldsymbol{z}) \, \mathrm{d}\boldsymbol{z} \neq \delta_{ij}, \tag{2.46}$$

with δ_{ij} the Kronecker delta. This way, they can be used to control the dependence between the intervals at two locations $\boldsymbol{z}$ and $\boldsymbol{z}'$ [Faes and Moens, 2020c]. The base functions can be constructed, e.g. by inverse distance weighting interpolation [Faes and Moens, 2020c] or local interval field decomposition [Imholz et al., 2015], as summarised in a recent review paper by Faes and Moens [2020b]. Furthermore, Faes and Moens [2019a] extended the concept of interval fields to also describe inter-dependencies between multivariate interval fields. Sofi et al. [2019] apply a response surface approach to propagate interval fields using interval FEM.

The mentioned methods are not further discussed here, as interval fields are not applied particularly in this work. However, the basic idea of interval fields becomes useful to describe imprecise random fields, which will be introduced in Subsection 2.3.2 before discussing and studying them intensively in Chapter 3.

2.3. Probability box theory for mixed uncertainties

In many cases of engineering application, both kind of uncertainties appear in a mixed manner. The theory of imprecise probabilities [Beer et al., 2013] provides a broad choice of approaches to model mixed uncertain parameters, as briefly reviewed in Subsection 1.1.3. In the following, the probability box (p-box) approach is introduced in further detail to model imprecise random variables. Afterwards, the concept of imprecise random variables is extended to the idea of imprecise random fields in Subsection 2.3.2, to describe uncertain parameters including both, imprecision and spatial variation.

2.3.1. Imprecise random variables

A p-box is a straightforward and flexible approach to describe imprecise random variables $[X](\omega) = X^I(\omega)$. Instead of a crisp CDF, the distribution of a p-box is enveloped by two probability bounds [Ferson et al., 2003], the left bound $\overline{F}_X(x)$ and the right bound $\underline{F}_X(x)$,

$$\mathcal{P} = \{P \mid \forall x \in \mathbb{R}, \ \underline{F}_X(x) \leq F_X(x) \leq \overline{F}_X(x)\}. \tag{2.47}$$

As exemplified in Figure 2.4, the bounds can be discrete or continuous. If all distributions $F_X^i(x) \in \mathcal{P}$ are discrete, this special case of the probability bounds analysis results in evidence theory. Furthermore, there are two ways to derive or interpret a p-box, as also depicted in Figure 2.4:

i) Considering a certain value x^*, the p-box provides an interval valued probability $F_*^I(x) = [\overline{F}_*(x), \underline{F}_*(x)]$, with $\overline{F}_*(x) = \overline{P}_{x^*} = \overline{P}(X \leq x^*)$ being the upper (left) bound and $\underline{F}_*(x) = \underline{P}_{x^*} = \underline{P}(X \leq x^*)$ being the lower (right) bound of the probability assigned to x^*, compare the red sketch in Figure 2.4.

ii) Considering a certain probability P^*, the p-box provides an interval valued parameter $x_*^I = [\underline{x}_{P^*}, \overline{x}_{P^*}]$, with $\underline{x}_{P^*}$ being the lower (left) bound and $\overline{x}_{P^*}$ being the upper (right) bound of the parameter assigned to P^*, compare the blue sketch in Figure 2.4.

Both ways result in the same p-box. Note that in any case, one bound of the p-box is assigned to the lower bound of the first but to the upper bound of the second interpretation. Therefore, the bounds are not referred to as lower and upper bounds as it is done for intervals but are called *left* and *right bound* instead.
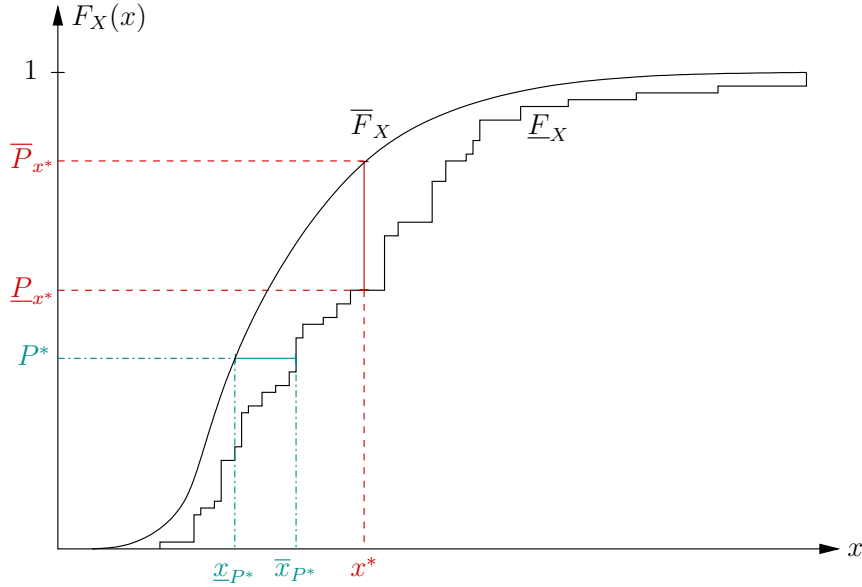
Figure 2.4: Probability box defined by a continuous left bound $\overline{F}_X = \overline{F}_X(x)$ and a discrete right bound $\underline{F}_X = \underline{F}_X(x)$, to be interpreted as an interval valued probability P^I or an interval valued parameter x^I.

A p-box is minimally defined by its left and right bound,

$$\mathcal{P} = [\overline{F}_X, \underline{F}_X], \tag{2.48}$$

leading to a *distribution free p-box*. Note that defining only the outer bounds theoretically may also include non-physical CDFs. On the other hand, a *parametric p-box* is a more restricted definition, e.g. in terms of the quintuple

$$\mathcal{P} = \langle \overline{F}_X, \underline{F}_X, \mu_X^I, \sigma_X^I, \mathcal{F} \rangle, \tag{2.49}$$

if more information is available [Beer et al., 2013, Faes et al., 2021]. For instance, the distribution family $\mathcal{F}$ might be known or the confidence intervals of the mean value μ_X^I or the variance $(\sigma_X^2)^I$ are given as

$$\int_{-\infty}^{\infty} x \, dF_X(x) \in \mu_X^I, \tag{2.50}$$

$$\left(\int_{-\infty}^{\infty} x^2 \, dF_X(x) \right) - \left(\int_{-\infty}^{\infty} x \, dF_X(x) \right)^2 \in (\sigma_X^2)^I. \tag{2.51}$$

As depicted in Figure 2.5, a p-box can be visualised in terms of its interval radii, Δx^I and ΔF_X^I, with respect to the corresponding interval midpoints $m(x^I)$ and $m(F_X^I)$. This representation is useful to compare results which are relatively similar in relation to the range of the CDF. Alternatively, a logarithmic scale can be used, which is however not as intuitively to read.
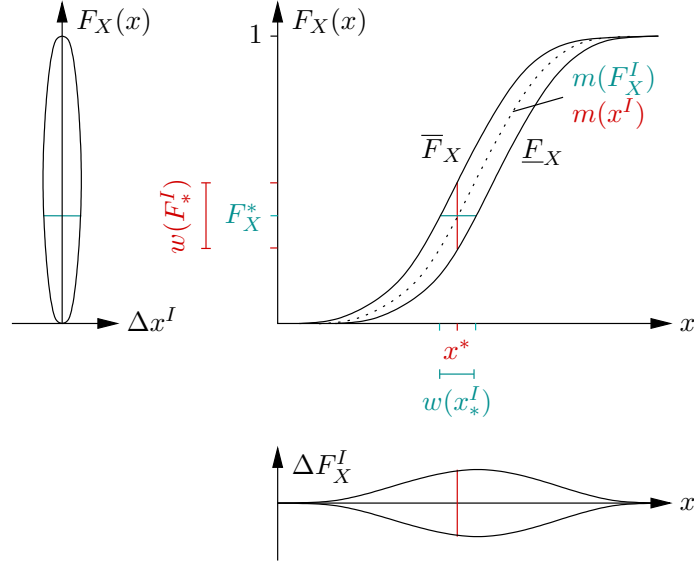
Figure 2.5: Classical visualisation of a probability box (top right), supplemented with its interval radii Δx^I (left) and ΔF_X^I (bottom) with respect to the corresponding midpoints $m(x^I)$ and $m(F_X^I)$ [Dannert et al., 2021a].

Several ways to construct a p-box are available, e.g. in terms of incomplete distribution properties, available data sets, aggregation methods or parametric construction. A sound review on these and dedicated methods has been recently published by Faes et al. [2021]. They furthermore review different ways to propagate p-box parameters. A very robust method is given by double loop approach which will be introduced in Section 3.3 to propagate imprecise random fields. Alternatively, decoupled approaches such as importance sampling or operator norm theory are available for parametric p-boxes, see Faes et al. [2021] and the literature provided therein. Schöbi and Sudret [2017] apply sparse polynomial chaos (PC) expansion as a surrogate model to propagate p-box valued parameters.

In this work, p-boxes are used to describe the quantity of interest (QoI) resulting from the propagation of (discretised) imprecise random fields. For this purpose, it is constructed by the minimum and maximum bounds of all input scenarios and therefore results in a parametric p-box containing at least information on the mean and standard deviation confidence intervals.

2.3.2.   Imprecise random fields

To quantify a random field, several hyper parameters are needed. For example, as described in Subsection 2.1.2, a Gaussian random field $X(\omega, \boldsymbol{z})$ requires information about its mean function $\mu_X(\boldsymbol{z})$ and its covariance function $C_X(\boldsymbol{z}, \boldsymbol{z}')$. The latter can be expressed as well by the standard deviation $\sigma_X(\boldsymbol{z})$ and the correlation function $\Gamma_X(\boldsymbol{z}, \boldsymbol{z}')$, see Eq. (2.19). These hyper parameters leave room for further uncertainties. While mean value and standard deviation

might be determined relatively easily by experiments, especially the correlation structure is difficult to measure and inherits a certain lack of knowledge. To consider also epistemic uncertainties, Dannert et al. [2018] and Faes and Moens [2019b] independently extended the idea of (aleatory) random fields towards imprecise random fields to model mixed uncertain, spatially (or temporally) varying parameters.

A straightforward way to model imprecision within the correlation function is to assume an interval valued correlation length L_X^I. Alternatively (or additionally), the correlation function itself could be considered with model uncertainty, i.e. regarding different correlation functions $\Gamma_X(\boldsymbol{z}, \boldsymbol{z}') \in \mathcal{C}$ with $\mathcal{C}$ the set of admissible correlation functions. However, this is beyond the scope of this dissertation. In this work, the focus is on interval valued correlation lengths.

Considering one or several hyper parameters to be interval valued, an imprecise random field is denoted by $[X](\omega, \boldsymbol{z})$ and can be described by the sextuplet

$$\mathcal{P} = \langle \overline{F}_X, \underline{F}_X, \mu_X^I, \sigma_X^I, \mathcal{F}, L_X^I \rangle. \tag{2.52}$$

In other words, an imprecise random field is a set of correlated p-boxes given at each location $\boldsymbol{z} \in \mathcal{D}$. This means that the state $[X_J](\omega) = [X](\omega, \boldsymbol{z}_J)$ at a certain location $\boldsymbol{z}_J \in \mathcal{D}$ is an imprecise random variable described by a p-box. On the other hand, a realisation $[X_j](\boldsymbol{z}) = [X](\omega_j, \boldsymbol{z})$ of an imprecise random field assigned to a certain sample ω_j is given by an interval field.

Instead of considering epistemic hyper parameters as intervals, they might also be described by fuzzy numbers or fuzzy intervals, leading to fuzzy random fields [Schietzold et al., 2019]. Indeed, imprecise random fields can be interpreted as a special case of fuzzy random fields with the membership function of the fuzzy quantity being either zero or one, see Figure 1.1 (d) and (g). However, despite this special case, fuzzy random fields require additional assumptions regarding the membership function and are therefore not further considered in this work.

3. Propagating Imprecise Random Fields

In Chapter 2, different ways to describe uncertain parameters in the input parameter space have been introduced, depending on whether the uncertainty is considered to be aleatory, epistemic or of mixed nature. Within this section the propagation of uncertain input parameters through a model is prepared.

A general model can be described, e.g. following Faes and Moens [2020b], as delineated. A random field realisation $\boldsymbol{x}_j(\boldsymbol{z}) = X(\omega_j, \boldsymbol{z})$ is propagated through a model $\mathcal{M}$ to obtain the model response $\boldsymbol{Y}_j(\boldsymbol{z}) = \mathcal{M}(\boldsymbol{x}_j)$ for a certain quantity of interest (QoI). The vector $\boldsymbol{Y}_j(\boldsymbol{z}) = (\boldsymbol{y}_1, \ldots, \boldsymbol{y}_n)_j$ contains all admissible model responses obtained by a set of function operators $M_i : \mathbb{R}^k \mapsto \mathbb{R}$,

$$\mathcal{M}(\boldsymbol{x}) : \boldsymbol{y}_i(\boldsymbol{z}) = M_i\left(\boldsymbol{x}(\boldsymbol{z})\right), \quad i = 1, \ldots, n, \tag{3.1}$$

where n depends on the model problem (e.g. number of elements regarding a spatial discretisation or the number of eigenpairs to be computed). For instance, a finite element (FE) model is usually considered in terms of solid mechanics in order to numerically solve the partial differential equation which describes the equilibrium of internal and external forces. Then, n is the number of degrees of freedom. If the solution scheme is non-intrusive, it can be used as a black-box within the framework of uncertainty quantification (UQ) and uncertainty propagation (UP). If the model response $\boldsymbol{Y}$ is related monotonically to the input vector $\boldsymbol{X}$ that has been propagated through the model $\mathcal{M}$, the model is referred to as *monotonic model.*

Independent of the input parameter being an uncertain variable or vector, the model response can be a variable Y or a vector $\boldsymbol{Y}$. This depends only on the QoI, e.g. it is a vector if the displacement field of the whole domain is required but a variable if only the maximum displacement (in one direction) is of interest.

To propagate an imprecise random field through a model, it needs to be discretised. For that purpose, the discretisation of (aleatory) random fields by Karhunen-Loève (KL) expansion is described in Subsection 3.1, while interval analysis is introduced in Subsection 3.2 to propagate (epistemic) interval variables. In Subsection 3.3, both methods are combined to a nested probability box (p-box) algorithm, to consider (mixed uncertain) imprecise random fields.

Model assumptions: The approaches introduced in this chapter are chosen according to the following model assumptions.

- The random field hyper parameters *mean value and standard deviation* can be determined sufficiently *exact*, e.g. by experiments.

- The *correlation length* is modelled as an *interval* as it is difficult or even impossible to be measured.

- The type of the correlation function (i.e. the smoothness of the random field) does not affect the model outcome as much as the correlation length (i.e. the variability of the random field). For this purpose, the *correlation function is chosen according to optimal conditions*, i.e. as a function for which an analytic solution is available while providing a good convergence.

- Only *Gaussian random fields* are considered which are assumed to be *homogeneous* and *isotropic*.

- Only a spatially *constant standard deviation* is applied, i.e. a Gaussian distributed random field can be obtained by scaling and shifting a standard normal distributed random field.

- Only *static problems* are investigated, there is *no cyclic loading*

- Only *monotonic models* are used, i.e. vertex propagation is assumed to be sufficient.

If appropriate for the sake of completeness or a better understanding, some further remarks beyond the topic are discussed, e.g. in terms of imprecise random fields arising from interval valued hyper parameters, but not investigated.

3.1. Karhunen-Loève expansion to discretise random fields

In order to propagate random fields through a model as described above, they need to be discretised. A widely used method to discretise continuous Gaussian random fields as defined in Subsection 2.1.2 is given by the KL expansion. A comprehensive introduction, derivation and discussion of the method is provided by Ghanem and Spanos [1991] or Sudret and Der Kiureghian [2000] and the fundamentals are only summarised here.

The basic idea of the KL expansion is to spectrally decompose the correlation structure $\Gamma_X(\boldsymbol{z}, \boldsymbol{z}') : \mathcal{D} \times \mathcal{D} \mapsto [0, 1]$ of the random field

$$\Gamma_X(\boldsymbol{z}, \boldsymbol{z}') = \sum_{i=1}^{\infty} \lambda_i \phi_i(\boldsymbol{z}) \phi_i(\boldsymbol{z}'), \tag{3.2}$$

where λ_i are the eigenvalues, sorted such that $\lambda_1 > \lambda_2 > \cdots > \lambda_\infty$, and $\phi_i(\boldsymbol{z})$ are the corresponding eigenfunctions. The eigenpairs are obtained by the Fredholm integral equation of the second kind,

$$\int_{\mathcal{D}} \Gamma_X(\boldsymbol{z}, \boldsymbol{z}') \phi_i(\boldsymbol{z}') \, \mathrm{d}\boldsymbol{z}' = \lambda_i \phi_i(\boldsymbol{z}). \tag{3.3}$$

In this context, $\Gamma_X(\boldsymbol{z}, \boldsymbol{z}')$ is also referred to as kernel function. In general, Eq. (3.3) needs to be solved numerically. For some special cases, analytical solutions are available, which are described in Subsection 3.1.3.

As $\Gamma_X(\boldsymbol{z}, \boldsymbol{z}')$ is bounded, symmetric and positive definite, λ_i are real and non-negative and $\phi_i(\boldsymbol{z})$ form a complete orthogonal basis on an $\mathcal{L}_2$ Hilbert space satisfying

$$\langle \phi_k(\boldsymbol{z}), \phi_l(\boldsymbol{z}) \rangle = \int_{\mathcal{D}} \phi_k(\boldsymbol{z}) \phi_l(\boldsymbol{z}) \, \mathrm{d}\boldsymbol{z} = \delta_{kl}, \tag{3.4}$$

where $\langle \cdot, \cdot \rangle : \mathcal{D} \times \mathcal{D} \mapsto \mathbb{R}$ is an inner product space and δ_{kl} is the Kronecker delta defined to be equal to 1 for $k = l$ and 0 for $k \neq l$.

A standard normal distributed random field $S(\omega, \boldsymbol{z}) \sim \mathcal{N}(0, 1)$ can then be described by the KL series expansion

$$S(\omega, \boldsymbol{z}) = \sum_{i=1}^{\infty} \sqrt{\lambda_i} \phi_i(\boldsymbol{z}) \xi_i(\omega). \tag{3.5}$$

Herein, it is $\sum_{i=1}^{\infty} \sqrt{\lambda_i} \phi_i(\boldsymbol{z}) = 1$ and $\xi_i(\omega) \sim \mathcal{N}(0, 1)$ is a standard normal distributed random variable following

$$\xi_i(\omega) = \frac{1}{\sqrt{\lambda_i}} \int_{\mathcal{D}} [X(\omega, \boldsymbol{z}) - \mu_X(\boldsymbol{z})] \, \phi_i(\boldsymbol{z}) \, \mathrm{d}\boldsymbol{z}, \quad i = 1, ..., \infty. \tag{3.6}$$

By this, the spatial dependency on $\boldsymbol{z}$ and the random dependency on ω of the random field are decoupled. Assuming a constant standard deviation within the domain, $\sigma_X(\boldsymbol{z}) = \sigma_X$, an arbitrary Gaussian random field $X(\omega, \boldsymbol{z}) \sim \mathcal{N}(\mu_X, \sigma_X)$ can be described by scaling Eq. (3.5) with σ_X and shifting the scaled field towards its mean value $\mu_X(\boldsymbol{z})$,

$$X(\omega, \boldsymbol{z}) = \mu_X(\boldsymbol{z}) + \sigma_X \sum_{i=1}^{\infty} \sqrt{\lambda_i} \phi_i(\boldsymbol{z}) \xi_i(\omega). \tag{3.7}$$

Note that in literature the KL expansion of a random field $X(\omega, \boldsymbol{z})$ is often introduced in terms of its covariance function

$$C_X(\boldsymbol{z}, \boldsymbol{z}') = \sigma_X(\boldsymbol{z}) \, \sigma_X(\boldsymbol{z}') \, \Gamma_X(\boldsymbol{z}, \boldsymbol{z}') \tag{3.8}$$

instead of its correlation function $\Gamma_X(\boldsymbol{z}, \boldsymbol{z}')$. Then, solving the Fredholm integral equation given in Eq. (3.3) with $C_X(\boldsymbol{z}, \boldsymbol{z}')$ used as the kernel function, the resulting eigenpairs $\{\lambda_i, \phi_i\}$ depend on the standard deviation $\sigma_X(\boldsymbol{z})$ and the sum in Eq. (3.7) is not multiplied by σ_X as this information is already included in λ_i and ϕ_i. The only advantage of using the covariance as kernel function is that the standard deviation can be assumed to be depending on space as well. On the contrary however, when a constant standard deviation $\sigma_X(\boldsymbol{z}) = \sigma_X$ is assumed, describing the KL expansion in terms of the correlation function has many benefits. At first, the formulation in terms of the correlation function is given by unitless eigenvalues and -functions[1] and a more straightforward understanding of the random field in Eq. (3.7) in terms of a scaled and shifted standard normal distributed random field is enabled. Furthermore, the KL expansion for a given kernel function and correlation length can be solved once as a standard normal

---

[1] This way, the unit of the random field is clearly connected to μ_X and σ_X.

distributed random field $S(\omega, \boldsymbol{z})$ and then be used for any arbitrary random field $X(\omega, \boldsymbol{z})$ as described above. This can reduce the computational cost when several random field parameters with the same correlation structure are considered. It will be discussed in Section 3.3 that this can become especially beneficial when imprecise random fields are investigated. In this contribution, only constant standard deviations are considered and the KL expansion is always expressed in terms of the correlation function.

To propagate a random field through a model, the sum of Eq. (3.7) needs to be truncated. For the resulting truncation error, different measures are introduced in the following subsection. Afterwards, different correlation structures are discussed in Subsection 3.1.2, before the solution of the Fredhold integral Eq. (3.3) is provided in Subsection 3.1.3.

3.1.1.   Truncation error of the Karhunen-Loève expansion

To propagate a random field $X(\omega, \boldsymbol{z})$ through a model, $\mathcal{M}(X(\omega, \boldsymbol{z}))$, the series needs to be truncated such that it retains only the T largest eigenvalues. This leads to an approximated random field,

$$\bar{X}(\omega, \boldsymbol{z}) = \mu_X(\boldsymbol{z}) + \sigma_X \sum_{i=1}^{T} \sqrt{\lambda_i} \phi_i(\boldsymbol{z}) \xi_i(\omega) \tag{3.9}$$

A realisation $\bar{x}_j(\boldsymbol{z}) = \bar{X}(\omega_j, \boldsymbol{z})$ can then be created by inserting one set $\boldsymbol{\xi}_j(\omega_i) = (\xi_1, \ldots, \xi_T)_j$ of standard normal distributed random variables, e.g. obtained by pseudo-randomly sampling.

Following Betz et al. [2014], the normalised local error variance $\epsilon_{\sigma^2}(\boldsymbol{z})$ remaining by truncating the random field is given by

$$\epsilon_{\sigma^2}(\boldsymbol{z}) = \frac{\text{Var}\left\{ X(\omega, \boldsymbol{z}) - \bar{X}(\omega, \boldsymbol{z}) \right\}}{\text{Var}\left\{ X(\omega, \boldsymbol{z}) \right\}} \tag{3.10}$$

and can be expressed globally by a scalar value in terms of the mean error variance

$$\bar{\epsilon}_{\sigma^2} = \frac{1}{|\mathcal{D}|} \int_{\mathcal{D}} \epsilon_{\sigma^2}(\boldsymbol{z}) \, \mathrm{d}\boldsymbol{z}. \tag{3.11}$$

With a constant variance $\sigma^2{}_X = \sigma^2{}_X(\boldsymbol{z})$, inserting $\text{Var}\left\{ X(\omega, \boldsymbol{z}) \right\} = \sigma^2{}_X$ into Eq. (3.10) and expressing $\text{Var}\left\{ \bar{X}(\omega, \boldsymbol{z}) \right\} = \bar{C}_X(\boldsymbol{z}, \boldsymbol{z}')$ in terms of the correlation function $\bar{\Gamma}_X(\boldsymbol{z}, \boldsymbol{z}')$ approximated by truncating Eq. (3.2),

$$\bar{C}_X(\boldsymbol{z}, \boldsymbol{z}') = \sigma^2{}_X \bar{\Gamma}_X(\boldsymbol{z}, \boldsymbol{z}') = \sigma^2{}_X \sum_{i=1}^{T} \sqrt{\lambda_i} \phi_i(\boldsymbol{z}) \xi_i(\omega), \tag{3.12}$$

Eq. (3.10) can be simplified to express the local truncation error in terms of the truncated correlation function,

$$\epsilon_{\bar{\Gamma}}(\boldsymbol{z}) = 1 - \sum_{i=1}^{T} \lambda_i \phi_i^2(\boldsymbol{z}). \tag{3.13}$$

Furthermore, with the orthogonality condition given in Eq. (3.4) the mean error variance in Eq. (3.11) can be transferred to the mean truncation error of the truncated correlation function

$$\bar{\epsilon}_{\bar{\Gamma}} = 1 - \frac{1}{|\mathcal{D}|} \sum_{i=1}^{T} \lambda_i. \tag{3.14}$$

Again, the error measures are mostly introduced in terms of the covariance function $\bar{C}_X(\boldsymbol{z}, \boldsymbol{z}')$ in literature [Betz et al., 2014], leading to the sums in Eq. (3.13) and Eq. (3.14) being scaled by $1/\sigma^2{}_X$ and consequently

$$\epsilon_{\bar{C}}(\boldsymbol{z}) = 1 - \frac{1}{\sigma^2{}_X} \sum_{i=1}^{T} \lambda_i \phi_i^2(\boldsymbol{z}), \tag{3.15}$$

$$\bar{\epsilon}_{\bar{C}} = 1 - \frac{1}{|\mathcal{D}|} \frac{1}{\sigma^2{}_X} \sum_{i=1}^{T} \lambda_i. \tag{3.16}$$

The truncation of the KL expansion is a crucial point when regarding imprecise random fields including imprecise correlation structures, as the truncation error does not only depend on T but also on the chosen correlation function as well as the correlation length. For this reason, the influence of the correlation function and its describing parameters is investigated intensively in Subsection 3.3.2.

3.1.2. Correlation structures

The correlation kernel $\Gamma_X(\boldsymbol{z}, \boldsymbol{z}')$ used in Eq. (3.3) is a function describing the correlation of two values $X(\omega, \boldsymbol{z})$ and $X(\omega, \boldsymbol{z}')$ at two arbitrary locations $\boldsymbol{z}$ and $\boldsymbol{z}'$ within the random field in terms of their distance $|\boldsymbol{z} - \boldsymbol{z}'|$. The larger the distance is, the less correlated the random variables located at these points within the field are. The decay can be described by the correlation length L_X, a measure driving the extend of the correlation and consequently the variability of the random field.

The simplest way to describe the correlation decay is given by the binary noise (BN) kernel [Ching and Phoon, 2019] as given in Table 3.1 (a). Here, the decay of the correlation $\Gamma_X(\boldsymbol{z}, \boldsymbol{z}')$ is described linearly in terms the distance $|\boldsymbol{z} - \boldsymbol{z}'|$, the slope depending on the correlation length L_X^{BN}. The drawback of this correlation model is its non-differentiability, not only at zero lag $|\boldsymbol{z} - \boldsymbol{z}'| = 0$ but also at the distance $|\boldsymbol{z} - \boldsymbol{z}'| \geq L_X^{\mathrm{BN}}$ where the correlation becomes zero.

A more general way to describe the correlation function is given by the Whittle-Matérn (WM) kernel family [Ching and Phoon, 2019]
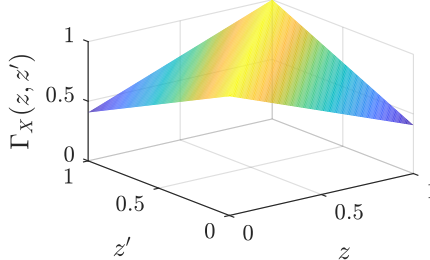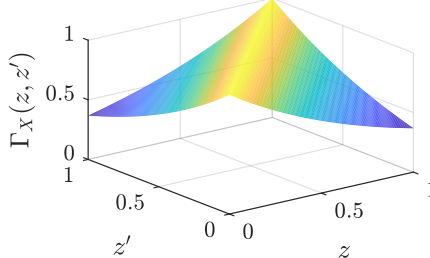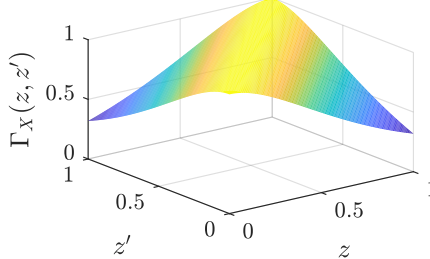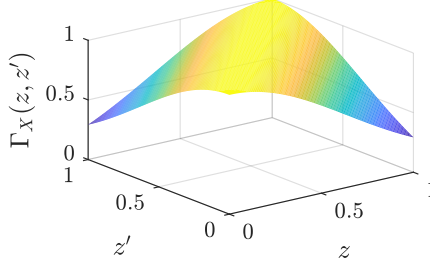
$$\Gamma_{X,\mathrm{WM}}^{\nu}(\boldsymbol{z}, \boldsymbol{z}') = \frac{2^{1-\nu}}{\gamma(\nu)} \left(\sqrt{2\nu} \, \frac{|\boldsymbol{z} - \boldsymbol{z}'|}{L_X} \right)^{\nu} K_{\nu} \left(\sqrt{2\nu} \, \frac{|\boldsymbol{z} - \boldsymbol{z}'|}{L_X} \right), \tag{3.17}$$

providing also a parameter ν to drive the smoothness of the random field variability. Here, $\gamma(\nu)$ is the Gamma function and K_{ν} the modified Bessel function of the second kind [Abramowitz

and Stegun, 1964]. For $\nu = p + 0.5$, $p \in \mathbb{N}^+$, Eq. (3.17) can be described in terms of an exponential function [Faes et al., 2022] as follows

$$\Gamma_{X,\text{WM}}^{p+0.5}(\boldsymbol{z}, \boldsymbol{z}') = \exp\left\{-\frac{\sqrt{2p+1}\,|\boldsymbol{z}-\boldsymbol{z}'|}{L_X}\right\}\frac{p!}{(2p)!}\sum_{i=1}^{p}\frac{(p+i)!}{i!(p-i)!}\left(\frac{2\sqrt{2p+1}\,|\boldsymbol{z}-\boldsymbol{z}'|}{L_X}\right)^{p-i}.$$

$$(3.18)$$

Table 3.1: Overviews of different correlation kernels with an effective correlation length $L_X = 1.0$, (b)-(d) belonging to the WM kernel family with p as given.

kernel	correlation surface	correlation function
(a) binary noise (BN)		$\Gamma_X(\boldsymbol{z},\boldsymbol{z}') = \max\left\{0\ ;\ 1 - \frac{|\boldsymbol{z}-\boldsymbol{z}'|}{L_X^{\text{BN}}}\right\}$ $L_X^{\text{BN}} = 1.6835$
(b) single exponential (SE)		$\Gamma_X(\boldsymbol{z},\boldsymbol{z}') = \exp\left\{-\frac{|\boldsymbol{z}-\boldsymbol{z}'|}{L_X^{\text{SE}}}\right\}$ $L_X^{\text{SE}} = 1.0$ $\left(\text{WM}: p = 0\ \rightarrow\ \Gamma_X = \Gamma_{X,\text{WM}}^{0.5}\right)$
(c) modified exponential (ME)		$\Gamma_X(\boldsymbol{z},\boldsymbol{z}') = \left(1 + \frac{|\boldsymbol{z}-\boldsymbol{z}'|}{L_X^{\text{ME}}}\right)\exp\left\{-\frac{|\boldsymbol{z}-\boldsymbol{z}'|}{L_X^{\text{ME}}}\right\}$ $L_X^{\text{ME}} = 0.4249$ $\left(\text{WM}: p = 1\ \rightarrow\ \Gamma_X = \Gamma_{X,\text{WM}}^{1.5}\right)$
(d) squared exponential (QE)		$\Gamma_X(\boldsymbol{z},\boldsymbol{z}') = \exp\left\{-\left(\frac{\boldsymbol{z}-\boldsymbol{z}'}{L_X^{\text{QE}}}\right)^2\right\}$ $L_X^{\text{QE}} = 0.9018$ $\left(\text{WM}: p = \infty\ \rightarrow\ \Gamma_X = \Gamma_{X,\text{WM}}^{\infty}\right)$

Three often used correlation kernels are the single exponential (SE) kernel ($p = 0$), the modified exponential (ME) kernel ($p = 1$) and the squared exponential (QE) kernel ($p = \infty$), see Table 3.1 (b) to (d), all of them belonging to the WM kernel familiy. Note that the correlation lengths of the different kernel types are not comparable with respect to how quickly the correlation decays. To compare the properties of different kernel functions, the corresponding

correlation length L_X^{kernel} should therefore be determined equivalently with respect to one reference kernel by means of minimising the mean squared error between the correlation function and the reference function [Spanos et al., 2007]. As the SE kernel is one of the most often used kernel functions, it is chosen as the refrence kernel within this contribution. The correlation length L_X^{SE} is then called the *effective correlation length*. In Table 3.1 the correlation surface of the different kernel types is each exemplified for a correlation length L_X, the corresponding equivalent correlation lengths L_X^{kernel} are given next to the correlation function[2].

As the kernels given in Table 3.1 (b) to (d) are described in terms of an exponential function, the correlation converges towards zero with increasing distance $|\boldsymbol{z} - \boldsymbol{z}'|$ and therefore do not involve non-differentiabilities at this point. However, like the BN kernel, the SE kernel is not differentiable at zero lag $|\boldsymbol{z} - \boldsymbol{z}'| = 0$. It can be seen in Figure 3.1 that this increases the number of required truncation terms T drastically. Here, the mean error $\bar{\epsilon}_{\bar{\Gamma}}$ corresponding to the truncation order T is compared for the SE (blue) and the ME (red) correlation function for three different correlation length ratios, $L_X/l = 0.1$ (solid line), $L_X/l = 1.0$ (dashed line) and $L_X/l = 10.0$ (dash-dotted line), regarding a one-dimensional (1D) random field. It can be seen that the mean error of the ME kernel decreases much faster than for the SE kernel. Furthermore, the larger the correlation length L_X is with respect to the domain length l, the smaller the mean truncation error. Note that also for the SE kernel, $\bar{\epsilon}_{\bar{\Gamma}}$ drops towards zero, as it can be noted for the ME kernel for $T > 170$. However, due to the slow convergence, much higher values of T are required, e.g. around $T = 1000$ terms for $L_X/l = 10.0$, and even higher ones for smaller correlation length ratios.
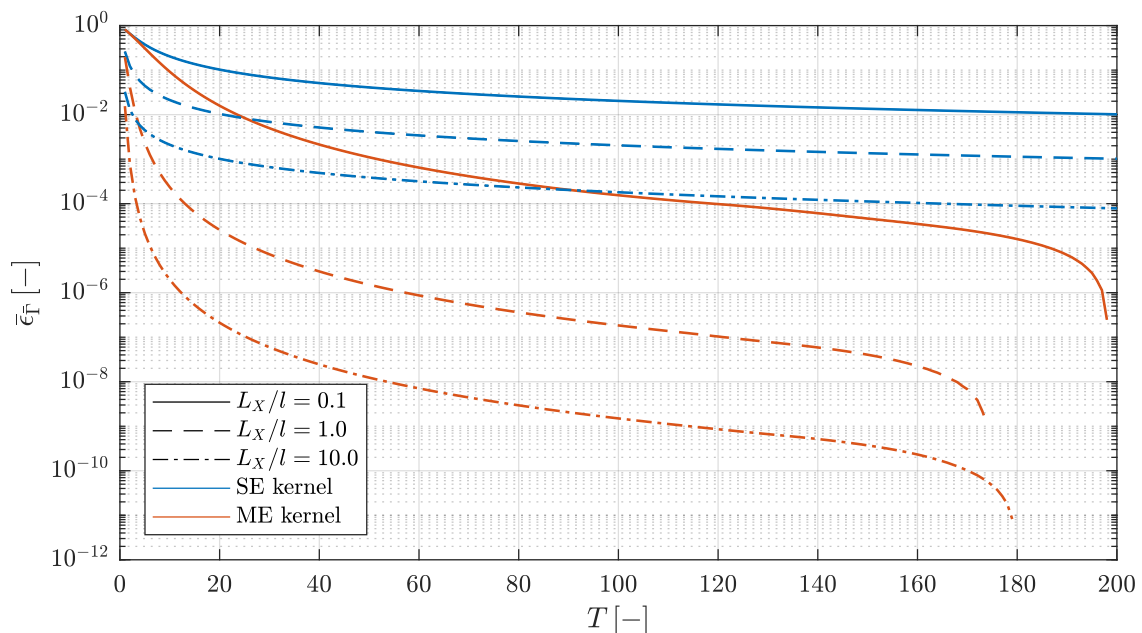
Figure 3.1: Mean truncation error $\bar{\epsilon}_{\bar{\Gamma}}$ corresponding to the truncation order T, regarding the analytic solution of the SE (blue) and the ME (red) correlation function $\Gamma_X(z, z')$ considering a one-dimensional random field for different correlation length ratios L_X/l.

---

[2]Note that $\Gamma_X(\boldsymbol{z}, \boldsymbol{z}')$ needs to be multiplied with $\sigma^2{}_X(\boldsymbol{z})$ if Eq. (3.3) is solved using the covariance function $C_X(\boldsymbol{z}, \boldsymbol{z}')$, which is often not differentiated consistently in literature.

The reason why the SE kernel is often applied nevertheless is the fact that an analytic solution is available for special cases, which is straightforward to implement [Sudret and Der Kiureghian, 2000]. The advantage of an analytic solution is not only that Eq. (3.3) is solved exactly and computationally more efficient than applying a numeric solution. Huang et al. [2001] further showed that the analytic solution also converges faster in terms of T than the numeric solution when comparing both solutions schemes for the single exponential kernel function. However, comparing the convergence rate of different kernel functions, due to their differentiability at zero lag the ME and QE kernels still converge much faster in terms of T than the SE kernel [Huang et al., 2001]. As the stochastic dimension N increases with T, this can become crucial in terms of the curse of dimensionality. Spanos et al. [2007] provide also an analytic solution for the ME kernel for 1D domains.

In the following, the SE correlation function,

$$\Gamma_X(z, z') = \exp\left\{ -\frac{|z - z'|}{L_X} \right\}, \tag{3.19}$$

and the ME correlation function,

$$\Gamma_X(z, z') = \left(1 + \frac{|z - z'|}{L_X^{\mathrm{ME}}} \right) \exp\left\{ -\frac{|z - z'|}{L_X^{\mathrm{ME}}} \right\}, \tag{3.20}$$

are compared in terms of a 1D random field. Both kernel functions are depicted in Figure 3.2 for the three different effective correlation length ratios, $L_X/l = 0.1$, $L_X/l = 1.0$ and $L_X/l = 10.0$. The correlation length L_X^{ME} is chosen such that the resulting correlation structure fits the one of the SE kernel. For the used effective correlation length ratios, the corresponding ME correlation length ratios $L_X^{\mathrm{ME}}/l = 0.0471$, $L_X^{\mathrm{ME}}/l = 0.4249$ and $L_X^{\mathrm{ME}}/l = 2.1114$ are obtained. Below each correlation function, three realisations of a standard normal distributed random field $\bar{s}_j = \bar{S}(\omega_j, z), j = 1, 2, 3$, according to the corresponding correlation length are depicted. For the sake of comparability, the same psuedo-randomly sampled sets $\boldsymbol{\xi}_1$, $\boldsymbol{\xi}_2$ and $\boldsymbol{\xi}_3$ have been used to create the three realisations. It can be seen that the random fields gained by the same set of $\boldsymbol{\xi}_j$ inherit the same global characteristic for the different correlation lengths, however, the local variation becomes higher for small correlation lengths.

For both kernel functions it can be noted that the variability of the random field depends on the correlation length L_X. For small values $L_X < l$, the random field is weakly correlated, i.e. the variability increases. On the other hand, the variability is reduced for highly correlated random fields, i.e. $L_X > l$. However, comparing the two different kernel functions with each other, it can be seen that the random fields resulting from the ME correlation function are much smoother than the ones resulting from the SE kernel. Note that the variability of an SE realisation increases with higher truncation terms without converging towards a certain state, as can be seen in Figure 3.3a. Decreasing the truncation error of the SE correlation function therefore leads to more and more fluctuating random field realisations. As can be seen in Figure 3.3b, this is not the case for the ME random field realisation, which converges towards a certain distribution with increasing T. This phenomenon is carefully studied and discussed by Faes et al. [2022], additionally also comparing both kernels to the QE correlation function, which does not provide an analytic solution.

In the following subsection, the numeric solution in general and the analytic solution for these two kernel functions are provided. However, for the reasons discussed above, i.e. the convergence of the mean truncation error as well as the convergence behaviour of an individual random field realisation with increasing T, only the ME correlation function is applied in Chapter 5 and Chapter 6.
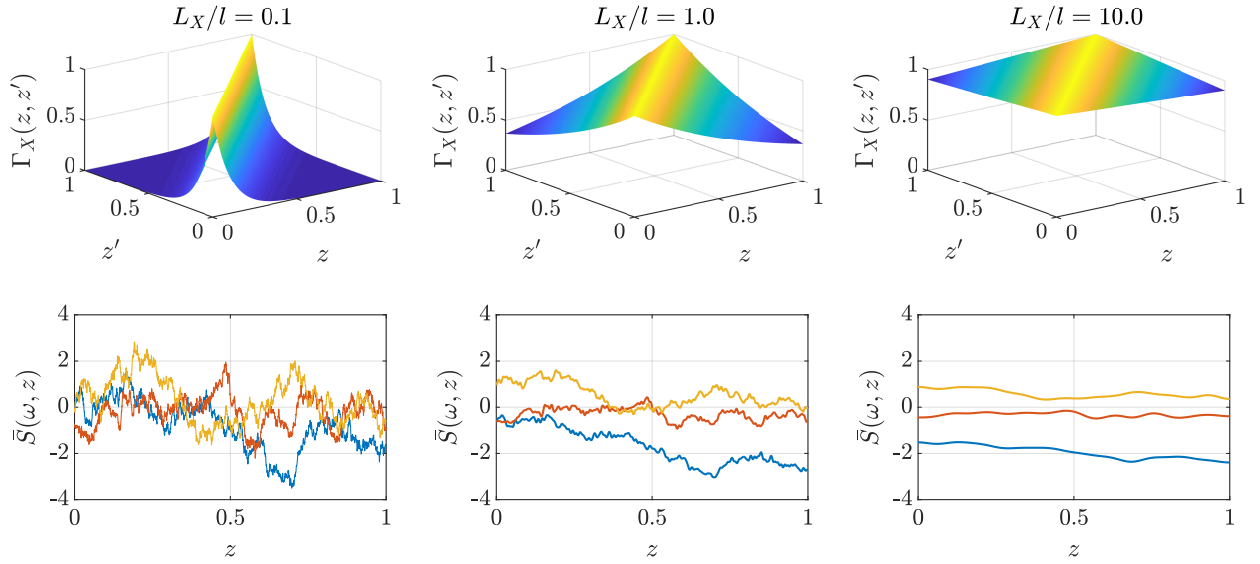
(a) single exponential correlation function
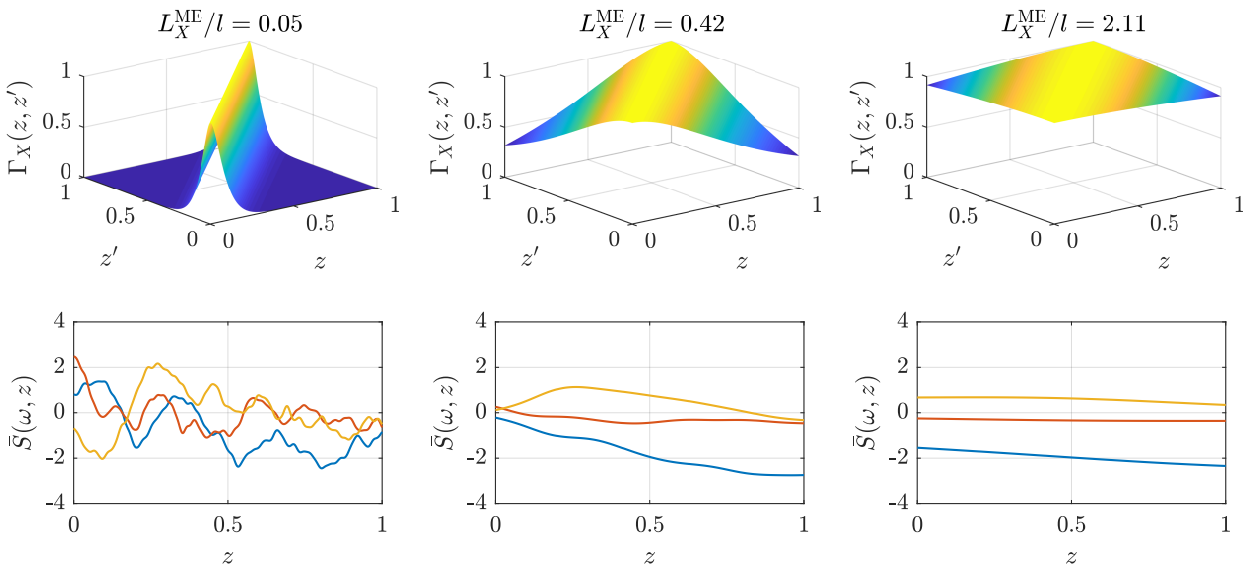
(b) modified exponential correlation function

Figure 3.2: Comparison of the correlation function in its closed form (each in top row) as well as three resulting standard normal distributed random field realisations (each in bottom row) for different correlation functions regarding three effective correlation length ratios, $L_X/l = 0.1$ (left), $L_X/l = 1.0$ (middle) and $L_X/l = 10.0$ (right), with respect to the domain length l of a one-dimensional random field.
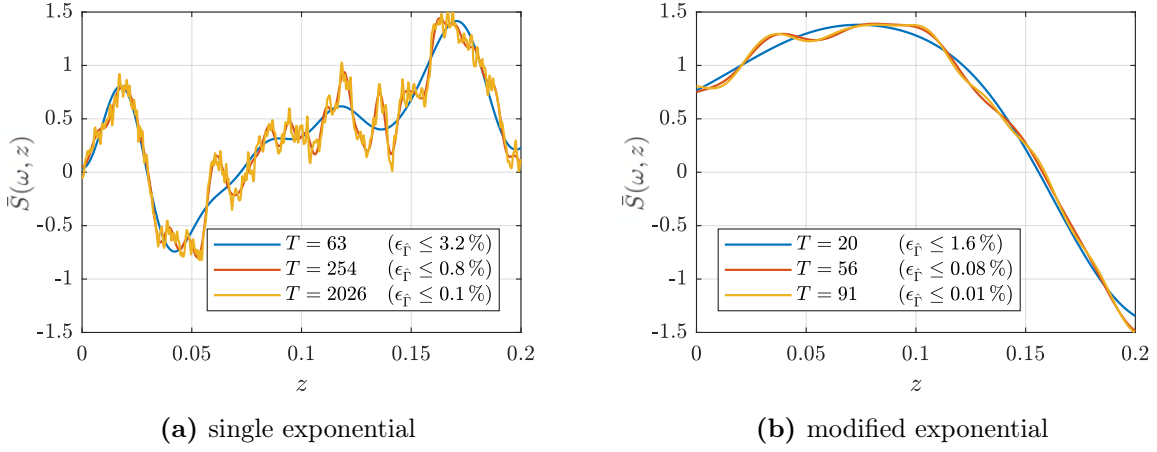
Figure 3.3: Extract $x \in [0, 0.2]$ of a standard normal distributed random field realisation $\bar{S}(\omega_j, x), x \in [0, 1]$, resulting from a fix effective correlation length ratio $L_X/l = 0.1$ obtained by different truncation orders.

3.1.3. Solution of the Fredhold integral equation

To obtain the eigenpairs (λ_i, ϕ_i) to be inserted into Eq. (3.9), the Fredholm integral equation given in Eq. (3.3) needs to be solved for the chosen kernel function $\Gamma(\boldsymbol{z}, \boldsymbol{z}')$. For 1D random fields described by an SE or ME correlation function an analytic solution of Eq. (3.3) is available. Considering other kernel functions, e.g. the QE correlation function, Eq. (3.3) needs to be solved numerically, which can become very costly. Furthermore, in any case of a multi-dimensional domain which is not rectangular but arbitrary, also for SE and ME correlation functions a numerical solution scheme is required.

Within this work, only problems enabling an analytic solution are considered. For this reason, only a short literature review on numeric solution schemes is provided in the following before summarising the analytic solution for both, SE and ME correlation functions.

Numeric solution schemes

In most cases, the Fredholm integral equation of second kind, given in Eq. (3.3), needs to be solved numerically. Atkinson and Han [2009] provide a broad overview on solution schemes for that purpose, which are for instance projection methods such as collocation or Galerkin method, or Nyström method. In the context of KL expansion, Galerkin methods are widely used and extended. The basic idea of Galerkin method [Ghanem and Spanos, 1991] is to discretise the d-dimensional domain $\mathcal{D} \subset \mathbb{R}^d$ by n_{el} elements and approximate the eigenfunctions $\phi_i(\boldsymbol{z}), i = 1, ..., n_{\mathrm{el}}$ by

$$\phi_i(\boldsymbol{z}) \approx \hat{\phi}_i(\boldsymbol{z}) = \sum_{k=1}^{n_{\mathrm{el}}} d_k^i h_k(\boldsymbol{z}), \tag{3.21}$$

where the basis functions $h_k(\boldsymbol{z})$ are spanned within $\mathcal{L}^2(\mathcal{D})$. The coefficients $d_k^i \in \mathbb{R}$ are determined solving the eigenvalue problem given by

$$\mathbf{CD} = \boldsymbol{\Lambda}\mathbf{BD}, \tag{3.22}$$

for $\mathbf{D} = \mathrm{D}_{ik} = d_k^i$ and $\mathbf{\Lambda} = \Lambda_{ik} = \lambda_i \delta_{ik}$ being a diagonal matrix containing the corresponding eigenvalues $\lambda_i, i = 1, ..., n_{\mathrm{el}}$. Furthermore, the symmetric positive definite matrix $\mathbf{B} = \mathrm{B}_{ik}$ and the symmetric positive semi-definite matrix $\mathbf{C} = \mathrm{C}_{ik}$ are obtained by

$$\mathrm{B}_{ik} = \int_{\mathcal{D}} h_i(\boldsymbol{z}) h_k(\boldsymbol{z}) \, \mathrm{d}\boldsymbol{z}, \tag{3.23}$$

$$\mathrm{C}_{ik} = \int_{\mathcal{D}} \int_{\mathcal{D}} C(\boldsymbol{z}, \boldsymbol{z}') h_i(\boldsymbol{z}), h_k(\boldsymbol{z}') \, \mathrm{d}\boldsymbol{z} \, \mathrm{d}\boldsymbol{z}', \tag{3.24}$$

with $C(\boldsymbol{z}, \boldsymbol{z}')$ the covariance function. Note that by this, maximally n_{el} eigenpairs are obtained and therefore $n_{\mathrm{el}} \geq T$ are needed to truncate the KL expansion in Eq. (3.9) after T terms. Furthermore, due to dense matrices, the traditional Galerkin method can become computational expensive, especially for two-dimensional (2D) or three-dimensional (3D) domains.

Several basis functions have been applied and investigated in literature, e.g. global Legendre polynomials [Papaioannou, 2012], Chebyshev polynomials [Liu and Zhang, 2017] or Haar wavelets [Phoon et al., 2002]. A Fourier KL discretisation is proposed by Li et al. [2008]. The disadvantage of such global interpolation schemes is that the accuracy can only be improved by an increased order of the basis functions, which can result in numerical instabilities.

Alternatively, the basis functions can be defined locally at each element of the discretised domain. For example, if the model propagation is performed by finite element method (FEM), the domain discretisation as well as the local piecewise linear Lagrange polynomials which are used as basis functions defined on the element domain can be recycled and used to solve Eq. (3.22) [Ghanem and Spanos, 1991]. Betz et al. [2014] propose an approach based on hierarchic basis functions defined by Gegenbauer polynomials, while Basmaji et al. [2022a] developed a discontinuous Legendre polynomial based Galerkin approach defining the Legendre polynomials locally but without considering continuity between the elements.

With regard to meshless approaches, Betz et al. [2014] propose to use the finite cell method as a quasi meshless approach. Furthermore, isogeometric Galerkin approaches using B-splines and NURBS have been investigated by Rahman [2018] as well as Mika et al. [2021].

Analytic solution for special cases

Considering a 1D random field described by an SE or ME correlation function the solution of Eq. (3.3) can be determined analytically. Furthermore, in case of 2D rectangular random fields the 2D solution can be obtained from the 1D solution corresponding to each dimension [Sudret and Der Kiureghian, 2000], i.e.

$$\lambda_i^{\mathrm{2D}} = \lambda_{i_1, z_1}^{\mathrm{1D}} \otimes \lambda_{i_2, z_2}^{\mathrm{1D}}, \tag{3.25}$$

$$\phi_i^{\mathrm{2D}}(\boldsymbol{z}) = \phi_{i_1}^{\mathrm{1D}}(z_1) \otimes \phi_{i_2}^{\mathrm{1D}}(z_2). \tag{3.26}$$

Note that the eigenvalues and corresponding eigenfunctions need to be sorted in descending order after applying the tensor product. Analogously, the same holds for 3D random fields in case of rectangular cubic domains. However, note that due to the multiplication of the values

$\lambda_i^{1D} \xrightarrow{i \to \infty} 0$, the convergence rate of the truncation error with respect to the truncation order T decreases when increasing the dimension. This can be directly seen when inserting λ_i^{2D} or λ_i^{3D} to Eq. (3.13) or Eq. (3.14) in order to determine the truncation error.

In the following, the analytic solution schemes for both, SE and ME correlation functions, are summarised considering a 1D random field given on the domain $\mathcal{D} = [-a, a]$. For the derivation, the reader is referred to the provided literature.

Single exponential (SE) correlation function: The Fredholm integral equation given in Eq. (3.3) can be solved analytically as described by Sudret and Der Kiureghian [2000]. The i-th eigenvalue is given by

$$\lambda_i = \frac{2L_X}{1 + w_i^2 L_X^2}, \tag{3.27}$$

with w_i being the solution of the transcendental equation

$$\begin{cases} \frac{1}{L_X} - w_i \tan(w_i a) = 0 & \text{in the range } \left[(i-1)\frac{\pi}{a}, \ (i - \frac{1}{2})\frac{\pi}{a}\right]; & \text{if } i \text{ is odd,} \\ \frac{1}{L_X} \tan(w_i a) + w_i = 0 & \text{in the range } \left[(i - \frac{1}{2})\frac{\pi}{a}, \ i\frac{\pi}{a}\right]; & \text{if } i \text{ is even.} \end{cases} \tag{3.28}$$

The corresponding eigenfunctions are then determined by

$$\phi_i(z) = \begin{cases} \left(a + \frac{\sin(2w_i a)}{2w_i}\right)^{-1/2} \cos(w_i z); & \text{if } i \text{ is odd,} \\ \left(a - \frac{\sin(2w_i a)}{2w_i}\right)^{-1/2} \sin(w_i z); & \text{if } i \text{ is even.} \end{cases} \tag{3.29}$$

The first twenty eigenvalues $\lambda_1, \ldots, \lambda_{20}$ of the SE kernel function are depicted in blue lines in Figure 3.4 for different correlation length ratios $L_X/l = 0.1$ (solid line), $L_X/l = 1.0$ (dahsed line) and $L_X/l = 10.0$ (dash-dotted line). It can be seen that λ_i converges towards zero faster the larger the correlation length L_X is with respect to the domain length l.
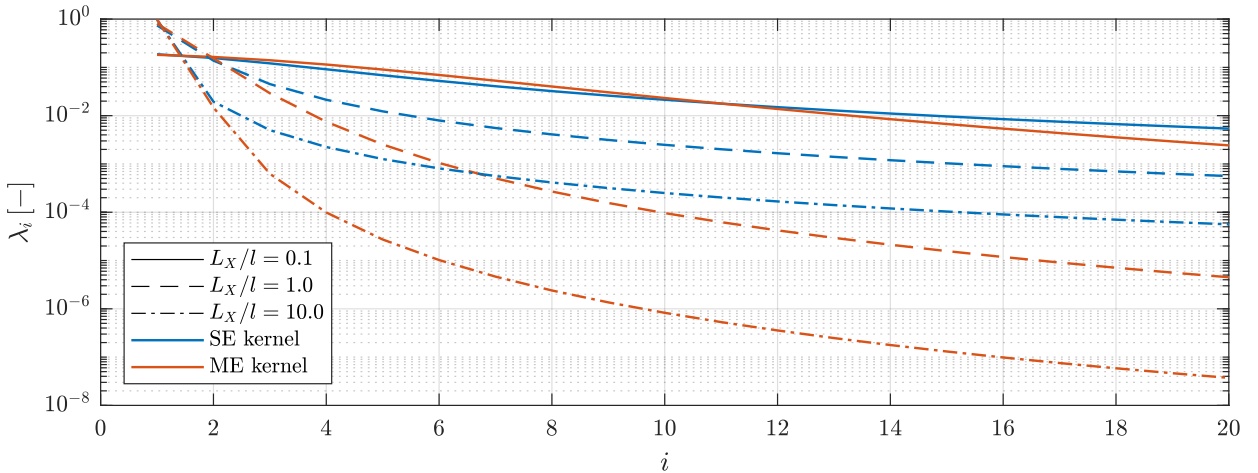
Figure 3.4: First twenty eigenvalues $\lambda_1, \ldots, \lambda_{20}$ obtained by the analytic solution of the SE (blue) and the ME (red) correlation function $\Gamma_X(z, z')$ considering a one-dimensional random field for different effective correlation length ratios L_X/l.

Modified exponential (ME) correlation function: The analytic solution of the modified exponential correlation function is derived in Spanos et al. [2007]. With the values w_1 and w_2,

$$w_1 = \sqrt{L_X^2 + \sqrt{4L_X^3\lambda_i^{-1}}}, \tag{3.30}$$

and

$$w_2 = \sqrt{L_X^2 - \sqrt{4L_X^3\lambda_i^{-1}}} \qquad \text{if} \qquad L_X^2 \geq \sqrt{4L_X^3\lambda_i^{-1}}, \tag{3.31}$$

$$w_2 = \sqrt{-L_X^2 + \sqrt{4L_X^3\lambda_i^{-1}}} \qquad \text{if} \qquad L_X^2 < \sqrt{4L_X^3\lambda_i^{-1}}, \tag{3.32}$$

the following coefficients can be determined:

$$A = (w_1^2 + 2L_Xw_1 + L_X^2)\exp(w_1a), \tag{3.33}$$

$$B = (w_1^2 - 2L_Xw_1 + L_X^2)\exp(-w_1a), \tag{3.34}$$

$$C = (L_X^2 - w_2^2)\cos(w_2a) - 2L_Xw_2\sin(w_2a), \tag{3.35}$$

$$D = (L_X^2 - w_2^2)\sin(w_2a) + 2L_Xw_2\cos(w_2a), \tag{3.36}$$

$$E = (w_1^3 - 3L_X^2w_1 - 2L_X^3)\exp(w_1a), \tag{3.37}$$

$$F = (-w_1^3 - 3L_X^2w_1 - 2L_X^3)\exp(-w_1a), \tag{3.38}$$

$$G = (w_2^3 + 3L_X^2w_2)\sin(w_2a) - 2L_X^3\cos(w_2a), \tag{3.39}$$

$$H = (-w_2^3 - 3L_X^2w_2)\cos(w_2a) - 2L_X^3\sin(w_2a). \tag{3.40}$$

Then, the odd-numbered eigenvalues λ_i are gained by solving

$$\det\begin{bmatrix} A+B & 2C \\ E+f & 2G \end{bmatrix} = 0 \tag{3.41}$$

and the even-numbered eigenvalues λ_i^* by solving

$$\det\begin{bmatrix} A-B & 2D \\ E-F & 2H \end{bmatrix} = 0. \tag{3.42}$$

With the scaling coefficients b_i and b_i^*,

$$b_i = \left[\frac{2}{w_{1i}}\sinh(2aw_{1i}) + \frac{1}{2w_{2i}}\left(\frac{A+B}{C}\right)^2\sin(2aw_{2i}) + a\left(\left(\frac{A+B}{C}\right)^2 + 4\right)\right.$$
$$\left. -2\frac{A+B}{C}\sqrt{\frac{\lambda_i}{L_X^3}}\left(w_{1i}\cos(aw_{2i})\sinh(aw_{1i}) + w_{2i}\sin(aw_{2i})\cosh(aw_{1i})\right)\right]^{-1/2}, \tag{3.43}$$

$$b_i^* = \left[\frac{2}{w_{1i}^*}\sinh(2aw_{1i}^*) - \frac{1}{2w_{2i}^*}\left(\frac{A^*-B^*}{D^*}\right)^2\sin(2aw_{2i}^*) + a\left(\left(\frac{A^*-B^*}{D^*}\right)^2 - 4\right)\right.$$
$$\left. +2\frac{A^*-B^*}{D^*}\sqrt{\frac{\lambda_i^*}{L_X^3}}\left(w_{2i}^*\cos(aw_{2i}^*)\sinh(a^*w_{1i}^*) - w_{1i}^*\sin(aw_{2i}^*)\cosh(aw_{1i}^*)\right)\right]^{-1/2}, \tag{3.44}$$

using w_{1i} and w_{2i} gained by the odd or even eigenvalues λ_i or λ_i^*, respectively, the corresponding normalised eigenfunctions are determined by

$$\phi_i(z) = \begin{cases} b_i \left[2\cosh(w_{1i}z) - \frac{A+B}{C} \cos(w_{2i}z) \right]; & \text{if } i \text{ is odd,} \\ b_i^* \left[2\sinh(w_{1i}^*z) - \frac{A^*-B^*}{D^*} \sin(w_{2i}^*z) \right]; & \text{if } i \text{ is even.} \end{cases} \tag{3.45}$$

In Figure 3.4, next to the first twenty eigenvalues corresponding to the SE kernel (depicted in blue), also the results $\lambda_1, \ldots, \lambda_{20}$ obtained by the analytic solution using the ME kernel function are depicted in red. Again, λ_i converges faster towards zero for larger correlation length ratios L_X/l. Comparing the two kernel types, it can be seen that for $L_X/l = 1.0$ and $L_X/l = 10.0$, the eigenvalues of the ME kernel drop much faster than the ones of the SE kernel. In case of $L_X/l = 0.1$, the ME kernel falls below the SE kernel only for $i \geq 12$. Still, as the number of required eigenvalues increases with decreasing L_X/l, the ME still outperforms the SE kernel in terms of convergence behaviour.

3.2. Interval analysis to consider interval variables

Propagating an interval variable or vector through a model, the response can be approximated by an interval as well, which bounds the true solution. The problem to be solved is then to find the minimum and maximum response, which means in general to find

$$M(X^I) = \left[\inf_{x \in X^I} (M(x)), \; \sup_{x \in X^I} (M(x)) \right], \tag{3.46}$$

if $M(X^I)$ is a continuous function on $\mathbb{R}$. The interval valued response for the QoI $Y^I = [\underline{Y}, \overline{Y}]$ is directly given by the bounds following from Eq. (3.46). However, as it is in the nature of interval vectors that there is no dependency between its entries, while the model might include a coupling between the model responses, Y^I can become non-physical and highly conservative. Furthermore, the intensity of this conservative overestimation increases proportionally with the number of interval valued input parameters as well as with their individual width $w(X^I)$. Generally, there exist a non-convex manifold $\tilde{Y} \in \mathbb{R}^n$ which is a subset of Y^I. However, its solution in a closed form is only obtainable when an explicit analytic solution of the problem exists [Faes and Moens, 2020b].

There have been several methods proposed by the research community which aim to limit the dependency phenomenon, e.g. the improved interval arithmetical technique [Muhanna and Mullen, 2001] or the affine arithmetic [Manson, 2005], which are however intrusive. A review of these advanced interval arithmetic methods and further extensions has been recently provided by Faes and Moens [2020b]. Alternatively, the dependency between different input interval parameters can be described in terms of an interval field $X^I(\boldsymbol{z})$. Then, $\tilde{Y}$ is approximated by propagating a set of of interval field realisations $x_j^I = X^I(\boldsymbol{z}_j)$ through the model. Depending on whether implicit or explicit interval fields are used, the propagation of them is performed non-intrusively or in terms of an optimisation approach, correspondingly [Verhaeghe et al., 2013]. A sound introduction into interval methods can be found in the dissertation by Faes [2017].

If the deterministic output of a model behaves monotonically, the interval valued results of a QoI can be determined directly by propagating all vertex combinations of the interval space through the model [Moens and Hanss, 2011]. In this case, classical interval arithmetic is sufficient to operate with interval inputs within the model. Then, the problem can be solved by a pure vertex propagation as briefly described in Subsection 3.2.1. Otherwise, a global optimisation approach is required, as outlined in Subsection 3.2.2. Additionally to these two methods, in their latest review paper Faes and Moens [2020b] also mention perturbation methods and hybrid approaches, which will not further be discussed in this work.

3.2.1. Vertex propagation

In case of monotonic problems, interval variables can be considered by pure vertex analysis. This means that only the interval bounds need to be propagated deterministically through the model. In case of a single interval variable as input, this means [Faes and Moens, 2020b]

$$M\left(X^I\right) = \begin{cases} \left[M\left(\underline{X}\right), \ M\left(\overline{X}\right)\right] & \text{if } M\left(\cdot\right) \text{ is monotonically increasing} \\ \left[M\left(\overline{X}\right), \ M\left(\underline{X}\right)\right] & \text{if } M\left(\cdot\right) \text{ is monotonically decreasing} \end{cases}. \tag{3.47}$$

When several input interval variables or an interval vector as input parameter are considered, the hyper cuboid vertices that have to be propagated are given by all combinations of the individual interval bounds [Moens and Hanss, 2011].

3.2.2. Global optimisation

Regarding an interval variable as input parameter X^I to be propagated through a general, non-monotonic model $\mathcal{M}$ as given in Eq. (3.1), the smallest conservative hyper cuboid approximation $\boldsymbol{Y}^I = \left(Y^I_1, \ldots, Y^I_n\right)$ of $\tilde{\boldsymbol{Y}}$ is determined by searching within X^I. Then, the i-th interval valued output quantity $Y^I_i = [\underline{Y}_i, \overline{Y}_i]$ out of n output quantities of the model (e.g. the degrees of freedom) can be found by optimising

$$\underline{Y}_i = \min_{x \in X^I} M_i(x), \quad i = 1, \ldots, n, \tag{3.48}$$

$$\overline{Y}_i = \max_{x \in X^I} M_i(x), \quad i = 1, \ldots, n. \tag{3.49}$$

When a global minimum and maximum can be obtained, the optimisation is successful and the smallest approximation of $\tilde{\boldsymbol{Y}}$ has been found. Note that only in this case conservatism can be guaranteed [Faes and Moens, 2020b].

Depending on the problem to be solved as well as the chosen model, the optimisation can become computationally costly, according to the computational time needed for a single model evaluation. However, as the global optimisation is completely non-intrusive, commercial solvers as well as any advanced solution scheme such as model order techniques can be easily used. A comprehensive discussion of these issues as well as a broad literature review on applied solution schemes is provided by Faes and Moens [2020b]. In this work, only monotonic models will be applied to propagate uncertain input parameters to receive a model response of a certain QoI. For this reason, global optimisation techniques are not further deepened.

3.3. Probability bounds analysis for imprecise random fields

If one or several hyper parameters of a random field are considered imprecise, an imprecise random field occurs, which includes both, aleatory and epistemic uncertainties. In this work, epistemic uncertainties are described by interval variables. Aleatory uncertainties are considered to be spatially dependent (i.e. modelled by random fields), following an isotropic correlation structure that is assumed to be known, e.g. in terms of an SE or ME correlation function. Furthermore, only constant mean values $\mu_X(z) = \text{const.}$ and standard deviations $\sigma_X := \sigma_X(z)$ are considered. If they were a function of the location z and additionally assumed to be an interval, the parameters would become an interval field. However, as will be pointed out in the following paragraphs, the crucial point is when an interval valued correlation length is used. This case has been addressed by Dannert et al. [2018, 2019] in terms of interval discretisation as well as by Faes and Moens [2019b] in terms of optimisation.

Following the notation of Faes and Moens [2019b], a Gaussian imprecise random field can be described by extending the KL expansion given in Eq. (3.7) towards

$$[X](\omega, z) = \mu_X^I(z) + \sigma_X^I \sum_{i=1}^{\infty} \sqrt{\lambda_i^I} \phi_i^I(z) \xi_i(\omega). \tag{3.50}$$

The interval valued eigenvalues $\lambda_i^I \in \mathbb{R}^+$ and corresponding interval fields $\phi_i^I(z) : \mathcal{D} \times \mathbb{R} \mapsto \mathbb{R}$, representing the bounds of the eigenfunctions, occur if an interval valued correlation length L_X^I is considered. Then, a realisation $[\bar{x}_j](z) = [\bar{X}](\omega_j, z)$ of an imprecise random field results in an interval field. It is obtained by truncating Eq. (3.50) after T terms and inserting a set $\boldsymbol{\xi}_j(\omega_i) = (\xi_1, \ldots, \xi_T)_j$ of standard normal distributed random variables.

In the next two paragraphs, the influence of the different hyper parameters being interval valued is discussed. Afterwards, a nested p-box algorithm to propagate imprecise random fields through an arbitrary, non-intrusive model is introduced.

Interval valued mean value and standard deviation: As discussed in Section 3.1, an arbitrary Gaussian random field $X(\omega, z) \sim \mathcal{N}(\mu_X, \sigma_X)$ can be understood as a standard normal distributed random field $S(\omega, z) \sim \mathcal{N}(0, 1)$ scaled by σ_X and shifted towards $\mu_X(z)$. This implies that both hyper parameters influence the random field monotonically and - applying a monotonic model $\mathcal{M}$ - a pure vertex analysis is sufficient regarding imprecise random fields occurring from the mean value $\mu_X^I(z)$ or the standard deviation σ_X^I being interval valued. By this, two scenarios have to be propagated through the model if one of the two hyper parameters is an interval variable while there is need for four scenarios in case of both hyper parameters are considered as interval variables.

Assuming the mean value and standard deviation additionally to be constant, yields another advantage. As the arbitrary Gaussian random field can be obtained from a unified, standard normal distributed random field in this case, Eq. (3.3) has to be solved only once (with respect to a certain spatial domain). This becomes beneficial when imprecise random fields and hence its individual interval realisations are applied on the same domain. Then, the computational

effort can be reduced by solving the KL expansion only once instead of for each (combination of) interval bound(s) resulting from μ_X^I and/or σ_X^I. This can become crucial when arbitrary 2D or 3D domains are used and numerical expensive solution schemes are required to solve the Fredholm integral equation.

Interval valued correlation length: In case of an interval valued correlation length, a pure vertex analysis can become insufficient. As can be seen in Figure 3.5, for $i > 1$ the eigenvalues λ_i - and hence the random field - are not monotonically depending on the correlation length L_X[3]. Note that also the phase and amplitude of the eigenfunctions $\phi_i(z)$ change according to L_X [Faes and Moens, 2019b]. However, for the sake of vividness, the following visual discussion is focused on the eigenvalues.
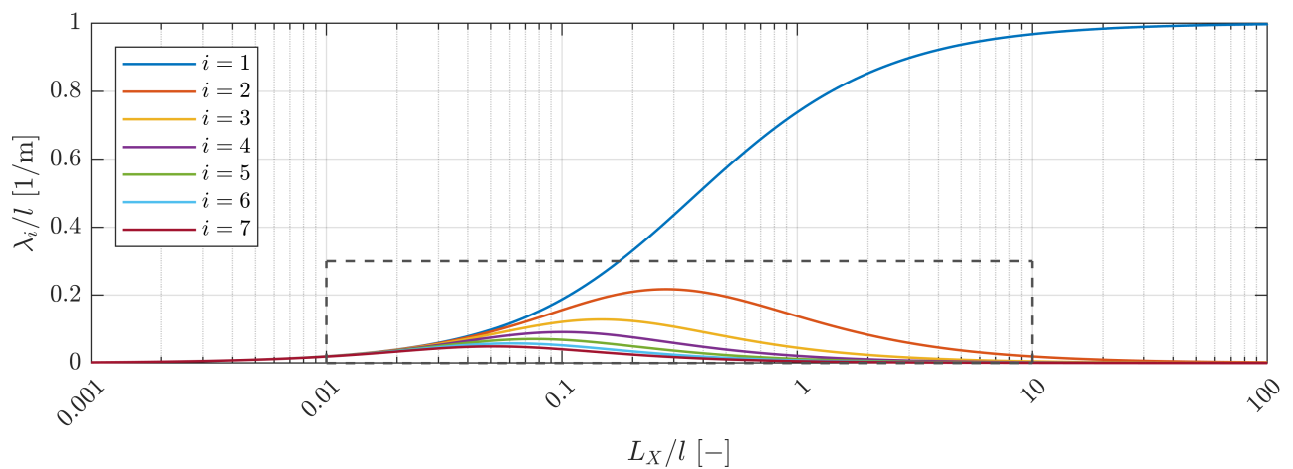
(a) λ_1/l converging monotonically towards one, while for $i > 1$ λ_i/l converges towards zero after reaching a maximum turning point
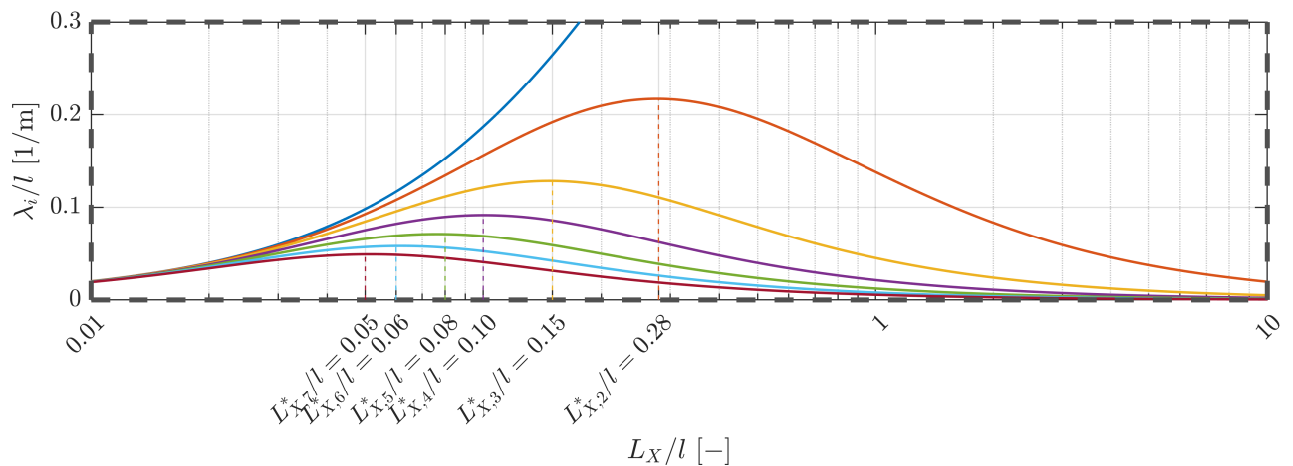
(b) intermediate correlation length ratios $L_{X,i}^*/l$ corresponding to the maximum turning point of the eigenvalue λ_i, $i = 2, \ldots, 7$

Figure 3.5: Normalised eigenvalues λ_i/l, $i = 1, \ldots, 7$ as a function of the correlation length ratio L_X/l, with l the domain length, obtained by a one-dimensional Gaussian random field considering a single exponential correlation kernel [Dannert et al., 2021a].

---

[3]Note that this is independent from the fact whether the model $\mathcal{M}$ through which the imprecise random field is propagated is monotonic or not.

In Figure 3.5, the first seven eigenvalues occurring from the analytic solution of a 1D random field with an SE correlation function are depicted as a function of the correlation length from a very small to a high range. Both, the eigenvalues and the correlation length are normalised by the domain length l, which has been chosen to be in meters for this example. For decreasing correlation length ratios L_X/l, all eigenvalues converge towards zero, as visible in Figure 3.5a. In case of an increase of the correlation length towards $L_X \gg l$, however, λ_1/l increases monotonically and finally converges towards one, while λ_i/l increase to a maximum turning point before decreasing again for $i > 1$ and finally converge to zero again. The turning points are depicted in Figure 3.5b in a closer view as indicated by the grey dashed box and will be discussed further in the context of the following optimisation procedure.

Due to the non-monotonic behaviour of the eigenvalues and -functions with respect to the correlation length, also values $L^*_X \in [\underline{L}_X, \overline{L}_X]$ can become significant for the bounds of the model response, even if the model itself is monotonic. These values L^*_X are referred to as *intermediate values*. This issue can be handled either by global optimisation [Faes and Moens, 2019b] or by discretising the interval valued correlation length [Dannert et al., 2018, 2019]. However, both approaches can become computational costly.

For a scenario where only monotonic models are applied to propagate imprecise random fields (as it will be done in this work), Faes and Moens [2019b] developed an efficient approach to determine L^*_X a priori and this way avoiding a global optimisation over the whole model propagation. The idea is to find the values L^*_X which lead to the extreme values in $\sqrt{\lambda_i}\phi_i(\boldsymbol{z})$. These can be obtained by optimising

$$\underline{L}^*_{X_i} = \arg\min_{\mathcal{G}(L_X)} \|\sqrt{\lambda_i}\phi_i(\boldsymbol{z})\|_2, \quad \text{s.t. } L_X \in L^I_X, \tag{3.51}$$

$$\overline{L}^*_{X_i} = \arg\max_{\mathcal{G}(L_X)} \|\sqrt{\lambda_i}\phi_i(\boldsymbol{z})\|_2, \quad \text{s.t. } L_X \in L^I_X, \tag{3.52}$$

for $i = 1, \ldots, T$, with $\mathcal{G}(\mathcal{D}, L_X) : \mathcal{D} \times L_X \mapsto \{\lambda_i, \phi_i(\boldsymbol{z})\}_{i=1}^{n_{\text{ep}}}$ being the process of solving Eq. (3.3) for n_{ep} eigenpairs given a crisp value L_X. As the $\mathcal{L}_2$ norm is differentiable, the resulting nonlinear approximation problem is smooth, convex and of limited dimension. Furthermore, a complete bounding set of the basis function in each mode is obtained by searching those L_X corresponding to the extrema of their $\mathcal{L}_2$ norm. The optimisation leads to maximally $2T$ solutions in a single vertex set $\mathbb{L}$,

$$\mathbb{L} = \{\underline{L}^*_{X_1}, \overline{L}^*_{X_1}, \ldots, \underline{L}^*_{X_T}, \overline{L}^*_{X_T}\}. \tag{3.53}$$

Note that the intermediate values $L^*_{X,i} \in L^I_X$ resulting for an interval valued correlation length L^I_X correspond to the maximum turning point values of the eigenvalues λ_i, laying within the considered interval, see Figure 3.5b.

In the context of damage mechanics, Dannert et al. [2021a] have shown that intermediate correlation length values do not have a significant effect on the resulting p-box, when monotonic, static problems are applied. Indeed, a small influence of the intermediate values was shown, however it has not proven to be of relevant impact to the p-box from the engineering point

of view. The focus of the following discussions and studies is therefore on the challenge of assuming different correlation length values in general, using three different ratios $L_X/l = 0.1$, $L_X/l = 1.0$ and $L_X/l = 10.0$ with respect to the domain length l, in order to investigate the influence and resulting problems raising from different magnitudes of correlation length ratios and the corresponding variability of the random field.

Double loop approach: Imprecise random fields can be propagated through a monotonic model as described in Algorithm 1. As the approach is non-intrusive, any monotonic model can be used as a black box and is therefore not discussed in this section. In the later applications, an FE model will be used considering linear elastic or elasto-plastic material behaviour. The algorithm is implemented in Matlab while Abaqus is used as FE solver. In order to use material data described by random fields, the subroutine `USDLFD`[4] of Abaqus is used to define the material data at the integration point level.

Before starting the algorithm, the imprecise random field parameters as well as their hyper parameters need to be defined. Furthermore, the parameters for the stochastic approach, e.g. the number of samples in case of a Monte Carlo (MC) approach, are required as well as the quantities of interest to be evaluated.

In the outer loop, the epistemic uncertainties, i.e. interval valued hyper parameters, are discretised. In analogy to the p-box propagation in terms of discretisation or sampling described by Zhang et al. [2010], the interval valued parameters might also be sampled. However, as pointed out before, in case of monotonic models a pure vertex analysis is sufficient. For more than one imprecise random field input parameter, this means that all vertex combinations are determined. If intermediate correlation length values are considered, also these values are combined with each value of the other parameter.

For each discretised epistemic parameter (combination), called *scenario c*, the following is performed. First, the crisp random field resulting for the current parameters is discretised by KL expansion. If the eigenpairs are already available for the current case, i.e. the Fredholm integral equation has been solved already for the current correlation length value regarding the underlying problem domain, the results can be recycled. Else, Eq. (3.3) needs to be solved either numerically or analytically.

In the inner loop, the aleatory uncertainties, i.e. the crisp random field resulting for the current parameters, are propagated. For each realisation number j out of a pre-defined number n_{s} of realisations, a deterministic random field realisation is created for every parameter that is considered to be uncertain. This is done by inserting the current hyper parameter values, the eigenpairs as well as $\boldsymbol{\xi}_j$ into Eq. (3.9). Different ways to choose $\boldsymbol{\xi}_j$ will be discussed in Chapter 5. The resulting realisation can then be propagated deterministically through the model and is stored in combination with the corresponding results of the model response.

As soon as all realisations have been propagated, the statistical evaluation is performed for each QoI (stochastic post-processing). This includes to determine the stochastic moments as well as the cumulative distribution function (CDF) of the current aleatory random field

---

[4]`https://abaqus-docs.mit.edu/2017/English/SIMACAESUBRefMap/simasub-c-usdfld.htm#simasub-c-usdfld`

Algorithm 1 Nested algorithm to propagate imprecise random fields based on interval valued parameters applying a monotonic model.

Require:
   monotonic model (black box)
   imprecise random field hyper parameters
   sample size n_s
   quantity of interest (QoI)

   % initialising
   if L_X is epistemic uncertain **then**
      % optimisation
      $c = (\underline{L}_X, L_{X,i}^*, \overline{L}_X)$
   else
      % vertex analysis
      $c = I^\times$
   end if

   % outer loop: discretise epistemic uncertainties
   for $i = c$ **do**

      % discretise random field
      if (λ, ϕ) available **then**
         load (λ, ϕ) of current correlation structure
      else
         solve Fredholm integral equation
         save (λ, ϕ) of current correlation structure
      end if

      % inner loop: propagate aleatory uncertainties
      for $j = n_\text{s}$ **do**
         generate random field realisation
         propagate through model   ▷ black box, e.g. FE solver by Abaqus
         save realisation and model response
      end for

      % stochastic post-processing (for each QoI)
      evaluate stochastic moments
      generate CDF
      save statistics

   end for

   % interval post-processing (for each QoI)
   determine interval bounds of stochastic moments
   determine CDF bounds
   save p-box results

---

propagation. Again, methods to be applied for this purpose are discussed further in Chapter 5. When the crisp random fields of all epistemic parameter combinations are propagated and evaluated, the double loop approach is finished. The resulting p-box is determined within the interval post-processing. From all epistemic scenarios, the minimum and maximum stochastic moments are identified. Furthermore, the left and right bound of the CDFs are determined.

Propagating imprecise random fields implies some additional challenges compared to the quests to be solved in terms of UQ and UP already. This applies especially for interval valued correlation lengths as studied in the following. In the subsections below, the main issues in terms of the computational cost, the influence of the truncation order as well as the spatial discretisation are investigated and discussed.

3.3.1. Computational cost

Due to the double loop approach as contoured in Algorithm 1, the computational cost can increase drastically depending on the number of imprecise random fields as well as the number of their interval valued hyper parameters. The effect of both is visualised in Figure 3.6. Each circle stands for the propagation of one scenario, i.e. a crisp random field, which may already include a high number n_s of deterministic model evaluations.

(a) one imprecise random field, one interval valued hyper parameter: $n_s \geq 2$

(b) one imprecise random field, two interval valued hyper parameters: $n_s \geq 4$

(c) two imprecise random fields, two interval valued hyper parameters: $n_s \geq 16$
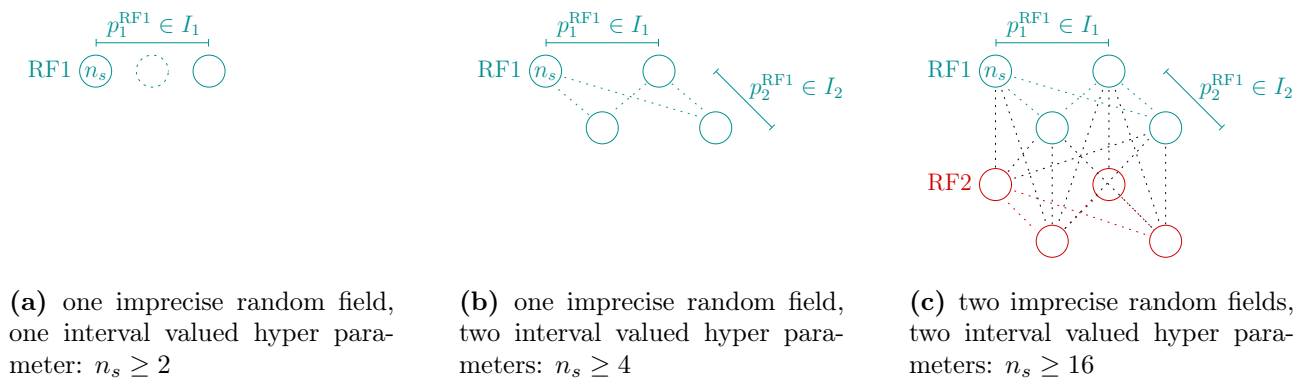
Figure 3.6: Computational cost depending on the number of crisp random field scenarios (each symbolised by a circle) to be propagated with a number n_s of realisations, according to the number of considered imprecise random fields and corresponding interval valued hyper parameters.

If one parameter RF1 is described by an imprecise random field, which results from only one interval valued hyper parameter p_1^{RF1}, at least two crisp random field scenarios have to be propagated, see Figure 3.6a. In case of intermediate values even more crisp random fields arise, as indicated by the dashed circle between the two circles assigned to the interval bounds. Considering a pure vertex analysis without intermediate values, this leads already to four scenarios when a second hyper parameter p_2^{RF1} of the first imprecise random field is considered to be interval valued (Figure 3.6b). Then, the computational cost to propagate this imprecise random field is already four times the computational cost required for an standard aleatory uncertainty analysis. Adding further interval valued hyper parameters or a second imprecise random field, the number of vertex combinations and therefore the number of crisp random fields to be propagated increases drastically, as exemplified in Figure 3.6c for two imprecise random fields including each two interval valued hyper parameters.

In order to keep the computational cost feasible, the individual model evaluation should be aimed to be as efficient as possible. This can be achieved by highly developed (commercial) solvers, parallel computing as well as model order reduction techniques. Additionally, the number of realisations to be propagated for each crisp random field should be kept as low as possible. For this purpose, different sophisticated sampling techniques are investigated and discussed in Chapter 5.

3.3.2. Influence of the truncation error

Considering an interval valued correlation length L_X^I, the truncation error of the input parameter is of high importance. As already pointed out in Subsection 3.1.2, the convergence rate of the truncation order depends on the type of the correlation function as well as on the correlation length ratio L_X/l with respect to the domain length. This means, if different correlation lengths are considered in terms of an interval valued correlation length hyper parameter, each individual crisp random field resulting from a certain value L_X has to be truncated at a different order. Otherwise, the resulting p-box might be not only affected by the uncertainty of the input, but also by a different approximation error. For this reason, according to the current correlation length, the truncation is usually chosen adaptively such that it falls below a certain predefined mean truncation error $\bar{\epsilon}_{\bar{\Gamma}} \leq \epsilon_{\max}$.

As an example, the truncation order T required to maintain a mean truncation error of $\bar{\epsilon}_{\bar{\Gamma}} \leq 0.015\,\%$ is compared for both kernel types in Table 3.2 considering the effective correlation length ratios $L_X/l = 0.1$, $L_X/l = 1.0$ and $L_X/l = 10.0$. In case of the smallest chosen correlation length, the SE kernel requires more than 130 times the number of truncation terms than the ME kernel. With regard to the curse of dimensionality, which will be further discussed in Chapter 5, the ME is therefore highly advantageous.

Table 3.2: Comparing the truncation order T required to obtain a comparable mean correlation error of $\bar{\epsilon}_{\bar{\Gamma}} \leq 0.015\,\%$ considering different effective correlation length ratios L_X/l assuming an SE or an ME correlation function for a 1D random field.

	$L_X/l\,[-]$	0.1	1.0	10.0
	$L_X^{\mathrm{SE}}/l\,[-]$	0.1	1.0	10.0
SE	$T\,[-]$	13472	1392	118
	$\bar{\epsilon}_{\bar{\Gamma}}\,[\%]$	0.01499	0.01498	0.01491
	$L_X^{\mathrm{ME}}/l\,[-]$	0.0471	0.4249	2.1114
ME	$T\,[-]$	102	12	3
	$\bar{\epsilon}_{\bar{\Gamma}}\,[\%]$	0.01468	0.01304	0.01475

Regarding the SE correlation function, a much higher mean truncation error has to be accepted, if small correlation lengths are considered. In Figure 3.7, the resulting truncation errors are compared for the different values L_X/l, regarding an SE correlation function.

Regarding the mean truncation error $\bar{\epsilon}_{\bar{\Gamma}}$ depicted in Figure 3.7a as a function of the truncation order T, a first challenge arises. As the truncation error decreases much faster for large

(a) mean truncation error $\bar{\epsilon}_{\bar{\Gamma}}$

(b) local truncation error $\epsilon_{\bar{\Gamma}}(z)$
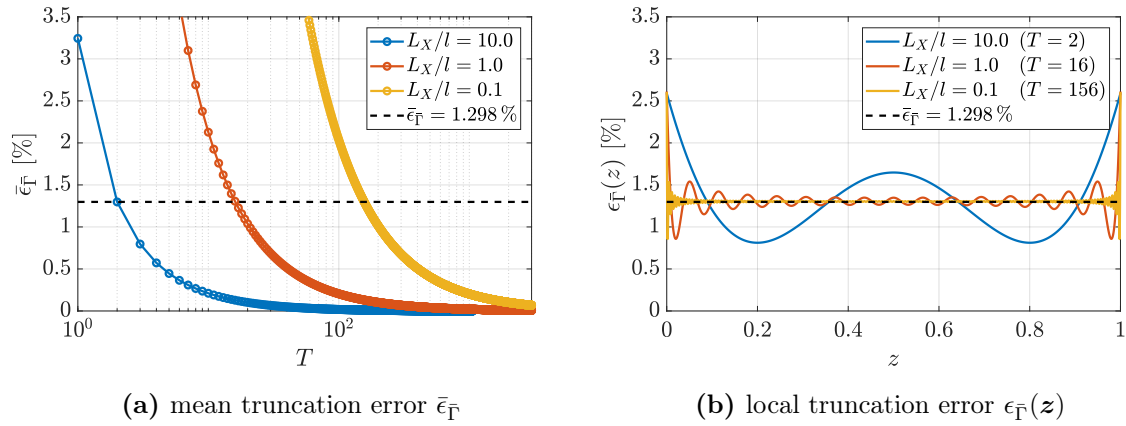
Figure 3.7: Comparing the mean and local truncation error of the single exponential correlation function regarding a one-dimensional random field obtained by different correlation length ratios L_X/l with respect to the domain length l.

correlation length ratios, not every arbitrary value $\bar{\epsilon}_{\bar{\Gamma}}$ can be chosen. For example, for $\bar{\epsilon}_{\bar{\Gamma}} \leq 3\%$, for $L_X/l = 10.0$, the next truncation error falling below this aimed value would be $\bar{\epsilon}_{\bar{\Gamma}} \approx 1.3\%$, using a truncation order of $T = 2$. However, the error resulting from the other correlation lengths would approximately fit the aim and this way the approximation error of the input is again not comparable. For this reason, the aimed error should always be oriented at the largest correlation length. On the other hand, as the error decreases that quickly in case of large values $L_X > l$, a further issue is then to maintain acceptable truncation orders for the small values $L_X < l$. As can be seen for an aimed value $\bar{\epsilon}_{\bar{\Gamma}} \leq 1.3\%$, this results in $T = 2$ in case of $L_X/l = 10.0$ but in $T > 150$ for $L_X/l = 0.1$ already.

In Figure 3.7b, the local truncation error $\epsilon_{\bar{\Gamma}}(z)$ is depicted with respect the domain. Again, the three different correlation length ratios are compared. Here, the local error is depicted for a mean truncation error $\bar{\epsilon}_{\bar{\Gamma}} \leq 1.3\%$, i.e. a different truncation order (as indicated in the legend) is chosen for each considered value L_X/l. It can be seen that in case of a large correlation length $L_X > l$, $\epsilon_{\bar{\Gamma}}(z)$ varies locally significantly around the aimed mean truncation error, while it is relatively close to $\bar{\epsilon}_{\bar{\Gamma}}$ within the whole domain for small values $L_X < 1$. This is another challenge to be addressed when dealing with imprecise random fields. Applying imprecise random fields to damage mechanics, Dannert et al. [2021a] have shown that a high local variation of $\epsilon_{\bar{\Gamma}}(z)$ can cause artificial localisation effects. Regarding large correlation lengths, the variation of the local truncation error can be reduced by increasing the truncation order. However, this leads again to a smaller global error $\bar{\epsilon}_{\bar{\Gamma}}$ and therefore higher required truncation terms regarding the small correlation length values.

This viscous circle cannot be broken without increasing the truncation order to very high values (then both errors converge towards zero), which is not feasible in terms of the curse of dimensionality. The problem can be reduced however by choosing correlation functions providing a fast convergence, e.g. the ME correlation function. As can be seen in Table 3.2 the ME kernel outperforms the SE kernel by far in terms of the required truncation order when a comparable effective correlation length is applied. In any case, dealing with imprecise random fields resulting from interval valued correlation lengths, the resulting truncation errors of the individual input fields must be carefully investigated and weighed appropriately.

3.3.3.   Influence of the spatial discretisation

Considering small correlation lengths, i.e. a high variability, the domain discretisation must be chosen accordingly. This is exemplified in Figure 3.8 for $n_{\mathrm{el}} = 5$ and $n_{\mathrm{el}} = 50$. If the number of elements is chosen too small, the resulting random field realisations are artificially smoothed. However, the computational cost of a single random field propagation usually increases according to the discretisation. Note that as an alternative (or additionally) to h-refinement, this problem can also be addressed by p-refinement.

(a) five elements   (b) fifty elements
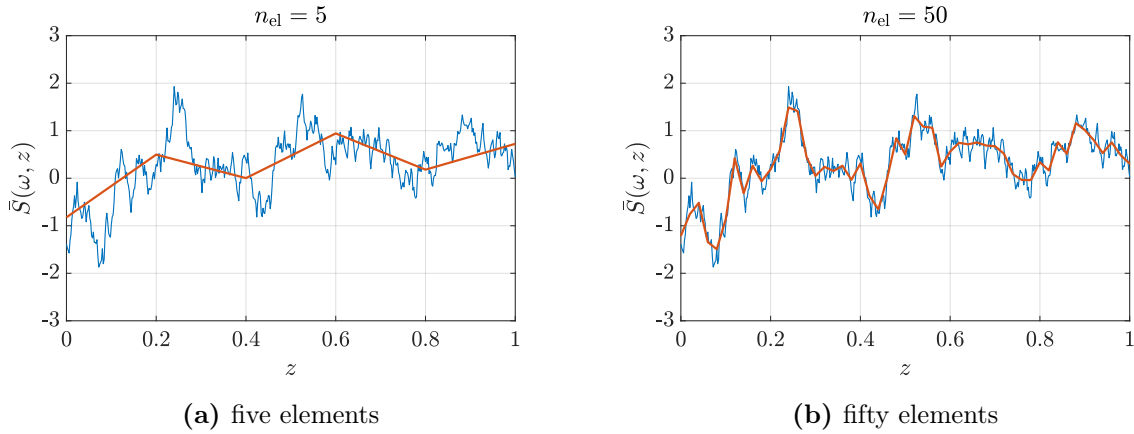
Figure 3.8: Random field realisation resulting from a single exponential correlation function with $L_X/l = 0.1$ (blue) as well as the values assigned to the discretised domain considering different numbers of elements n_{el}.

Sudret and Der Kiureghian [2000] conclude from their literature review that the element length should be chosen approximately between $L_X/4$ and $L_X/2$. They further emphasise that, in the context of FE analysis, it might additionally be essential to consider singular points when creating the FE mesh. In this case, solving the KL expansion and the FE problem based on different meshes can become useful to reduce the computational cost for solving Eq. (3.22). Still, the FE mesh needs to be fine enough to capture the variability of the random field.

4. Solid Mechanics

Scientific and engineering problems are usually described by ordinary or, more generally, partial differential equations (PDEs). Given a spatial d-dimensional bounded domain $\mathcal{D} \subset \mathbb{R}^d$, with $d = 1, 2, 3$, a PDE is given by

$$\begin{cases} \mathcal{L}(\boldsymbol{z}; y) = f(\boldsymbol{z}; y), & \boldsymbol{z} \in \mathcal{D} \\ \mathcal{B}(\boldsymbol{z}; y) = g(\boldsymbol{z}; y), & \boldsymbol{z} \in \partial\mathcal{D} \end{cases}, \tag{4.1}$$

with $\mathcal{L}$ denoting a linear or non-linear differential operator and $\mathcal{B}$ describing the boundary conditions at the body surface $\partial\mathcal{D}$, see Figure 4.1. The aim is to solve the PDE for the (usually spatial dependent) primary variable $y = y(\boldsymbol{z})$. It is distinguished into Dirichlet boundary conditions, defining the primary variables at the boundary $\partial_u\mathcal{D}$, and Neumann boundary conditions, when the spatial gradient of the primary variables is described at $\partial_t\mathcal{D}$.
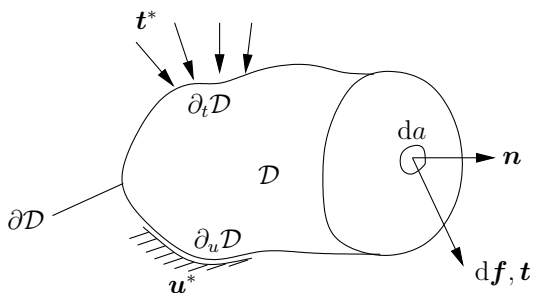
Figure 4.1: Arbitrary cut through a continuous body including general definitions.

When the PDE cannot be solved analytically, numerical methods are required to approximate the solution y. For instance, in the finite element method (FEM) y is defined based on a piecewise continuous basis by dividing the domain $\mathcal{D}$ into an arbitrary amount $i = 1, \ldots, n_{\text{el}}$ of finite sub-domains $\mathcal{D}_{\text{e},i}$, so-called finite elements (FEs). Before introducing the main idea of FEM in Section 4.3, Eq. (4.1) is specified in the context of the continuum mechanical framework in Section 4.1 and the used material laws are described in Section 4.2.

Model assumptions: In this work, linear-elastic and elasto-plastic material laws are used, the latter including linear hardening. For the purpose of all studies, the following model assumptions are made.

- Only *static problems* without cyclic loading, i.e. a one-way loading history, are considered. Therefore, isotropic and kinematic hardening are indistinguishable.

- Only *isotropic materials* are applied, i.e. the material response does not depend on the loading direction.

- For the scope of this chapter, *homogeneous materials* are considered, although spatial uncertain material properties are investigated in the later studies[1].

- All examples are applied assuming *small strains* ($\varepsilon < 5\,\%$) and *small rigid body rotations*, i.e. all quantities can be defined in the reference configuration and the linear strain tensor can be decomposed additively into an elastic and a plastic part.

- A *Cartesian coordinate system* is used, i.e. tensor notations (e.g. denoted by $\boldsymbol{a} := a_i \boldsymbol{e}_i$ or $\boldsymbol{A} := A_{ij}\boldsymbol{e}_i \otimes \boldsymbol{e}_j$) can be simplified by a pure matrix notation in terms of their coefficient matrix, neglecting the base unit vectors (i.e. $\mathbf{a} := a_i$ and $\mathbf{A} := A_{ij}$).

- In case of elasto-plasticity, the plastic behaviour is independent of the hydrostatic stress state, i.e. the yield criterion depends only on the deviatoric part and the plastic deformations are considered to be volume conservative (*von Mises plasticity*).

- Only *isothermal processes* are considered, i.e. the temperature does not change.

The focus of this chapter lays on describing the framework adjusted to these model assumptions rather than covering the whole generalised concept. As FEM in the context of solid mechanics using linear-elastic and elasto-plastic material descriptions is well established and will be applied as a black box model in the context of a uncertainty propagation (UP), only the main terms and equations are provided here. For detailed derivations and further extensions, e.g. with regard to large deformations, the reader is referred to additional literature, such as the books by Holzapfel [2000], de Souza Neto et al. [2008], Altenbach [2015].

4.1.   Continuum mechanical framework

A continuum is understood to be a domain of closed region (also called body) which is described by a continuous set of material points, at which the properties of the continuum are defined. In general, this can imply fluids or solid bodies but only the latter are considered and discussed in this work. The aim of continuum mechanics is to describe the kinematic and kinetic behaviour of continua. A more detailed introduction into continuum mechanics as well as into the underlying tensor algebra can be found e.g. in the books by Altenbach [2015] or Holzapfel [2000].

Considering the continuum to be an arbitrary solid body as exemplified in Figure 4.1, external impacts such as forces or (prohibited) displacements may cause deformations, translations and/or an internal stress state. Particularly, when large deformations can occur, it is distinguished into reference and current configuration. These are often labelled by capital and lower-case letters [Holzapfel, 2000], respectively, e.g. 'dZ' and 'dz' to denote an incremental length or 'Grad $(\cdot)$' and 'grad $(\cdot)$' as gradient operator. Regarding any material point given by the vector $\boldsymbol{Z}$ in the current configuration, with $\boldsymbol{z}$ being the corresponding point in the reference configuration, the displacement vector can be found by $\boldsymbol{u} = \boldsymbol{z} - \boldsymbol{Z}$. Based on this connection, the stress and strain measures need to be defined in both configurations and can

---

[1]Varying material data can be considered straightforwardly at the Gauss point level when assembling the stiffness matrix within FEM.

be connected via push-forward and pull-back relations. However, assuming only small strains, the gradient of the displacement with respect to the current configuration, $\operatorname{Grad} \boldsymbol{u} = \partial u_i / \partial Z_J$, and with respect to the reference configuration, $\operatorname{grad} \boldsymbol{u} = \partial u_i / \partial z_j$, are approximately equal, i.e. $\operatorname{Grad} \boldsymbol{u} \approx \operatorname{grad} \boldsymbol{u}$. Then, the linear strain tensor is defined by

$$\boldsymbol{\varepsilon} = \frac{1}{2} \left(\operatorname{grad} \boldsymbol{u} + \operatorname{grad}^{\mathrm{T}} \boldsymbol{u} \right), \tag{4.2}$$
$$\varepsilon_{ij} = \frac{1}{2} \left(\frac{\partial u_i}{\partial z_j} + \frac{\partial u_j}{\partial z_i} \right),$$

i.e. the continuum mechanical framework can be exclusively described in terms of the reference configuration. Note that the linear strain tensor is symmetric, i.e. $\varepsilon_{ij} = \varepsilon_{ji}$. As all examples in this work are based on small strain assumptions, all equations and formulations described in the following are directly discussed in the reference configuration only.

The stress state of a continuum results from the internal forces. Regarding an arbitrary cut through the body $\mathcal{D}$, as visualised in Figure 4.1, and therein an infinitesimal small area $\mathrm{d}a$, the vector of tension $\boldsymbol{t}$ is defined as

$$\boldsymbol{t} = \frac{\mathrm{d}\boldsymbol{f}}{\mathrm{d}a}, \tag{4.3}$$

where $\mathrm{d}\boldsymbol{f}$ is the force acting on $\mathrm{d}a$. Applying Cauchy's theorem, $\boldsymbol{t} = \boldsymbol{\sigma} \cdot \boldsymbol{n}$, with $\boldsymbol{n}$ the normal vector on the surface $\mathrm{d}a$, the tension $\boldsymbol{t}$ can be expressed as the Cauchy stress tensor $\boldsymbol{\sigma} := \boldsymbol{\sigma}(\boldsymbol{z})$, with

$$\boldsymbol{\sigma} = \begin{bmatrix} \sigma_{11} & \sigma_{12} & \sigma_{13} \\ & \sigma_{22} & \sigma_{23} \\ \text{sym.} & & \sigma_{33} \end{bmatrix}. \tag{4.4}$$

By that, the stress state is described precisely at a certain point $\boldsymbol{z} \in \mathcal{D}$ in terms of the normal stresses σ_{ii} in the direction of the corresponding orthonormal cut $\boldsymbol{n}_i$ and the shear stresses σ_{ij}.

In the following subsection, the balance equations required for the scope of this work are briefly discussed, before introducing the constitutive relations to describe the considered material behaviour in Subsection 4.1.2.

4.1.1. Balance equations

The following universal balance laws are required to describe physical systems in general.

i) Assuming a mass conserving system, the *balance of mass* describes the change of the mass density ρ due to volume change. In this work, the mass of the body is considered time invariant, i.e. $\frac{\mathrm{d}m}{\mathrm{d}t} = 0$.

ii) The *balance of momentum* describes the equilibrium of the internal and external forces to be fulfilled over time.

iii) From the *balance of angular momentum*, the symmetry of the Cauchy stress tensor, $\boldsymbol{\sigma} = \boldsymbol{\sigma}^{\mathrm{T}}$, can be derived.

iv) The *balance of energy*, also called the first law of thermodynamics, describes the equilibrium of the thermodynamic properties of a system.

v) The *balance of entropy* (second law of thermodynamics) is an inequality condition providing the direction of energy transfer of a process.

In the following paragraphs, the balance laws (ii), (iv) and (v) are described more detailed with respect to the applications provided in this work as they are of specific importance.

Balance of momentum: Newton's law of motion describes the time dependent change in the momentum of a mechanical system resulting from the internal forces and external forces, i.e. the body forces and the applied forces. Applying Cauchy's theorem and the divergence theorem, the momentum balance can be transformed to the linear momentum equation,

$$\rho \frac{\mathrm{d}\boldsymbol{v}}{\mathrm{d}t} = \rho \boldsymbol{b} + \operatorname{div} \boldsymbol{\sigma}, \tag{4.5}$$

to be fulfilled at an arbitrary material point $\boldsymbol{z} \in \mathcal{D}$. Here, the rate of the linear momentum $\rho \boldsymbol{v}$ is equal to the external forces, composed by the body forces $\boldsymbol{b} := \boldsymbol{b}(\boldsymbol{z})$ and the internal forces $\operatorname{div} \boldsymbol{\sigma}$. The density ρ is independent of time and space. Furthermore, in case of a static problem, the velocity $\boldsymbol{v} := \boldsymbol{v}(\boldsymbol{z})$ is zero and the left side vanishes, leading to Cauchy's equilibrium equation,

$$\rho \boldsymbol{b} + \operatorname{div} \boldsymbol{\sigma} = \boldsymbol{0}. \tag{4.6}$$

The boundary conditions are given by the (applied or restricted) deflections as well as the external forces,

$$\boldsymbol{u} = \boldsymbol{u}^* \quad \text{on} \quad \partial_u \mathcal{D}, \tag{4.7}$$

$$\boldsymbol{t} = \boldsymbol{\sigma} \cdot \boldsymbol{n} = \boldsymbol{t}^* \quad \text{on} \quad \partial_t \mathcal{D}. \tag{4.8}$$

The PDE given in Eq. (4.6) is solved in terms of FEM as described in Section 4.3.

Balance of energy: The first law of thermodynamics can be transformed into the local form of the energy balance given by

$$\rho \dot{e} = \boldsymbol{d} \cdot \cdot \boldsymbol{\sigma} + \rho r - \operatorname{div} \boldsymbol{q}, \tag{4.9}$$

where e is the internal energy, $\boldsymbol{d}$ the strain velocity tensor, r the radiant heat and $\boldsymbol{q}$ the heat flux vector. In case of small deformations, it is $\boldsymbol{d} = \dot{\boldsymbol{\varepsilon}}^{\mathrm{p}}$, with $\dot{\boldsymbol{\varepsilon}}^{\mathrm{p}}$ the plastic strain rate.

Balance of entropy: From the second law of thermodynamics, the local form of the entropy balance can be derived as

$$\rho \vartheta \dot{s} \geq \rho r - \operatorname{div} \boldsymbol{q} + \frac{1}{\vartheta} \boldsymbol{q} \cdot \operatorname{grad} \vartheta, \tag{4.10}$$

with s the specific entropy and ϑ the temperature. The free Helmholtz energy ψ is defined by

$$\psi = e - \vartheta s. \tag{4.11}$$

Inserting Eq. (4.9) and Eq. (4.10) into $\rho\dot{\psi} = \rho\dot{e} - \rho\vartheta\dot{s}$ and assuming small strains, i.e. $\boldsymbol{d} = \dot{\boldsymbol{\varepsilon}}$, it follows for the dissipation

$$D = \underbrace{\dot{\boldsymbol{\varepsilon}}^{\mathrm{p}} \cdot\cdot \boldsymbol{\sigma} - \rho\left(\dot{\psi} + \dot{\vartheta}s\right)}_{D^{\mathrm{in}}} - \underbrace{\frac{1}{\vartheta}\boldsymbol{q} \cdot \operatorname{grad}\vartheta}_{D^{\mathrm{th}}} \geq 0. \tag{4.12}$$

Note that the first term follows from $\boldsymbol{d} = \dot{\boldsymbol{\varepsilon}}$ as the elastic part of the strain tensor is not dissipative. The total dissipation is decomposed into the internal and the thermal dissipation, D^{in} and D^{th}, respectively. It describes the irreversible conversion of potential energy and is important for deriving physically consistent material models.

4.1.2. Constitutive theory

Describing the thermodynamic state of a material point within a continuum, it is distinguished into independent variables, i.e. the spatial location $\boldsymbol{z}$ and the temperature ϑ of the material point at time t, and dependent (constitutive) variables, e.g. the free energy ψ, the specific entropy s, the stress tensor $\boldsymbol{\sigma}$ and the heat flux vector $\boldsymbol{q}$. In general, the constitutive variables may depend on the location, (the rate and/or gradient of) the temperature, the strain (rate) or the density. Considering small strains and homogeneous materials, the dependency on the location and the density vanishes. Furthermore, assuming moderate deformation rates, all time dependent terms can be neglected. For isothermal processes, also the dependency on the temperature disappears and it remains

$$\psi = \tilde{\psi}\left(\boldsymbol{\varepsilon}\right), \tag{4.13}$$

$$\boldsymbol{\sigma} = \tilde{\boldsymbol{\sigma}}\left(\boldsymbol{\varepsilon}\right), \tag{4.14}$$

Substituting the time derivation $\dot{\psi}$ to the remaining terms of Eq. (4.12),

$$\left(\boldsymbol{\sigma} - \rho\frac{\partial\psi}{\partial\boldsymbol{\varepsilon}}\right) \cdot\cdot \dot{\boldsymbol{\varepsilon}}^{\mathrm{p}} \geq 0, \tag{4.15}$$

it follows that

$$\boldsymbol{\sigma} = \rho\frac{\partial\psi}{\partial\boldsymbol{\varepsilon}}. \tag{4.16}$$

Material symmetry: Regarding elastic material behaviour under small deformations, the stress state $\boldsymbol{\sigma}$ is depending linearly on the strains $\boldsymbol{\varepsilon}$ as defined by the generalised Hooke's law,

$$\boldsymbol{\sigma} = \mathbb{C} \cdot\cdot \boldsymbol{\varepsilon}, \tag{4.17}$$

$$\sigma_{ij} = C_{ijkl}\,\varepsilon_{kl}, \tag{4.18}$$

with $\mathbb{C} = C_{ijkl}$ the fourth order linear elastic material tensor. The free energy function can be expressed in terms of the linear strain tensor,

$$\psi = \frac{1}{2}\boldsymbol{\varepsilon} \cdot\cdot \left(\mathbb{C} \cdot\cdot \boldsymbol{\varepsilon}\right) = \frac{1}{2}C_{ijkl}\varepsilon_{ij}\varepsilon_{kl}. \tag{4.19}$$

Due to the symmetry of stress and strain tensor, $\sigma_{ij} = \sigma_{ji}$ and $\varepsilon_{kl} = \varepsilon_{lk}$, it is consequently $C_{ijkl} = C_{jikl} = C_{ijlk}$ and the general 81 components of $\mathbb{C}$ reduce to 36 constants. Referring to Cartesian coordinates, this enables a simple matrix formulation becoming handy for an FE implementation. Writing the unique components of the symmetric stress and strain tensor as a column matrix,

$$\boldsymbol{\sigma} = \begin{bmatrix} \sigma_{11} & \sigma_{22} & \sigma_{33} & \sigma_{12} & \sigma_{23} & \sigma_{31} \end{bmatrix}^{\mathrm{T}}, \tag{4.20}$$

$$\boldsymbol{\varepsilon} = \begin{bmatrix} \varepsilon_{11} & \varepsilon_{22} & \varepsilon_{33} & 2\varepsilon_{12} & 2\varepsilon_{23} & 2\varepsilon_{31} \end{bmatrix}^{\mathrm{T}}, \tag{4.21}$$

Eq. (4.17) becomes

$$\boldsymbol{\sigma} = \mathbf{C}\,\boldsymbol{\varepsilon}, \tag{4.22}$$

with $\mathbf{C}$ being a 6×6 material matrix. Furthermore, with $\mathbb{C}$ being the second partial derivative of the free energy function,

$$\mathbb{C} = \frac{\partial \boldsymbol{\sigma}}{\partial \boldsymbol{\varepsilon}} = \frac{\partial^2 \psi}{\partial \boldsymbol{\varepsilon} \partial \boldsymbol{\varepsilon}} = \frac{\partial^2 \psi}{\partial \varepsilon_{ij} \partial \varepsilon_{kl}} = \frac{\partial^2 \psi}{\partial \varepsilon_{kl} \partial \varepsilon_{ij}}, \tag{4.23}$$

it is $C_{ijkl} = C_{klij}$ and $\mathbf{C}$ can be expressed symmetrically in terms of 21 material parameters,

$$\mathbf{C} = \begin{bmatrix} C_{1111} & C_{1122} & C_{1133} & C_{1112} & C_{1123} & C_{1131} \\ & C_{2222} & C_{2233} & C_{2212} & C_{2223} & C_{2231} \\ & & C_{3333} & C_{3312} & C_{3323} & C_{3331} \\ & & & C_{1212} & C_{1223} & C_{1231} \\ & \text{sym.} & & & C_{2323} & C_{2331} \\ & & & & & C_{3131} \end{bmatrix} = \begin{bmatrix} C_{11} & C_{12} & C_{13} & C_{14} & C_{15} & C_{16} \\ & C_{22} & C_{23} & C_{24} & C_{25} & C_{26} \\ & & C_{33} & C_{34} & C_{35} & C_{36} \\ & & & C_{44} & C_{45} & C_{46} \\ & \text{sym.} & & & C_{55} & C_{56} \\ & & & & & C_{66} \end{bmatrix}.$$

In Subsection 4.2.1, the material matrix $\mathbf{C}$ is further specified in terms of an isotropic, linear-elastic material behaviour. Then the number of independent elastic constants reduces to two material parameters.

Internal variables and dissipation: For the description of inelastic material behaviour, Eq. (4.13) and Eq. (4.14) are supplemented by internal variables, which can be understood as unobservable state variables $\boldsymbol{\beta}_i, i = 1, \ldots, n$. These are determined in terms of evolution equations given by functions of the constitutive variables and the internal variables. For the model assumptions stated earlier in this work, this results in

$$\frac{\mathrm{d}\boldsymbol{\beta}_i}{\mathrm{d}t} = \dot{\boldsymbol{\beta}}_i(\boldsymbol{\varepsilon}, \boldsymbol{\beta}_1, \ldots, \boldsymbol{\beta}_n). \tag{4.24}$$

The evolution equations have to be integrated numerically, e.g. by implicit Euler method. If the system is not time dependent, a so-called pseudo-time is introduced to develop the non-linear response step by step. For example, considering quasi-static problems, the load can be applied incrementally by introducing such a pseudo-time.

Describing the free energy given in Eq. (4.13) not only as a function of the strain $\boldsymbol{\varepsilon}$ but also of the internal variables $\boldsymbol{\beta}_i$,

$$\psi = \tilde{\psi}\left(\boldsymbol{\varepsilon}, \boldsymbol{\beta}_1, \ldots, \boldsymbol{\beta}_n\right), \tag{4.25}$$

the internal dissipation D^{in} given in Eq. (4.12) describes the mechanical dissipation resulting from inelastic material behaviour,

$$D^{\text{in}} = \boldsymbol{\sigma} \cdot \cdot \, \dot{\boldsymbol{\varepsilon}}^{\text{p}} - \rho \sum_{i=1}^{n} \frac{\partial \tilde{\psi}}{\partial \boldsymbol{\beta}_i} \cdot \cdot \, \dot{\boldsymbol{\beta}}_i \geq 0. \tag{4.26}$$

The time rate variables are called thermodynamic fluxes, while $B_i = -\partial \psi / \partial \boldsymbol{\beta}_i$ describe the thermodynamic forces.

In the context of elasto-plastic material behaviour, the internal variable is given by the plastic strain rate tensor $\dot{\boldsymbol{\varepsilon}}^{\text{p}}$. If hardening is considered, this internal variable is supplemented by a scalar valued internal variable to describe the isotropic hardening and/or a tensor valued internal variable in case of kinematic hardening. An elasto-plastic material model considering linear hardening is introduced in Subsection 4.2.2.

4.2. Material descriptions in terms of small strains

To simulate the behaviour of solids under loading, the response needs to be modelled properly according to the typical behaviour of the underlying material. For example, the behaviour of steel can be described as linear-elastic as long as the stress occurring due to loading maintains a certain threshold. Afterwards, the material starts to deform irreversibly and plastic material laws need to be considered.

Apart from (linear) elastic material models, there exist many well established laws to model elasto-plasticity, including hardening effects as the circumstances require. In the following, the fundamentals of isotropic linear-elastic material behaviour are summarised in Subsection 4.2.1 and supplemented by a standard elasto-plastic material law including linear hardening in Subsection 4.2.2, according to the constitutive relations introduced in Subsection 4.1.2. If not indicated differently, this section is based on the book by de Souza Neto et al. [2008]. However, the equations are reduced to the scope of the examples applied in this work, based on the model assumptions introduced in the beginning of this chapter.

4.2.1. Linear-elasticity

Assuming an isotropic material such as steel, the number of different entries in the material matrix $\mathbf{C}$ can be further reduced. Then, the model response is a function only of the Young's modulus E and the Poisson's ratio ν and Eq. (4.22) can be written with the components

$$\text{C}_{11} = \text{C}_{22} = \text{C}_{33} = \frac{E(1-\nu)}{(1+\nu)(1-2\nu)},$$

$$\text{C}_{12} = \text{C}_{23} = \text{C}_{13} = \frac{E\nu}{(1+\nu)(1-2\nu)},$$

$$\text{C}_{44} = \text{C}_{55} = \text{C}_{66} = \frac{E(1-2\nu)}{2(1+\nu)(1-2\nu)},$$

and all other entries C $= 0$. Alternatively, Eq. (4.22) can be described in terms of the bulk modulus κ and the shear modulus G,

$$\sigma_{ij} = \underbrace{\kappa\,\varepsilon_{kk}\delta_{ij}}_{-p\,\mathbf{I}} + \underbrace{2G\left(\varepsilon_{ij} - \frac{1}{3}\varepsilon_{kk}\delta_{ij}\right)}_{\tilde{\sigma}}, \tag{4.27}$$

which represents the stress tensor by the hydrostatic pressure

$$p = -\frac{1}{3}\mathrm{tr}\,\boldsymbol{\sigma} \tag{4.28}$$

and its deviatoric part $\tilde{\boldsymbol{\sigma}} = \boldsymbol{\sigma} + p\,\mathbf{I}$, with $\mathbf{I}$ the identity matrix. Analogously to this hydrostatic-deviatoric split, the strain tensor can be decomposed into

$$\boldsymbol{\varepsilon} = \frac{1}{3}v\mathbf{I} + \tilde{\boldsymbol{\varepsilon}}. \tag{4.29}$$

The first term represents the volumetric part in terms of the volume dilatation $v = \mathrm{tr}\,\boldsymbol{\varepsilon}$ and the second term is the deviatoric part. This tensor decomposition becomes important in the following subsection, where the plastic deformation is assumed to be volume conservative, i.e. the plastic flow does not change the volume significantly (von Mises plasticity).

4.2.2. Elasto-plasticity

Plastic flow means an irreversible deformation of the material. Regarding elasto-plastic material models, it is assumed that the response of a material is elastic (i.e. reversible) as long as a certain threshold, the yield stress σ_{y}, is not reached. When the yield stress is exceeded, plastic flow occurs associated with plastic deformations.

Assuming small rigid body rotations, the linear strain tensor can be decomposed into a part of elastic strains $\boldsymbol{\varepsilon}^{\mathrm{e}}$ and the remaining plastic strains $\boldsymbol{\varepsilon}^{\mathrm{p}}$,

$$\boldsymbol{\varepsilon} = \boldsymbol{\varepsilon}^{\mathrm{e}} + \boldsymbol{\varepsilon}^{\mathrm{p}}. \tag{4.30}$$

Furthermore, for isothermal processes the free energy is a function only of the elastic strains, i.e. $\psi := \psi(\boldsymbol{\varepsilon}^{\mathrm{e}})$ while the internal dissipation depends on the plastic strain rate,

$$D^{\mathrm{in}} = \boldsymbol{\sigma} \cdot\cdot\, \dot{\boldsymbol{\varepsilon}}^{\mathrm{p}} \geq 0. \tag{4.31}$$

Following the principle of maximum internal dissipation, i.e. maximising D^{in} by convex optimisation leads to a stationary saddle point problem to be solved,

$$\mathcal{L} = -D^{\mathrm{in}}(\boldsymbol{\sigma}) + \dot{\gamma}f(\boldsymbol{\sigma}), \tag{4.32}$$

with $\dot{\gamma}$ being a Lagrange multiplier used as plastic parameter in this context. The associated flow rule follows from differentiating $\mathcal{L}$ with respect to $\boldsymbol{\sigma}$,

$$\frac{\partial\mathcal{L}}{\boldsymbol{\sigma}} = -\dot{\boldsymbol{\varepsilon}}^{\mathrm{p}} + \dot{\gamma}\frac{\partial f}{\partial\boldsymbol{\sigma}} = \mathbf{0}, \tag{4.33}$$

$$\Rightarrow \dot{\boldsymbol{\varepsilon}}^{\mathrm{p}} = \dot{\gamma}\frac{\partial f}{\partial\boldsymbol{\sigma}}. \tag{4.34}$$

The yield criterion f (also called flow law) is chosen according to the assumptions made for plastic flow, e.g. by the von Mises yield criterion as described in the next paragraph. The fact that either the flow law is fulfilled ($f < 0$), i.e. elastic behaviour occurs and the plastic parameter is zero, or the plastic region is reached and the plastic parameter appears, is summarised in the Kuhn-Tucker conditions

$$\dot{\gamma} \geq 0, \quad f \leq 0, \quad \dot{\gamma}f = 0. \tag{4.35}$$

Then, the plastic parameter $\dot{\gamma}$ is obtained from the consistency condition $\dot{f} = 0$ if $f = 0$.

Von Mises plasticity: Concerning the material behaviour of metals, the plastic flow does not affect the volume. This means that plasticity is independent of the hydrostatic stress, i.e. the yield criterion depends only on the stress deviator $\tilde{\boldsymbol{\sigma}}$,

$$f(\tilde{\boldsymbol{\sigma}}) \leq 0, \tag{4.36}$$

and the plastic strain rate given in Eq. (4.34) becomes

$$\dot{\boldsymbol{\varepsilon}}^{\mathrm{p}} = \dot{\gamma} \frac{\partial f}{\partial \tilde{\boldsymbol{\sigma}}}. \tag{4.37}$$

Under this assumption as well as considering isotropic material behaviour, the von Mises yield criterion can be applied. By this hypothesis it is assumed that plastic flow depends on the equivalent von Mises stress σ_{vM},

$$f = \sigma_{\mathrm{vM}} - \sigma_{\mathrm{y}} \leq 0. \tag{4.38}$$

The plastic region is reached and yielding starts as soon as the equivalent von Mises stress

$$\sigma_{\mathrm{vM}} = \sqrt{\frac{3}{2} \, \tilde{\boldsymbol{\sigma}} \cdot \cdot \, \tilde{\boldsymbol{\sigma}}} = \sqrt{\frac{3}{2}} \, \|\tilde{\boldsymbol{\sigma}}\| \tag{4.39}$$

exceeds the yield stress σ_{y}, i.e. when the yield criterion

$$f = \|\tilde{\boldsymbol{\sigma}}\| - \sqrt{\frac{2}{3}} \sigma_{\mathrm{y}} \leq 0, \tag{4.40}$$

is violated. For ideal plasticity, the plastic parameter $\dot{\gamma}$ is obtained by inserting Eq. (4.40) to the consistency condition, leading to

$$\dot{\gamma} = \boldsymbol{n} \cdot \cdot \, \dot{\boldsymbol{\varepsilon}}, \quad \text{with} \quad \boldsymbol{n} = \frac{\tilde{\boldsymbol{\sigma}}}{\|\tilde{\boldsymbol{\sigma}}\|}. \tag{4.41}$$

Here, $\boldsymbol{n}$ is a second order tensor normal to the yield function, pointing into the direction of the deviatoric stress.

Hardening: When hardening effects occur, the material can bear a further increase of stress also after yielding starts. There are two kinds of linear hardening, isotropic and kinematic. While the first is physically associated with dislocations of the crystal lattice, the latter is caused by the resulting residual stress.

Hardening is described by further internal variables, a scalar internal variable a in case of isotropic hardening and a tensor valued internal variable $\boldsymbol{\beta}$ in case of kinematic hardening. The free energy is then supplemented by these internal variables, $\psi := \psi(\boldsymbol{\varepsilon}^{\text{e}}, a, \boldsymbol{\beta})$ and the internal dissipation in Eq. (4.31) becomes

$$D^{\text{in}} = \boldsymbol{\sigma} \cdot \cdot \, \dot{\boldsymbol{\varepsilon}}^{\text{p}} \underbrace{- \frac{\partial \psi}{\partial a}}_{\alpha} \dot{a} \underbrace{- \frac{\partial \psi}{\partial \boldsymbol{\beta}}}_{\boldsymbol{\tau}} \dot{\boldsymbol{\beta}}. \tag{4.42}$$

Due to the hardening, the yield surface changes and the flow law needs to be adapted, e.g. in case of linear hardening

$$f = \|\tilde{\boldsymbol{\sigma}} - \boldsymbol{\tau}\| - \sqrt{\frac{2}{3}}(\sigma_{\text{y}} + \alpha) \leq 0. \tag{4.43}$$

In terms of isotropic hardening, this can be interpreted as an increase of the yield surface, i.e. the initial yield stress σ_{y} raises by α. Alternatively (or additionally), the yield surface is shifted in the deviatoric space by the stress back tensor $\boldsymbol{\tau}$ in the case of kinematic hardening.

In case of a monotonically increasing load, the two hardening laws are indistinguishable as the different effects of the hardening types start to occur due to reverse loading. As only monotonic loading is applied in this work, assuming an elasto-plastic material with linear kinematic hardening is therefore sufficient. The commercial software Abaqus is used to solve the corresponding FE problem. Abaqus provides von Mises plasticity combined with a linear kinematic hardening model based on the linear hardening law by Ziegler [1959],

$$\dot{\boldsymbol{\tau}} = H \frac{1}{\sigma_{\text{y}}} \left(\boldsymbol{\sigma} - \boldsymbol{\tau} \right) \dot{\bar{\varepsilon}}^{\text{p}}, \tag{4.44}$$

with H the hardening parameter and the scalar

$$\dot{\bar{\varepsilon}}^{\text{p}} = \sqrt{\frac{2}{3} \dot{\boldsymbol{\varepsilon}}^{\text{p}} \cdot \cdot \, \dot{\boldsymbol{\varepsilon}}^{\text{p}}} = \sqrt{\frac{2}{3}} \|\dot{\boldsymbol{\varepsilon}}^{\text{p}}\| \tag{4.45}$$

describing the equivalent plastic strain rate.

4.3.   Non-linear finite element method

The FEM is a well established approach to approximate the solution of PDEs in terms of its weighted integral mean, by multiplying the strong form by a test function $\delta\boldsymbol{u}$ and integrating over the domain, which is then called the weak form of the PDE. In this section, the basic concept of (non-linear) FEM is briefly exemplified using the momentum balance given in Eq. (4.6) under the boundary conditions Eq. (4.7) and Eq. (4.8). Note that for bar and beam elements, the underlying PDE is given by the corresponding differential equations describing the deflection of a bar and the bending of a beam, respectively. For these examples as well as further derivations regarding the given example, the reader is referred to the book by Bathe [1996], on which this section is based.

The weak form of Eq. (4.6) is obtained as described above and results in

$$\int_{\mathcal{D}} \delta \boldsymbol{u} \cdot (\operatorname{div} \boldsymbol{\sigma} + \rho \boldsymbol{b}) \, \mathrm{d}v = 0. \tag{4.46}$$

In the context of solid mechanics, the test function $\delta \boldsymbol{u}$ can be interpreted as a virtual displacement. After a partial integration and applying the Gaussian divergence theorem, the weak form results in the mechanical equilibrium

$$\int_{\mathcal{D}} \operatorname{grad}(\delta \boldsymbol{u}) \cdot \cdot \boldsymbol{\sigma} \, \mathrm{d}v - \int_{\mathcal{D}} \delta \boldsymbol{u} \cdot \rho \boldsymbol{b} \, \mathrm{d}v - \int_{\partial_t \mathcal{D}} \delta \boldsymbol{u} \cdot \boldsymbol{t}^* \, \mathrm{d}a = 0. \tag{4.47}$$

The first term describes the virtual work of the internal forces, while the second and third terms are the virtual works of the body forces and the surface forces, subsumed to the virtual work of the external forces.

Spatial discretisation: To solve the weak form for the displacement field $\boldsymbol{u}$, the domain $\mathcal{D}$ is discretised into n_{el} elements $\mathcal{D}_{\mathrm{e}}$,

$$\mathcal{D} \simeq \mathcal{D}_h = \bigcup_{e=1}^{n_{\mathrm{el}}} \mathcal{D}_{\mathrm{e}}, \tag{4.48}$$

accepting a certain discretisation error. In Figure 4.2a the discretisation of an arbitrary two-dimensional (2D) domain $\mathcal{D}$ by 18 four-node elements is exemplified.
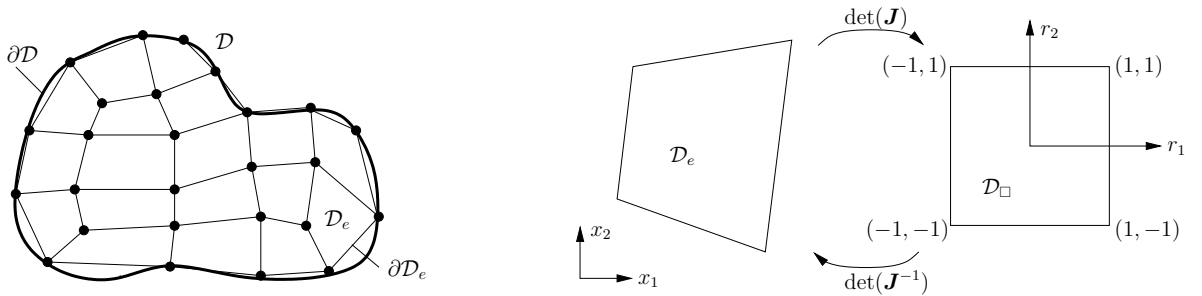
(a) Discretisation of the domain $\mathcal{D}$ into n_{el} elements $\mathcal{D}_{\mathrm{e}}$

(b) Relation between an element $\mathcal{D}_{\mathrm{e}}$ and the reference element $\mathcal{D}_{\square}$

Figure 4.2: Spatial discretisation of a domain $\mathcal{D}$ and the transformation of a finite element $\mathcal{D}_{\mathrm{e}}$ to a reference element $\mathcal{D}_{\square}$.

The weak form can then be solved for each element $\mathcal{D}_{\mathrm{e}}$, using shape functions $h_i(\boldsymbol{r})$ which are defined at a reference element $\mathcal{D}_{\square}$ given in a reference coordinate system $\boldsymbol{r}$. For that purpose, each FE is transformed to the reference element by the Jacobian determinant,

$$\det \mathbf{J} = \det \frac{\partial \boldsymbol{z}}{\partial \boldsymbol{r}}. \tag{4.49}$$

The transformation of a four-node element into a unified reference square is exemplified in Figure 4.2b. The shape functions have to fulfil the conditions of being complete and differentiable

as well as the requirements on the continuity of the model. In classical FE applications, this implies C_0-continuous shape functions, except for beam elements, where C_1-continuous shape functions are required. In this work, examples using one-dimensional (1D) bar elements, 1D beam elements and bi-linear 2D four-node elements are applied.

Isogeometric concept: The body geometry can be approximated locally for each element in terms of the shape functions by

$$z \approx \sum_{i=1}^{n_\mathrm{n}} h_i(\boldsymbol{r}) \boldsymbol{z}_i, \tag{4.50}$$

with n_n the number of nodes at each element. Storing the shape functions of each node in the **H**-matrix, this leads to the matrix formulation $\mathbf{z} = \mathbf{H}\,\hat{\mathbf{z}}$, where $\hat{\mathbf{z}}$ denotes the values determined at the nodes. Applying the isoparametric concept, displacements are approximated by the same shape functions, i.e.

$$\boldsymbol{u} \approx \sum_{i=1}^{n_\mathrm{n}} h_i(\boldsymbol{r}) \boldsymbol{u}_i, \tag{4.51}$$

$$\mathbf{u} = \mathbf{H}\,\hat{\mathbf{u}} \quad \text{and} \quad \delta\mathbf{u} = \mathbf{H}\,\delta\hat{\mathbf{u}}. \tag{4.52}$$

Furthermore, with the **B**-matrix containing the spatial derivations of the shape functions with respect to the global coordinates $\partial h_i/\partial z_j$, the strain $\boldsymbol{\varepsilon} = \operatorname{grad}\boldsymbol{u}$ can be obtained using matrix notation,

$$\boldsymbol{\varepsilon} = \mathbf{B}\,\hat{\mathbf{u}} \quad \text{and} \quad \delta\boldsymbol{\varepsilon} = \mathbf{B}\,\delta\hat{\mathbf{u}}. \tag{4.53}$$

Assembling: Using matrix instead of tensor notation, Eq. (4.47) can be formulated at each element by inserting Eq. (4.22) and Eq. (4.53),

$$\delta\hat{\mathbf{u}}^{\mathrm{T}} \left[\underbrace{\int_{\mathcal{D}_e} \mathbf{B}^{\mathrm{T}}\mathbf{C}\mathbf{B}\,\mathrm{d}v}_{\mathbf{K}_e}\,\hat{\mathbf{u}} - \underbrace{\int_{\mathcal{D}_e} \mathbf{H}^{\mathrm{T}}\rho\mathbf{b}\,\mathrm{d}v - \int_{\partial_t\mathcal{D}_e} \mathbf{H}^{\mathrm{T}}\mathbf{t}^*\,\mathrm{d}a}_{\hat{\mathbf{f}}_e} \right] = 0. \tag{4.54}$$

Here, $\mathbf{K}_e$ is the so-called element stiffness matrix and $\hat{\mathbf{f}}_e$ includes both, the body and the surface forces. The integrals are solved numerically, e.g. by Gaussian quadrature. Reassembling the FEs $\mathcal{D}_e$ to the complete domain $\mathcal{D}_h$ as given in Eq. (4.48),

$$\bigcup_{e=1}^{n_\mathrm{el}} \left[\mathbf{K}_e\,\hat{\mathbf{u}}_e - \hat{\mathbf{f}}_e \right] = 0, \tag{4.55}$$

the global mechanical equilibrium equation results in the linear equation system

$$\mathbf{K}\,\hat{\mathbf{u}} = \hat{\mathbf{f}}. \tag{4.56}$$

From the primary variables $\mathbf{u}$, the secondary variables at each element are obtained within the postprocessing, e.g. the strains by $\boldsymbol{\varepsilon} = \mathbf{B}\,\hat{\mathbf{u}}$ and the stresses by $\boldsymbol{\sigma} = \mathbf{C}\mathbf{B}\,\hat{\mathbf{u}}$.

Linearisation: Regarding non-linear material laws, the load is applied in incremental steps and the material matrix ${}^t\mathbf{C} = \frac{\partial\boldsymbol{\sigma}}{\partial\boldsymbol{u}}|_t$ has to be determined depending on the current primary variables within each step. For this purpose, a pseudo-time t is introduced in case of static problems. Then, the linearised equilibrium is given by

$$
{}^{t+\Delta t}\boldsymbol{\sigma} = {}^t\boldsymbol{\sigma} + {}^t\mathbf{C}\,\Delta\hat{\mathbf{u}} \tag{4.57}
$$

and Eq. (4.54) results in

$$
\delta\hat{\mathbf{u}}^{\mathrm{T}}\left[\underbrace{\int_{\mathcal{D}_e}\mathbf{B}^{\mathrm{T}}{}^t\mathbf{C}\mathbf{B}\,\mathrm{d}v}_{{}^t\mathbf{K}_e}\,\Delta\hat{\mathbf{u}} - \underbrace{\int_{\mathcal{D}_e}\mathbf{H}^{\mathrm{T}}\rho\,{}^{t+\Delta t}\mathbf{b}\,\mathrm{d}v - \int_{\partial_t\mathcal{D}_e}\mathbf{H}^{\mathrm{T}}\,{}^{t+\Delta t}\mathbf{t}^*\,\mathrm{d}a}_{{}^{t+\Delta t}\hat{\mathbf{f}}_e^{\mathrm{ex}}} + \underbrace{\int_{\mathcal{D}_e}\mathbf{B}^{\mathrm{T}}{}^t\boldsymbol{\sigma}\,\mathrm{d}v}_{{}^t\hat{\mathbf{f}}_e^{\mathrm{in}}}\right] = 0. \tag{4.58}
$$

Assembling the elements to the global element stiffness matrix as well as the external and internal forces to a global column matrix, the linearised equation system at time t reads

$$
{}^t\mathbf{K}\,\Delta\hat{\mathbf{u}} = {}^{t+\Delta t}\hat{\mathbf{f}}^{\mathrm{ex}} - {}^t\hat{\mathbf{f}}^{\mathrm{in}}. \tag{4.59}
$$

While the load increment is increased with each pseudo-time step in an outer loop, the equilibrium Eq. (4.59) needs to be solved iteratively for each load step in an inner loop, e.g. by the Newton-Raphson method.

5. Sampling Based Stochastic Finite Element Methods

When aleatory uncertain quantities are considered as input parameters within a partial differential equation (PDE), Eq. (4.1) can be extended to a stochastic partial differential equation (SPDE),

$$\begin{cases} \mathcal{L}(\omega, \boldsymbol{z}; Y) = f(\omega, \boldsymbol{z}), & \boldsymbol{z} \in \mathcal{D} \\ \mathcal{B}(\omega, \boldsymbol{z}; Y) = g(\omega, \boldsymbol{z}), & \boldsymbol{z} \in \partial\mathcal{D} \end{cases}, \tag{5.1}$$

which additionally holds within the probability space $(\Omega, \mathcal{F}, P)$ as defined in Section 2.1. The aim of a stochastic finite element method (SFEM) is to find the stochastic function $Y = Y(\omega, \boldsymbol{z}) : \Omega \times \Omega \mapsto \mathbb{R}$, which is the solution for P-almost everywhere $\omega \in \Omega$ [Xiu and Hesthaven, 2005]. The dimension N of the sample space $\Omega = \Omega_1 \times \cdots \times \Omega_N$, $\Omega_i \subset \mathbb{R}$, $i = 1, \ldots, N$ depends on the amount of considered random input quantities. Especially when random fields are included, N increases quickly as it is driven by the chosen truncation order T in this case. In general, the stochastic dimension is given by

$$N = n_{\mathrm{RV}} + \sum_{i=1}^{n_{\mathrm{RF}}} T_i, \tag{5.2}$$

where n_{RV} is the number of random variables and n_{RF} the number of random fields which are considered as random input quantities. Concerning sophisticated sampling techniques, the stochastic dimension can become challenging in terms of the curse of dimensionality.

There exist intrusive SFEM as well as non-intrusive, i.e. sampling based approaches. In this work, only the latter are considered as the applicability of intrusive SFEM is quite limited. Note that besides SFEM, there exist also the interval finite element method [Moens and Vandepitte, 2005, Moens and Hanss, 2011] to consider epistemic (i.e. interval valued) parameters in finite element (FE) problems. This approach is however not considered in this work.

In this chapter, three well-established, sampling based approaches are introduced in Section 5.1 in order to solve SPDEs. Afterwards, the methods are applied to one-dimensional (1D) and two-dimensional (2D) stochastic FE problems in Section 5.2. Here, the focus is on the propagation of random fields, which involves high stochastic dimensions. Furthermore, the applicability of the methods regarding non-linear material models is investigated. Finally, the approaches are compared and discussed in Section 5.3.

Model assumptions: Additionally to the model assumptions stated in Chapter 4 in terms of the mechanical conditions, the following model assumptions are made with respect to the uncertainties.

- Only *aleatory* uncertainties are considered in this chapter. The propagation of mixed (i.e. aleatory and epistemic) uncertainties is discussed in Chapter 6.

- All aleatory input quantities are considered *Gaussian distributed*, although this is physically not consistent with the used material parameters. In terms of the largest considered relative standard deviation of $\sigma_X = 0.1\mu_X$, this means a probability of $f_X(x < 0) = 7.62 \times 10^{-24}$ to obtain a negative sample. It is assured during all simulations that no negative samples occurred.

- Input random quantities are assumed to be *independent*, i.e. the joint probability density function (PDF) can be obtained by Eq. (2.15). This holds for both, for an input random vector $\boldsymbol{X} = (X_1(\omega), \ldots, X_N(\omega))$ of different parameters or for the components $\boldsymbol{\xi} = (\xi_1, \ldots, \xi_T)$ corresponding to an input random field.

- All applied models are assumed to be sufficiently *smooth*. In Subsection 5.2.2 it will be shown that this is not always appropriate and the consequences following in that case are discussed.

- Only *static* problems are considered, i.e. there are no (time depending) random processes.

- Each quantity of interest (QoI) is considered as an *individual scalar stochastic response field* $Y(\boldsymbol{x}, \boldsymbol{z})$, e.g. the displacements $u_1(\boldsymbol{x}, \boldsymbol{z})$ and $u_2(\boldsymbol{x}, \boldsymbol{z})$, instead of summarising them into vector fields, $\boldsymbol{Y}(\boldsymbol{x}, \boldsymbol{z})$ accordingly.

The aim of this chapter is to introduce and apply well-known global sampling techniques. All of them have some severe drawbacks which will be discussed and exemplified. There has been (and still is) a great effort in the research community to overcome these challenges for each of the described approaches, no matter whether they occur in terms of high dimensionality, non-linearity or computational effort. However, when different correlation length scenarios are compared within an imprecise random field, assuring an appropriate input description is already challenging, as pointed out in Section 3.3. Introducing further difficult to control error sources in the model propagation by applying highly sophisticated sampling techniques featuring adaptive or anisotropic refinements seems therefore not appropriate at this state of research concerning imprecise random fields. Therefore, advanced techniques are mentioned incidentally but not discussed further in this work.

5.1.   Sampling approaches

The fundamental idea of all sampling approaches is to propagate individual realisations deterministically through a given model. Regarding input parameters which are described by a random variable, a realisation $x_j = X(\omega_j)$ follows directly from ω_j. On the other hand, a random field realisation $\bar{x}_j(\boldsymbol{z}) = \bar{X}(\omega_j, \boldsymbol{z})$ described by a truncated Karhunen-Loève (KL) expansion is generated by inserting a set of independent standard normal distributed random variables $\boldsymbol{\xi}_j(\omega_i) = (\xi_1, \ldots, \xi_T)_j$ into Eq. (3.9). These values $\boldsymbol{\xi}_j$ can be either sampled pseudo-randomly or chosen artificially, depending on the applied approach.

Three sampling techniques are briefly introduced in the following. In each of the approaches, Eq. (5.1) is solved repetitively in terms of the deterministic PDE

$$\begin{cases} \mathcal{L}(\boldsymbol{x}_j, \boldsymbol{z}; y_j) = f(\boldsymbol{x}_j, \boldsymbol{z}), & \boldsymbol{z} \in \mathcal{D} \\ \mathcal{B}(\boldsymbol{x}_j, \boldsymbol{z}; y_j) = g(\boldsymbol{x}_j, \boldsymbol{z}), & \boldsymbol{z} \in \partial\mathcal{D} \end{cases} \tag{5.3}$$

resulting for each N-dimensional realisation $\boldsymbol{x}_j, j = 1, \ldots, n_{\mathrm{s}}$, with n_{s} the number of realisations [Xiu and Hesthaven, 2005]. The approaches differ in the way of choosing $\boldsymbol{x}_j$ and consequently in the way of evaluating the stochastic response $Y(\boldsymbol{x}, \boldsymbol{z})$ from the model evaluations $y_j = \mathcal{M}(\boldsymbol{x}_j)$.

The approaches are valid for both, random vector (or variable) input parameters $\boldsymbol{X}(\omega)$ and random field parameters $X(\omega, \boldsymbol{z})$. Therefore, when random input quantities are denoted by $\boldsymbol{X}$ or input realisations by $\boldsymbol{x}_j$, this can always mean both, a random vector $\boldsymbol{X} := \boldsymbol{X}(\omega)$ or a random field $\boldsymbol{X} := X(\omega, \boldsymbol{z})$, and consequently a random vector realisation $\boldsymbol{x}_j := \boldsymbol{X}(\omega_j)$ or a random field realisation $\boldsymbol{x}_j := x_j(\boldsymbol{z}) = X(\omega_j, \boldsymbol{z})$. The model response $y_j(\boldsymbol{z}) = \mathcal{M}(\boldsymbol{x}_j, \boldsymbol{z})$ of a propagated realisation $\boldsymbol{x}_j$ is a deterministic function. Analogously to the state of a random field, the state of the stochastic response field at a specific point $\boldsymbol{z}_J$ is denoted by $Y_J(\boldsymbol{x}) = Y(\boldsymbol{x}, \boldsymbol{z}_J) = \mathcal{M}(\boldsymbol{X}, \boldsymbol{z}_J)$.

As mechanical problems given on a physical domain $\mathcal{D}$ are considered in this work, the stochastic response $Y(\boldsymbol{x}, \boldsymbol{z}) = \mathcal{M}(\boldsymbol{X}, \boldsymbol{z})$ is generally described by a stochastic response field, independent of the random input parameter $\boldsymbol{X}$ being a random vector (or variable) $\boldsymbol{X} := \boldsymbol{X}(\omega)$ or a (or several) random field $\boldsymbol{X} := X(\omega, \boldsymbol{z})$. Regarding the used FE models, this means that the stochastic response is available for the node values $\hat{\mathbf{z}}$, i.e. the statistic evaluations can be straightforwardly performed at each individual node value. To keep this in mind, the spatial coordinate $\hat{\mathbf{z}}$ is kept in the equations to emphasise the spatial dependency of the stochastic response and to make clear that each equation is evaluated individually at each FE node.

5.1.1. Monte Carlo simulation

A straightforward method to use random quantities within a stochastic simulation is given by Monte Carlo (MC) methods [Fishman, 1996]. In case of a brute force MC simulation, n_{MC} realisations $\boldsymbol{x}_j, j = 1, \ldots, n_{\mathrm{MC}}$ are sampled pseudo-randomly, either in terms of the random variable input parameters or the set of standard normal distributed random variables $\boldsymbol{\xi}_j$ to obtain a random field realisation. Eq. (5.3) is then solved for each realisation by propagating $\boldsymbol{x}_j$ directly through the considered model,

$$y_j(\hat{\mathbf{z}}) = \mathcal{M}(\boldsymbol{x}_j, \hat{\mathbf{z}}), \quad j = 1, \ldots, n_{\mathrm{MC}}. \tag{5.4}$$

As the sampled input parameters follow the chosen distribution, the stochastic response $Y(\boldsymbol{x}, \hat{\mathbf{z}})$ of the quantity of interest can be determined directly by a statistical evaluation of the model outcome $y_j(\hat{\mathbf{z}})$ - e.g. in terms of an empirical PDF $f_Y(y_i)$ or an empirical cumulative distribution function (CDF) $F_Y(y_i)$ - if the sample size n_{MC} is sufficiently large. Furthermore, the stochastic moments can be evaluated by statistics as well. For instance, the mean value follows as

$$\mu\{Y\}(\hat{\mathbf{z}}) = \frac{1}{n_{\mathrm{MC}}} \sum_{i=1}^{n_{\mathrm{MC}}} y_j(\hat{\mathbf{z}}) \tag{5.5}$$

and the standard deviation $\sigma\{Y\}(\hat{\mathbf{z}})$ can be obtained from the variance, which is given by

$$\sigma^2\{Y\}(\hat{\mathbf{z}}) = \frac{1}{n_{\mathrm{MC}} - 1} \sum_{i=1}^{n_{\mathrm{MC}}} \left[\, y_j(\hat{\mathbf{z}}) - \mu\{Y\}(\hat{\mathbf{z}}) \,\right]^2 . \tag{5.6}$$

The stochastic moments are suited to evaluate the convergence. If several MC simulations with each $j = 1, \ldots, n_{\mathrm{MC}}$ realisations result in sufficiently similar stochastic moments, the simulations can considered to be converged. Alternatively, an MC simulation can be enlarged gradually by further realisation sets, until the relative error of the new sample set with regard to the old one is sufficiently small.

The main advantages [Le Maître and Knio, 2010] of brute force MC method are its independence from the stochastic dimension as well as its straightforward implementation. Furthermore it is very robust, i.e. it is applicable for any model, no matter whether it is monotonic or not, linear or non-linear, smooth or non-smooth and so on. The number of sample propagations can be increased until a required error is achieved. Results that are already obtained can be simply enriched by further realisations. However, the complexity of the model naturally affects the computation time of each individual realisation. In this case, MC method can become computationally expensive due to its poor convergence rate of $1/\sqrt{n_{\mathrm{MC}}}$. This often leads to about $n_{\mathrm{MC}} = 10^4$ samples to be propagated to obtain sufficiently converged stochastic moments. Furthermore, if a probability of failure of 10^{-p} is supposed to be estimated, $n_{\mathrm{MC}} = 10^{p+2}$ samples are required [Sudret, 2015]. For example, if a reliability of 99.9 % is required, i.e. the probability of failure is $0.001 = 10^{-3}$, this results in $n_{\mathrm{MC}} = 10^5$ MC samples to be propagated.

There are many attempts to improve MC method in terms of the convergence rate, but they restrict the brute force approach with regard to its general applicability discussed above. For instance, the samples can be chosen more expedient by using Sobol sequences (quasi MC method) [Kuo et al., 2012] or Latin hypercube sampling [Helton and Davis, 2003]. While the first is only applicable for low-dimensional problems, the second approach most notably suffers from the fact that already obtained simulations cannot be recycled by adding further samples, if a required error is not achieved. Alternatively, multi-level MC methods [Giles, 2015] aim to reduce the computational cost by introducing different levels of mesh refinements, using only small sample sizes for the higher resolutions. A more general approach enabling all different kinds of high- and low-fidelity measures is given by multi-fidelity MC method [Peherstorfer et al., 2018].

5.1.2.   Stochastic collocation method

The main idea of the stochastic collocation (SC) method [Xiu and Hesthaven, 2005] is to choose the random input from a pre-defined grid, so-called *collocation points*, instead of sampling it pseudo-randomly. Given a set of n_{SC} collocation points $\mathcal{X}^N = (\boldsymbol{x}_1, \ldots, \boldsymbol{x}_{n_{\mathrm{SC}}})$, each N-dimensional collocation point $\boldsymbol{x}_j = (x_1, \ldots, x_N)_j$ defines one realisation of N independent random variables with the joint PDF $f_{\boldsymbol{X}}(\boldsymbol{x})$ as given in Eq. (2.15). For each collocation point, Eq. (5.3) is solved repetitively by deterministic model evaluations inserting $\boldsymbol{x}_j$. In order to use SC method to propagate random fields, each random field realisation $\bar{x}_j = \bar{X}(\omega_j, \hat{\mathbf{z}}), j =$

$1, \ldots, n_{\mathrm{SC}}$, is obtained by inserting the coordinates of one N-dimensional collocation point $\boldsymbol{x}_j = (x_1, \ldots, x_{N=T})$ into the standard normal distributed random variables $\boldsymbol{\xi}_j(\omega_i) = (\xi_1, \ldots, \xi_T)$ required for the truncated KL expansion given in Eq. (3.9).

Assuming the stochastic response $Y(\boldsymbol{x}, \hat{\mathbf{z}})$ to be sufficiently smooth within the random space $\zeta \subseteq \mathbb{R}^N$ and obtaining the solution $y_j(\hat{\mathbf{z}}) = \mathcal{M}(\boldsymbol{x}_j, \hat{\mathbf{z}})$ of Eq. (5.3) by propagating each collocation point $\boldsymbol{x}_j$, the stochastic response $\tilde{Y}(\boldsymbol{x}, \hat{\mathbf{z}})$ is approximated globally by interpolation within the N-dimensional random space ζ,

$$\tilde{Y}(\boldsymbol{x}, \hat{\mathbf{z}}) = \tilde{\mathcal{M}}(\boldsymbol{x}, \hat{\mathbf{z}}) = \sum_{j=1}^{n_{\mathrm{SC}}} y_j(\hat{\mathbf{z}}) H_j(\boldsymbol{x}), \quad \hat{\mathbf{z}} \in \mathcal{D}, \quad \boldsymbol{x} \in \zeta, \tag{5.7}$$

with $H_j(\boldsymbol{x}) \in V$ being Lagrange polynomials within the interpolation space V fulfilling $H_j(x_i) = \delta_{ij}$, $i = 1, \ldots, N$, $j = 1, \ldots, n_{\mathrm{SC}}$ for each collocation point $\boldsymbol{x}_j$ [Xiu and Hesthaven, 2005]. The multivariate Lagrange polynomials $H_j(\boldsymbol{x})$ can be constructed by divided differences, e.g. recursively in terms of the Newton scheme or adaptively using the Aitken-Neville algorithm [Jablonski, 2014]. In case of $\zeta_1 = \cdots = \zeta_N$ and $f_{X_1}(x_1) = \cdots = f_{X_N}(x_N)$ - as it is the case for Gaussian random fields described by KL expansion - a univariate quadrature rule is enabled for the same quadrature level.

Using the metamodel $\tilde{\mathcal{M}}$ given by Eq. (5.7), the solution of Eq. (5.3) can be estimated for any randomly sampled input realisation without propagating it through the model again. Doing so for a sufficiently large sample size, the stochastic response can be obtained by statistics [Bressolette et al., 2010]. Additionally, the stochastic moments can be determined directly by interpolation, for instance it is for the expected value and variance,

$$\mu\{\tilde{Y}\}(\hat{\mathbf{z}}) = \sum_{j=1}^{n_{\mathrm{SC}}} y_j(\hat{\mathbf{z}}) \int_\zeta H_j(\boldsymbol{x}) f_{\boldsymbol{X}}(\boldsymbol{x}) \, \mathrm{d}\boldsymbol{x}, \tag{5.8}$$

$$\sigma^2\{\tilde{Y}\}(\hat{\mathbf{z}}) = \sum_{j=1}^{n_{\mathrm{SC}}} \left[y_j(\hat{\mathbf{z}}) - \mu\{\tilde{Y}\}(\hat{\mathbf{z}}) \right]^2 \int_\zeta H_j(\boldsymbol{x}) f_{\boldsymbol{X}}(\boldsymbol{x}) \, \mathrm{d}\boldsymbol{x}. \tag{5.9}$$

Here, the information about the input distribution is not incorporated by the sampling process but in terms of the joint probability function $f_{\boldsymbol{X}}(\boldsymbol{x})$ [Xiu and Hesthaven, 2005]. Note that solving the N-dimensional integral can become computational expensive for high stochastic dimensions. However, when Gaussian random fields are considered using KL expansion, the integrals corresponding to j only need to be solved (and stored) once for each grid type of predefined collocation points according to N, as the underlying random variables $\boldsymbol{\xi}$ are always standard normal distributed.

Smolyak algorithm: A straightforward approach to construct the set $\mathcal{X}^N$ of N-dimensional collocation points is to apply the full tensor product $\mathcal{X}^N = \left(\mathcal{X}^{(i_1)} \otimes \cdots \otimes \mathcal{X}^{(i_N)} \right)$ on the 1D collocation point sets $\mathcal{X}^{(i)}$, each containing m_i nodes. However, with $n_{\mathrm{SC}} = m_i^N$ the number of collocation points increases quickly for high stochastic dimensions, which is known as the curse of dimensionality.

As introduced by Xiu and Hesthaven [2005], the aim of applying Smolyak algorithm is to reduce the number of collocation points by neglecting certain polynomial order combinations in the higher dimensions, which do not have a significant effect to the result. This is achieved by combining only these 1D collocation point sets, for which the multi-index $\boldsymbol{\alpha} = (\alpha_1, \ldots, \alpha_N) \in \mathbb{N}_+^N$ fulfils

$$k + 1 \leq |\boldsymbol{\alpha}| \leq k + N, \quad \text{with} \quad |\boldsymbol{\alpha}| = \alpha_1 + \cdots + \alpha_N, \tag{5.10}$$

where k is the Smolyak level controlling the univariate polynomial order. Consequently, only these indices α_i are contained in the index set $\mathcal{A}(k, N)$, for which Eq. (5.10) is fulfilled. By this, the number of collocation points n_{SC} contained in the sparse grid depends on both, the Smolyak level k and the stochastic dimesnion N. Note that there are also further (isotropic and anisotropic) rules to select $\boldsymbol{\alpha}$, as reviewed e.g. by Jablonski [2014]. However, in this work only the rule given by Eq. (5.10) is used.

Based on the index set $\mathcal{A} := \mathcal{A}(k, N)$, a sparse set of collocation points is obtained by

$$\mathcal{X}_{\mathrm{s}}^N = \bigcup_{\boldsymbol{\alpha} \in \mathcal{A}} \left(\mathcal{X}_{\mathrm{s}}^{(\alpha_1)} \times \cdots \times \mathcal{X}_{\mathrm{s}}^{(\alpha_N)} \right), \tag{5.11}$$

which is called sparse grid in the following. The Smolyak metamodel is then given by

$$\tilde{Y}(\boldsymbol{x}, \hat{\mathbf{z}}) = \tilde{\mathcal{M}}(\boldsymbol{x}, \hat{\mathbf{z}}) = \sum_{\boldsymbol{\alpha} \in \mathcal{A}} \eta(|\boldsymbol{\alpha}|) \cdot \left(\mathcal{I}^{(\alpha_1)} \times \cdots \times \mathcal{I}^{(\alpha_N)} \right), \tag{5.12}$$

with the 1D interpolants

$$\mathcal{I}^{(\alpha_i)} := \mathcal{I}(\tilde{Y}) \left(x^{(\alpha_i)}, \hat{\mathbf{z}} \right) = \sum_{k=1}^{m_\alpha} y \left(x_k^{(\alpha_i)}, \hat{\mathbf{z}} \right) \cdot H_k^{(\alpha_i)}(x) \tag{5.13}$$

and the factor $\eta(|\boldsymbol{\alpha}|)$ defined as

$$\eta(|\boldsymbol{\alpha}|) = (-1)^{k+N-|\boldsymbol{\alpha}|} \cdot \binom{N-1}{k+N-|\boldsymbol{\alpha}|}. \tag{5.14}$$

The number m_{α_i} of collocation points used within the dimension i is chosen by the rule

$$m_{\alpha_i} = \begin{cases} 1 & \text{if } \alpha_i = 1 \\ 2^{\alpha_i - 1} + 1 & \text{if } \alpha_i > 1 \end{cases}. \tag{5.15}$$

For the stochastic moments given before, it is now

$$\mu\{\tilde{Y}\}(\hat{\mathbf{z}}) = \sum_{\boldsymbol{\alpha} \in \mathcal{A}} \eta(|\boldsymbol{\alpha}|) \sum_{k_1=1}^{m_{\alpha_1}} \cdots \sum_{k_N=1}^{m_{\alpha_N}} y \left(x_{k_1}^{(\alpha_1)}, \ldots, x_{k_N}^{(\alpha_N)}, \hat{\mathbf{z}} \right) \cdot \mathcal{J}(k, \alpha), \tag{5.16}$$

$$\sigma^2\{\tilde{Y}\}(\hat{\mathbf{z}}) = \sum_{\boldsymbol{\alpha} \in \mathcal{A}} \eta(|\boldsymbol{\alpha}|) \sum_{k_1=1}^{m_{\alpha_1}} \cdots \sum_{k_N=1}^{m_{\alpha_N}} \left[y \left(x_{k_1}^{(\alpha_1)}, \ldots, x_{k_N}^{(\alpha_N)}, \hat{\mathbf{z}} \right) - \mu\{\tilde{Y}\}(\hat{\mathbf{z}}) \right]^2 \cdot \mathcal{J}(k, \alpha), \tag{5.17}$$

with the N-dimensional integral

$$\mathcal{J}(k, \alpha) = \int_\zeta \left(H_{k_1}^{\alpha_1}(\boldsymbol{x}) \otimes \cdots \otimes H_{k_N}^{\alpha_N}(\boldsymbol{x}) \right) f_{\boldsymbol{X}}(\boldsymbol{x}) \, \mathrm{d}\boldsymbol{x}. \tag{5.18}$$

Note that the stochastic dimension has not changed using the Smolyak algorithm and therefore, solving Eq. (5.18) is computationally as expensive as solving the integral for the full grid. Still, compared to the full grid SC method, the efficiency is improved significantly by requiring far less model evaluations. For high stochastic dimensions, solving Eq. (5.18) by Gauss cubature or similar integration schemes can become too expensive. Instead, the integral can be solved by deterministic MC or collocation methods.

As N is usually fixed, the accuracy of the sparse SC method is improved by increasing the Smolyak level k. However, for higher stochastic dimensions, this may lead to a significant increase of n_{SC} from one level to the next. For this reason, the number of collocation points cannot be chosen in a flexible manner. Furthermore, due to the use of global interpolation, Smolyak algorithm requires a sufficiently smooth solution within the random space in order to achieve a fast convergence. Several extensions have been proposed regarding the challenges occurring from non-smooth or high-dimensional problems, e.g. spatially adaptive [Pflüger, 2010] or anisotropic [Nobile et al., 2008] sparse grids. A sound survey of different sparse grids and interpolation strategies in terms of general collocation methods regarding PDEs is provided by Bungartz and Griebel [2004].

Choice of nodal points: Multiple sparse grid definitions are available based on different choices regarding the 1D collocation point set including m_{α_i} points. An often applied sparse grid is the Clenshaw-Curtis grid, obtained by choosing the extrema of Chebyshev polynomials for the 1D point set, but also Gauss points can be considered [Xiu and Hesthaven, 2005]. However, these grids are defined on a bounded domain $\zeta = [-1, 1]^N$ but unbounded grids $\zeta = (-\infty, \infty)^N$ appear more useful in terms of KL expansion, where the collocation points are used to model standard normal distributed (i.e. unbounded) random variables. For that purpose, unbounded sparse grids can be obtained by Gauss-Hermite points [Jablonski, 2014], Kronrod-Patterson sequences [Genz and Keister, 1996] or Gauss-Leja points [Narayan and Jakeman, 2014].

All three unbounded sparse grid types have been investigated intensively in a recent survey by Dannert et al. [2022] regarding their applicability in terms of high stochastic dimensions and non-linear material models. It has been shown in this study that global SC method is not appropriate to propagate (high-dimensional) random fields through non-linear problems, especially when they are not sufficiently smooth. Although the grid size of the Kronrod-Patterson sparse grid increases much faster than the grid sizes of the alternative sparse grid formulations, it has proven to be the most robust one with respect to the given application. For this reason, the Kronrod-Patterson grid is used in this work, when comparing different sampling approaches in Section 5.2. The 2D SC grids obtained by Kronrod-Patterson sequence are exemplified for an increasing Smolyak level $k = 1, \ldots, 4$ in Figure 5.1.

While the full grid is depicted in grey circles, the sparse grid points are given as black points. It can be seen that the number of collocation points is reduced drastically using sparse grids. Furthermore, it can be noticed that the collocation points spread in the random space with increasing k. Note that Kronrod-Patterson grids are nested (i.e. $\mathcal{X}_{k_1}^N \subset \mathcal{X}_{k_2}^N$ if $k_1 < k_2$) and symmetric but the underlying quadrature rule does not provide strictly positive weights.
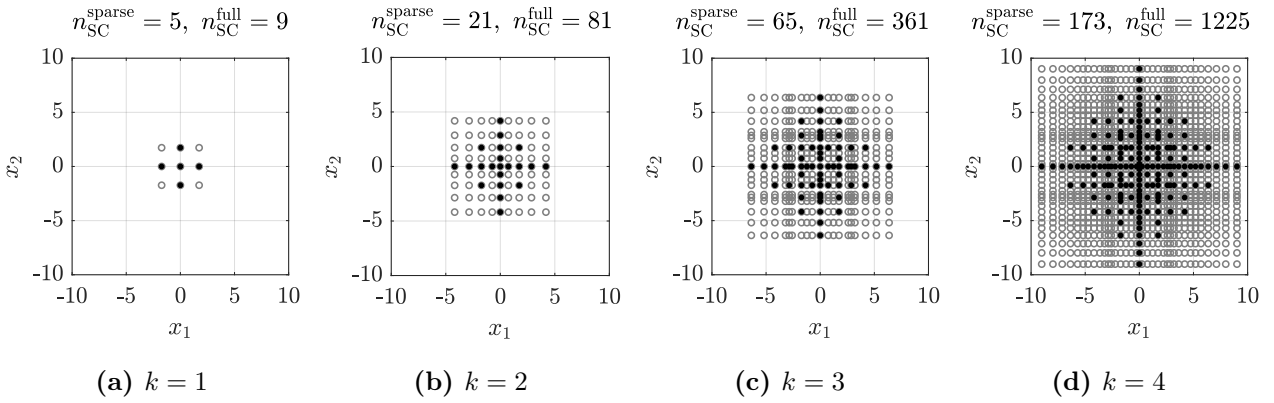
Figure 5.1: Two-dimensional sparse grids (black points) of the unbounded Kronrod-Patterson grid with its grid size n_{SC} increasing with a raising Smolyak level k as well as the corresponding full grids (grey circles) [Dannert et al., 2022].

Error measure: Starting the SC simulation with $k = 1$ and increasing the level step by step, a relative error of any quantity $\{\cdot\}$ (e.g. the stochastic moments of a QoI) can be quantified for each level k in comparison to the level before,

$$\epsilon_k\{\cdot\} = \frac{|\{\cdot\}_k - \{\cdot\}_{k-1}|}{|\{\cdot\}_k|}. \tag{5.19}$$

The deterministic solution (i.e. all random parameters considered with their mean values) is defined to be $\{\cdot\}_{k=0}$. It corresponds to a sparse grid containing only one collocation point, i.e. the point $[0]^N$. During an SC simulation, k is increased until a required error ϵ_k is achieved or the number of collocation points n_{SC} exceeds a predefined threshold.

Note that the result of a propagated collocation point from the lower levels can be reused, if the collocation point is also included in the grid obtained by the higher level. For this purpose, nested grids such as the Kronrod-Patterson sparse grid are particularly beneficial to save computational effort.

5.1.3. Polynomial chaos expansion

Also for polynomial chaos (PC) expansion methods [Sudret, 2015], the realisations are sampled pseudo-randomly, as it is done for the brute force MC method and the SPDE to be solved follows as given in Eq. (5.3). In the context of PC expansion, the sampled input realisations $\boldsymbol{x}_j, j = 1, \ldots, n_{\mathrm{PC}}$ and corresponding solutions $y_j(\hat{\boldsymbol{z}}) = \mathcal{M}(\boldsymbol{x}_j, \hat{\boldsymbol{z}})$ are called *experimental design* and can be obtained by brute force MC or any advanced sampling of $\boldsymbol{x}_j$. However, the concept is then to create a metamodel from a set of propagated samples which is much smaller than the number of MC samples, i.e. $n_{\mathrm{PC}} \ll n_{\mathrm{MC}}$. Then, similar to the use of the SC metamodel, the response of further samples can be estimated directly by the PC metamodel and do not have to be propagated.

In the case of PC methods, a stochastic response $\tilde{Y}(\boldsymbol{x}, \hat{\boldsymbol{z}})$ with finite variance can be described by an orthonormal basis $\Psi_{\boldsymbol{\alpha}}(\boldsymbol{x})$ using the metamodel

$$\tilde{Y}(\boldsymbol{x}, \hat{\boldsymbol{z}}) = \tilde{\mathcal{M}}(\boldsymbol{x}, \hat{\boldsymbol{z}}) = \sum_{\boldsymbol{\alpha} \in \mathcal{A}} \hat{a}_{\boldsymbol{\alpha}}(\hat{\boldsymbol{z}}) \Psi_{\boldsymbol{\alpha}}(\boldsymbol{x}), \tag{5.20}$$

with the coefficients $\hat{a}_{\boldsymbol{\alpha}}(\hat{\mathbf{z}})$ to be determined from the experimental design as described later. The multivariate polynomials $\Psi_{\boldsymbol{\alpha}}(\boldsymbol{x})$ corresponding to the multi-index $\boldsymbol{\alpha} = (\alpha_1, \ldots, \alpha_N), \alpha_i \in \mathbb{N}^N$, are obtained from the univariate polynomials $\psi_{\alpha_i}^{(i)}(x_i)$,

$$\Psi_{\boldsymbol{\alpha}}(\boldsymbol{x}) = \prod_{i=1}^{N} \psi_{\alpha_i}^{(i)}(x_i), \tag{5.21}$$

with $\psi_{\alpha_i}^{(i)}(x_i)$ being (normalised) 1D orthonormal polynomials according to the polynomial degree p. For Gaussian random quantities, Hermite polynomials are the optimal choice, which is also known as homogeneous chaos expansion [Wiener, 1938]. Using the Askey scheme of orthogonal polynomials, Xiu and Karniadakis [2002] generalised the PC approach to converge optimally according to an arbitrary underlying probability distribution on $\boldsymbol{x} \in \zeta \subseteq \mathbb{R}^N$.

Next to a statistical evaluation of the samples propagated by the metamodel in Eq. (5.20), the stochastic moments can be determined directly from the coefficients $\hat{a}(\hat{\mathbf{z}})$, e.g. it is for the expected value and the variance

$$\mu\{\tilde{Y}\}(\hat{\mathbf{z}}) = \hat{a}_0(\hat{\mathbf{z}}), \tag{5.22}$$

$$\sigma^2\{\tilde{Y}\}(\hat{\mathbf{z}}) = \sum_{\boldsymbol{\alpha} \in \mathcal{A} \setminus 0} \hat{a}_{\boldsymbol{\alpha}}^2(\hat{\mathbf{z}}). \tag{5.23}$$

The index set $\mathcal{A}$ can be determined according to different truncation schemes as described in the following.

Truncation scheme: The multi index $\boldsymbol{\alpha} \in \mathcal{A}$ depends on the stochastic dimension N and a chosen polynomial degree p as follows

$$\mathcal{A}(N, p) = \{\boldsymbol{\alpha} \in \mathbb{N}^N : |\boldsymbol{\alpha}| \leq p\}, \tag{5.24}$$

$$|\boldsymbol{\alpha}| = \alpha_1 + \ldots + \alpha_N.$$

Instead of using the total polynomial degree p, the set can be further reduced by choosing a hyperbolic truncation, i.e.

$$\mathcal{A}(N, p, q) = \{\boldsymbol{\alpha} \in \mathbb{N}^N : ||\boldsymbol{\alpha}||_q \leq p\}, \tag{5.25}$$

$$||\boldsymbol{\alpha}||_q = (\alpha_1^q + \ldots + \alpha_N^q)^{1/q}.$$

In Figure 5.2 three index sets $\boldsymbol{\alpha} = (\alpha_1, \alpha_2)$ for $N = 2$ are depicted for different q-norms regarding the polynomial degrees $p = 3$ and $p = 6$. The index set of the q-norm $||\boldsymbol{\alpha}||_1 \leq p$ is equivalent to the total polynomial degree $|\boldsymbol{\alpha}| \leq p$.

Determine the coefficients: The coefficients $\hat{a}_{\boldsymbol{\alpha}}(\hat{\mathbf{z}})$ can be obtained by the experimental design using projection methods or a regression approach [Sudret, 2015]. In case of projection, an N-dimensional integral needs to be solved, limiting the approach in terms of high stochastic dimensions similarly to the integral in Eq. (5.18). For this reason, only the regression approach based on least-square minimisation is used in this work. The aim of the underlying least-square

minimisation approach is to find the set of coefficients $\hat{a}(\hat{\mathbf{z}}) = \{\hat{a}_{\boldsymbol{\alpha}}(\hat{\mathbf{z}}), \boldsymbol{\alpha} \in \mathcal{A}\}$ for which the mean square error

$$\mathrm{E}\left[\epsilon^2\right] = \mathrm{E}\left[\left(\mathcal{M}(\boldsymbol{x}_j, \hat{\mathbf{z}}) - \tilde{\mathcal{M}}(\boldsymbol{x}, \hat{\mathbf{z}})\right)^2\right] \tag{5.26}$$

is minimised. Note that the first term is given by the model evaluation of the sampled realisations (i.e. the experimental design) while the second term is the metamodel given by Eq. (5.20). With the information matrix $\mathbf{A}$ containing the values of the orthonormal basis of $\boldsymbol{x}$, i.e. $A_{ji} = \Psi_{\alpha_j}(\boldsymbol{x}_j)$, the solution of Eq. (5.26) can be found by

$$\hat{a}(\hat{\mathbf{z}}) = (\mathbf{A}^{\mathrm{T}}\mathbf{A})^{-1}\mathbf{A}^{\mathrm{T}}\,\mathcal{Y}(\hat{\mathbf{z}}), \tag{5.27}$$

where the column matrix $\mathcal{Y}(\hat{\mathbf{z}}) = (y_1(\hat{\mathbf{z}}), \dots, y_{n_{\mathrm{PC}}}(\hat{\mathbf{z}}))^{\mathrm{T}}$ contains the experimental design $y_j(\hat{\mathbf{z}}) = \mathcal{M}(\boldsymbol{x}_j, \hat{\mathbf{z}}), j = 1, \dots, n_{\mathrm{PC}}$.
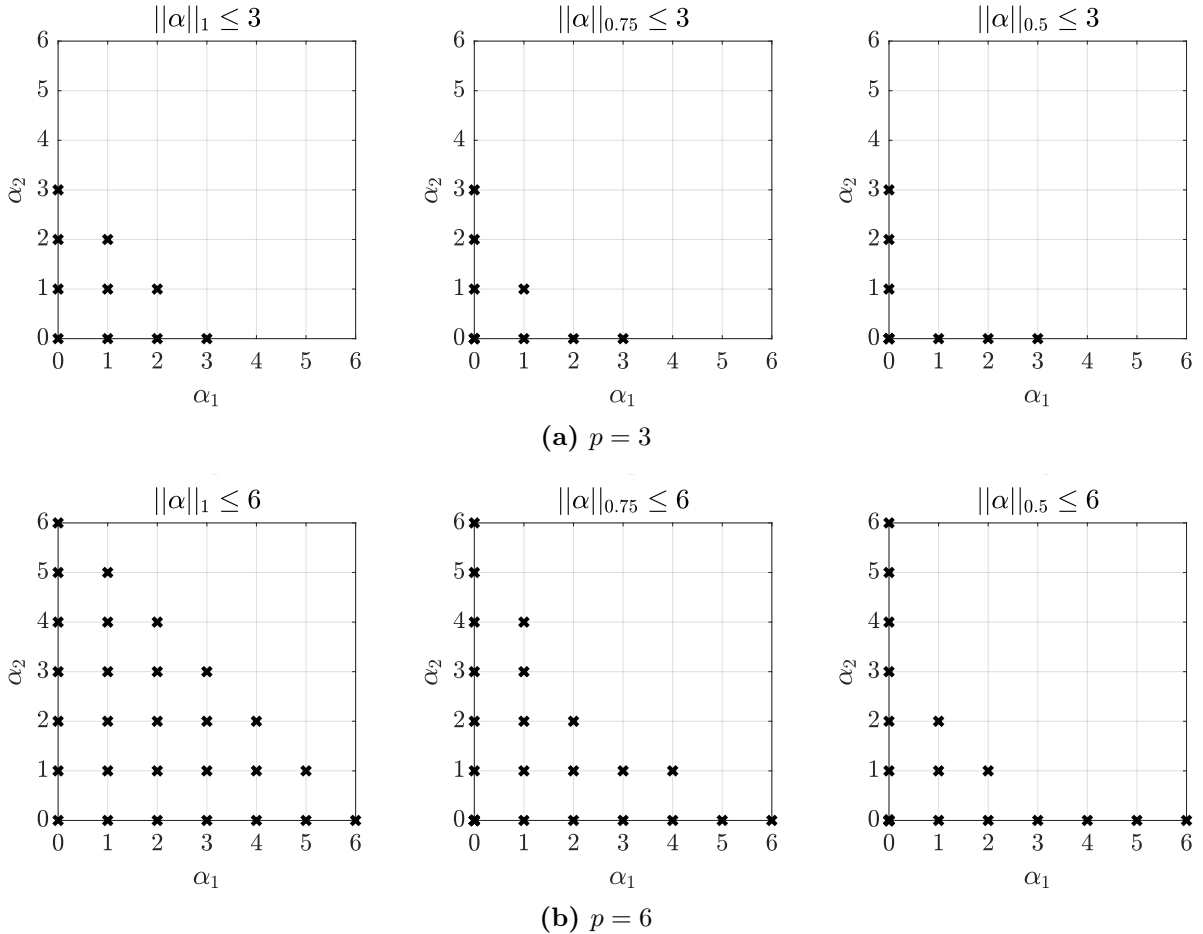
Figure 5.2: 2D index sets $\boldsymbol{\alpha} = (\alpha_1, \alpha_2)$ of two different polynomial degrees p corresponding to different q-norms, $\|\boldsymbol{\alpha}\|_1 = |\boldsymbol{\alpha}| \leq p$ (left), $\|\boldsymbol{\alpha}\|_{0.75} \leq p$ (centre) and $\|\boldsymbol{\alpha}\|_{0.5} \leq p$ (right).

Sparse polynomial chaos expansion: For high stochastic dimensions, general PC expansion method suffers from the curse of dimensionality, i.e. many samples are required to obtain sufficiently converged results. To overcome this issue, Blatman and Sudret [2008] propose a sparse PC expansion approach, which is also used in this work. The idea is to further reduce the set $\mathcal{A}$ by determining the optimal basis of the candidate set in an adaptive algorithm.

Starting with an initial experimental design, i.e. a sampled candidate set $\mathcal{X} = (\boldsymbol{x}_1, \ldots, \boldsymbol{x}_{n_{\mathrm{PC}}})$ and the corresponding response $\mathcal{Y}(\hat{\mathbf{z}}) = (y_1(\hat{\mathbf{z}}), \ldots, y_{n_{\mathrm{PC}}}(\hat{\mathbf{z}}))^{\mathrm{T}}$, the optimal PC basis $\mathcal{A}^*$ is selected as follows. The optimal basis $\mathcal{A}^{(p)}$ with regard to the polynomial order p is obtained from the candidate basis $\mathcal{A}$ for a pre-defined q-norm based on least angle regression [Blatman and Sudret, 2011]. For that purpose, the leave-one-out error ϵ_{LOO} is determined for each candidate set point $\boldsymbol{x}_j \in \mathcal{X}$ to estimate its influence to the experimental design, i.e.

$$\epsilon_{\mathrm{LOO}}(\hat{\mathbf{z}}) = \frac{1}{n_{\mathrm{PC}}} \sum_{j=1}^{n_{\mathrm{PC}}} \left(\mathcal{M}(\boldsymbol{x}_j, \hat{\mathbf{z}}) - \tilde{\mathcal{M}}_{\mathcal{A}}^{(-j)}(\boldsymbol{x}_j, \hat{\mathbf{z}}) \right)^2, \tag{5.28}$$

with $\tilde{\mathcal{M}}_{\mathcal{A}}^{(-j)}$ being the metamodel built from the experimental design based on the candidate set $\mathcal{X} \backslash (\boldsymbol{x}_j)$. When the coefficients $\hat{a}(\hat{\mathbf{z}})$ are determined by least-square regression as described above, the leave-one-out error can be obtained directly from the metamodel based on the original experimental design as follows

$$\epsilon_{\mathrm{LOO}}(\hat{\mathbf{z}}) = \frac{1}{n_{\mathrm{PC}}} \sum_{j=1}^{n_{\mathrm{PC}}} \left(\frac{\mathcal{M}(\boldsymbol{x}_j, \hat{\mathbf{z}}) - \tilde{\mathcal{M}}_{\mathcal{A}}(\boldsymbol{x}_j, \hat{\mathbf{z}})}{1 - h_j} \right)^2, \tag{5.29}$$

where h_j is the j-th diagonal term of $\mathbf{A} \left(\mathbf{A}^{\mathrm{T}} \mathbf{A} \right)^{-1} \mathbf{A}^{\mathrm{T}}$ with $A_{ji} = \Psi_{\alpha_j}(\boldsymbol{x}_j)$. Furthermore, ϵ_{LOO} can be normalised by the variance $\sigma^2\{Y\}$ and corrected by a factor accounting for the limit size of the experimental design, resulting in the relative leave-one-out error

$$\epsilon_{\mathrm{LOO}}{}^*(\hat{\mathbf{z}}) = \frac{1}{n_{\mathrm{PC}} - P} \left(\frac{1 + \frac{1}{n_{\mathrm{PC}}} \mathrm{tr}\, \mathbf{C}_{\mathrm{emp}}^{-1}}{\sigma^2\{Y\}} \right) \epsilon_{\mathrm{LOO}}(\hat{\mathbf{z}}), \tag{5.30}$$

with $P = \mathrm{card}\, \mathcal{A}$ and $\mathbf{C}_{\mathrm{emp}} = \frac{1}{n_{\mathrm{PC}}} \Psi^{\mathrm{T}} \Psi$ [Sudret, 2015].

When $\epsilon_{\mathrm{LOO}}{}^*$ increases twice in a row, this indicates an overfitting of the metamodel to the given basis and the initial experimental design needs to be enriched by further candidate samples $\mathcal{X}^+$ and corresponding model responses $\mathcal{Y}^+$. As soon as a required error is achieved, the optimal PC basis $\mathcal{A}^*$ is obtained and the corresponding coefficients $\hat{a}^*(\hat{\mathbf{z}})$ can be determined by least-square regression.

As an alternative to sparse PC expansion, also anisotropic PC expansion methods [Jakeman et al., 2015, Zygiridis, 2021] have been proposed to reduce the curse of dimensionality. As the sparse SC method introduced in Subsection 5.1.2, the sparse PC expansion is based on global polynomials within the sample space. For this reason, also for sparse PC expansion the stochastic response is required to be sufficiently smooth. To be applicable also for non-smooth responses, adaptive multi-element PC expansion methods [Wan and Karniadakis, 2005, Li and Stinis, 2016] may become necessary. Basmaji et al. [2022b] combine both, the anisotropic and the adaptive multi-element approach towards an hp-adaptive framework.

Error measure: Besides the leave-one-out error used within the sparse PC algorithm, a second error measure can be used to validate the quality of the metamodel obtained from

the optimal PC basis a posteriori. For this purpose, a validation set $\mathcal{X}_{\text{val}}$ is sampled and the validation error then follows as

$$\epsilon_{\text{val}}(\hat{\mathbf{z}}) = \frac{1}{n_{\text{val}}} \sum_{j=1}^{n_{\text{val}}} \left(\mathcal{M}(\boldsymbol{x}_j, \hat{\mathbf{z}}) - \tilde{\mathcal{M}}_{\mathcal{A}}(\boldsymbol{x}_j, \hat{\mathbf{z}}) \right)^2. \tag{5.31}$$

Here, $\mathcal{M}(\boldsymbol{x}_j, \hat{\mathbf{z}})$ is the regular model evaluation of each realisation $\boldsymbol{x}_j \in \mathcal{X}_{\text{val}}$, $j = 1, \ldots, n_{\text{val}}$ and $\tilde{\mathcal{M}}(\boldsymbol{x}_j, \hat{\mathbf{z}})$ the metamodel evaluation of the same realisation $\boldsymbol{x}_j$.

5.2.   Comparison in terms of solid mechanical applications

In the following, the three sampling based SFEM approaches are compared in terms of their general applicability regarding an efficient and accurate propagation of random fields. For this purpose, the propagation of different correlation length scenarios and the impact of the - under some circumstances high - stochastic dimension due to the truncated KL expansion is studied at first in Subsection 5.2.1 for 1D random fields in terms of linear-elastic material behaviour. Afterwards, propagating a 2D random field through a non-linear material model (i.e. an elasto-plastic material including linear hardening) is studied in Subsection 5.2.2. Note that the MC and SC results have already been published as a part of a broader investigation on SC methods [Dannert et al., 2022].

Remarks on the implementation: As described before in Section 3.3, Abaqus is used as a black-box FE solver, using the subroutine USDLFD to define material parameters described by a random field at the integration point level. However, on the contrary to the mixed uncertain approach described by Algorithm 1, only aleatory uncertainties are considered in this chapter, i.e. the initialising of epistemic parameters, the outer loop and the interval post-processing are not necessary. Depending on the applied SFEM approach, the following functions or toolkits are used for the stochastic framework.

- Brute force MC method: The samples $\boldsymbol{\xi}_j = (\xi_1, \ldots, \xi_T)_j$, $j = 1, \ldots, n_{\text{MC}}$ to create n_{MC} random field realisations truncated at T, are generated pseudo-randomly by the random number generator `xi_j = randn([1,N])` provided by Matlab. The default generator (Mersenne Twister) is used while its seed is initialised by the current time by `rng('shuffle')` to ensure unique samples when a given sample set is enlarged by further samples. The statistical evaluation is performed using the respective Matlab functions.

- Sparse SC method: The Kronrod-Patterson sparse grid and the corresponding interpolants are generated using the toolbox *Sparse Grids Matlab Kit*[1] [Bäck et al., 2011]. Each N-dimensional collocation point $\boldsymbol{x}_j = (x_1, \ldots, x_{N=T})$ is inserted to $\boldsymbol{\xi}_j = (\xi_1, \ldots, \xi_T)_j$ to obtain a random field realisation.

---

[1]©2009-2018 L. Tamellini and F. Nobile: `https://sites.google.com/view/sparse-grids-kit`, release "Esperanza" (10/2018)

- Sparse PC expansion: The sample set to generate the experimental design is generated by brute force MC sampling as described above. With these, the sparse PC is determined using the toolkit *UQLab*[2] [Marelli and Sudret, 2014, Marelli et al., 2022].

In order to obtain a fair comparison between the approaches, besides their individual relative error measures, a comparable reference error of each method m = MC, m = SC and m = PC is determined based on a reference solution,

$$\epsilon_{\text{ref}}\{\cdot\} = \frac{\|\{\cdot\}^{\text{m}} - \{\cdot\}_{\text{ref}}\|}{\|\{\cdot\}_{\text{ref}}\|}. \tag{5.32}$$

The reference solution is generated by brute force MC with $n_{\text{MC}}^{\text{ref}} \gg n_{\text{MC}}$. In the following, the mean value and standard deviation of the QoI are inserted to the placeholder $\{\cdot\}$. However, any quantity can be considered.

5.2.1. One-dimensional example including high stochastic dimensions

The three approaches are applied to estimate the maximum deflection w_{max} of the steel beam depicted in Figure 5.3 assuming linear elasticity. While the line load $q_0 = 50\,\text{kN}\,\text{m}^{-1}$ is considered constant, the Young's modulus $E(\omega, z)$ is modelled as a 1D Gaussian random field described by constant hyper parameters, $\mu_E = 210\,\text{GPa}$ and $\sigma_E = 0.1\mu_E$.
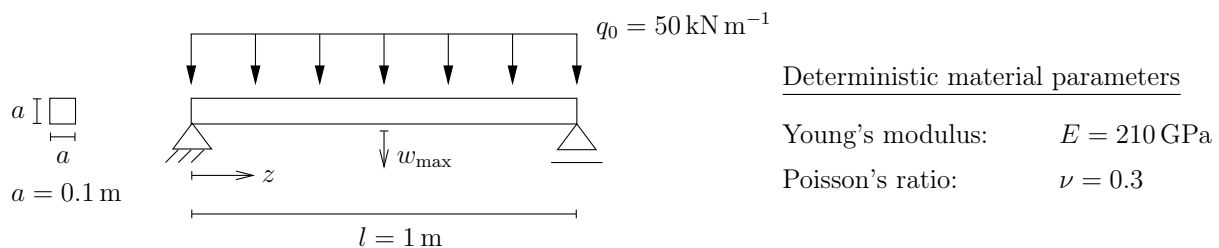

Figure 5.3: Linear-elastic steel beam model under a constant line load q_0 with the deterministic solution resulting in a maximal deflection $w_{\text{max}} = 0.37\,\text{mm}$ [Dannert et al., 2022].

Three correlation length ratios $L_E/l = 0.1$, $L_E/l = 1.0$ and $L_E/l = 10.0$ are studied, applying a modified exponential (ME) correlation function. For each correlation length scenario, the truncation term T is chosen such that a comparable mean truncation error $\bar{\epsilon}_{\bar{\Gamma}} = 0.08\,\%$ is achieved, i.e. $T = 56$ for $L_E/l = 0.1$, $T = 7$ for $L_E/l = 1.0$ and $T = 2$ for $L_E/l = 10.0$. Note that the correlation lengths are chosen in different magnitudes despite the physical meaning for steel, as the aim is to investigate the general effect of the correlation length and truncation order to the applicability of the provided methods. The beam is discretised by $n_{\text{el}} = 50$ beam elements using a third order quadrature scheme for integration. The mean value $\mu\{w_{\text{max}}\}$ and standard deviation $\sigma\{w_{\text{max}}\} = \sqrt{\sigma^2\{w_{\text{max}}\}}$ of the maximum beam deflection w_{max} are estimated, respectively, by Eq. (5.5) and Eq. (5.6) in case of MC method, by Eq. (5.16) and Eq. (5.17) in case of sparse SC method and by Eq. (5.22) and Eq. (5.17) in case of sparse PC method.

---

[2]©2018-2022 S. Marelli and B. Sudret: `https://www.uqlab.com/`, release 2.0.0

The internal error measures of the SC and PC approach are depicted in Figure 5.4. For the SC method, the relative error ϵ_k is obtained adaptively with the Smolyak level k for both quantities, the mean value $\mu\{w_{\max}\}$ and the standard deviation $\sigma\{w_{\max}\}$ of the maximum beam deflection $w_{\max}$, see Figure 5.4a. On the contrary, the PC expansion provides two more general error measures of the metamodel, the leave-one-out error $\epsilon_{\mathrm{LOO}}\{w_{\max}\}$ and the validation error $\epsilon_{\mathrm{val}}\{w_{\max}\}$ in Figure 5.4b.

(a) SC method using the Kronrod-Patterson sparse grid
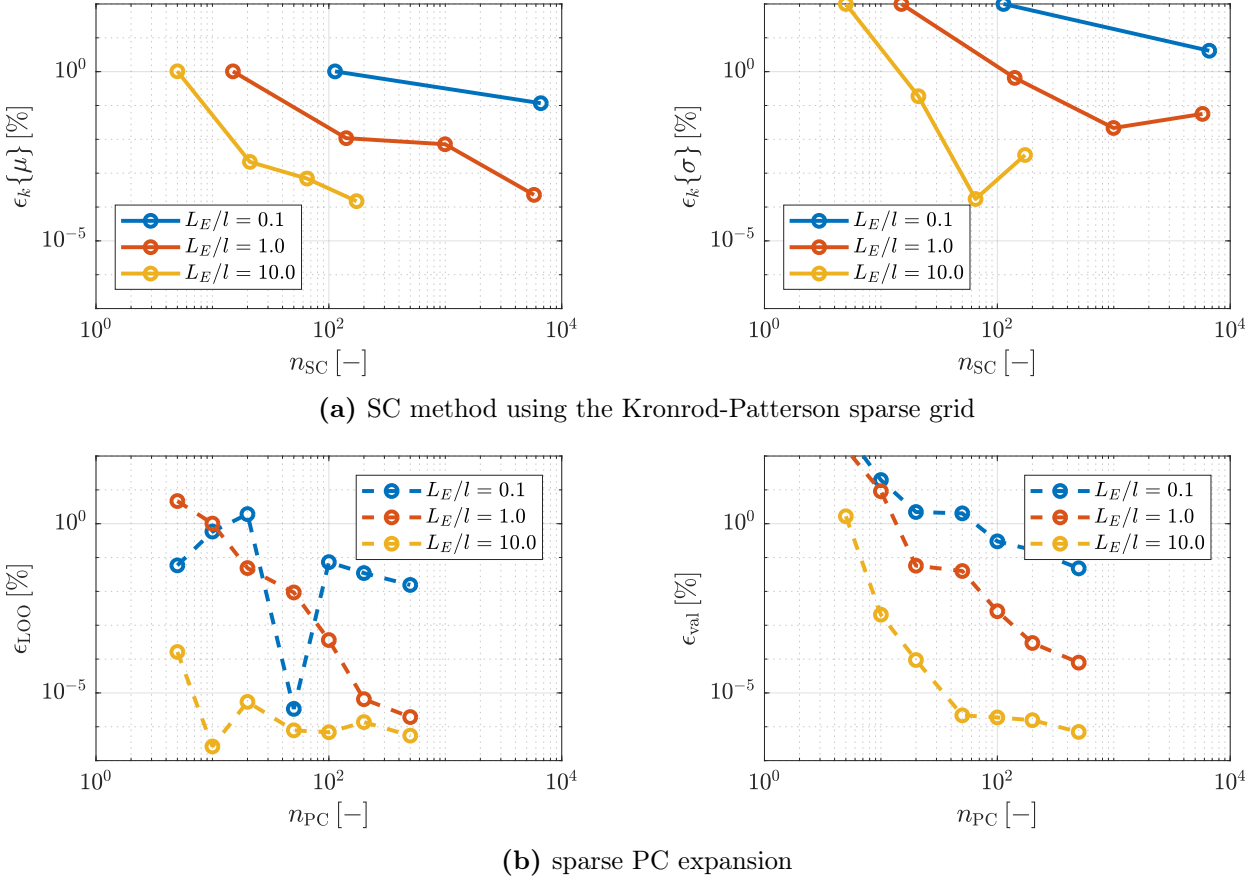

(b) sparse PC expansion

Figure 5.4: Relative error measures of the sparse SC and the sparse PC methods obtained for the estimate of the maximum beam deflection $w_{\max}$ with respect to the sample size, comparing different correlation length ratios L_E/l and accordingly different stochastic dimensions.

For both methods, it can be seen that the error converges faster for large correlation length ratios, i.e. less stochastic dimensions are required to obtain the chosen mean truncation error of the input random field. For $L_E/l = 0.1$, including $N = T = 56$ (results depicted in blue), both methods show difficulties regarding the convergence. Still, the results of the sparse PC expansion are much better even for less samples ($n_{\mathrm{PC}} = 500$) than the results of the SC method, where the relative error of the standard deviation is larger than one percent, although the grid size is already quite large ($n_{\mathrm{SC}} = 6609$). Increasing the Smolyak level once more would result in a grid size which cannot compete with a brute force MC simulation anymore. Another disadvantage of SC method is the fact that the grid size n_{SC} depends on the stochastic dimension N, while n_{PC} can be chosen flexibly for the sparse PC expansion. However, note that the time required to obtain the sparse PC basis raises drastically for large stochastic dimensions. For this reason, also for sparse PC method the sample size is limited with regard to efficiency, independent of the computational cost caused by the propagation of the sample set.

(a) $L_E/l = 0.1$ $(T = 56)$

(b) $L_E/l = 1.0$ $(T = 7)$

(c) $L_E/l = 10.0$ $(T = 2)$
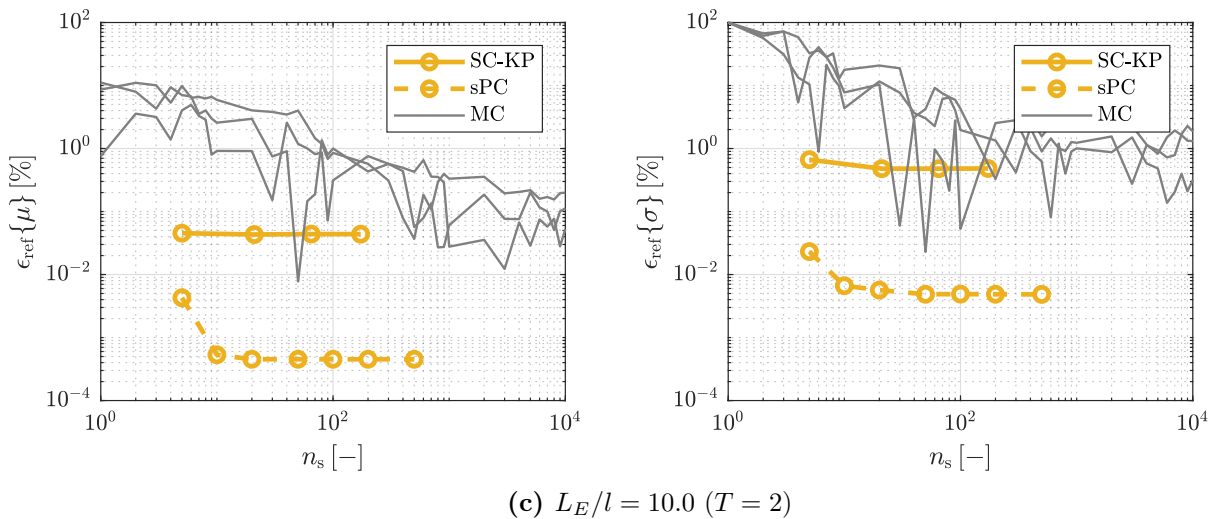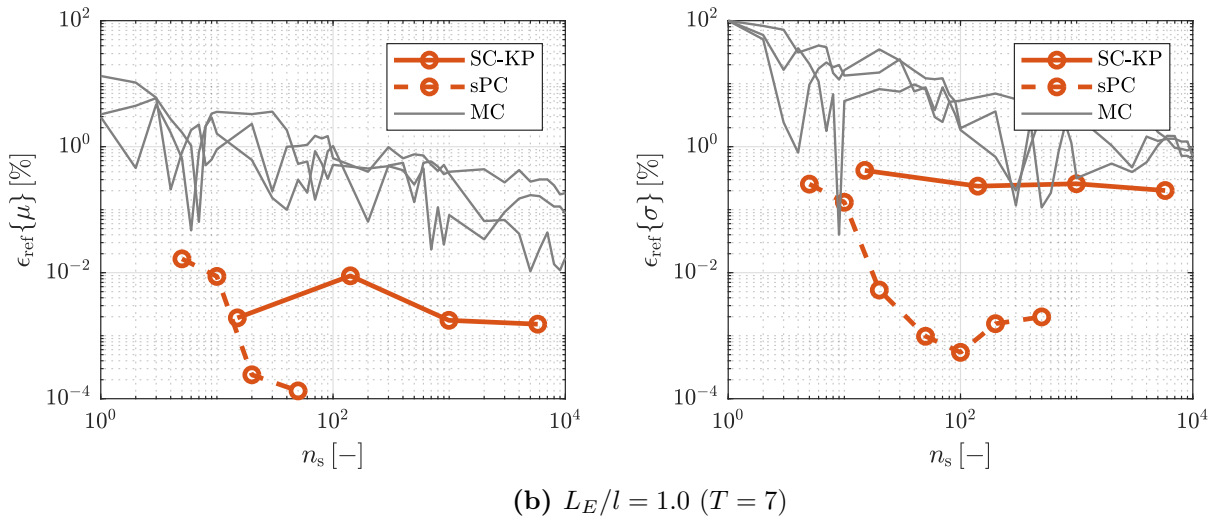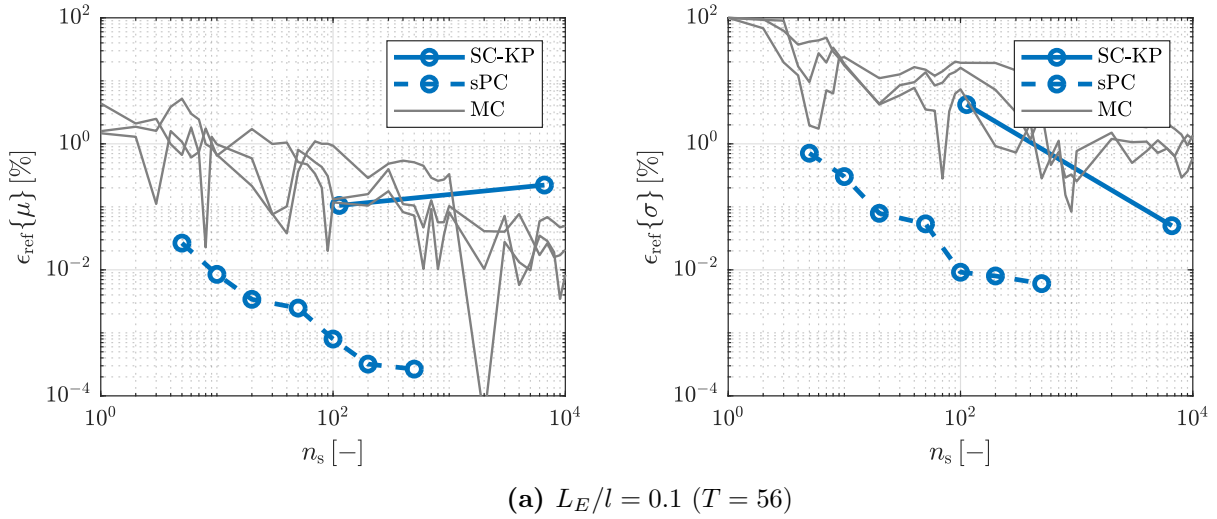
Figure 5.5: Comparing the reference error $\epsilon_{\mathrm{ref}}\{\cdot\}$ of the mean value $\mu\{w_{\mathrm{max}}\}$ (left) and the standard deviation $\sigma\{w_{\mathrm{max}}\}$ (right) of the maximum beam deflection w_{max} for different correlation length ratios L_E/l. The coloured solid lines represent the results of sparse SC method using the Kronrod-Patterson sparse grid, the dashed lines the results of the sparse PC expansion and the grey lines three MC trajectories, each with $n_{\mathrm{MC}} = 1 \times 10^4$ samples. The reference solution is obtained by brute force MC method using $n_{\mathrm{MC}}^{\mathrm{ref}} = 5 \times 10^4$ samples.

The internal error measures of SC and PC method each provide a convergence estimate to run (and stop) the simulation without any reference solution available. However, as they are obtained differently, they are actually not comparable for the two methods. For a fair comparison, the relative error of the mean value $\mu\{w_{max}\}$ and the standard deviation $\sigma\{w_{max}\}$ is determined by Eq. (5.32) for each method. For this purpose, a brute force MC reference solution with $n_{MC}^{ref} = 5 \times 10^4$ samples is used. The results are depicted in Figure 5.5. As a comparison, also three brute force MC trajectories are depicted, each obtained by $n_{MC} = 1 \times 10^4$ samples. It can be noted that for large stochastic dimensions, SC method does not even compete with the brute force MC method. This improves a bit for moderate stochastic dimensions but still the SC method does not appear much beneficial. On the contrary, the sparse PC expansion results in a much better convergence in terms of the reference error obtained by a certain sample size. For this reason and as the sample size can be chosen flexibly, sparse PC expansion is found to be the best choice regarding the given example, i.e. propagating (in some circumstances high-dimensional) 1D random fields through a linear-elastic material model. In the next section, a 2D random field is investigated in terms on non-linear material behaviour.

5.2.2.   Two-dimensional example including a non-linear model

In the following the approaches are investigated for non-linear model propagation. For this purpose, the one square-meter sized steel plate depicted in Figure 5.6 is pulled at its top by a constant line load $q_0 = 400\,\mathrm{MN\,m^{-1}}$. An elasto-plastic material law including linear hardening is applied. In the deterministic case with $E = 210\,\mathrm{GPa}$, the yield stress of σ_y is exceeded by the resulting stress state and therefore hardening occurs with a linear hardening parameter $H = 1.5\,\mathrm{GPa}$. Then, the maximum deflection is constantly $u_2 = 68.36\,\mathrm{mm}$ along the whole top of the square and the equivalent plastic strain $\bar{\varepsilon}^p = 6.65\,\%$ is constant in the whole domain. The FE model is applied with a domain discretisation of $n_{el} = 10 \times 10$ bi-linear four-node elements.
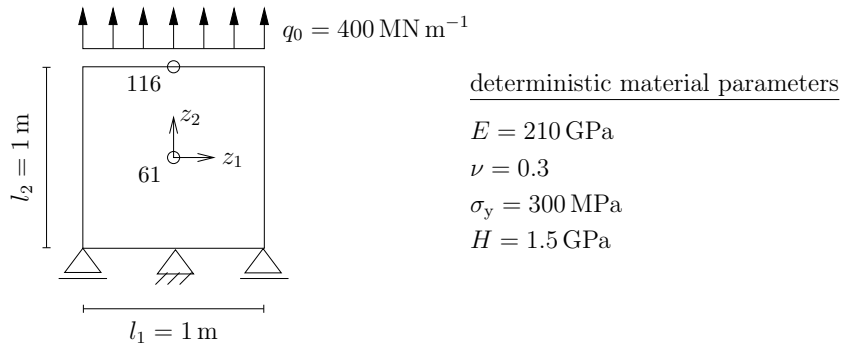
Figure 5.6: Elasto-plastic steel plate model pulled by a constant line load q_0 with the deterministic solution resulting in the maximum deflection $u_2 = 68.36\,\mathrm{mm}$ and a constant equivalent plastic strain $\bar{\varepsilon}_p = 6.65\,\%$. The quantities of interest are investigated at node (61) in case of u_2 and at node (116) in case of $\bar{\varepsilon}_p$ as marked by circles [Dannert et al., 2022].

Describing the Young's modulus as a 2D random field with $\mu_E = 210\,\mathrm{GPa}$, $\sigma_E = 0.1\mu_E$ and $L_E = 2\,\mathrm{m}$, the constant behaviour of the QoI is not observable for the individual realisations but again achieved for the stochastic moments, i.e. $\mu\{Y, \boldsymbol{z}\}$ and $\sigma\{Y, \boldsymbol{z}\}$, if the results are sufficiently converged. The QoI Y is further investigated in terms of the deflection u_2 at node 116 and of the equivalent plastic strain $\bar{\varepsilon}^p$ at node 61, both nodes marked by circles in Figure 5.6.

(a) SC method using the Kronrod-Patterson sparse grid

(b) sparse PC expansion

Figure 5.7: Relative error measures of the sparse SC method and the sparse PC method with respect to the sample size, obtained for the estimate of the deflection u_2 at node 116 and of the equivalent plastic strain $\bar{\varepsilon}^{\mathrm{p}}$ at node 61, describing the Young's modulus as a random field truncated at $T = 5$.

The SC and PC method are applied to solve the FE problem with a chosen truncation order $T = 5$ leading to a mean truncation error $\bar{\epsilon}_{\bar{\Gamma}} = 1.38\,\%$. T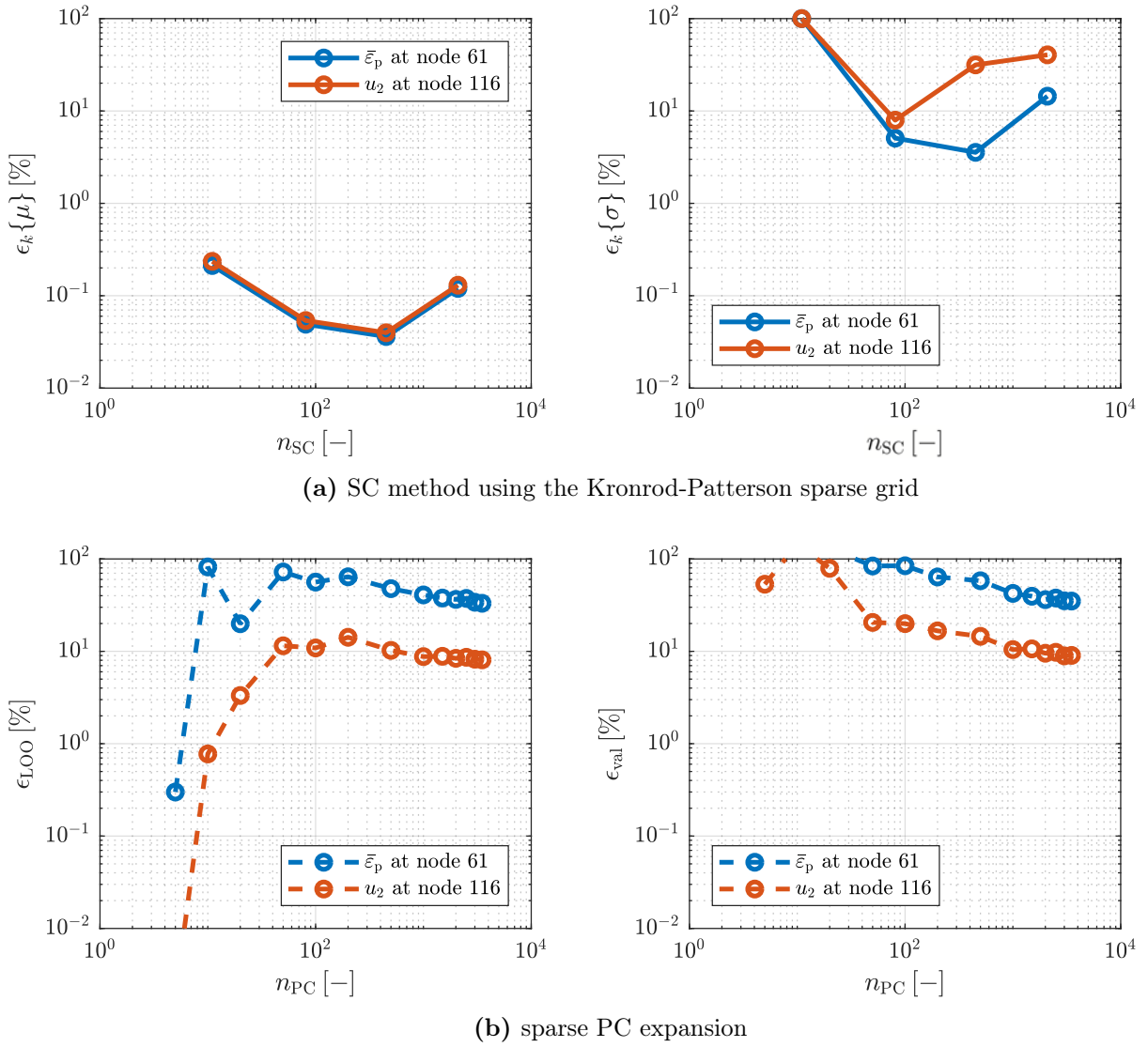he corresponding internal error measures are depicted in Figure 5.7. In Figure 5.7a, the relative error ϵ_k of the mean value $\mu\{Y\}$ (left) and the standard deviation $\mu\{Y\}$ (right) is depicted as a function of the grid size n_{SC} resulting for the Smolyak levels $k = 1, \ldots, 4$. Below, the leave-one-out error ϵ_{LOO} (left) and the validation error ϵ_{val} (right) obtained for the PC metamodels describing the QoI are depicted in Figure 5.7b. It can be found that for both QoI only $\epsilon_k\{\mu\}$ becomes small though not convergent. All other error measures result in values around ten percent and beyond, which is not acceptable. Increasing the sample size is not expedient as it would lead to a number of required realisations that could not further compete with the MC method.

However, regarding the corresponding reference errors depicted in Figure 5.8, it is remarkable that the PC metamodel still appears to provide good results. The reference error of both, the mean value and the standard deviation, for both QoI outperforms the three trajectories of

the MC simulations with each $n_{MC} = 1 \times 10^4$ samples by far. As a reference solution, again a brute force MC simulation with $n_{MC} = 5 \times 10^4$ samples has been used. Still, a reference solution is usually not available and therefore the error must be quantified internally during the engineering design process.

(a) displacement: $Y = |u_2|$ at node 116

(b) equivalent plastic strain: $Y = \bar{\varepsilon}^p$ at node 61
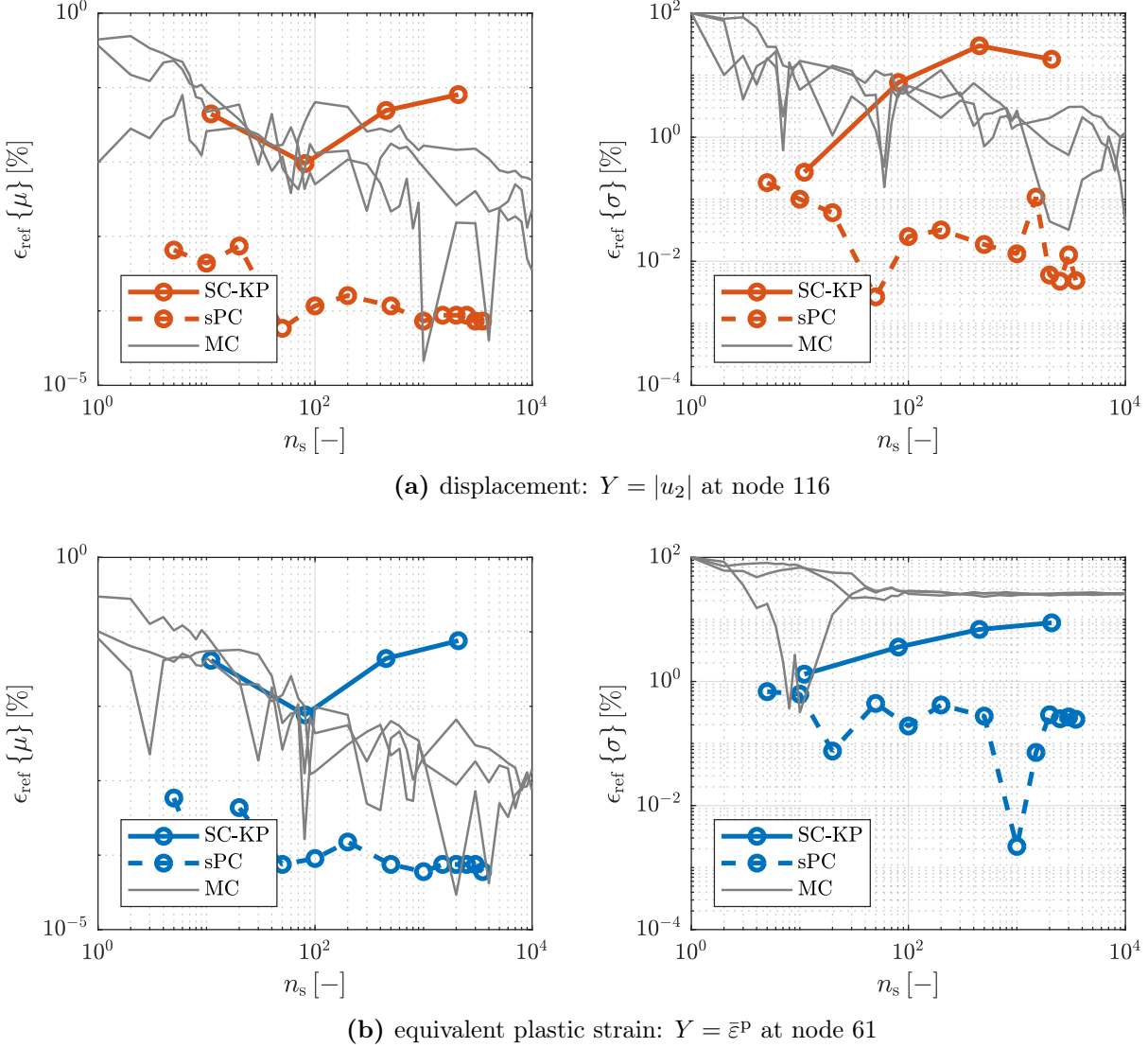
Figure 5.8: Comparing the reference error $\epsilon_{ref}\{\cdot\}$ of the mean value $\mu\{Y\}$ (left) and the standard deviation $\sigma\{Y\}$ (right) of two different quantities of interest Y. The coloured solid lines represent the results of SC method using the Kronrod-Patterson sparse grid, the dashed lines the results of the sparse PC expansion and the grey lines three MC trajectories, each with $n_{MC} = 1 \times 10^4$ samples. The reference solution is obtained by brute force MC method using $n_{MC}^{ref} = 5 \times 10^4$ samples.

Regarding the results of the SC method, it is observed that they do not only exceed the error of the MC simulations but also appear to become worse with increasing sample size. This can be traced back to instabilities in the Smolyak algorithm due to negative weights [van den Bos et al., 2017]. Additionally, the Lagrangian polynomials tend to oscillate for large grid sizes [Jablonski, 2014]. These issues can even lead to negative stochastic moments in some cases [Dannert et al., 2022].

5.3. Summary and concluding remarks

In this chapter, SC and PC methods have been reviewed as two well established alternative approaches towards MC method. The applicability of the SC method using Kronrod-Patterson sparse grids and of sparse PC expansion has been investigated for high-dimensional as well as non-linear problems and compared to the performance of a brute force MC simulation.

Although both of the two sophisticated sampling methods suffer from the curse of dimensionality, it has been shown in Subsection 5.2.1 that the sparse PC expansion outperforms the sparse SC method by far. The latter is even not applicable at all in some cases (i.e. using $L_E/l = 0.1$ with $N = 56$), while sparse PC expansion provided a slower convergence in high-dimensional cases but still outperformed MC method. Furthermore, the advantage of PC expansion over SC method is that the sample size n_{PC} is not defined by the stochastic dimension N. For this reason the sample size can be chosen more precisely in this case, while the number of collocation points n_{SC} increases quickly from one level to the next. Concerning 2D or three-dimensional (3D) random fields, but also a case where several random field input parameters are considered, N increases too fast for SC method being a suitable sampling technique.

The SC method could be further improved by applying anisotropic sparse grids [Nobile et al., 2008], where the multi-index is not chosen equally in each dimension but adaptively according to the influence of the random variable corresponding to a certain dimension. This can become especially beneficial regarding random field input parameters which are described by KL expansion, as the influence of the expansion terms decreases with an increasing number of the eigenvalues. Regarding sparse PC method, this phenomenon is automatically incorporated indirectly by searching the optimal basis.

Regarding the non-linear FE problem exemplified in Subsection 5.2.2, both sophisticated techniques did not appear suitable. Although the reference error of the sparse PC expansion outperforms the results of a brute force MC simulation, the leave-one-out and validation error do not decrease sufficiently. The limitations of sparse PC expansion regarding non-linear material responses also have been reported recently by Voelsen et al. [2023] in terms of elasto-plasticity as well as problems in damage mechanics. As no reference solution is available in general, these error measures are required as an internal stopping criterion.

The reason for the slow convergence can be found in the non-linear model demanding much more samples to obtain enough information about the stochastic response. As will be shown in Subsection 6.3.2 non-linear models may even include non-differential regions in the response, which cannot be considered to be a smooth response anymore. However, sufficient smoothness has been a model assumption on which both, SC and PC approaches have been based on, as global polynomials are used.

Regarding non-smooth stochastic responses, both approaches can still be improved by spatially adaptive techniques using local polynomials, see e.g. Pflüger [2010] for adaptive SC methods or Wan and Karniadakis [2005], Li and Stinis [2016] for multi-element PC expansion. By this a refinement of the random space discretisation at critical regions is enabled. Basmaji et al. [2022b] improve the efficiency of an adaptive multi-element PC expansion by combining

it with an anisotropic PC approach. This general procedure is conceivable also for SC method. However, as it has been shown for sparse PC expansion in this chapter, it is difficult to control the error measure and corresponding stopping criterion a priori. Considering imprecise random fields occurring by interval valued correlation lengths, ensuring a comparable input is crucial to ensure the resulting probability box (p-box) not to be traced back to approximation errors. For this reason, applying such sophisticated sampling techniques introduces too many difficulties to control error variables in the propagation process to enable a reliable statement about the resulting QoI p-boxes.

6. Limit Representation of Imprecise Random Fields

As discussed intensively in Section 3.3, the propagation of imprecise random fields needs to be well pondered and can become very difficult. The main challenges are recapped once more in Figure 6.1. Whichever hyper parameter(s) of the random field is or are described by an interval, a cost-increasing double loop arises within the probability box (p-box) approach. It requires to simulate at least two interval bound scenarios but the number of scenarios may blow up rapidly with increasing number of interval valued hyper parameters or input parameters considered as imprecise random fields. For this reason, an important aim is to reduce the computational cost of an individual interval parameter scenario. This can be achieved by reducing the number of samples required to simulate a scenario c, e.g. in terms of sophisticated sampling techniques. Alternatively, the cost to solve the problem for each sample can be decreased by model reduction techniques. Within this research project, the focus has been on investigating the first of these two opportunities. For this purpose, stochastic collocation (SC) method and polynomial chaos (PC) expansion have been studied intensively in Chapter 5.
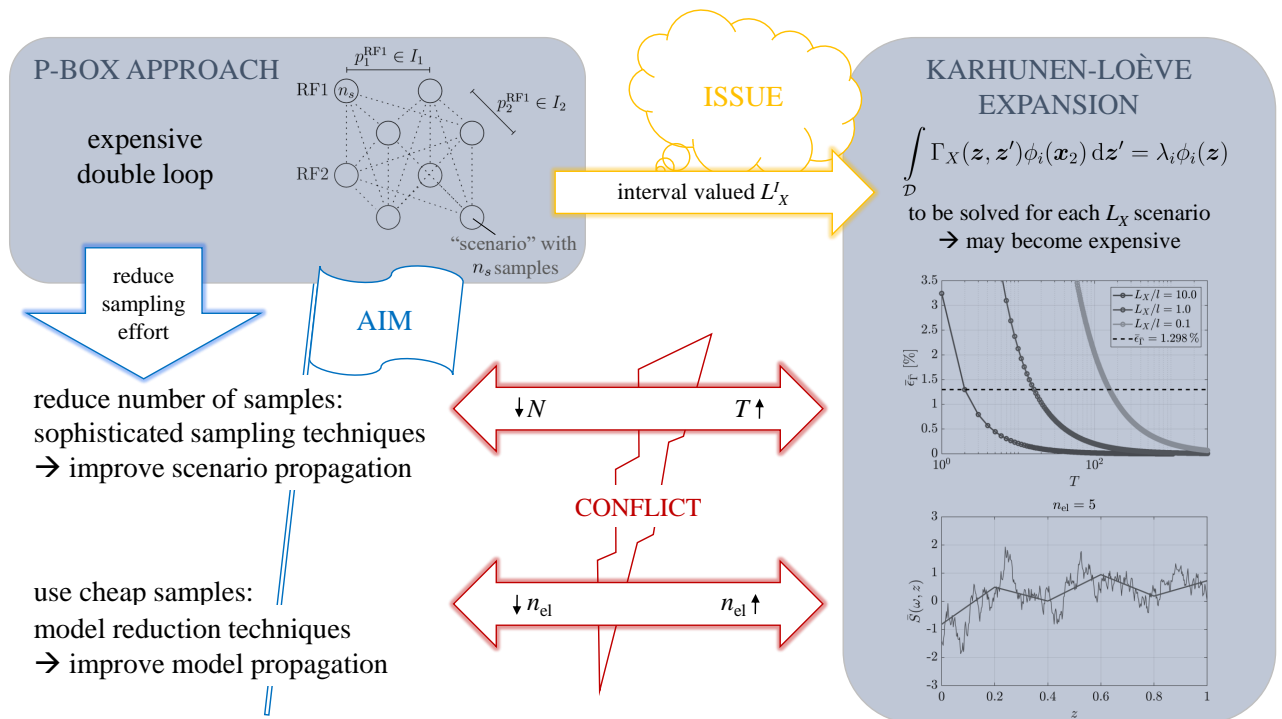

Figure 6.1: Challenges in propagating imprecise random fields.

However, considering interval valued correlation lengths L_X^I, another issue arises which can cause conflicts with the aim of reducing the sampling effort. Using different correlation length values, while demanding a comparable truncation error of the corresponding input random

fields can lead to high truncation orders T and this way increase the stochastic dimension N drastically. This can conflict with using sophisticated sampling techniques, which suffer usually from the curse of dimensionality. Additionally, highly variable random fields occurring from small correlation lengths may require to discretise the domain with a high h- or p-refinement in order to not smoothen the random field artificially. Here, the conflict arises with the aim to use cheap samples, which is however beyond the scope of this work. Note that the need to solve the Fredholm integral equation several times for different correlation length values may additionally increase the computational cost, especially when arbitrary domain shapes or correlation functions are used, which do not provide an analytic solution.

In this chapter, a decoupled interpolation approach is introduced, with which the expensive double loop can be avoided. Furthermore, with the new approach the discussed conflicts can be evaded up to a certain point underlying certain model assumptions. It has been observed in Chapter 5 that the correlation length mainly impacts the standard deviation of the outcome quantity of interest (QoI), but hardly its mean value. Furthermore, the higher the variability (i.e. the smaller the correlation length) of the input random field is, the smaller the standard deviation of the QoI and vice versa. In other words, highly correlated random fields (i.e. large correlation lengths) result in larger standard deviations of the QoI than those with small correlation lengths. This means that the variability of the QoI increases with decreasing variability of the input random field.

To understand this phenomenon, the influence of the correlation length to the input random field is further investigated in Section 6.1. Based on the observations made in there, the mentioned interpolation approach is proposed in Section 6.2. In Section 6.3, the new approach is studied intensively for one-dimensional (1D) problems regarding linear and non-linear propagation in terms of both, the material behaviour and the stochastic response. Afterwards, the approach is applied to propagate two-dimensional (2D) imprecise random fields through a non-linear finite element (FE) problem in Section 6.4. The main results of the provided studies are concluded in Section 6.5.

Model assumptions: With regard to propagating imprecise random fields through linear or non-linear monotonic models, the following model assumptions are made.

- The hyper parameters μ_X and σ_X can be determined sufficiently exact by experiments and are therefore considered as *crisp scalar values*.

- The correlation length is interval valued, a pure *vertex analysis* is sufficient, i.e. no intermediate values $L_X^* \in L_X^I$ are required to be propagated.

- *No localisation effects* occur due to a locally varying truncation error if the mean truncation error is chosen sufficiently small.

- There is a *monotonic dependence* of the output QoI stochastic moments on the correlation length.

- The output distribution can be of arbitrary family but this *distribution family is independent from the correlation length.*

- *No cyclic loading* is applied.

Note that the approach has already been proposed and investigated using the single exponential (SE) correlation kernel during this research project [Dannert et al., 2021b]. However, the approach is applied to the modified exponential (ME) correlation function in the following, which provides a much better convergence behaviour than the SE kernel.

6.1. Investigation on the correlation length

In this section, the impact of the correlation length towards the random field input is investigated more carefully. For a 1D standard normal distributed random field $S(\omega, z)$, an ME correlation function is assumed and different effective correlation length ratios L_S/l with respect to the domain length l are studied, $L_S/l = 0.1$, $L_S/l = 1.0$ and $L_S/l = 10.0$. As discussed in Subsection 3.1.2, a small value $L_S < l$ implies a high variability within the field and vice versa. Furthermore, increasing $L_S \gg l$, i.e. $L_S/l \to \infty$, the random field converges towards a random variable. Regarding the other extreme, $L_S/l \to 0$, the random field is completely uncorrelated, i.e. it results in white noise.

Recapitulating the theory of Gaussian random fields, given a large number of realisations, their values at a certain state $S_J(\omega) = S(\omega, z_J)$ are Gaussian distributed as well, see Figure 2.3 in Subsection 2.1.2. For an increasing number of realisations $s_j(z) = S(\omega_j, z)$, the mean value $\mu\{s_j(z_J)\}$ and standard deviation $\sigma\{s_j(z_J)\}$ at a certain z_J are therefore expected to converge towards the hyper parameters $\mu_S = 0$ and $\sigma_S = 1$ of the standard normal distributed random field $S(\omega, z)$. This behaviour is independent of the considered correlation length. However, observing only the values at a certain position z_J of the random field neglects the fact that its values are more or less correlated within the field. For this reason, the statistical behaviour of the average values of the random field realisations is investigated more carefully in the following. Given one realisation $s_j(z) = S(\omega_j, z)$, its average value over z is called its corresponding individual mean value $\hat{\mu}_{s,j}$.

In Figure 6.2, the correlation functions (on the left) and each three exemplary truncated standard normal distributed random field realisations $\bar{s}_j(z) = \bar{S}(\omega_j, z), j = 1, 2, 3$, (on the right) are depicted for the five discussed correlation length ratios. For this purpose, the domain $\mathcal{D} = [0, 1]$ is discretised by $n_{\text{el}} = 500$ elements. For the sake of comparability, the same set of standard normal distributed random variables $\boldsymbol{\xi}_j = (\xi_1, \ldots, \xi_T)_j$ are used for each corresponding ω_j of the ratios L_S/l. Note that in order to maintain a comparable mean variance error of $\bar{\epsilon}_{\bar{\Gamma}} \leq 0.015\,\%$ for the different correlation lengths, Eq. (3.9) and such the set $\boldsymbol{\xi}_j = (\xi_1, \ldots, \xi_{501})_j$ is truncated individually at $T \leq 501$, depending on the correlation length ratio L_S/l. In case of white noise, the full sets $\boldsymbol{\xi}_j = (\xi_1, \ldots, \xi_{501})_j$ are used for each $j = 1, 2, 3$ while for the three random variables the sets are given by the first entry, i.e. $(\xi_1)_j$. For the sake of clarity, only one white noise realisation is plotted in Figure 6.2a (grey line), although all three realisations have been created as described above. Additionally to each realisation $\bar{s}_j(z) = \bar{S}(\omega_j, z)$, its

(a) $L_S/l \to 0$ (white noise)

(b) $L_S/l = 0.1,\ T = 102$ [*]

(c) $L_S/l = 1.0,\ T = 12$ [*]

(d) $L_S/l = 10.0,\ T = 3$ [*]
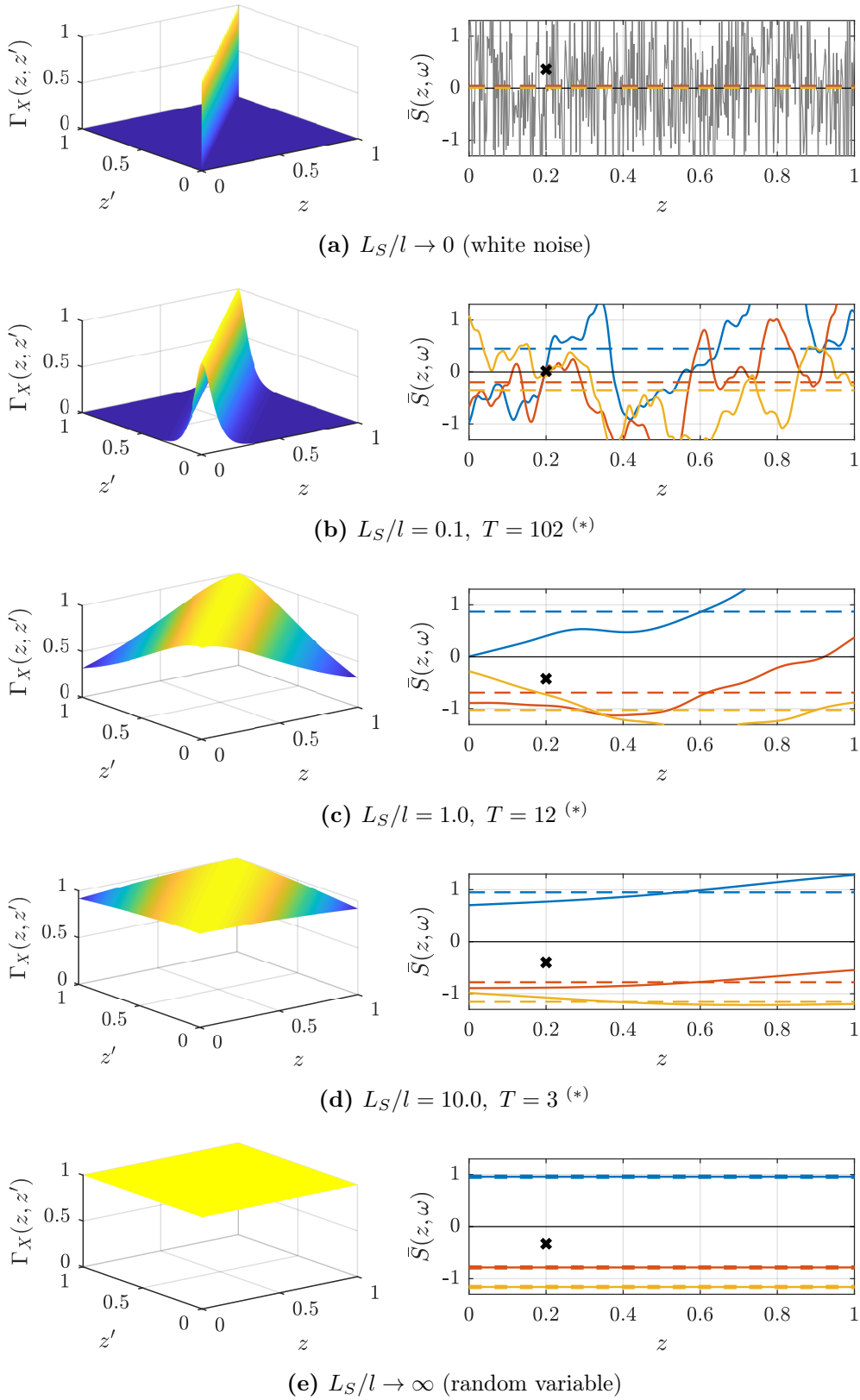
(e) $L_S/l \to \infty$ (random variable)

Figure 6.2: Influence of the correlation length ratio on the modified exponential correlation function in its closed form (left) and the resulting random fields (right).

[*] Random fields discretised by Karhunen-Loève expansion truncated such that $\bar{\epsilon}_\Gamma = 0.015\,\%$.

individual mean value $\hat{\mu}_{s,j}$ over the domain z is depicted in a dashed line of the corresponding colour. For the state $S_J(\omega) = S(\omega, z_J)$ of the random fields, each mean value $\mu\{S_J\}$ of the three realisations is exemplified at $z = 0.2$ by a black cross[1]. Although only one realisation is plotted for the white noise, also here three mean values $\hat{\mu}_{s,j}$ are depicted, the first obtained from the grey realisation, the other two corresponding to the two created but not plotted realisations. The same holds for the mean value of the three states at $z = 0.2$. Note that these individual mean values are the main interest of the following discussion. For this reason the y-axes are chosen in a smaller range (each the same one for comparability), although the random field realisations are not depicted completely this way, in order to see the influence of the correlation length to the individual mean value more clearly.

It can be observed from Figure 6.2a that the individual mean values $\hat{\mu}_{s,j}$ of the white noise realisations lay very close to the hyper parameter $\mu_S = 0$ of the standard normal distributed white noise. This is plausible as the mean of a large number of pseudo-randomly sampled, independent random variables should again result in the mean value used as the sampling input. Regarding now a weakly correlated random field, e.g. $L_S/l = 0.1$ as exemplified in Figure 6.2b, the mean values of each individual realisation are slightly varying from the Karhunen-Loève (KL) hyper parameter $\mu_S = 0$, inserted to Eq. (3.9) to create the three realisations. Increasing the correlation length ratio further towards $L_S/l = 1.0$ or $L_S/l = 10.0$, it can be seen that the individual mean values $\hat{\mu}_{s,j}$ of the random field realisations $s_j(z) = S(\omega_j, z)$ spread more and more. For an infinite correlation length ratio, $\hat{\mu}_{s,j}$ converge towards the same constant value as sampled for the random variable $s_j = S(\omega_j)$, see Figure 6.2e.

(a) mean value $\mu\{\hat{\mu}_{s,j}\}$

(b) standard deviation $\sigma\{\hat{\mu}_{s,j}\}$
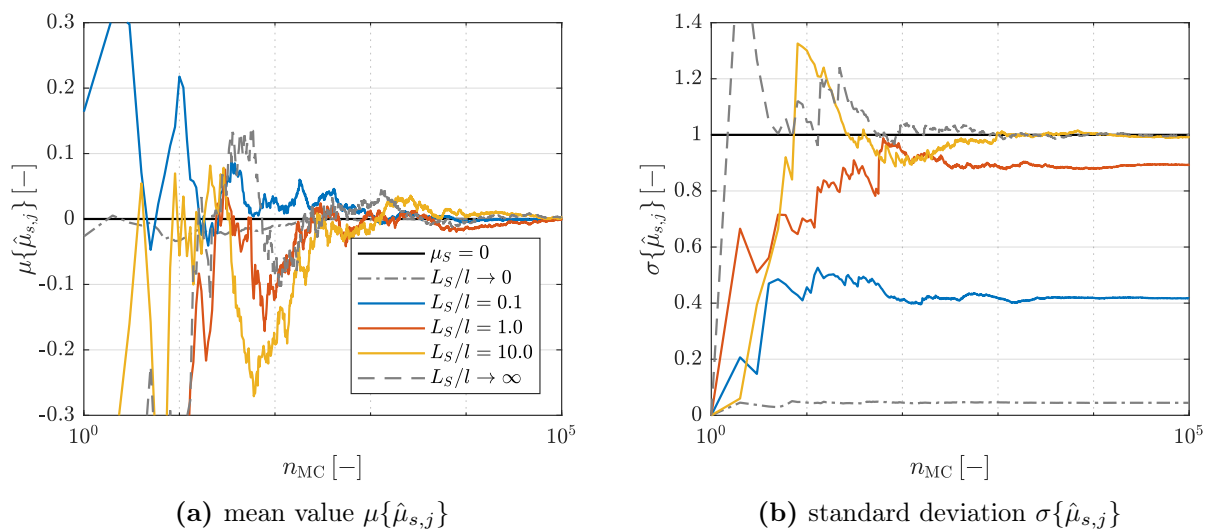
Figure 6.3: Convergence of the stochastic moments of the individual realisation mean values $\hat{\mu}_{s,j}$ of $j = 1, \ldots, n_{\text{MC}}$ standard normal distributed random field realisations $\bar{s}_j(z) = \bar{S}(\omega_j, z)$, the legend given in (a) is valid for both plots.

To sum up, it can be observed that for a highly varying random field, each realisation results in an average value close to the mean value used as input hyper parameter. On the contrary, large correlation lengths lead to a higher variability of the individual realisation mean values $\hat{\mu}_{s,j}$, while each realisation itself becomes more and more constant with increasing L_S/l. As

---

[1]However, note that three realisations are by far not enough to observe $\mu\{S_J\}$ to converge towards $\mu_S = 0$.

three realisations are lucid for visualisation but by far not enough to make a clear statement, the statistical behaviour of the individual mean values $\hat{\mu}_{s,j}$ is studied regarding a large number of realisations obtained by Monte Carlo (MC) sampling. For each investigated correlation length ratio, the mean value $\mu\{\hat{\mu}_{s,j}\}$ and the standard deviation $\sigma\{\hat{\mu}_{s,j}\}$ of the individual realisations mean values are depicted as a function of the sample size n_{MC} in Figure 6.3.

As can be seen in Figure 6.3a, for a high number of random field realisations, the mean $\mu\{\hat{\mu}_{s,j}\}$ of all individual realisation mean values $\hat{\mu}_{s,j}, j = 1, \ldots, n_{\mathrm{MC}}$, converges to the hyper parameter mean value of the random field, i.e. $\mu_S = 0$, independent of the correlation length ratio. On the contrary, the corresponding standard deviation $\sigma\{\hat{\mu}_{s,j}\}$ converges towards different values depending on the correlation length ratio, see Figure 6.3b. More precisely, $\sigma\{\hat{\mu}_{s,j}\}$ converges towards smaller values in case of small and larger values in case of large correlation length ratios. In the extremes, it converges towards zero in case of white noise[2] and towards $\sigma_S = 1$ in case of a random variable. This confirms the assumption which has been made regarding the three exemplified random field realisations given in Figure 6.2 and the following can be concluded:

- Small correlation length ratios L_S/l lead to a high variation within each standard normal distributed random field realisation $s_j(z) = S(\omega_j, z)$ but to a small variation of the corresponding individual mean values $\hat{\mu}_{s,j}$ with respect to the underlying hyper parameter $\mu_S = 0$.

- Large correlation length ratios L_S/l result in relatively constant random field realisations $s_j(z) = S(\omega_j, z)$ but the corresponding individual mean values $\hat{\mu}_{s,j}$ vary much more from the underlying hyper parameter $\mu_S = 0$.

$\Rightarrow$ For this reason, the standard deviation $\sigma\{\hat{\mu}_{s,j}\}$ of the individual mean values $\hat{\mu}_{s,j}$ converges to different values for different ratios L_S/l, bounded by

$$\sigma\{\hat{\mu}_{s,j}\} = \begin{cases} 0 & \text{for } L_S/l \to 0 \\ \sigma_S & \text{for } L_S/l \to \infty \end{cases}, \tag{6.1}$$

where $\sigma_S = 1$ is hyper parameter standard deviation of the standard normal distributed random field, inserted to Eq. (3.9). The mean value $\mu\{\hat{\mu}_{s,j}\}$ of the individual random field mean values $\hat{\mu}_{s,j}$ however converges towards the hyper parameter mean value $\mu_S = 0$.

Describing a general, d-dimensional Gaussian random field $X(\omega, z) \sim \mathcal{N}(\mu_X, \sigma_X), z \in \mathcal{D}^d$ as a standard normal distributed random field $S(\omega, z)$ scaled by σ_X and shifted towards μ_X,

$$X(\omega, z) = \mu_X + \sigma_X \cdot S(\omega, z), \tag{6.2}$$

---

[2]Note that this is only the case for an infinite number of elements $n_{\mathrm{el}} \to \infty$, however, $n_{\mathrm{el}} = 500$, are sufficient to achieve a small value, but not $\sigma\{\hat{\mu}_{s,j}\} \to 0$.

it can be concluded that the mean value $\mu\{\hat{\mu}_{x,j}\}$ of the individual mean values $\hat{\mu}_{x,j}$ converges towards the hyper parameter μ_X of the random field and $\sigma\{\hat{\mu}_{x,j}\}$ is bounded by

$$\sigma\{\hat{\mu}_{x,j}\} = \begin{cases} 0 & \text{for } L_X/l \to 0 \\ \sigma_X & \text{for } L_X/l \to \infty \end{cases}, \qquad (6.3)$$

This finding regarding the statistical behaviour of the individual random field mean values is used in the next section to provide a decoupled interpolation approach based on preliminary knowledge about the input random field.

6.2. Decoupled interpolation approach

It has been found in Section 6.1 that the correlation length mainly affects the standard deviation $\sigma\{\hat{\mu}_{x,j}\}$ of the individual realisations mean value $\hat{\mu}_{x,j}$ but rarely the mean value $\mu\{\hat{\mu}_{x,j}\}$ of the input random field. The same has been observed for the mean value $\mu\{y\}$ and standard deviation $\sigma\{y\}$ of the output QoI y in Subsection 5.2.1, where the maximum beam deflection $w_{\max}$ has been investigated for different correlation length ratios, $L_E/l = 0.1$, $L_E/l = 1.0$ and $L_E/l = 10.0$. The resulting standard deviations $\sigma\{w_{\max}\}$ versus the corresponding value $\sigma\{\hat{\mu}_{E,j}\}$ of the Young's modulus E considered as input random field are depicted in Figure 6.4. Additionally, a linear regression obtained from the three pairs is depicted in a blue dashed line.
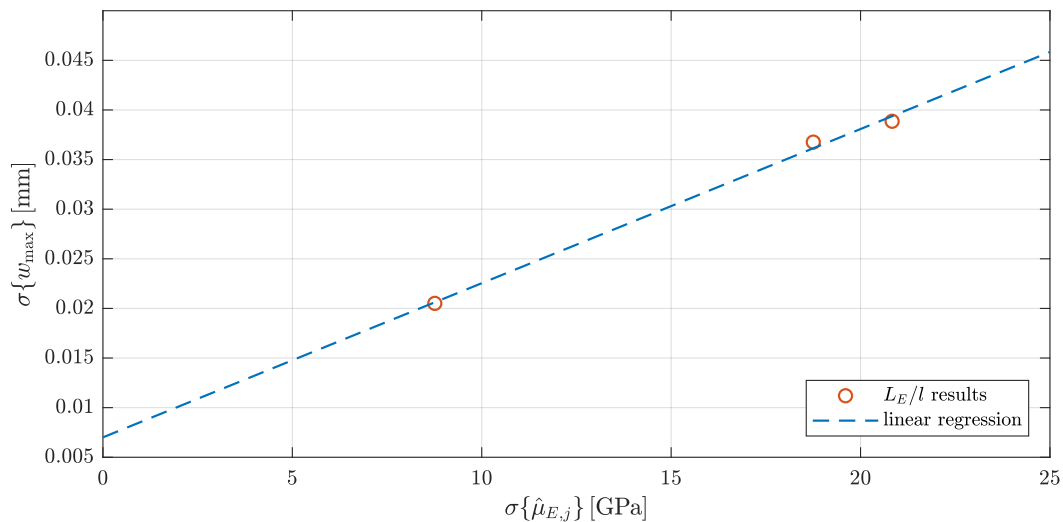
Figure 6.4: Dependence between the standard deviation $\sigma\{\hat{\mu}_{E,j}\}$ of the Young's modulus realisations individual mean values and the standard deviation $\sigma\{w_{\max}\}$ of the output quantity of interest, resulting from the Monte Carlo simulations from Subsection 5.2.1.

Note that, although a linear-elastic material law has been applied in this example, the mechanical response to a varying Young's modulus is non-linear as it is in the denominator when solving the bending problem for the beam deflection. Still, the dependency between $\sigma\{\hat{\mu}_{E,j}\}$ and $\sigma\{w_{\max}\}$ appears to be approximately linear. Therefore, for the decoupled interpolation approach developed in the following, a linear dependency is assumed. Afterwards, the assumption is examined for different cases in Section 6.3 and Section 6.4.

In the following subsection, the interpolation approach is introduced from a descriptive point of view, considering one uncertain input parameter. Afterwards, the general algorithmic treatment is provided, before defining different error measures in Subsection 6.2.3.

6.2.1.   General idea

The concept of imprecise random fields considers a lack of knowledge regarding one or more random field hyper parameters, e.g. described by intervals. In this context, assuming an interval valued correlation length has shown to be the most challenging, both in terms of propagation but also in terms of estimating the interval bounds at all, as the correlation structure is difficult (if at all) to be measured. A first step is therefore to consider the concept of having absolutely no idea on the correlation length, i.e. $L_X \in (0, \infty)$. This means to assume the random field to be anything between white noise (WN), $L_X \to 0$, and a random variable (RV), $L_X \to \infty$. It is assumed (and later studied) that also the standard deviation of a QoI considering WN converges towards zero, $\sigma\{y\} \to 0$. Then, with the mean value $\mu\{y\}$ being independent from the correlation length, an output QoI can be described by the p-box resulting from

$$\overline{F}_Y = \min\left\{ F_Y^{\mathrm{RV}}(y),\ \mu_{\mathrm{RV}}\{y\} \right\}, \tag{6.4}$$

$$\underline{F}_Y = \max\left\{ F_Y^{\mathrm{RV}}(y),\ \mu_{\mathrm{RV}}\{y\} \right\}. \tag{6.5}$$

As this p-box results from the correlation length to be any value, the resulting $\mathcal{P}_0^\infty = [\overline{F}_Y, \underline{F}_Y]_0^\infty$ is called *absolutely no idea probability box (ani-p-box)*. The benefit of simulating an ani-p-box is mainly given by the stochastic dimension to be propagated, which is $N = n_{\mathrm{RV}}$, i.e. only driven by the number of uncertain parameters considered in the input. On the contrary, when also random fields are involved, the stochastic dimension is generally obtained by Eq. (5.2) and therefore increases rapidly even for a low number n_{RF} of random fields.

In a second step, the idea is to exploit the prior knowledge about the converged value $\sigma\{\hat{\mu}_{x,j}\}$ of an input random field corresponding to a certain correlation length L_X as well as a certain (linear) dependence between input and output. Assuming the output distribution family to be independent of the correlation length, this enables to interpolate the results from the ani-p-box instead of propagating the random field through the model. As soon as the Fredholm integral equation is solved, creating a high number of random field realisations $x_j(\boldsymbol{z}) = X(\omega_j, \boldsymbol{z})$, and then their individual mean values $\hat{\mu}_{x,j}$ and the resulting standard deviation $\sigma\{\hat{\mu}_{x,j}\}$ is very cheap. The computational cost would occur from the propagation of the realisations through the model. Furthermore, when the random field can be described in terms of a standard normal distributed random field, $X(\omega, \boldsymbol{z}) = \mu_X + \sigma_X \cdot S(\omega, \boldsymbol{z})$, the standard deviation $\sigma\{\hat{\mu}_{s,j}\}$ can be determined and stored once as a function of the correlation length ratio L_X/l for a given correlation kernel. The converged standard deviation of an arbitrary Gaussian random field $X(\omega, \boldsymbol{z}) \sim \mathcal{N}(\mu_X, \sigma_X)$ corresponding to a certain correlation length ratio $L = L_X/l$ can then be directly obtained from

$$\sigma_L\{\hat{\mu}_{x,j}\} = \sigma_X \cdot \sigma_L\{\hat{\mu}_{s,j}\}. \tag{6.6}$$

The general idea of the interpolation approach based on an ani-p-box is visualised in Figure 6.5 considering one uncertain input parameter and assuming a linear dependence between input and output.
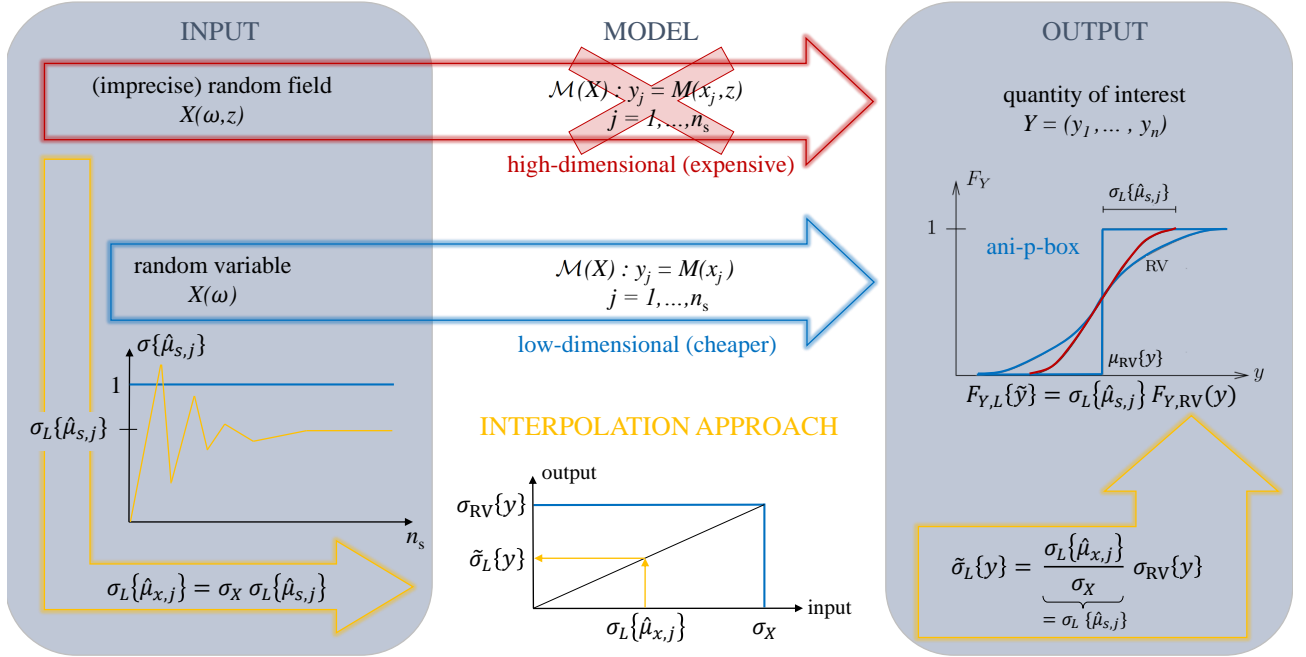

Figure 6.5: Interpolation approach based on an ani-p-box.

As described before, instead of an (imprecise) random field $[X](\omega, \boldsymbol{z})$ (red), a random variable $X(\omega)$ (blue) with the same μ_X and σ_X is propagated through the model to determine the ani-p-box. The linear connection is obtained from the points $(0,0)$ and $(\sigma_X, \sigma_{\mathrm{RV}}\{y\})$, where $\sigma_{\mathrm{RV}}\{y\})$ is the standard deviation of the QoI obtained by propagating the random variable. Then, determining the standard deviation $\sigma\{\hat{\mu}_{x,j}\}$ of the individual realisations mean values corresponding to the correlation length ratio $L = L_X/l$, the resulting standard deviation $\sigma_L\{y\}$ of an input random field can be estimated directly from the standard deviation $\sigma_{\mathrm{RV}}\{y\}$ obtained by the random variable input,

$$\tilde{\sigma}_L\{y\} = \underbrace{\frac{\sigma_L\{\hat{\mu}_{x,j}\}}{\sigma_X}}_{=\sigma_L\{\hat{\mu}_{s,j}\}} \cdot \sigma_{\mathrm{RV}}\{y\}. \tag{6.7}$$

The factor $\sigma_L\{\hat{\mu}_{x,j}\}/\sigma_X$ is determined from the linear connection and is equal to the standard deviation $\sigma_L\{\hat{\mu}_{s,j}\}$ obtained from the individual mean values of the standard normal distributed random field realisations. It can further be used to interpolate the cumulative distribution function (CDF) $F_{Y,L}(\tilde{y})$ by discretising the ani-p-box horizontally and interpolate the value $F_i(\tilde{y})$ from the corresponding interval $y_i^I = [\underline{y}_i, \overline{y}_i]$, i.e.

$$F_{Y,L}(\tilde{y}) = \sigma_L\{\hat{\mu}_{s,j}\} \cdot F_{Y,\mathrm{RV}}(y). \tag{6.8}$$

The tilde symbol indicates that the corresponding value has been obtained by interpolation. By this approach, the double loop of the probability bounds analysis described in Algorithm 1 is decoupled into two separate loops. The first one is the aleatory loop propagating a random

variable input to obtain the ani-p-box of the QoI. If this is done, the epistemic uncertainties are discretised in a second loop but the resulting scenarios are not propagated but only interpolated within the ani-p-box.

If only one input parameter is considered as (imprecise) random field, just one scenario (this very parameter considered as a random variable) needs to be propagated, as depicted in Figure 6.5. If several (imprecise) random fields are applied, multiple scenarios arise, occurring from each combination of $L_{X,i}/l = (0,\infty), i = 1,\ldots,n_{\mathrm{RF}}$. As white noise converges towards the same mean value but to a standard deviation of zero, the parameter can be assumed to be deterministic instead, assigning the mean value to it. By this, it is not necessary to propagate any white noise, what can become computationally costly too, as a high mesh resolution is required to capture the variability.

Regarding two imprecise random field parameters $[X_1](\omega, \boldsymbol{z})$ and $[X_2](\omega, \boldsymbol{z})$, this leads to three scenarios to be propagated,

- both parameters as random variable: $X_1(\omega)$, $X_2(\omega)$,

- the first parameter as random variable, the second deterministic: $X_1(\omega)$, $X_2 = \mu_{X_2}$,

- the first parameter deterministic, the second as random variable: $X_1 = \mu_{X_1}$, $X_1(\omega)$.

The stochastic dimension of each scenario is $N \leq n_{\mathrm{IRF}} = 2$. The standard deviation $\sigma\{y\}$ of the QoI corresponding to the pair (L_{X_1}, L_{X_2}) is then estimated from the bi-linear surface obtained by the scenarios given above (and additionally the point zero for both parameters assumed to be white noise) spanned over $[0, \sigma\{\hat{\mu}_{X_1,j}\}] \times [0, \sigma\{\hat{\mu}_{X_2,j}\}]$. Applying three imprecise random field parameters, seven scenarios occur with each a stochastic dimension of $N \leq n_{\mathrm{IRF}} = 3$. Note that, applying an appropriate sophisticated sampling technique, the propagation of these scenarios is assumed to be much less expensive than propagating the imprecise random fields directly, where due to high truncation orders often only a brute force MC simulation is possible.

6.2.2.   Algorithmic treatment

The decoupled approach outlined above is described by Algorithm 2. Again, only non-intrusive stochastic methods, i.e. sampling based approaches, are used and FE models will be applied as black box model in later applications using Abaqus. The algorithm itself is implemented in Matlab.

The first part is the aleatory propagation of the random variables. For that purpose, the RV scenarios occurring from the IRF input parameters are determined. These arise from combining each IRF parameter $[X_i](\omega, \boldsymbol{z})$ considered (i) as a random variable $X_i(\omega)$ with the same hyper parameters μ_{X_i} and σ_{X_i} and (ii) as a deterministic value with $X_i = \mu_{X_i}$. Then, the ani-p-box can be determined based on the chosen model and (sophisticated) sampling technique using Algorithm 3.

After the ani-p-box is obtained, the (discretised) epistemic uncertainties are considered in the second part of Algorithm 2. Note that also a purely aleatory random field propagation could be replaced by this interpolation method if the ani-p-box exists. Then, only one scenario

---

Algorithm 2 Decoupled approach to propagate imprecise random fields (IRFs) occurring from interval valued correlation lengths L_X^I.

Require:
  monotonic model (black box)
  quantity of interest (QoI)
  (sophisticated) sampling technique
  number of samples n_s
  number of IRF parameters n_{IRF}
  hyper parameters $\mu_X = (\mu_{X_1}, \mu_{X_2}, \dots)$, $\sigma_X = (\sigma_{X_1}, \sigma_{X_2}, \dots)$, $L_X^I = (L_{X_1}^I, L_{X_2}^I, \dots)$

  % determine RV scenarios c_{RV}
  if $n_{IRF} = 1$ **then**
    % one scenario
    $c_{RV} = X(\omega)$ with μ_X and σ_X
  else
    % vertex analysis
    $c_{RV} = [X_i(\omega), X_i]^\times, \quad X_i(\omega)$ with μ_{X_i} and σ_{X_i} and $X_i = \mu_{X_i}$ deterministic
  end if

  % propagate aleatory uncertainties
  determine ani-p-box   ▷ **Algorithm 3**: model, sampling technique, n_s, c_{RV}

  % determine random field (RF) scenarios c_{RF}
  if only RF input **then**
    % one scenario
    $c_{RF} = L_{X_i}$
  else
    % vertex analysis
    $c_{RF} = [\underline{L}_{X_i}, \overline{L}_{X_i}]^\times$
  end if

  % interpolate epistemic uncertainties
  determine p-box by interpolation   ▷ **Algorithm 4**: ani-p-box, c_{RF}, n_{IRF}

  % finalise simulation
  visualise p-box results for QoI
  save p-box results

---

occurs regarding directly the crisp correlation lengths L_{X_i} assigned to each considered random field $X_i(\omega, \mathbf{z})$. For imprecise random fields, the different scenarios are obtained by combining each of corresponding interval bounds $[\underline{L}_{X_i}, \overline{L}_{X_i}]$. This is only possible, when the influence of intermediate values is negligible, as it has been shown to be for static problems in the context of solid mechanics [Dannert et al., 2021a]. The CDF or p-box resulting from the random field or imprecise random field, respectively, can then be interpolated from the ani-p-box using Algorithm 4.

The two algorithms to determine the ani-p-box and the interpolated p-box are described in more detail in the following two paragraphs.

Determine the ani-p-box: Based on the RV scenarios obtained in Algorithm 2 by the random variables and deterministic values corresponding to the (imprecise) random fields, the corresponding ani-p-box is obtained by Algorithm 3. Each scenario needs to be propagated through the black box model according to the chosen (sophisticated) sampling technique. For each generated sample, a deterministic model evaluation is performed. The computational cost is therefore mainly depending on the chosen sampling technique, i.e. the required number of samples n_s. After the repetitive deterministic model evaluations, the stochastic response in terms of the stochastic moments or the CDF is determined according to the chosen sampling technique, e.g. by statistical evaluation (MC method) or the meta model provided by PC or SC method.

The ani-p-box is obtained afterwards from the different scenarios. The mean value $\mu_\mathrm{RV}\{y\}$ is assumed to be crisp and equal to the deterministic solution y_0 assuming $X_i = \mu_{X,i}$. Note that for the later interpolation, the standard deviation $\sigma_c\{y\}$ of each scenario needs to be stored in $\sigma_{\mathrm{RV},c}$, not only the minimum and maximum bound. The bounds of the ani-p-box are determined by minimising and maximising the CDFs obtained from the different scenarios including the CDF corresponding to white noise, which is assumed to be a vertical line equal to the mean value $\mu_\mathrm{RV}\{y\} = y_0$ for an infinite number of elements, $n_\mathrm{el} \to \infty$.

Determine the p-box by interpolation: When the ani-p-box is available for a certain set of random variable input parameters, any p-box resulting from one or more of these parameters being an (imprecise) random field can be estimated directly from the ani-p-box according to Algorithm 4. For each scenario c, the standard deviation $\sigma_L\{\hat{\mu}_{x_i,j}\}$ of the individual mean value $\hat{\mu}_{x_i,j}$ corresponding to the random field $X_i(\omega, \mathbf{z})$ with the correlation length ratio $L = L_X/l$, can be estimated by the unified results obtained by a standard normal distributed random field as given in Eq. (6.6). Then, the standard deviation $\tilde{\sigma}_{L,c}\{y\}$ of the output QoI y corresponding to the scenario c and the underlying correlation length ratio $L = L_X/l$ can be estimated by linear interpolation from the RV scenarios. If only one (imprecise) random field is considered as input parameter, this is equivalent to scaling the random field result by the unified standard deviation of the individual standard normal distributed random field realisations mean values, see Eq. (6.7). With this estimated standard deviation, the CDF corresponding to the scenario c given $L = L_X/l$ is interpolated within the ani-p-box, see Eq. (6.8). For that purpose, the

CDF is discretised into horizontal intervals, which are then scaled by $\tilde{\sigma}_{L,s}\{y\}$ and added to the mean value $\mu_{\mathrm{RV}}\{y\} = y_0$,

$$\tilde{y}_{L,c} = \mu_{\mathrm{RV}}\{y\} + \tilde{\sigma}_{L,c}\{y\} \cdot (y_{\mathrm{RV}} - \mu_{\mathrm{RV}}\{y\}). \tag{6.9}$$

From the CDFs of all scenarios, the p-box bounds are determined by minimisation and maximisation. The same is done for the interval valued standard deviation $\tilde{\sigma}^I\{y\}$. The mean value is again assumed to be crisp and equal to the mean value obtained from the random variable scenarios.

Algorithm 3 Approach to determine a p-box based on having absolutely no idea (ani-p-box) about the correlation length, i.e. $L_X \in (0, \infty)$.

Require:
    monotonic model (black box)
    (sophisticated) sampling technique
    number of samples n_{s}
    random variable (RV) scenarios c_{RV}

    % simulate scenarios
    for each $c \in c_{\mathrm{RV}}$ **do**

        % propagate aleatory uncertainties
        for $j = n_{\mathrm{s}}$ **do**
            generate random variable realisation j
            propagate j through model   ▷ black box, e.g. FE solver by Abaqus
            save realisation and model response
        end for
        determine $\mu_c\{y\}$, $\sigma_c\{y\}$ and $F_{Y,c}(y)$ of QoI   ▷ according to sampling technique

    end for

    % determine statistical information corresponding to each IRF parameter X_i
    $\mu_{\mathrm{RV}}\{y\} = y_0$ (deterministic solution assuming μ_{X_i})
    $\sigma_{\mathrm{RV},c} = (\sigma_1\{y\}, \sigma_2\{y\}, \dots)$

    % determine ani-p-box
    left bound $\overline{F}_Y^{\mathrm{RV}} = \min\{F_{Y,c}(y), \mu_{\mathrm{RV}}\{y\}\}$
    right bound $\underline{F}_Y^{\mathrm{RV}} = \max\{F_{Y,c}(y), \mu_{\mathrm{RV}}\{y\}\}$

    return ani-p-box: $[\overline{F}_Y^{\mathrm{RV}}, \underline{F}_Y^{\mathrm{RV}}]_0^\infty$, $\mu_{\mathrm{RV}}\{y\}$, $\sigma_{\mathrm{RV},c}$

Algorithm 4 Interpolate a cumulative distribution function or a probability box within the corresponding ani-p-box.

Require:
   absolutely no idea probability box (ani-p-box)
   random field (RF) scenarios c_{RF}
   number of imprecise random field (IRF) parameters n_{IRF}

   % discretise epistemic uncertainties
   for each $c \in c_{\mathrm{RF}}$ **do**

      % get input statistics of standard normal distributed RF
      if $\sigma\{\hat{\mu}_{s,j}\}$ available **then**
         load $\sigma_L\{\hat{\mu}_{s,j}\}$ of current correlation structure
      else
         determine converged $\sigma_L\{\hat{\mu}_{s,j}\}$ by KL expansion
         save $\sigma_L\{\hat{\mu}_{s,j}\}$
      end if

      % determine input information of each IRF parameter X_i
      $\sigma_L\{\hat{\mu}_{x_i,j}\} = \sigma_{X_i} \cdot \sigma_L\{\hat{\mu}_{s,j}\}$

      % estimate output standard deviation of the random field scenario
      if $n_{\mathrm{IRF}} > 1$ **then**
         interpolate $\tilde{\sigma}_{L,c}\{y\}$ from $\sigma_{\mathrm{RV},c}$ vs. $\sigma\{\hat{\mu}_{x_i,j}\}$
      else
         $\tilde{\sigma}_{L,c}\{y\} = (\sigma\{\hat{\mu}_{x,j}\}/\sigma_X)\,\sigma_{\mathrm{RF}}\{y\}$
      end if

      % interpolate output y of current random field scenario (for each QoI)
      $\tilde{y}_{L,c} = \mu_{\mathrm{RV}}\{y\} + \tilde{\sigma}_{L,c}\{y\} \cdot (y_{\mathrm{RV}} - \mu_{\mathrm{RV}}\{y\})$
      determine CDF $F_Y(\tilde{y}_{L,c})$

   end for

   % post-processing: determine p-box (for each QoI)
   left bound $\overline{F}_{\tilde{Y}} = \min\left\{\, F_Y(\tilde{y}_{L,c}) \,\right\}$
   right bound $\underline{F}_{\tilde{Y}} = \max\left\{\, F_Y(\tilde{y}_{L,c}) \,\right\}$
   $\tilde{\mu}\{y\} \simeq \mu_{\mathrm{RV}}\{y\}$
   $\tilde{\sigma}^I\{y\} = [\, \min\{\tilde{\sigma}_{L,c}\{y\}\},\ \max\{\tilde{\sigma}_{L,c}\{y\}\} \,]$

   return p-box: $[\overline{F}_{\tilde{Y}}, \underline{F}_{\tilde{Y}}]$, $\tilde{\mu}\{y\}$, $\tilde{\sigma}^I\{y\}$

6.2.3. Error measures

The interpolated p-box results of the provided decoupled algorithm based on an ani-p-box is validated with brute force MC simulations. The accuracy can then be quantified by error measures relative to the MC results. For example, the distance between the interpolated and the sampled results can be obtained and depicted similarly to the interval radii description of a p-box introduced in Figure 2.5. This means in the horizontal case to discretise $F_Y(y)$ into $i = 1, \ldots, n_F$ intervals of y^I,

$$\tilde{\Delta} y_i = y_i^{\mathrm{MC}} - \tilde{y}_i, \tag{6.10}$$

and plot the distance vertically as a function of $F_{Y,i}(y)$. Additionally, the vertical distance is obtained by discretising y into into $i = 1, \ldots, n_y$ intervals of $F_Y^I(y)$,

$$\tilde{\Delta} F_{Y,i} = F_{Y,i}^{\mathrm{MC}}(y) - F_{Y,i}(\tilde{y}), \tag{6.11}$$

and plotting the results horizontally as a function of y_i.

Alternatively, Eq. (6.10) can be unified by determining the relative error given by

$$\tilde{\epsilon}\{y_i\} = \frac{|y_i^{\mathrm{MC}} - \tilde{y}_i|}{|y_i^{\mathrm{MC}}|}. \tag{6.12}$$

Note that a relative error obtained from the vertical distance in Eq. (6.11) is not an appropriate error measure, as the denominator can become (too close to) zero for the left tail $F_Y^{\mathrm{MC}}(y) \to 0$ of the CDF. However, as the CDF is always defined on the unit range, $F_Y \in [0, 1]$, the distance is naturally a relative measure and can be compared for different simulations directly.

6.3. Study on one-dimensional random fields

The decoupled interpolation approach proposed in Section 6.2 is studied carefully regarding 1D random fields in the following. For that purpose, two different scenarios are investigated. In Subsection 6.3.1, the algorithm is applied to a problem considering linear-elastic material behaviour. Afterwards, a non-linear problem is studied in Subsection 6.3.2 regarding elasto-plastic material behaviour including linear hardening. Both problems are applied to a 1D physical model such that the individual sample propagation is relatively cheap in terms of computational cost. This way, for each simulation a MC sampling with a high sample number $n_{\mathrm{MC}} = 1 \times 10^5$ is feasible to investigate the general applicability.

6.3.1. Bending beam with linear-elastic material behaviour

In this study, the interpolation algorithm is applied to the bending beam already introduced in Figure 5.3 of Subsection 5.2.1. However, the beam of length $l = 1\,\mathrm{m}$ is here discretised by $n_{\mathrm{el}} = 500$ beam elements to represent white noise properly. As the QoI, the maximum beam deflection w_{max} in the beam centre is investigated. The deterministic result considering a Young's modulus $E = 210\,\mathrm{GPa}$ and a constant line load $q_0 = 50\,\mathrm{kN}\,\mathrm{m}^{-1}$ is $w_{\mathrm{max}} = 0.37\,\mathrm{mm}$.

In the following, two input parameters are investigated as input random fields, the line load $q(\omega, z)$ and the Young's modulus $E(\omega, z)$. Afterwards, a study considering both parameters as input random fields is provided. These three examples have already been studied intensively by Dannert et al. [2021b] for the proposed interpolation approach regarding the SE correlation kernel. Note that within the mentioned contribution, the correlation length has been discretised by much more scenarios than the three scenarios used here. The assumption of a monotonic dependence of the output QoI is supported by the results provided therein. In contrast, the ME correlation function is used here, regarding three different correlation length ratios, $L_X/l = 0.1$, $L_X/l = 1.0$ and $L_X/l = 10.0$.

The response of the QoI $w_{\max}$ of both parameters is depicted in Figure 6.6 as a function of the parameter range resulting from the corresponding mean value and a certain standard deviation. For a Gaussian random variable, 99.73% of the samples lay within the range $\mu_X \pm 3\sigma_X$. The resulting ranges corresponding to different assumptions on the relative standard deviation, $\sigma_X = r \cdot \mu_X$, are depicted in vertical lines. The dashed lines mark the range $\mu_X \pm 3\sigma_X^{5\%}$ when $r = 0.05$ is assumed, the dash-dotted lines correspond to $r = 0.1$ and the dotted lines to $r = 0.2$.
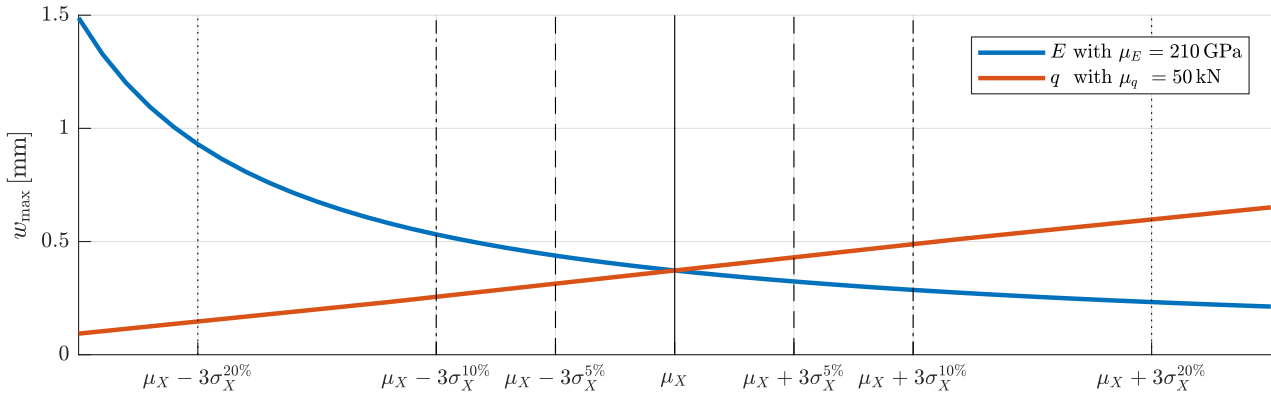

Figure 6.6: Maximal beam deflection $w_{\max}$ of the linear-elastic beam as a function of different input parameters.

Regarding the line load, it can be seen that the response is depending linearly on its value, independent from the assumed relative standard deviation. This is plausible as the line load can be found in the numerator of the bending equation. On the contrary, the Young's modulus is located in the denominator, leading to a non-linear response. However, for small relative standard deviations, e.g. $r = 0.05$, the response can still be considered to be almost linear. In order to see the effect of a slightly non-linear response, a relative standard deviation of ten percent is chosen in the following studies.

Investigations for a linear response

The line load $q(\omega, z)$ is considered as random field with a mean value $\mu_q = 50\,\text{kN}\,\text{m}^{-1}$ and a standard deviation $\sigma_q = 0.1\mu_q$. First, the assumption of linear dependency between the standard deviation of the individual input realisations mean values $\sigma\{\hat{\mu}_{q,j}\}$, and the standard deviation $\sigma\{w_{\max}\}$ of the QoI resulting from sampling is reviewed in Figure 6.7. For that purpose, the result considering a random variable is given in a grey circle and the linear dependency is depicted in a blue line from the point $(0,0)$ to the random variable result.
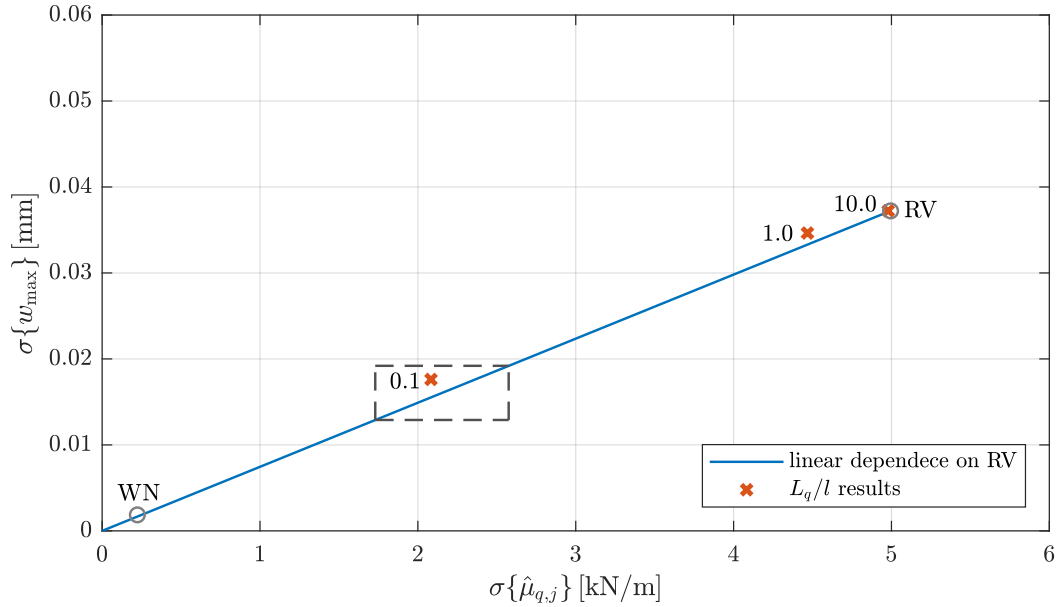
Figure 6.7: Almost linear dependence between the input standard deviation $\sigma\{\hat{\mu}_{q,j}\}$ of the individual realisations mean value $\hat{\mu}_{q,j}$ and the standard deviation $\sigma\{w_{\max}\}$ of the output maximum beam deflection $w_{\max}$ obtained by $n_{\mathrm{el}} = 500$ and $n_{\mathrm{MC}} = 1 \times 10^5$ for each scenario, considering the line load $q(\omega, z)$ as random field input.
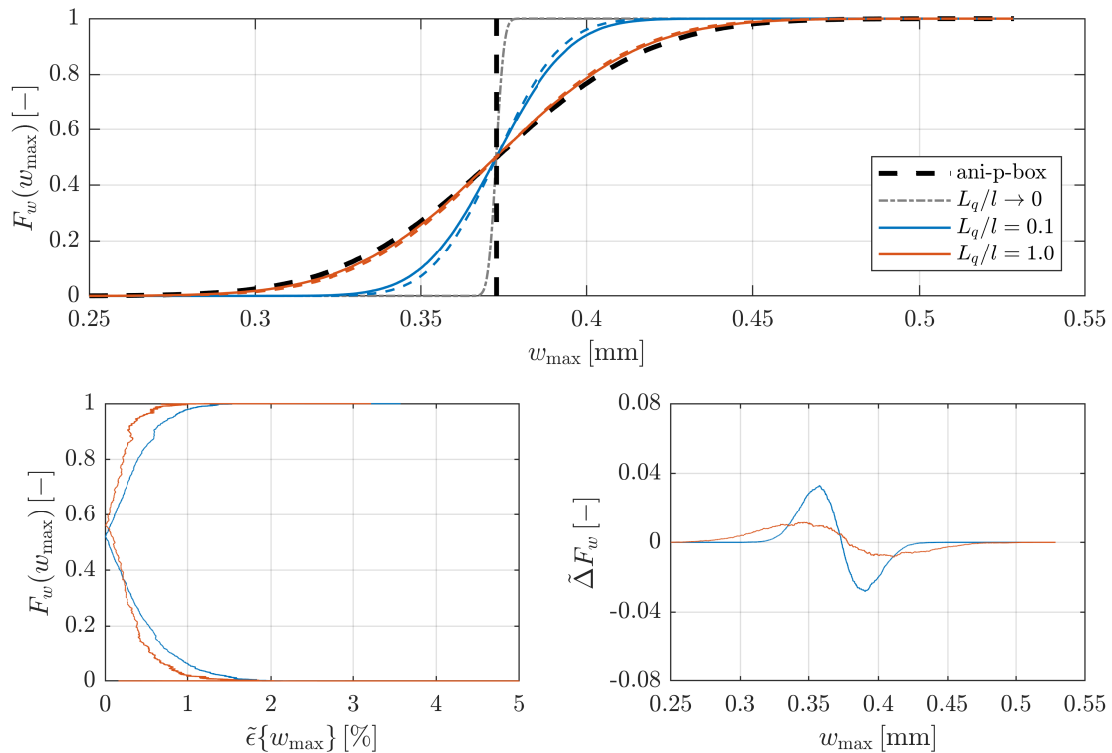
Figure 6.8: Cumulative distribution functions for two correlation length ratios, $L_q/l = 0.1$ (blue) and $L_q/l = 1.0$ (red), obtained by sampling with $n_{\mathrm{MC}} = 1 \times 10^5$ MC samples (solid lines) as well as resulting from a linear interpolation within the ani-p-box (dashed lines), complemented with the corresponding error measures $\tilde{\epsilon}\{w_{\max}\}$ (bottom left) and $\tilde{\Delta}F_w$ (bottom right), when considering the line load $q(\omega, z)$ as an input random field.

Each pair $(\sigma\{\hat{\mu}_{q,j}\}, \sigma\{w_{\max}\})$ corresponding to the different values L_q/l is depicted as a red cross. It can be seen that the results lay slightly above the blue line visualising the linear dependency. For that reason, the interpolated standard deviation $\tilde{\sigma}\{w_{\max}\}$ slightly underestimates the standard deviation obtained from sampling. This could be ascribed to approximation errors, e.g. in terms of the chosen number of elements n_{el}, truncation order T or sample size n_{MC}. All three parameters are therefore investigated in the further course for the correlation length ratio $L_q/l = 0.1$, regarding the close up area as indicated with the grey dashed lined box. The result corresponding to the correlation length ratio $L_q/l = 10.0$ lays already very close to the one obtained by the random variable. Additionally, the result assuming white noise (with regard to $n_{\mathrm{el}} = 500$) is depicted in a grey circle. It can be seen that it lays close to the origin but is not zero for both, input and output standard deviation. However, with an increasing element number, the result would converge towards zero.

The results obtained from the interpolation algorithm are depicted in Figure 6.8. In the top figure, the ani-p-box is depicted in black, dashed lines. Furthermore, the CDF of the white noise result is given in a grey line. It can be assumed that it converges towards the vertical line of the ani-p-box for $n_{\mathrm{el}} \to \infty$. The CDFs gained by sampling and propagating the random fields are depicted in solid lines, blue for $L_q/l = 0.1$ and red for $L_q/l = 1.0$. The corresponding CDFs resulting from interpolation are depicted in dashed lines of the same colours. The results of $L_q/l = 10.0$ are neglected in this figure as they are effectively similar with the ones obtained from the random variable, i.e. the non-vertical bound of the ani-p-box.

The two figures in the bottom of Figure 6.8 depict the relative error $\tilde{\epsilon}\{w_{\max}\}$ defined by Eq. (6.12) on the left, while the distance $\tilde{\Delta}F_w$ is given as a function of $w_{\max}$ on the right[3]. At the very tails, the error $\tilde{\epsilon}\{w_{\max}\}$ can become very high due to the sparsity of the unlikely events. However, regarding $\tilde{\Delta}F_w$ it can be seen that the distance converges towards zero in the tails. Besides the tails, the error can be quantified to be $\tilde{\epsilon}\{w_{\max}\} \leq 2\,\%$ in case of $L_q/l = 0.1$ and $\tilde{\epsilon}\{w_{\max}\} \leq 1\,\%$ for $L_q/l = 1.0$.

As the largest error is obtained for the correlation length ratio $L_q/l = 0.1$, the influence of different approximation errors is investigated in the following. For that purpose, each one of the parameters, (i) the element number n_{el}, (ii) the truncation order T and (iii) the sample size n_{MC}, is varied while the other two parameters stay fixed. For each of these adjustments, five simulation packages with each new samples are performed, to ensure that observable effects are not traced back to randomness. Note that for this extensive study, only $n_{\mathrm{MC}} = 1 \times 10^4$ samples are used for each simulation package to reduce the computational effort.

Number of elements: At first, the effect of the number of elements is investigated regarding the correlation length ratio $L_q/l = 0.1$. For that purpose, five simulations are performed, each with $n_{\mathrm{el}} = 10$ (blue circles), $n_{\mathrm{el}} = 50$ (yellow circles), $n_{\mathrm{el}} = 100$ (violet circles) and $n_{\mathrm{el}} = 500$ (red crosses) element numbers. The results are depicted in Figure 6.9 in the closed up region as marked in Figure 6.7.

---

[3]Note that the axes of the relative error, $\tilde{\epsilon}\{w_{\max}\} = [0, 5]$, and the distance, $\tilde{\Delta}F_w = [-0.08, 0.08]$, are chosen in this scale in order to be comparable with later results.
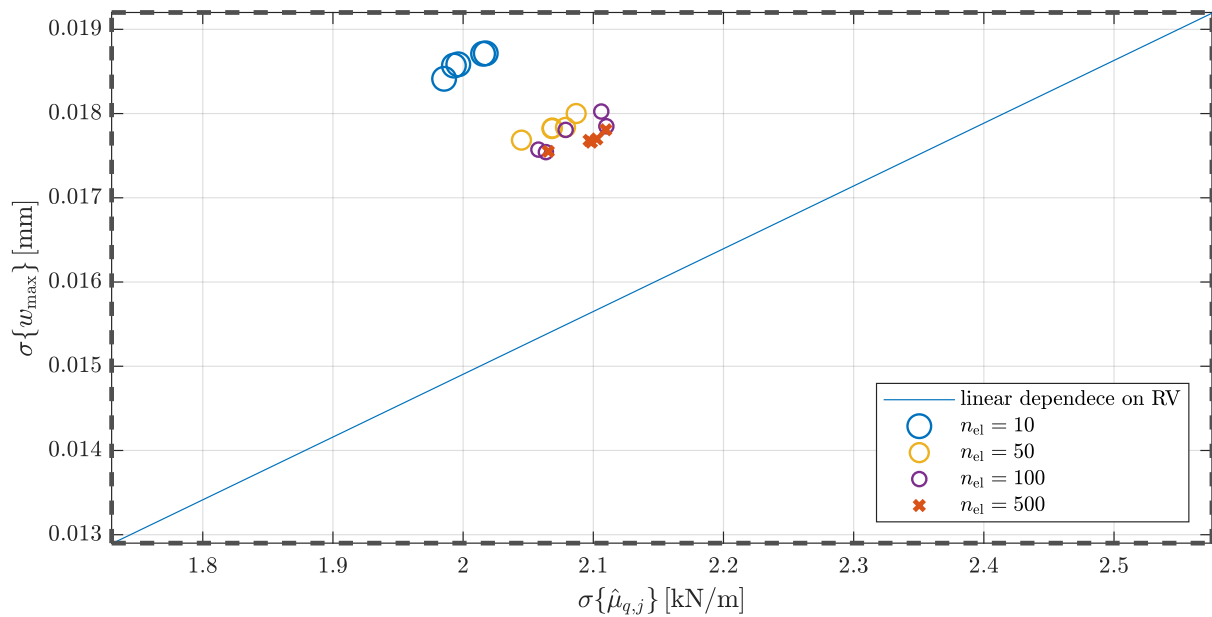
Figure 6.9: Influence of the number of FE elements n_{el} on the dependency between input and output standard deviation, applying the correlation length ratio $L_q/l = 0.1$, with $T = 102$ and $n_{\mathrm{MC}} = 1 \times 10^4$ for each scenario.

It can be seen that the results corresponding to the same number of elements are still varying slightly. This is due to the relatively small sample size $n_{\mathrm{el}} = 1 \times 10^4$. However, as n_{el} is always the same for each simulation, the results do not scatter more or less for the different values of n_{el}. Increasing the number of elements, the results get closer to the line symbolising the linear dependence of the random variable results. The approximation error due to the element number therefore has an effect on the dependency between $\sigma\{w_{\mathrm{max}}\}$ and $\sigma\{\hat{\mu}_{q,j}\}$. Still, the results are already converging for $n_{\mathrm{el}} = 500$ and it cannot be assumed that increasing the element number further would achieve results matching with the linear dependence line. Regarding the computational cost involved for high mesh precision, increasing n_{el} further for just a little effect seems not worth the effort.

Truncation order: In a next step, the influence of the truncation order T is studied. For that purpose, T is chosen such that it reduces the truncation error by the factor ten for each step. The truncation terms needed for an aimed mean truncation error, $\bar{\epsilon}_{\bar{\Gamma}} \leq 15\,\%$, $\bar{\epsilon}_{\bar{\Gamma}} \leq 1.5\,\%$, $\bar{\epsilon}_{\bar{\Gamma}} \leq 0.15\,\%$ and $\bar{\epsilon}_{\bar{\Gamma}} \leq 0.015\,\%$, are given in Table 6.1. For the sake of transparency, the actually resulting mean truncation error is stated below, as a certain aimed error cannot necessarily be achieved. However, for the purpose of studying the general influence of T, the given actual errors are accepted.

Table 6.1: Truncation order T and resulting mean truncation error $\bar{\epsilon}_{\bar{\Gamma}}$, corresponding to different aimed truncation errors $\bar{\epsilon}$, assuming a correlation length ratio $L_q/l = 0.1$.

aimed mean truncation error	$\bar{\epsilon}_{\bar{\Gamma}} \leq 15\,\%$	$\bar{\epsilon}_{\bar{\Gamma}} \leq 1.5\,\%$	$\bar{\epsilon}_{\bar{\Gamma}} \leq 0.15\,\%$	$\bar{\epsilon}_{\bar{\Gamma}} \leq 0.015\,\%$
truncation order $T\,[-]$	8	21	46	102
resulting mean truncation error $\bar{\epsilon}_{\bar{\Gamma}}\,[\%]$	14.5700	1.3820	0.1409	0.0147

The results of each five simulations for the different truncation orders $T = 8$, $T = 21$, $T = 46$ and $T = 102$ are depicted in Figure 6.10. Note that for the sake of comparability, the same close up interval is chosen as before. It can be seen that the influence of the truncation order is much smaller than the influence of the mesh size. Increasing T further would not lead to a better approximation and therefore cannot show evidence for an actually linear dependency.
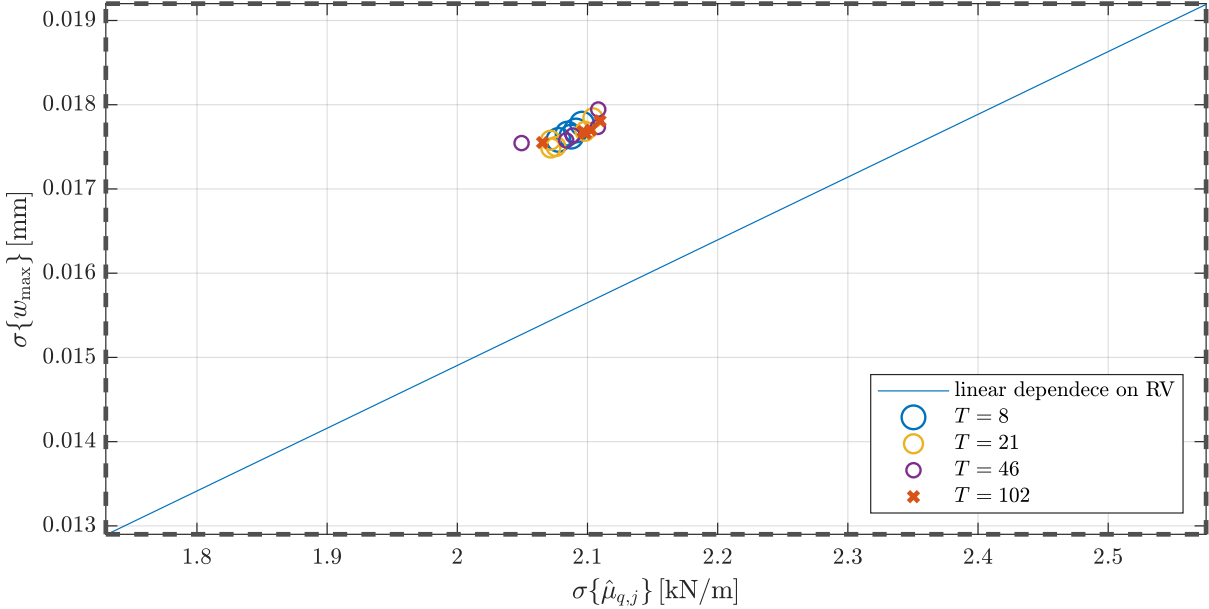

Figure 6.10: Influence of the truncation order T on the dependency between input and output standard deviation, applying the correlation length ratio $L_q/l = 0.1$, with $n_{el} = 500$ and $n_{MC} = 1 \times 10^4$ for each scenario.

Number of samples: At last the effect of the sample size n_{MC} is investigated. Here, also $n_{MC} = 1 \times 10^5$ is included, as this is the sample size used in the studies before. As the convergence of the stochastic moments depends on the sample size, a high variation of the results is expected for small sample sizes. This can indeed be observed in Figure 6.11. While the results scatter relatively wide for $n_{MC} = 100$ and $n_{MC} = 1000$, they concentrate more for $n_{MC} = 1 \times 10^4$ and are almost not distinguishable for $n_{MC} = 1 \times 10^5$. However, increasing the sample size does not have the effect of resulting closer to the linear dependency line.

Summary: In Figure 6.7 it has been observed that the assumption of a linear dependency between $\sigma\{w_{max}\}$ and $\sigma\{\hat{\mu}_{q,j}\}$ is not perfectly correct. In order to investigate whether this is just an issue of convergence, the influence of different parameters affecting the approximation error has been studied in the last paragraphs. The element number n_{el} has been the only parameter for which an effect could be shown with respect to approaching the linear dependency line for higher values. However, the results appeared to converge to a value which is still above the linear dependency line. While, compared to the element number, the truncation order T did not have a significant effect on the results, the sample size n_{MC} has shown a huge influence, but mainly on the scattering and rarely on the convergence of the results towards the linear dependency line.
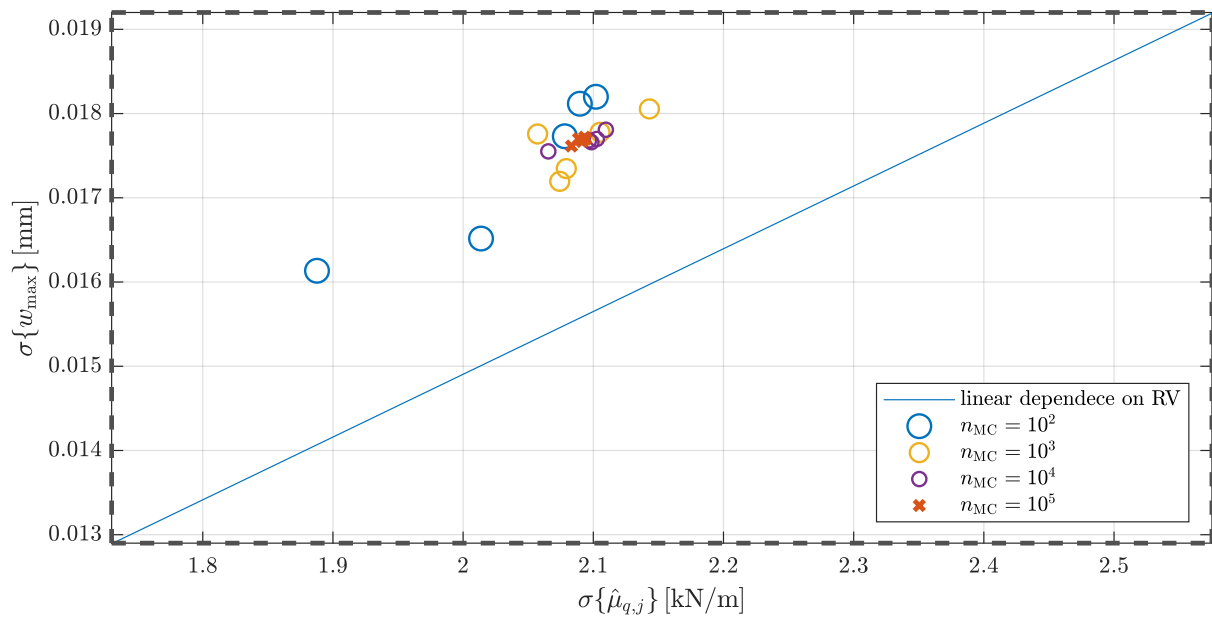
Figure 6.11: Influence of the number of MC samples n_{MC} on the dependency between input and output standard deviation, applying the correlation length ratio $L_q/l = 0.1$, with $n_{el} = 500$ and $T = 102$.

It can be concluded that the dependency is indeed not perfectly linear. In other words, a true linear dependency cannot be achieved by more accurate simulations. Still, the assumption of a linear dependency appears appropriate for an estimate, especially when the propagation of imprecise random fields involves a much higher computational cost than determining the anip-box for $L_q/l = (0, \infty)$. Furthermore, as the true correlation structure and correlation length are unknown anyway and the whole simulation is based on imprecise model assumptions, the inaccuracy resulting from the decoupled interpolation algorithm can be justified.

Investigations for a non-linear response

The study is repeated considering the Young's modulus as input random field with $\mu_E = 210\,\text{GPa}$ and $\sigma_E = 0.1\mu_E$, leading to a moderately non-linear response. As can be seen in Figure 6.12, this has an influence on the accuracy regarding a linear estimate of the output standard deviation. Especially for the small correlation length ratio $L_E/l = 0.1$ the standard deviation obtained from sampling is significantly underestimated by the interpolated pendant assuming linear dependence. It has been shown for the case of a random field line load that increasing the precision of the - already relatively precise - simulations will not improve the results to be more linearly dependent. For that reason, the convergence study is not repeated for the Young's modulus once more.

The resulting interpolated CDFs for the ratios $L_E/l = 0.1$ and $L_E/l = 1.0$ are investigated in Figure 6.13. Here, the impact of underestimating the standard deviation can clearly be seen. While the CDF corresponding to $L_E/l = 1.0$ appears to be interpolated sufficiently (and provide also a relative error of $\tilde{\epsilon}\{w_{max}\} \leq 2\,\%$), the difference between the interpolated and the sampled CDF obtained by $L_E/l = 0.1$ is already clearly noticeable in the CDF itself. The error in the lower tail becomes about $\tilde{\epsilon}\{w_{max}\} = 4\,\%$. Furthermore, a distinct difference of the
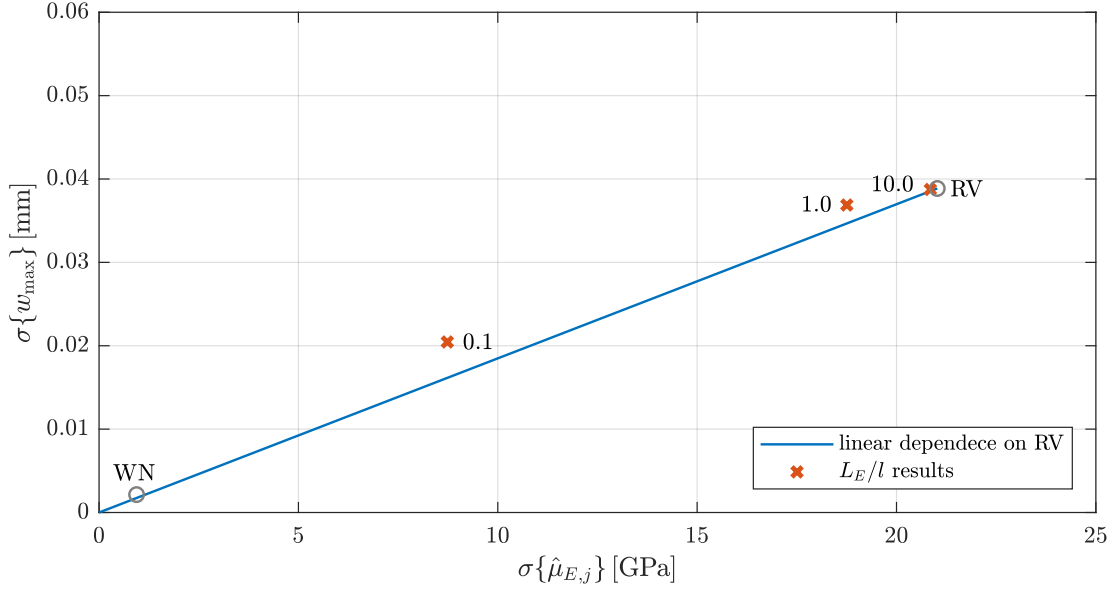
Figure 6.12: Slightly non-linear dependence between the input standard deviation $\sigma\{\hat{\mu}_{E,j}\}$ of the individual mean value $\hat{\mu}_{E,j}$ and the standard deviation $\sigma\{w_{\max}\}$ of the output maximum beam deflection $w_{\max}$ obtained by $n_{\mathrm{el}} = 500$ and $n_{\mathrm{MC}} = 1 \times 10^5$ for each scenario, considering the Young's modulus $E(\omega, z)$ as random field input.
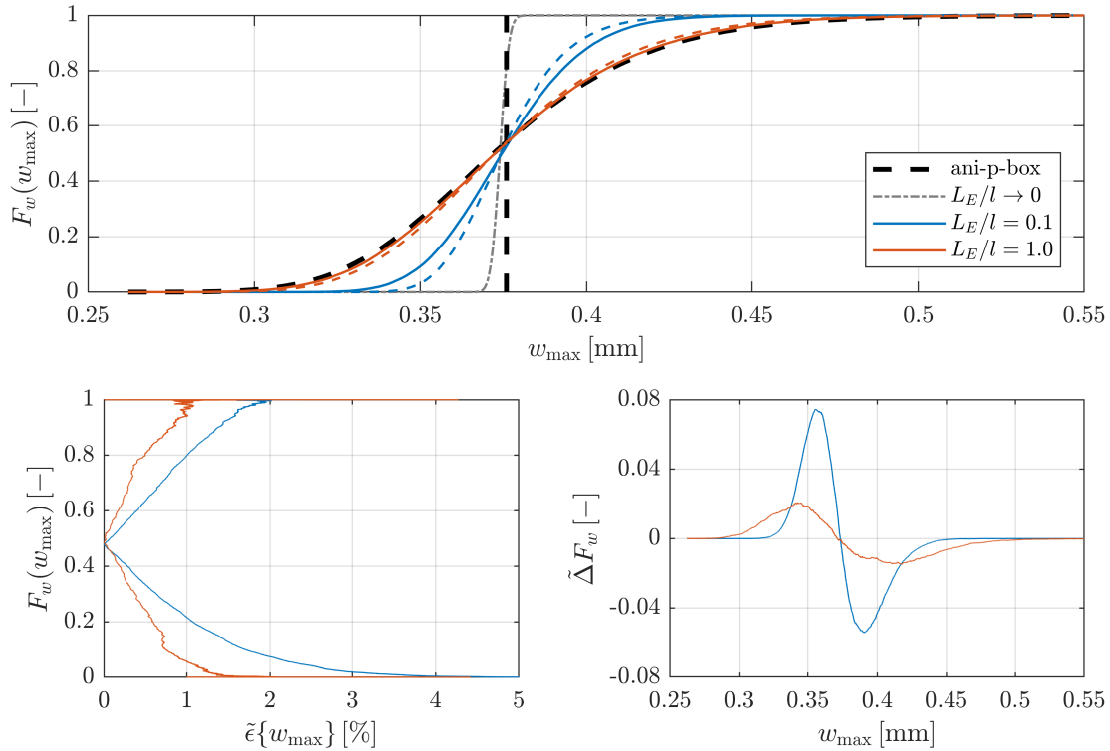
Figure 6.13: Cumulative distribution functions for two correlation length ratios, $L_E/l = 0.1$ (blue) and $L_E/l = 1.0$ (red), obtained by sampling with $n_{\mathrm{MC}} = 1 \times 10^5$ MC samples (solid lines) as well as resulting from a linear interpolation within the ani-p-box (dashed lines), complemented with the corresponding error measures $\tilde{\epsilon}\{w_{\max}\}$ (bottom left) and $\tilde{\Delta}F_w$ (bottom right), when considering the Young's modulus $E(\omega, z)$ as an input random field.

errors in the upper and lower tail is visible regarding both, the relative error and the distance measure. This has not been observed (that pronounced) in the first study based on a random field line load. This is attributed to the fact that, due to the non-linear response, the Gaussian distribution of the input is not propagated towards a Gaussian distributed output anymore. For this reason, the impact of the underestimated standard deviation varies along the CDF. This suggests the idea to "correct" the linearly assumed dependency by incorporating higher moments of the QoI, but this is part of future research.

Investigations for two random field input parameters

The interference of both parameters, the line load $q(\omega, z)$ and the Young's modulus $E(\omega, z)$, being a random field is studied in the following. The hyper parameters and correlation lengths for both parameters are considered the same as before. The bi-linear dependency between the QoI $w_{\max}$ and the corresponding input values $\sigma\{\hat{\mu}_{q,j}\}$ and $\sigma\{\hat{\mu}_{E,j}\}$ is symbolised with a blue surface in Figure 6.14. The surface is obtained by the scenarios described by the combination of deterministic and random variable simulations. The four scenarios resulting from each parameter being assumed as a random variable or white noise are depicted as grey circles, to verify the assumption of the white noise converging towards zero. The results obtained by sampling and propagating the random fields according to the random field scenario $(L_q/l, L_E/l)$ are given by red crosses. The corresponding interpolated result laying on the surface is depicted as a black dot. Furthermore, to facilitate the view on the distance between the sampled and the interpolated result, the red crosses and the corresponding black points are connected by a black line. If the line is not or only barely visible, the both results coincide. This is the case for many correlation length combinations.
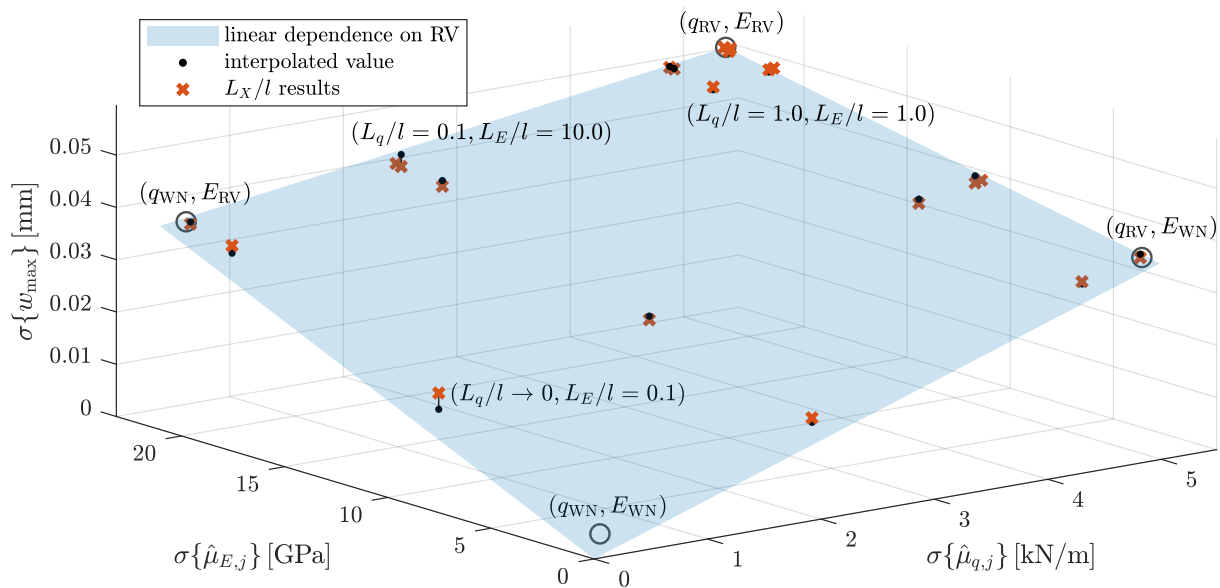
Figure 6.14: Bi-linear dependence between the input standard deviations $\sigma\{\hat{\mu}_{q,j}\}$ and $\sigma\{\hat{\mu}_{E,j}\}$ of the individual mean values $\hat{\mu}_{q,j}$ and $\hat{\mu}_{E,j}$ and the standard deviation $\sigma\{w_{\max}\}$ of the output maximum beam deflection $w_{\max}$ obtained by $n_{\mathrm{el}} = 500$ and $n_{\mathrm{MC}} = 1 \times 10^5$ for each scenario, considering the line load $q(\omega, z)$ and the Young's modulus $E(\omega, z)$ as input random fields.

The largest distance can be observed for $(L_q/l \to \infty, L_E/l = 0.1)$. For this (i) scenario and two further examples, i.e. (ii) $(L_q/l = 0.1, L_E/l = 10.0)$ and (iii) $(L_q/l = 1.0, L_E/l = 1.0)$, the resulting CDFs are investigated further in Figure 6.15. As to be expected, the difference between the interpolated and the sampled results is most distinct for scenario (i), where both correlation lengths are small. However, regarding the error in the left tails, with $\tilde{\epsilon}\{w_{\max}\} \le 4\,\%$ scenario (ii) results in a larger error than the first scenario ($\tilde{\epsilon}\{w_{\max}\} \le 2.5\,\%$). When both correlation length ratios are moderate, as given in scenario (iii), the interpolation fits the sampled result very well. Besides the effects of not being perfectly linear, which have already been observed in the cases of one random field input, the interference of two random field input parameters does not appear to diminish the applicability of the proposed interpolation approach.
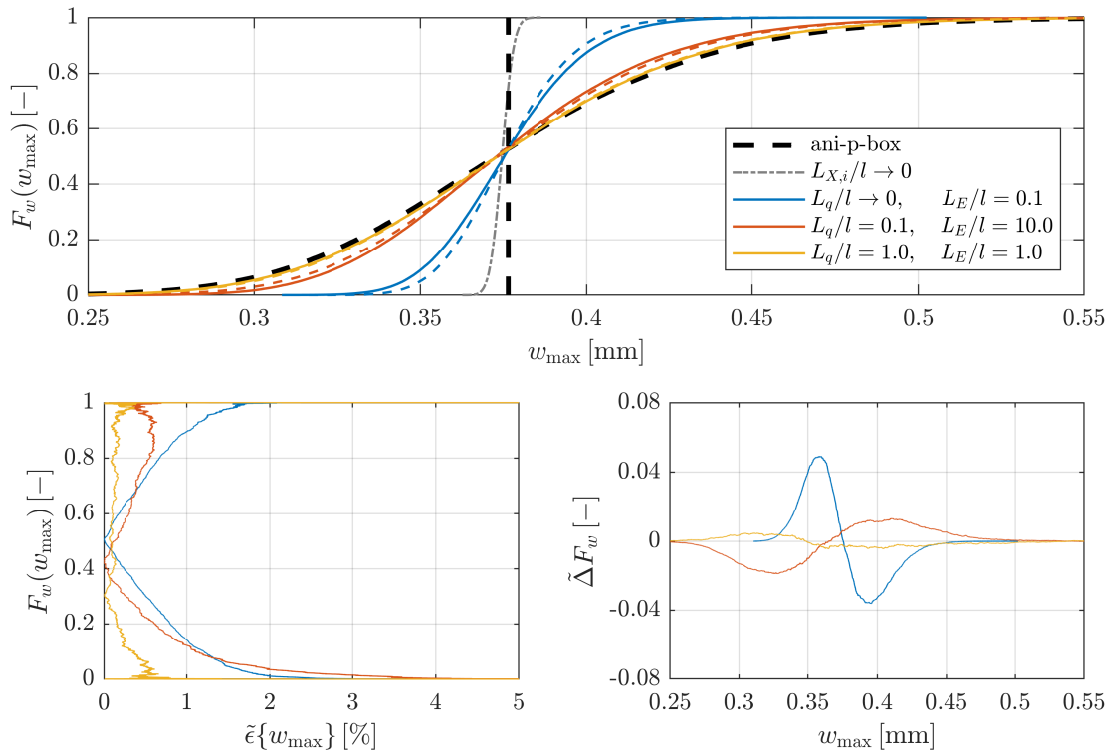

Figure 6.15: Cumulative distribution functions for three correlation length combinations obtained by sampling with $n_{\mathrm{MC}} = 1 \times 10^5$ MC samples (solid lines) as well as resulting from a linear interpolation within the ani-p-box (dashed lines), complemented with the corresponding error measures $\tilde{\epsilon}\{w_{\max}\}$ (bottom left) and $\tilde{\Delta} F_w$ (bottom right), when considering both, the line load $q(\omega, z)$ and the Young's modulus $E(\omega, z)$ as input random fields.

6.3.2.   Tensile bar with elasto-plastic material behaviour

In the following study, the interpolation algorithm is applied to a simple mechanical problem providing a non-linear model, i.e. in terms of an elasto-plastic material behaviour including linear kinematic hardening. A bar of length $l = 1\,\mathrm{m}$ and cross section $A = 0.01\,\mathrm{m}^2$ is clamped at its one end and loaded by a single tensile force $F = 3.2\,\mathrm{MN}$, as depicted in Figure 6.16. The QoI is the maximal deflection $u_{\max}$ at the free end. The bar is discretised by $n_{\mathrm{el}} = 500$ rod elements. Again, steel with a Young's modulus $E = 210\,\mathrm{GPa}$ is used. Furthermore, for the deterministic case, a yield stress $\sigma_{\mathrm{y}} = 300\,\mathrm{MPa}$ and a hardening parameter $H = 1.5\,\mathrm{GPa}$ are assumed, leading to a deterministic deflection of $u_{\max} = 14.86\,\mathrm{mm}$.

Deterministic material parameters

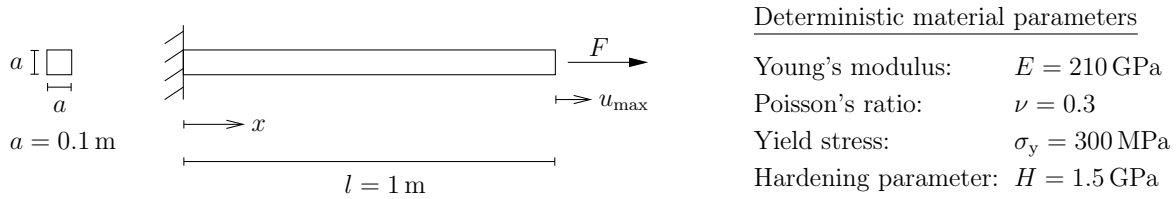|	
Young's modulus:	$E = 210\,\text{GPa}$
Poisson's ratio:	$\nu = 0.3$
Yield stress:	$\sigma_\text{y} = 300\,\text{MPa}$
Hardening parameter:	$H = 1.5\,\text{GPa}$

$a = 0.1\,\text{m}$

$l = 1\,\text{m}$

Figure 6.16: Elasto-plastic bar under axial loading $F = 3.2\,\text{MN}$, resulting in a deterministic maximal deflection: $u_\text{max} = 14.86\,\text{mm}$.

In Figure 6.17, the model response is depicted as a function of the different material parameters. Note that the response with respect to the Young's modulus is still non-linear but the influence of E is rather small compared to the yield stress σ_y. Furthermore, the response of the latter is non-differentiable due to the fact that for large values of σ_y, the yield stress is not reached regarding the given load. In the following, the interpolation approach is studied with regard to the non-linear response resulting from the hardening parameter H, as it has a slightly higher influence than E, and afterwards with regard to the non-differentiable response. Again, ten percent standard deviation are assumed for each case and the three correlation length ratios $L_X/l = 0.1$, $L_X/l = 1.0$ and $L_X/l = 10.0$ are considered. Note that regarding the range of possible samples, $\mu_{\sigma_\text{y}} \pm 3\sigma_{\sigma_\text{y}}^{10\%}$, deflections of $u_\text{max} > 50\,\text{mm}$, i.e. larger than five percent are not unlikely to be obtained. This violates the assumption of small strains. However, as this example is just applied to test the proposed algorithm in general and is not used for a real engineering design, this concern is secondary at this point. The most interesting part of the simulation is expected in the area of non-differentiability, where the deflection is small.
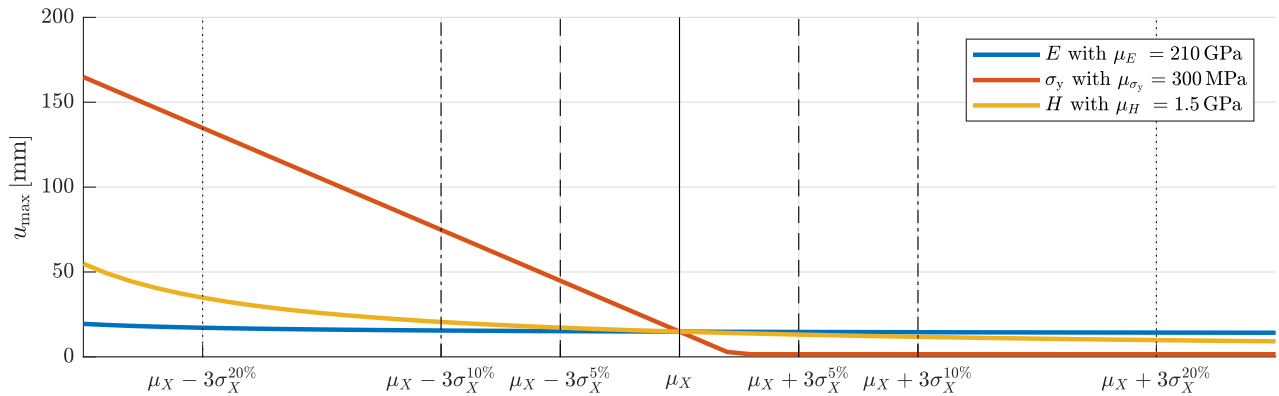

Figure 6.17: Maximal bar deflection u_max as a function of different input parameters considering an elasto-plastic material.

Investigations for a non-linear response

The elasto-plastic bar study is first performed with the hardening parameter $H(\omega, z)$ as an input random field. The mean value is chosen as $\mu_H = 1.5\,\text{GPa}$, the standard deviation is $\sigma_H = 0.1\mu_H$. Furthermore, the same three correlation length scenarios are considered as before. The dependency of the QoI standard deviation $\sigma\{u_\text{max}\}$ and the standard deviation $\sigma\{\hat{\mu}_{H,j}\}$ of the individual input realisation mean values are depicted in Figure 6.18. Again, the assumed linear dependence on the random variable is symbolised by a blue line connecting the origin (i.e. converged white noise) and the random variable result. It can be seen that the assumption of a linear dependence fits the sampled random field results very well.

Figure 6.18: Linear dependence between the input standard deviation $\sigma\{\hat{\mu}_{H,j}\}$ of the individual mean value $\hat{\mu}_{H,j}$ and the standard deviation $\sigma\{u_{\max}\}$ of the output maximum bar deflection $u_{\max}$, considering the hardening parameter $H(\omega, z)$ as random field input, obtained by $n_{\mathrm{el}} = 500$ and $n_{\mathrm{MC}} = 1 \times 10^5$ for each scenario.

Figure 6.19: Cumulative distribution functions for two correlation length ratios, $L_H/l = 0.1$ (blue) and $L_H/l = 1.0$ (red), obtained by sampling with $n_{\mathrm{MC}} = 1 \times 10^5$ MC samples (solid lines) as well as resulting from a linear interpolation within the ani-p-box (dashed lines), complemented with the corresponding error measures $\tilde{\epsilon}\{u_{\max}\}$ (bottom left) and $\tilde{\Delta} F_u$ (bottom right), when considering the hardening parameter $H(\omega, z)$ as an input random field.

As can be seen in Figure 6.19, this leads to a much better interpolation of the corresponding CDFs as well, even for the correlation length ratio $L_H/l = 0.1$. It can be concluded that the accuracy of an interpolation within the ani-p-box seems not only to depend on the system response towards a certain parameter but also on the model itself.

Investigation for a non-differentiable response

In a second study, the applicability of the decoupled interpolation algorithm towards a non-differentiable response is investigated. Again, the non-linear elasto-plastic material model including linear hardening is assumed. However, here the yield stress σ_y is considered as the random field input parameter, following a mean value of $\mu_{\sigma_y} = 300\,\text{MPa}$ and ten percent standard deviation, $\sigma_{\sigma_y} = 0.1\mu_{\sigma_y}$. Although the QoI response $u_{\max}$ shows a non-differentiability within the range of possible outcomes $\mu_{\sigma_y} \pm 3\sigma_{\sigma_y}$, the standard deviation $\sigma\{u_{\max}\}$ of the output depends linearly on the input value of $\sigma\{\hat{\mu}_{\sigma_y,j}\}$, as can be seen in Figure 6.20.
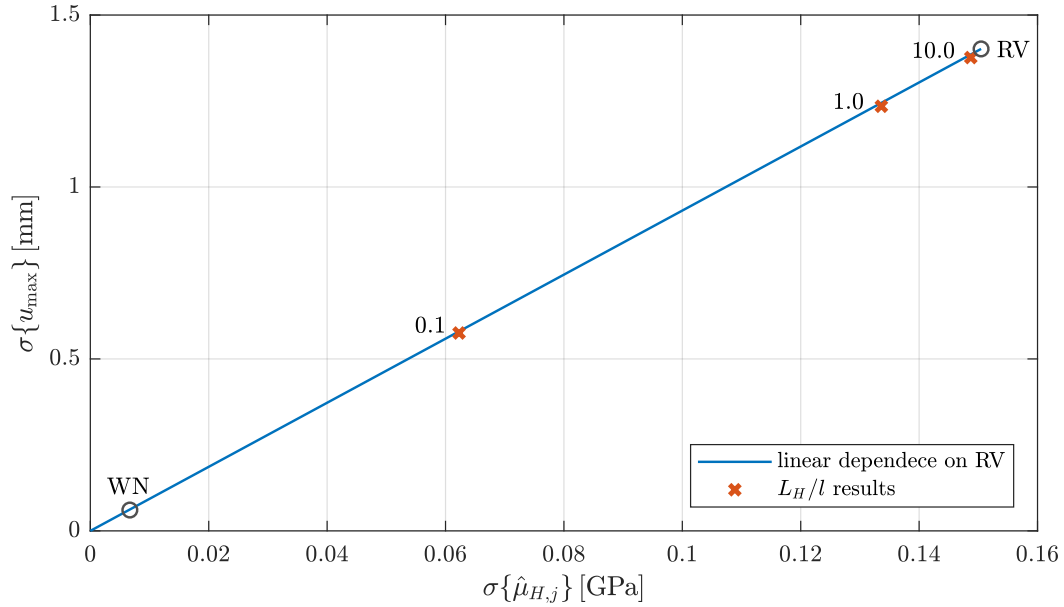

Figure 6.20: Linear dependence between the input standard deviation $\sigma\{\hat{\mu}_{\sigma_y,j}\}$ of the individual mean value $\hat{\mu}_{\sigma_y,j}$ and the standard deviation $\sigma\{u_{\max}\}$ of the output maximum bar deflection $u_{\max}$, considering the yield stress $\sigma_y(\omega, z)$ as random field input, obtained by $n_{\text{el}} = 500$ and $n_{\text{MC}} = 1 \times 10^5$ for each scenario.

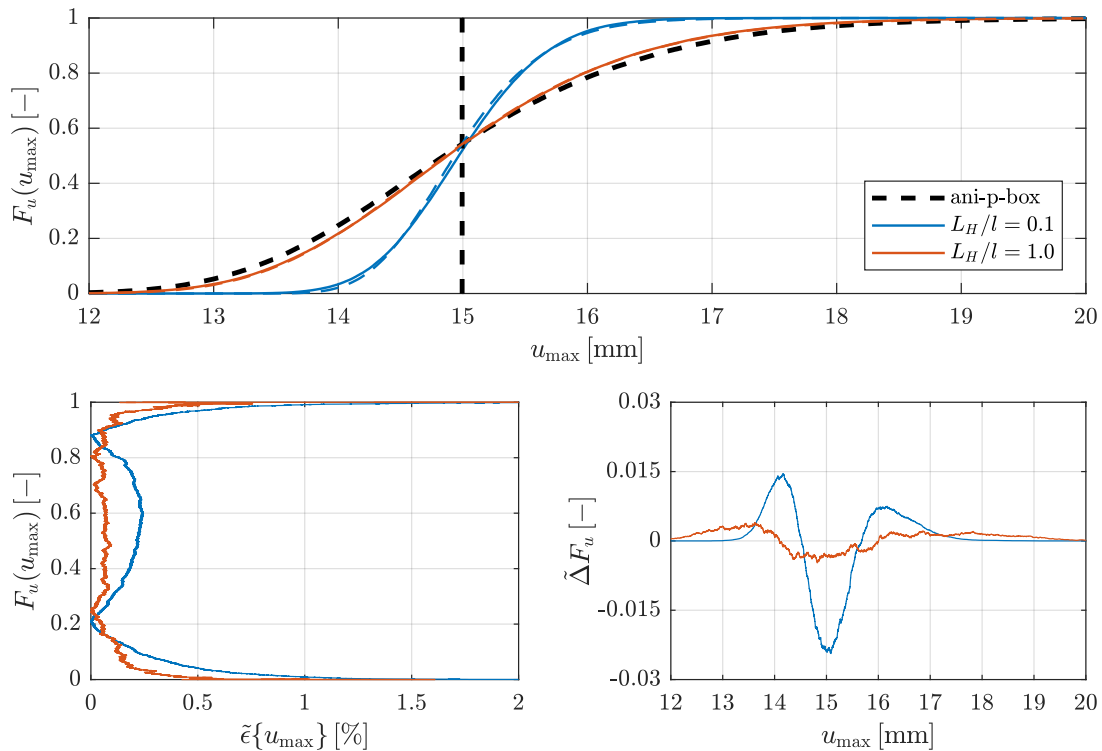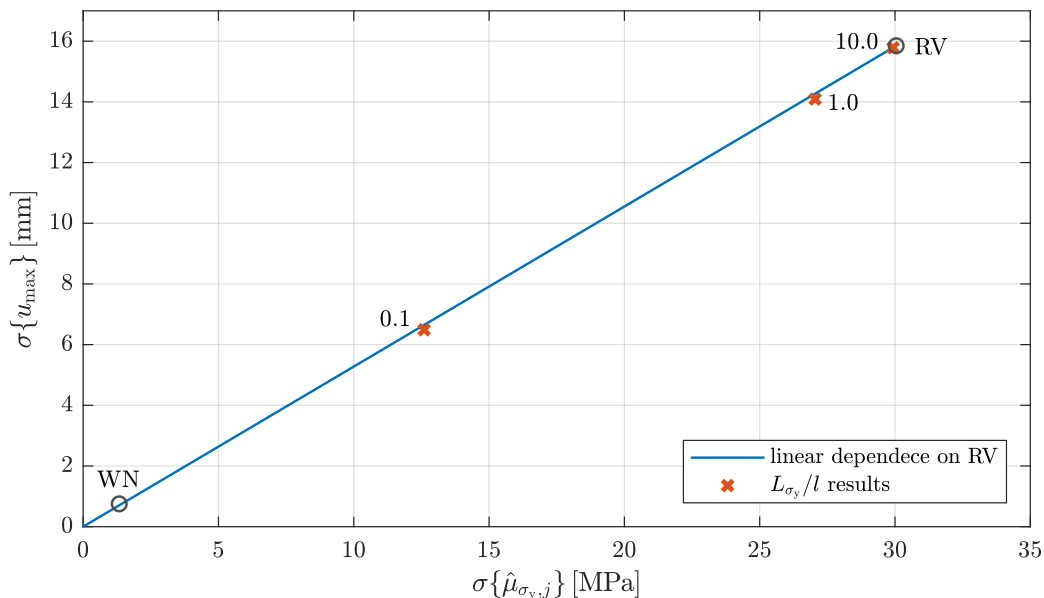Nevertheless, the interpolation within the ani-p-box does not work properly in this case, as can be observed in Figure 6.21. This is due to the non-differentiable behaviour of the response in the region where the yield stress becomes too high for the bar starting to yield at all, given the load F. Regarding a random variable, the value of the yield stress is constant for each realisation. This means that the bar starts to yield everywhere at the same time and with the same intensity or, if the yield stress realisation is too high, not at all. In the latter case, the corresponding realisations are effectively deterministic, it does not matter what exact value the yield stress realisation becomes if this stress is not reached given the applied load. The vertical part of the CDF obtained by the random variable is therefore driven by quasi deterministic realisations which are purely linear-elastic. As soon as yielding occurs, the

deflection increases so quickly that a kink in the CDF occurs. This kink is interpolated one-to-one for the correlation length scenarios. On the contrary to the random variable, however, the random fields yield stress value is not constant over the whole domain. Therefore, yielding might start in some elements already while others are still in the linear-elastic region. The higher the variability of the random field is (i.e. the smaller the correlation length is), the more unlikely it is to obtain quasi deterministic realisations in the linear-elastic region. For this reason, the vertical part is much shorter for the correlation length ratio $L_{\sigma_y}/l = 1.0$ and disappears completely for $L_{\sigma_y}/l = 0.1$. Consequently, a very large error can be obtained in the left tail, where the interpolation entails the kink of the random variable while the sampled CDF does show a smoother behaviour.
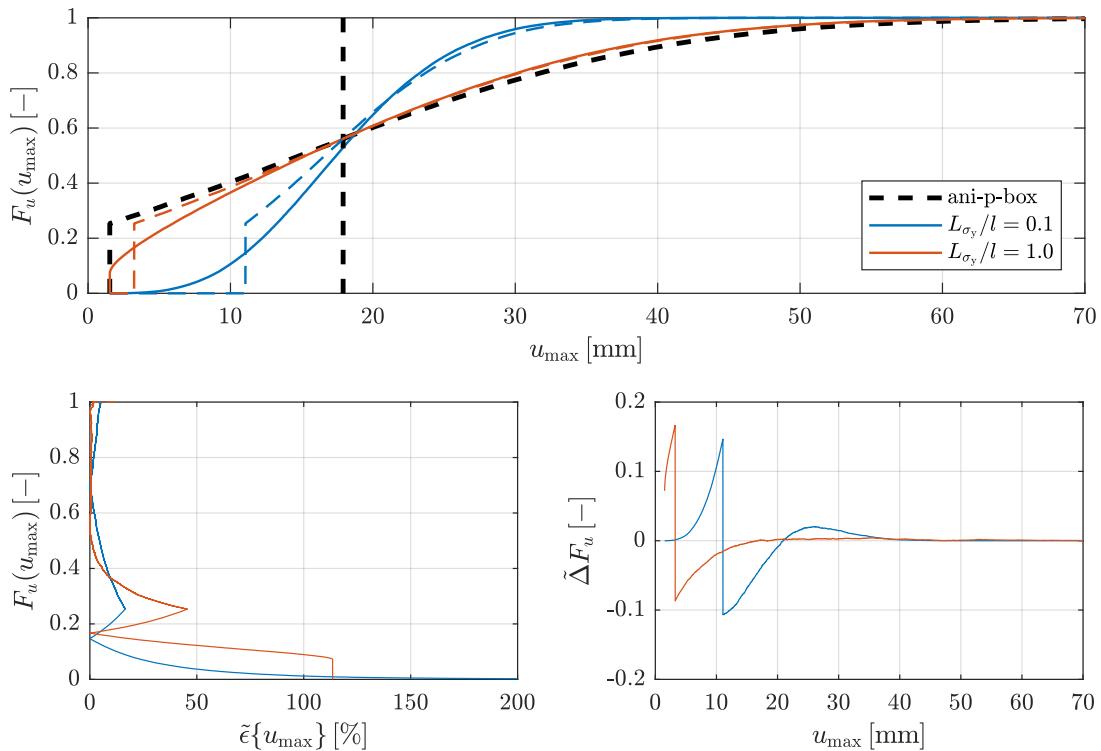
Figure 6.21: Cumulative distribution functions for two correlation length ratios, $L_{\sigma_y}/l = 0.1$ (blue) and $L_{\sigma_y}/l = 1.0$ (red), obtained by sampling with $n_{MC} = 1 \times 10^5$ MC samples (solid lines) as well as resulting from a linear interpolation within the ani-p-box (dashed lines), complemented with the corresponding error measures $\tilde{\epsilon}\{u_{max}\}$ (bottom left) and $\tilde{\Delta}F_u$ (bottom right), when considering the yield stress $\sigma_y(\omega, z)$ as an input random field.

On the other side, the errors of the right tails are relatively small, indicating a good interpolation of the sampled results. As the right tail is usually of higher interest from the engineering point of view, as it covers the case where plastic deformation happens, the interpolation approach might be useful for some applications nevertheless. However, using it should be carefully pondered. With regard to engineering application, the rebalancing of stresses in 2D and three-dimensional (3D) problems might become useful as well, in order to avoid hard kinks in case of a random variable. For this reason, the influence of the yield stress is studied once more in the next caption for a 2D example.

6.4. Application to a two-dimensional random field

To investigate the ani-p-box approach for a non-linear model including a 2D random field, the numerical example of Subsection 5.2.2 is slightly modified. The elasto-plastic material model including linear hardening as well as the deterministic material parameters stay the same as before. The yield stress is again considered as the random field input parameter, the hyper parameters are chosen as $\mu_{\sigma_y} = 300\,\text{MPa}$ and $\sigma_{\sigma_y} = 0.05\,\mu_{\sigma_y}$. A ME correlation kernel is used and different effective correlation length ratios are studied, i.e. $L_{\sigma_y}/l = 0.4$, $L_{\sigma_y}/l = 0.6$ and $L_{\sigma_y}/l = 0.8$. The corresponding correlation lengths $L_{\sigma_y}^{\text{ME}}$ and truncation orders T to achieve a mean truncation error of $\bar{\epsilon}_{\bar{\Gamma}} \leq 1.0\,\%$ are given in Table 6.2.

Table 6.2: Truncation order T required to obtain a comparable mean correlation error of $\bar{\epsilon}_{\bar{\Gamma}} \leq 1.0\,\%$ considering different effective correlation length ratios L_{σ_y}/l assuming an ME correlation function for a 2D random field.

$L_{\sigma_y}/l\,[-]$	0.4	0.6	0.8
$L_{\sigma_y}^{\text{ME}}/l\,[-]$	0.1839	0.2699	0.3503
$T\,[-]$	47	24	16
$\bar{\epsilon}_{\bar{\Gamma}}\,[\%]$	0.9816	0.9997	0.9688

As depicted in Figure 6.22, the one square-meter sized plate is only pulled at its top along its right half side by the constant line load $q_0 = 300\,\text{MPa}$. By this, the stress state is not constant anymore and a rebalancing of the stresses is achieved. As can be seen in Figure 6.23, this smoothens the QoI responses a bit, at least for some nodes, e.g. node 66. In this figure, the model responses of the displacement u_2 (left) and the equivalent plastic strain $\bar{\varepsilon}^p$ (right) are depicted for the FE nodes 61, 66 and 121 as a function of the yield stress σ_y. The black dashed vertical lines represent the stochastic domain $\mu_{\sigma_y} \pm 3\sigma_{\sigma_y}$ within which 99.73 % of the samples are included.
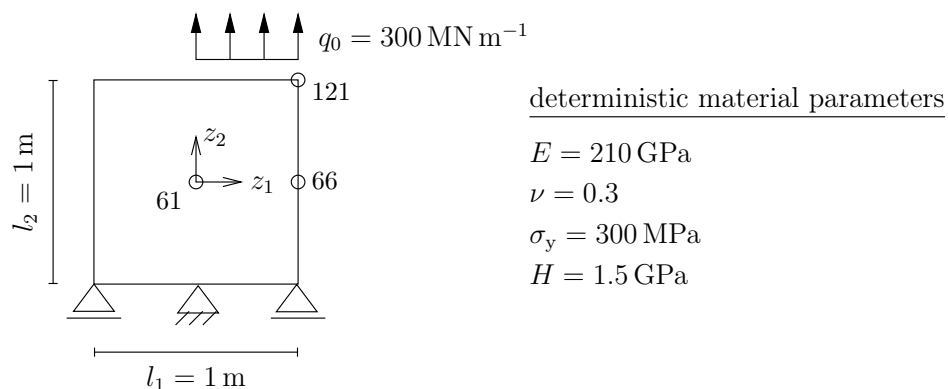
Figure 6.22: Elasto-plastic steel plate model pulled at its right side by a constant line load q_0. The quantities of interest are investigated at the nodes which marked by circles.

The maximum deflection u_2 is now expected to be at node 121. Furthermore, it can be seen for node 61 (which has been used as node of interest in Subsection 5.2.2) that $\bar{\varepsilon}^p$ is zero within the range of likely events (black dashed lines). For this reason, the equivalent plastic strain is investigated at node 66 in this example.

(a) displacement u_2 **(b)** equivalent plastic strain $\bar{\varepsilon}^{\mathrm{p}}$
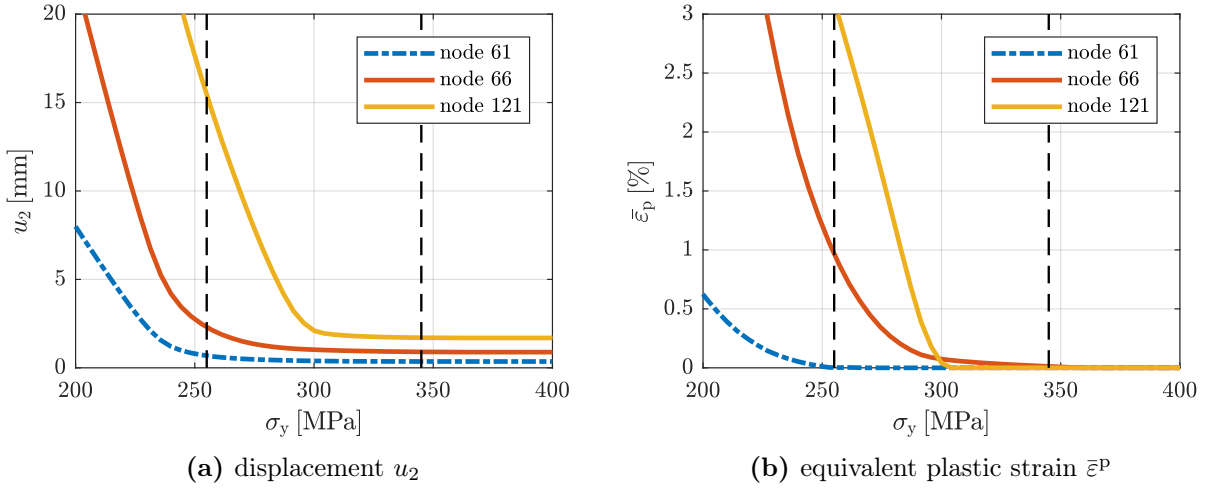
Figure 6.23: Model response of the quantity of interest at different nodes as a function of the yield stress σ_{y}.

In the following subsection, the convergence behaviour of the mean value and standard deviation for both QoI is studied. Afterwards, the ani-p-box resulting for the displacment at node 121 and the equivalent plastic strain at node 66 are depicted and discussed in Subsection 6.4.2.

6.4.1.   Investigation on the convergence behaviour

The convergence of the stochastic moments with an increasing sample size n_{MC} is depicted in Figure 6.24, using a brute force MC simulation. In Figure 6.24a, the mean value $\mu\{\hat{\mu}_{\sigma_{\mathrm{y}},j}\}$ (left) and standard d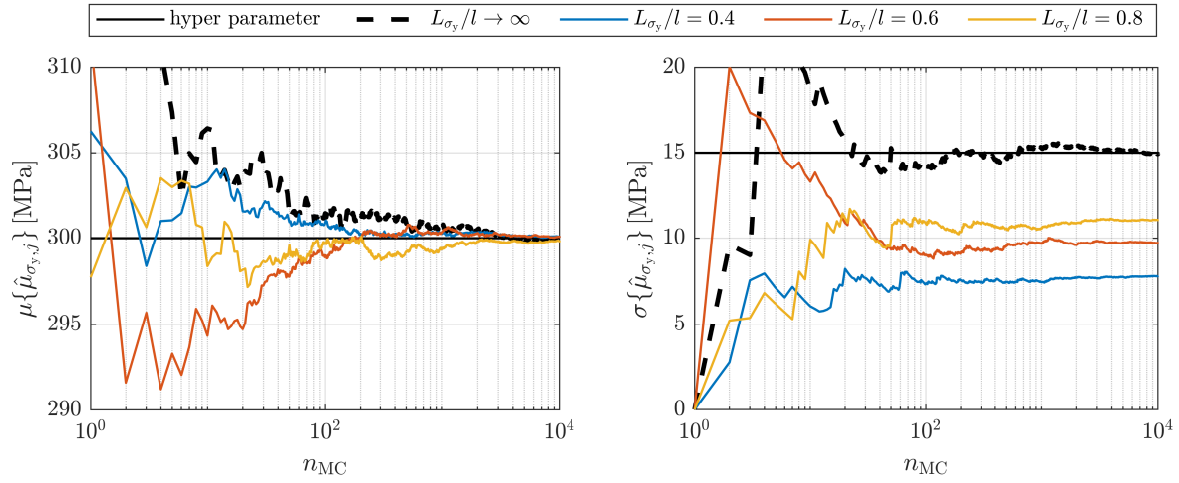eviation $\sigma\{\hat{\mu}_{\sigma_{\mathrm{y}},j}\}$ (right) of the individual random field realisation mean values $\hat{\mu}_{\sigma_{\mathrm{y}},j}$ of the input random field yield stress $\sigma_{\mathrm{y}}(\omega, \boldsymbol{z})$ are depicted for the different correlation length ratios in different colours. The convergence of the mean value and the standard deviation of the random variable realisations $(L_{\sigma_{\mathrm{y}}}/l \to \infty)$ is given in a black dashed line. The input hyper parameters $\mu_{\sigma_{\mathrm{y}}} = 300\,\mathrm{MPa}$ and $\sigma_{\sigma_{\mathrm{y}}} = 0.1\mu_{\sigma_{\mathrm{y}}} = 15\,\mathrm{MPa}$ are depicted in a black solid line.

As to be expected from the investigations in Section 6.1, $\mu\{\hat{\mu}_{\sigma_{\mathrm{y}},j}\}$ converges towards $\mu_{\sigma_{\mathrm{y}}}$ independently of the correlation length, while $\sigma\{\hat{\mu}_{\sigma_{\mathrm{y}},j}\}$ converges towards different values between zero and $\sigma_{\sigma_{\mathrm{y}}}$ depending on $L_{\sigma_{\mathrm{y}}}/l$. So far, a similar behaviour has been observed for the mean value $\mu\{Y\}$ and standard deviation $\sigma\{Y\}$ of the QoI $Y(\omega, \boldsymbol{z})$. As can be seen on the right side of Figure 6.24b for the displacement $Y(\omega) = u_2(\omega, \hat{\boldsymbol{z}}_{121})$ at node 121 and the equivalent plastic strain $Y(\omega) = \bar{\varepsilon}^{\mathrm{p}}(\omega, \hat{\boldsymbol{z}}_{66})$ at node 66, this still holds true for the standard deviation. However, the convergence of the corresponding mean values, depicted on the left side of Figure 6.24b now also appears to be dependent on the correlation length. As a first assumption the converged mean value is expected to follow the same ratio depending on $L_{\sigma_{\mathrm{y}}}/l$ as the converged standard deviation. However while the latter lays between zero and the random variable result, the mean value lays between the deterministic result (depicted as a constant in a black solid line) and the random variable result. Actually, defining the standard deviation of a deterministic solution to be zero, the statement can be generally expressed as the assumption that the stochastic moments resulting from $L_{\sigma_{\mathrm{y}}}/l \in (0, \infty)$ are bounded by the deterministic value and the random variable results. This still holds for the results obtained before in Section 6.3, observing the mean values to be close or almost equal to the deterministic result.

(a) mean value $\mu\{\hat{\mu}_{\sigma_\mathrm{y},j}\}$ (left) and standard deviation $\sigma\{\hat{\mu}_{\sigma_\mathrm{y},j}\}$ (right) of the individual random field realisation mean values $\hat{\mu}_{\sigma_\mathrm{y},j}$ of the input random field yield stress $\sigma_\mathrm{y}(\omega, \boldsymbol{z})$
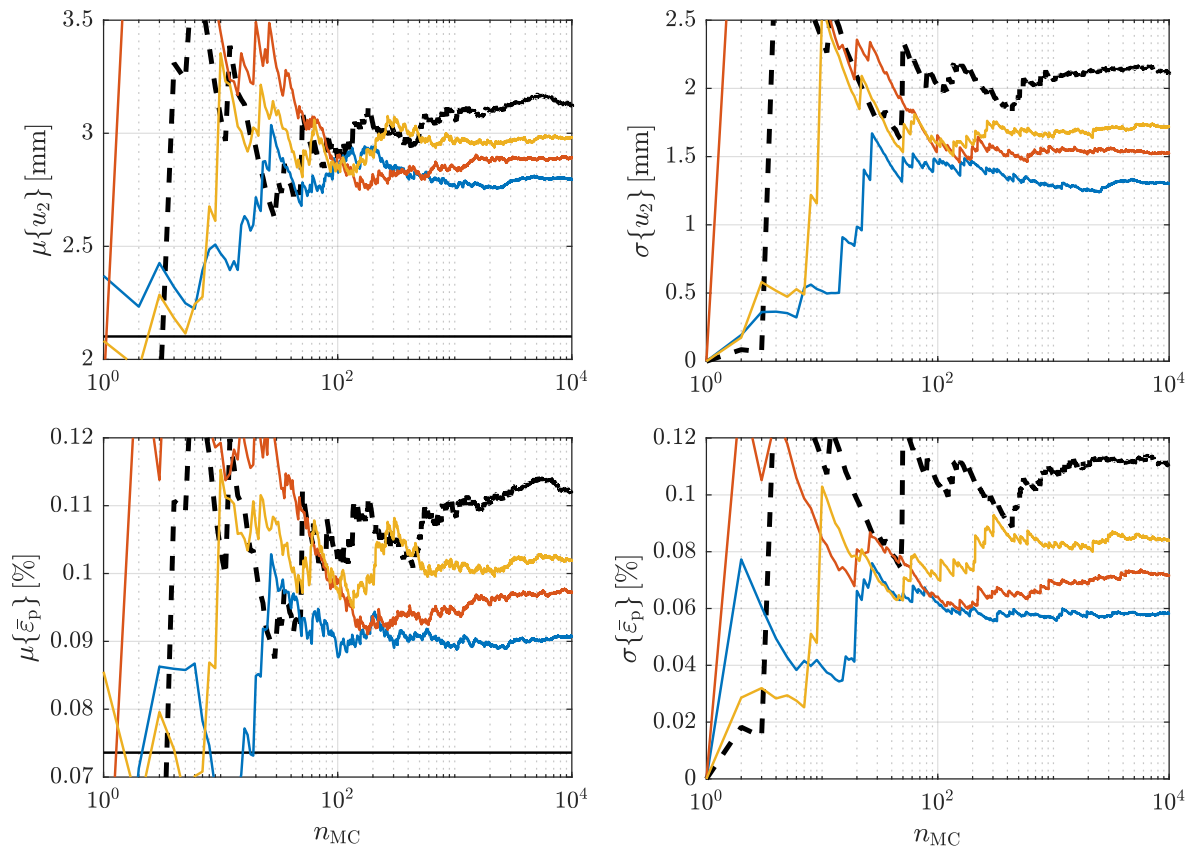
(b) mean value $\mu\{Y\}$ (left) and standard deviation $\sigma\{Y\}$ (right) of the QoI, i.e. the displacement $Y(\omega) = u_2(\omega, \hat{\boldsymbol{z}}_{121})$ (top) and the equivalent plastic strain $Y(\omega) = \bar{\varepsilon}^\mathrm{p}(\omega, \hat{\boldsymbol{z}}_{66})$ (bottom)

Figure 6.24: Convergence behaviour of the input realisations as well as the QoI obtained by an elasto-plastic material model including linear hardening.

To investigate the dependency between the converged mean value $\mu\{Y\}$ and standard deviation $\sigma\{Y\}$ of the output QoI $Y(\omega)$ and the underlying mean and standard deviation of the individual input realisation mean values, both moments are each plotted for both QoI against $\mu\{\hat{\mu}_{\sigma_y,j}\}$ and $\sigma\{\hat{\mu}_{\sigma_y,j}\}$ in Figure 6.25. The different colours represent the results obtained at the different nodes to be investigated. The assumed linear dependency between the deterministic and the random variable results is visualised by a solid line. Its left end represents the deterministic result, its right end the results of the random variable, both marked by a circle. The results corresponding to the three different correlation length ratios L_{σ_y}/l are depicted as crosses in the corresponding colour.

(a) displacement $Y(\omega) = u_2(\omega, \hat{\mathbf{z}}_{121})$

(b) equivalent plastic strain $Y(\omega) = \bar{\varepsilon}^{\mathrm{p}}(\omega, \hat{\mathbf{z}}_{66})$
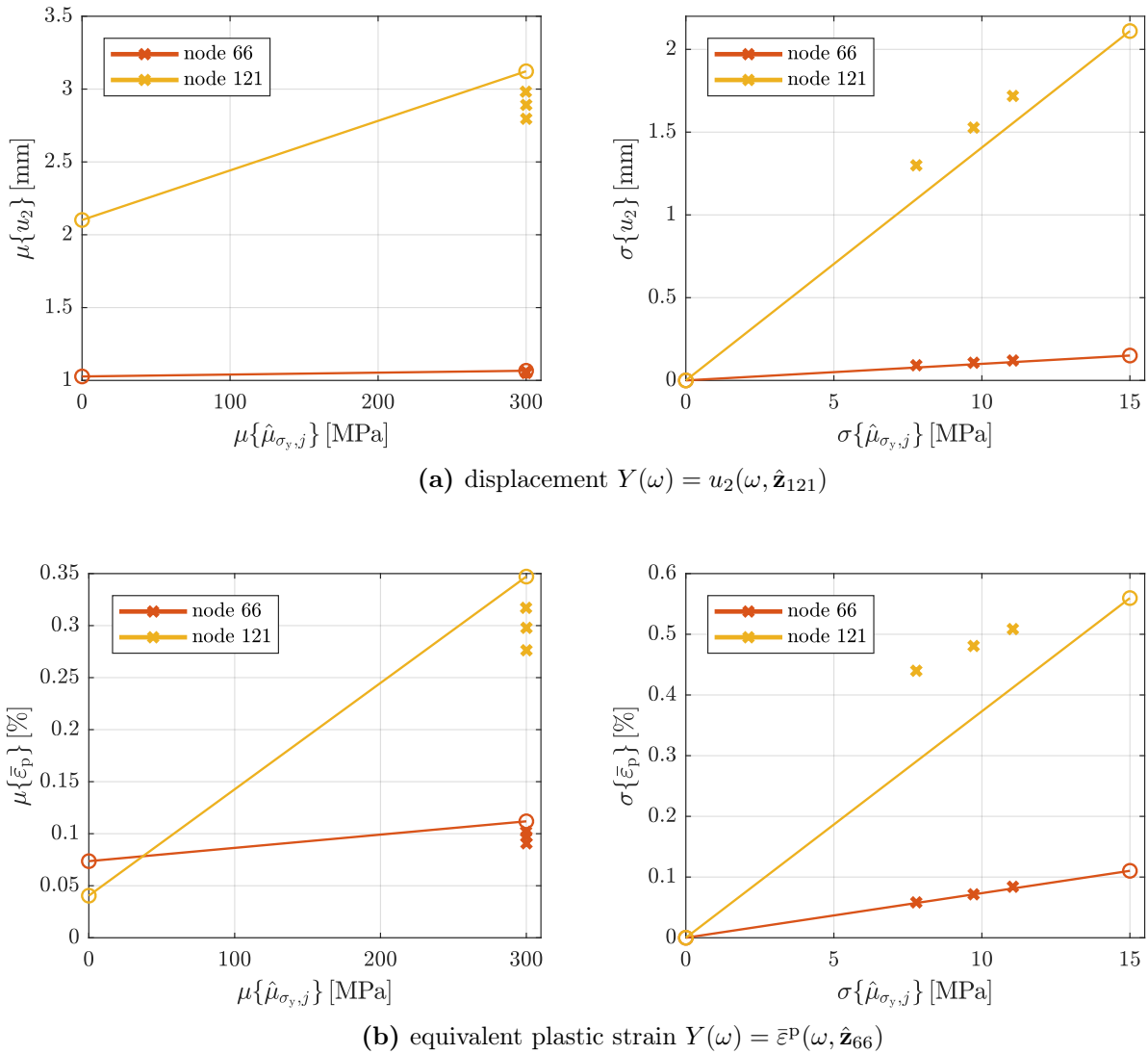
Figure 6.25: Dependency between the converged mean value $\mu\{Y\}$ (left) and standard deviation $\sigma\{Y\}$ (right) of the QoI $Y(\omega)$ and the underlying mean and standard deviation of the individual input realisation mean values, $\mu\{\hat{\mu}_{\sigma_y,j}\}$ and $\sigma\{\hat{\mu}_{\sigma_y,j}\}$.

Regarding the standard deviation depicted at the right side of Figure 6.25, it can be seen that the assumption of a linear dependency again underestimates the true value. This may become especially critical for large deformations as obtained e.g. at node 121. Furthermore, in case of the equivalent plastic strain, the deviation becomes larger for smaller correlation length ratios, see Figure 6.25b. As the mean values of the input is still converging towards the hyper

parameter μ_{σ_y} independently of the correlation length, the mean values of the output line up on a vertical line underneath the random variable results, see the left side of Figure 6.25. For the following study, it is assumed that the ratio of the standard deviation can be mapped linearly to this vertical dependency between the deterministic result y_0 and the random variable mean value μ_{RV} of the output, i.e.

$$\tilde{\mu}_L\{y\} = y_0 + \underbrace{\frac{\sigma_L\{\hat{\mu}_{x,j}\}}{\sigma_X}}_{=\sigma_L\{\hat{\mu}_{s,j}\}} \cdot \left(\mu_{RV}\{y\} - y_0 \right). \tag{6.13}$$

By this, Eq. (6.8) is generalised towards

$$F_{Y,L}(\tilde{y}) = \tilde{\mu}_L\{y\} + \sigma_L\{\hat{\mu}_{s,j}\} \cdot F_{Y,RV}(y). \tag{6.14}$$

Validating this assumption in general as well as investigating also higher moments with regard to their input output dependency remains a goal of future research.

6.4.2. Results obtained by the interpolation approach

The generalised interpolation approach is investigated for the given problem by propagating each random field and random variable scenario by a brute force MC simulation using each $n_{MC} = 1 \times 10^4$ samples. The ani-p-box resulting for the propagated random field and its assigned mean value regarding the displacement u_2 at node 121 is depicted in a black dashed line in Figure 6.26. Furthermore, the deterministic result is given as a vertical black solid line. The CDFs resulting from propagating the random fields using different correlation length ratios are depicted in solid lines. In dashed lines of corresponding colour, the results obtained by interpolating within the ani-p-box are depicted. As before, the corresponding error measures $\tilde{\epsilon}\{u_2\}$ and $\tilde{\Delta} F_u$ are depicted below the ani-p-box.

It can be noticed that there is no perfectly vertical part in the CDF of the random variable as observed for the 1D example. This is due to the rebalancing of stresses in the domain. However, the left tail corresponding to small displacements is still very steep. Furthermore, the tails of the random field CDFs appear to converge to the same origin, while the correlation length mainly affects the right tail, which corresponds to the realisations resulting in remarkable plastic deformations. This cannot be incorporated by the interpolation of the CDFs, resulting in a poor result of the left tails. Concerning the right tails, the interpolated results fit the sampled ones much butter. Still, also here an increasing error is observed for a decreasing correlation length.

On the contrary to the 1D examples where the resulting CDFs appeared (approximately) Gaussian (despite the kink occurring under certain circumstances), the distribution family of the displacement is clearly non Gaussian. This is properly the reason why the mean value $\mu\{u_2\}$ is much more affected by the correlation length than the mean of the QoI in Section 6.3. This further suggests the assumption that studying the dependency of higher moments on the correlation length could attain further knowledge to improve the interpolation approach.

The results obtained by the interpolation approach to estimate the equivalent plastic strain $\bar{\varepsilon}^{\mathrm{p}}$ at node 66 are depicted in Figure 6.27. Although the left tail is not as steep as for the displacement, the error made by interpolation is even higher. Furthermore, the left tails of the sampled CDFs corresponding to the three different random field scenarios even lay outside the ani-p-box. This violates the model assumption of a monotonic dependency between the QoI stochastic moments and the correlation length. Consequently, also the assumption of intermediate values $L_{\sigma_{\mathrm{y}}}^{*} \in L_{\sigma_{\mathrm{y}}}^{I}$ has to be questioned with regard to this example. On the contrary to the assumptions made before, it can be concluded that stress rebalancing effects do not improve the applicability of the interpolation approach regarding non-linear models.
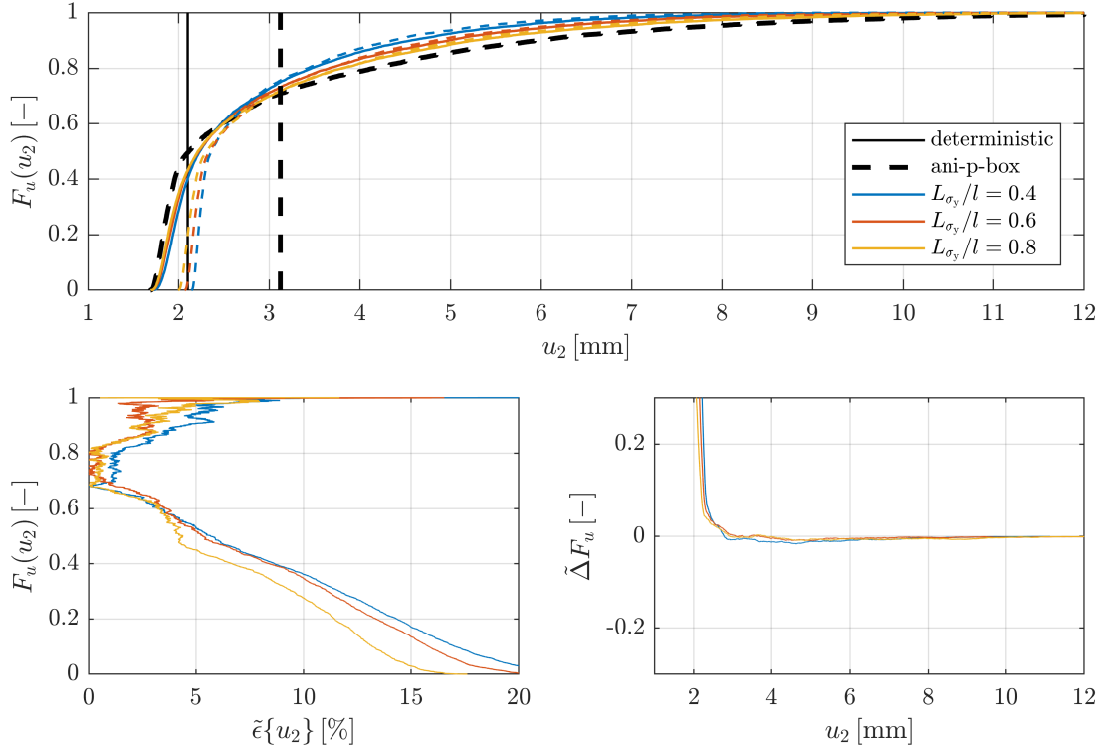

Figure 6.26: Cumulative distribution functions of the deflection u_2 at node 121, considering three correlation length ratios, $L_{\sigma_{\mathrm{y}}}/l = 0.4$ (blue), $L_{\sigma_{\mathrm{y}}}/l = 0.6$ (red) and $L_{\sigma_{\mathrm{y}}}/l = 0.8$ (yellow), each scenario obtained by sampling with $n_{\mathrm{MC}} = 1 \times 10^4$ MC samples (solid lines) as well as resulting from a linear interpolation within the ani-p-box (dashed lines), complemented with the corresponding error measures $\tilde{\epsilon}\{u_2\}$ (bottom left) and $\tilde{\Delta}F_u$ (bottom right), considering the yield stress $\sigma_{\mathrm{y}}(\omega, z)$ as an input random field.

6.5.   Summary and concluding remarks

In the studies provided in Chapter 5, global sparse SC as well as global sparse PC approaches have been shown to be limited by the curse of dimensionality and especially in terms of non-linear model propagation. Due to the amount of model assumptions and approximation errors already made for the KL expansion considering imprecise random fields, more sophisticated SC and PC approaches, e.g. in terms of an adaptive local refinement within the stochastic space, have not been considered appropriate in order to guarantee the resulting p-box not being mainly caused artificially by a combination of several errors.
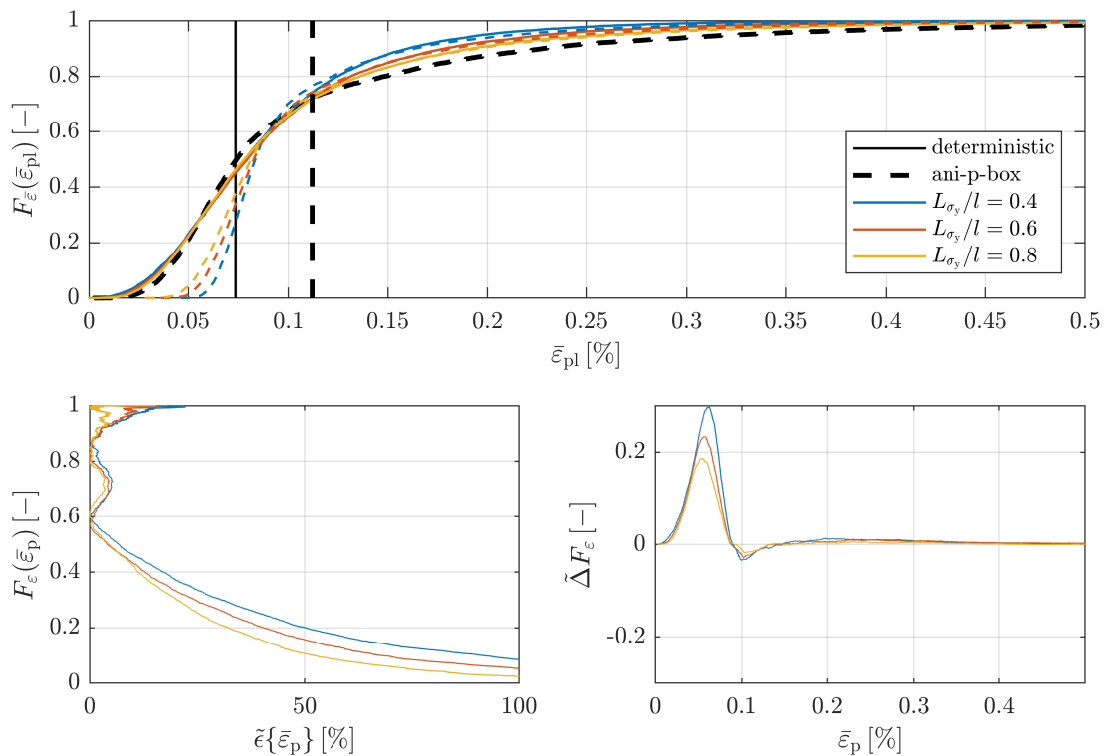
Figure 6.27: Cumulative distribution functions of the equivalent plastic strain $\bar{\varepsilon}^{\mathrm{p}}$ at node 66, considering three correlation length ratios, $L_{\sigma_{\mathrm{y}}}/l = 0.4$ (blue), $L_{\sigma_{\mathrm{y}}}/l = 0.6$ (red) and $L_{\sigma_{\mathrm{y}}}/l = 0.8$ (yellow), each scenario obtained by sampling with $n_{\mathrm{MC}} = 1 \times 10^4$ MC samples (solid lines) as well as resulting from a linear interpolation within the ani-p-box (dashed lines), complemented with the corresponding error measures $\tilde{\epsilon}\{\bar{\varepsilon}^{\mathrm{p}}\}$ (bottom left) and $\tilde{\Delta}F_{\varepsilon}$ (bottom right), considering the yield stress $\sigma_{\mathrm{y}}(\omega, z)$ as an input random field.

As a dependency on the correlation length between input and output has been observed in the studies before, this dependency has been intensively studied for the mean value and the standard deviation in this chapter. Based on these findings, the p-box of having absolutely no idea (ani-p-box) about the correlation length, i.e. $L_X \in (0, \infty)$, has been introduced to describe the outest bounds possible regarding interval valued correlation lengths. Then, a decoupled interpolation has been proposed to interpolate the results corresponding to a random field of certain correlation length from the ani-p-box.

The approach has been studied for 1D and 2D random fields concerning linear and non-linear material models. It has been shown that the CDF can be sufficiently estimated when the output follows approximately a Gaussian distribution. However, if the model response is non-differentiable, the part of the CDF corresponding to the non-differentiable region cannot be represented satisfactory. If the results are described by a non Gaussian distribution family, the interpolation approach fails. It remains to be studied in future research whether the convergence behaviour of higher moments can be used to further improve the interpolation approach with this respect.

In general, the approach is expected only to be applicable under certain model assumptions, as stated in the beginning of this chapter. Especially regarding non-monotonic models, the use of the interpolation approach has to be questioned. This includes also monotonic models involving cyclic loading.

A severe drawback is the fact that no internal error measure is available. So far, the results have only been validated in terms of a reference error but a reference solution is usually not available. Still, understanding also the impact of higher moments, this approach can be useful to obtain estimates in engineering application, as the computational cost can be reduced drastically by only propagating a random variable instead of several random fields. Concerning non-linear problems, by the fact of propagating only one (low-dimensional) scenario per uncertain input parameter, also more sophisticated sampling techniques than the studied global approaches can become useful again. To draw more generic conclusions from the observation, the approach should further be validated in terms of more complex geometries.

7. Conclusion and Perspectives

Uncertainties appear in different extends, kinds and situations during the engineering design process. They can imply varying material properties, imperfect geometries or unpredictable loading conditions and may change in time or space. While epistemic uncertainties can be (theoretically) reduced by getting more data, knowledge or precision, aleatory uncertainties depend on chance. Often a mixture of both uncertainties is required to model real conditions.

In this work, different concepts to quantify and propagate different kinds of uncertainties have been described and examined. This included Gaussian random variables and fields to describe aleatory uncertain scalar values or spatially varying values, respectively. To model epistemic uncertainties, the focus has been on interval valued parameters. Consequently, mixed uncertainties have been described by the combination of both theories, resulting in a probability box (p-box). The double loop approach is an often applied and straightforward method to propagate such imprecise probabilities. The interval valued parameters are discretised in an outer loop while each resulting aleatory scenario can be propagated within the inner loop, e.g. by Monte Carlo (MC) sampling. Finally, the quantity of interest (QoI) as the outcome of the model propagation can again be described by a p-box.

The application focus of this thesis was on mixed uncertain material properties including a spatial variation. For this purpose, imprecise random fields were introduced and intensively investigated. While it has been assumed that mean value and standard deviation can be determined sufficiently exact by experiments, the difficulty or even impossibility to measure the correlation length has been acknowledged by an interval valued correlation length. The random fields resulting for each correlation length scenario have been discretised by a truncated Karhunen-Loève (KL) expansion. It has been shown that this may involve difficulties regarding the truncation error corresponding to the correlation length scenarios to be comparable. Otherwise, it cannot be estimated how much the resulting p-box is just a consequence of different truncation errors. Furthermore, the computational cost in terms of the double loop propagation as well as due to the physical discretisation has been addressed.

To reduce the computation time, two alternative sampling techniques than MC method have been investigated, the sparse stochastic collocation (SC) method as well as a sparse polynomial chaos (PC) expansion. Both methods aim at reducing the number of samples to be propagated and have shown high efficiency for linear and smooth models. While sparse SC method suffers from the curse of dimensionality regarding large truncation terms, sparse PC expansion outperformed both, SC and MC method also for high stochastic dimensions. However, concerning the propagation through a non-linear material law, only the robust MC method achieved satisfactory results.

In the studies during this research project, it has been observed that the correlation length mainly affects the standard deviation of the QoI but rarely the mean value. In any case, both parameters appeared to decrease monotonically (though not linearly) with an increasing correlation length. Consequently, it has been assumed and shown in a first study that the results were bounded by the infinite bounds of the correlation length, i.e. assuming white noise (the correlation length converges towards zero) on the one side and a random variable (convergence towards infinity) on the other side. Based on this study, a decoupled interpolation approach has been proposed. The basic idea is to interpolate the result of an arbitrary correlation length scenario within the so-called absolutely no idea probability box (ani-p-box). As the propagation of white noise converges towards the deterministic result, the ani-p-box can be obtained by a deterministic and a random variable propagation. Ideally, the simulation of the latter is much cheaper than for a random field, as the stochastic dimension is usually much smaller and sophisticated sampling techniques can be applied. The interpolation factor is determined by the ratio of the standard deviation of the individual input realisation mean values corresponding to the applied correlation length and the standard deviation of the QoI obtained by the random variable. The first is estimated by sampling (but not propagating) a large number of random field realisations, taking the mean of each realisation and evaluating the standard deviation of these realisation mean values statistically.

The proposed decoupled interpolation approach has been investigated for one-dimensional (1D) and two-dimensional (2D) random field problems regarding linear and non-linear material models. The approach yields a good approximation if the stochastic response is sufficiently smooth. However, the error turned out to be higher if the correlation length is small. Additionally, assuming a linear dependency between the input and output standard deviations, the true standard deviation of the QoI has been slightly underestimated in some cases. If the stochastic response is locally changing significantly or even is non-differentiable, the interpolated results include a high error at the probabilities assigned to this region in the response. In case of the provided studies, this has been the case when the elastic region transits to the plastic region. Therefore, further investigations on the input output dependency of higher moments are suggested for future research, aiming to improve the interpolation by this knowledge. Additionally, an internal error estimate to quantify the quality of the results without a reference solution must be developed to achieve applicability in engineering practise.

For these cases where the interpolation approach is beneficial, it is of high benefit in terms of computational cost. First, the double loop approach is decoupled and only the scenarios corresponding to the uncertain parameters modelled by random variables need to be propagated. This is less than the according random field scenarios, even if only a vertex analysis was applied for the latter case. Second and consequently, no random field propagation is required, solving the challenge regarding different truncation orders and corresponding stochastic dimensions. Third, the physical mesh discretisation must only be chosen as fine as necessary to gain convergence for constant material data and not according to the variability of the random field, which reduced the simulation cost of an individual realisation. At last, due to the usually moderate stochastic dimensions in terms of random variables, sophisticated sampling methods

can be used which would suffer from the curse of dimensionality in case of high-dimensional random fields. Furthermore, as the change of stochastic dimensions due to different required truncation orders is avoided, also anisotropic and/or adaptive multi-element approaches can be considered to propagate random variables through non-smooth models, without risking multiple approximation errors to interfere and resulting in an artificial error induced p-box.

Bibliography

M. Abramowitz and I.A. Stegun. *Handbook of mathematical functions with formulas, graphs and mathematical tables*. Department of commerce, National Bureau of Standards, 10 edition, 1964.

H. Altenbach. *Kontinuumsmechanik - Einführung in die materialunabhängigen und material-abhängigen Gleichungen*. Springer Vieweg, 3 edition, 2015.

K. Atkinson and W. Han. *Numerical Solution of Fredholm Integral Equations of the Second Kind*, pages 473–549. Springer New York, New York, NY, 2009. doi: 10.1007/978-1-4419-0458-4_12.

J. Bäck, F. Nobile, L. Tamellini, and R. Tempone. Stochastic spectral Galerkin and collocation methods for PDEs with random coefficients: a numerical comparison. In J.S. Hesthaven and E.M. Ronquist, editors, *Spectral and High Order Methods for Partial Differential Equations*, volume 76 of *Lecture Notes in Computational Science and Engineering*, pages 43–62. Springer, 2011. Selected papers from the ICOSAHOM '09 conference, June 22-26, Trondheim, Norway.

A.A. Basmaji, M.M. Dannert, and U. Nackenhorst. Implementation of Karhunen-Loève expansion using discontinuous Legendre polynomial based Galerkin approach. *Probabilistic Engineering Mechanics*, 67:103176, 2022a. doi: 10.1016/j.probengmech.2021.103176.

A.A. Basmaji, A. Fau, J.H. Urrea-Quintero, M.M. Dannert, E. Voelsen, and U. Nackenhorst. Anisotropic multi-element polynomial chaos expansion for high-dimensional nonlinear structural problems. *Probabilistic Engineering Mechanics*, 70:103366, 2022b. doi: 10.1016/j.probengmech.2022.103366.

K.-J. Bathe. *Finite Element Procedures*. Prentice-Hall Inc., 1996.

M. Beer, S. Ferson, and V. Kreinovich. Imprecise probabilities in engineering analyses. *Mechanical Systems and Signal Processing*, 37(1):4–29, 2013. doi: 10.1016/j.ymssp.2013.01.024.

W. Betz, I. Papaioannou, and D. Straub. Numerical methods for the discretization of random fields by means of the Karhunen-Loève expansion. *Computer Methods in Applied Mechanics and Engineering*, 271:109–129, 2014.

G. Blatman and B. Sudret. Sparse polynomial chaos expansions and adaptive stochastic finite elements using a regression approach. *Comptes Rendus Mecanique*, 336(6):518–523, 2008. doi: 10.1016/j.crme.2008.02.013.

G. Blatman and B. Sudret. Adaptive sparse polynomial chaos expansion based on least angle regression. *Journal of Computational Physics*, 230(6):2345–2367, 2011. doi: 10.1016/j.jcp.2010.12.021.

P. Bressolette, M. Fogli, and C. Chauvière. A stochastic collocation method for large classes of mechanical problems with uncertain parameters. *Probabilistic Engineering Mechanics*, 25 (2):255–270, 2010. doi: 10.1016/j.probengmech.2010.01.002.

H.-J. Bungartz and M. Griebel. Sparse grids. *Acta Numerica*, 13:147–269, 2004. doi: 10.1017/S0962492904000182.

J. Ching and K.-K. Phoon. Impact of autocorrelation function model on the probability of failure. *Journal of Engineering Mechanics*, 145(1):04018123, 2019.

M.M. Dannert, A. Fau, R.M.N. Fleury, M. Broggi, U. Nackenhorst, and M. Beer. A probability-box approach on uncertain correlation lengths by stochastic finite element method. *PAMM*, 18(1):e201800114, 2018. doi: 10.1002/pamm.201800114.

M.M. Dannert, R.M.N. Fleury, A. Fau, and U. Nackenhorst. Non-linear finite element analysis under mixed epistemic and aleatory uncertain random field input. In M. Beer and E. Zio, editors, *Proceedings of the 29th European Safety and Reliability Conference*, pages 2693–2698, 2019. doi: 10.3850/978-981-11-2724-3_0286-cd.

M.M. Dannert, M.G.R. Faes, R.M.N. Fleury, A. Fau, U. Nackenhorst, and D. Moens. Imprecise random field analysis for non-linear concrete damage analysis. *Mechanical Systems and Signal Processing*, 150:107343, 2021a. doi: 10.1016/j.ymssp.2020.107343.

M.M. Dannert, J.L. Häufler, and U. Nackenhorst. Limit representations of imprecise random fields. In M. Papadrakakis, V. Papadopoulos, and G. Stefanou, editors, *4th ECCOMAS Thematic Conference on Uncertainty Quantification in Computational Sciences and Engineering (UNCECOMP)*, pages 82–99, 2021b. doi: 10.7712/120221.8024.19110.

M.M. Dannert, F. Bensel, A. Fau, R.M.N. Fleury, and U. Nackenhorst. Investigations on the restrictions of stochastic collocation methods for high dimensional and nonlinear engineering applications. *Probabilistic Engineering Mechanics*, 69:103299, 2022. doi: 10.1016/j.probengmech.2022.103299.

E.A. de Souza Neto, D. Perić, and D.R.J. Owen. *Computational Methods for Plasticity: Theory and Applications*. John Wiley & Sons, 1 edition, 2008.

A.P. Dempster. Upper and lower probability inferences based on a sample from a finite univariate population. *Biometrika*, 54(3,4):515–528, 1967.

A. Der Kiureghian and O. Ditlevsen. Aleatory or epistemic? does it matter? *Structural Safety*, 31(2):105–112, 2009.

A. Der Kiureghian, H.-Z. Lin, and S.-J. Hwang. Second-order reliability approximations. *Journal of Engineering Mechanics, ASCE*, 113(8):1208–1225, 1987. doi: 10.1061/(ASCE)0733-9399(1987)113:8(1208).

I. Elishakoff and F. Elettro. Interval, ellipsoidal, and super-ellipsoidal calculi for experimental and theoretical treatment of uncertainty: Which one ought to be preferred? *International Journal of Solids and Structures*, 51(7):1576–1586, 2014. doi: 10.1016/j.ijsolstr.2014.01.010.

M. Faes. *Interval methods for the identification and quantification of inhomogeneous uncertainty in finite element models.* PhD thesis, KU Leuven, 2017.

M. Faes and D. Moens. Multivariate dependent interval finite element analysis via convex hull pair constructions and the extended transformation method. *Computer Methods in Applied Mechanics and Engineering*, 347:85–102, 2019a. doi: 10.1016/j.cma.2018.12.021.

M. Faes and D. Moens. Imprecise random field analysis with parametrized kernel functions. *Mechanical Systems and Signal Processing*, 134:106334, 2019b. doi: 10.1016/j.ymssp.2019.106334.

M. Faes and D. Moens. On auto- and cross-interdependence in interval field finite element analysis. *International Journal for Numerical Methods in Engineering*, 121(9):2033–2050, 2020a. doi: 10.1002/nme.6297.

M. Faes and D. Moens. Recent trends in the modeling and quantification of non-probabilistic uncertainty. *Archives of Computational Methods in Engineering*, 27:633–671, 2020b. doi: 10.1007/s11831-019-09327-x.

M. Faes and D. Moens. On auto- and cross-interdependence in interval field finite element analysis. *International Journal for Numerical Methods in Engineering*, 121(9):2033–2050, 2020c. doi: 10.1002/nme.6297.

M. Faes, M. Broggi, E. Patelli, Y. Govers, J. Mottershead, M. Beer, and D. Moens. A multivariate interval approach for inverse uncertainty quantification with limited experimental data. *Mechanical Systems and Signal Processing*, 118:534–548, 2019. doi: 10.1016/j.ymssp.2018.08.050.

M.G.R. Faes, M. Daub, S. Marelli, E. Patelli, and M. Beer. Engineering analysis with probability boxes: A review on computational methods. *Structural Safety*, 93:102092, 2021. doi: 10.1016/j.strusafe.2021.102092.

M.G.R. Faes, M. Broggi, P.D. Spanos, and M. Beer. Elucidating appealing features of differentiable auto-correlation functions: a study on the modified exponential kernel. *Probabilistic Engineering Mechanics*, 69:103269, 2022. doi: 10.1016/j.probengmech.2022.103269.

S. Ferson and W. Troy Tucker. Sensitivity analysis using probability bounding. *Reliability Engineering & System Safety*, 91(10):1435–1442, 2006. doi: 10.1016/j.ress.2005.11.052.

S. Ferson, V. Kreinovich, L. Ginzburg, D.S. Myers, and K. Sentz. Constructing probability boxes and dempster-shafer structures. Technical report, Sandia National Laboratories, 2003. Sand Report - SAND2002-4015.

M. Fina. *Polymorphe Unschärfemodellierung in der nichtlinearen Strukturmechanik - Stabilität von Schalentragwerken, räumliche Variabilität und Metamodellierung*. PhD thesis, Karlsruher Institut für Technologie, 2020.

M. Fina, P. Weber, and W. Wagner. Polymorphic uncertainty modeling for the simulation of geometric imperfections in probabilistic design of cylindrical shells. *Structural Safety*, 82: 101894, 2020. doi: 10.1016/j.strusafe.2019.101894.

G. Fishman. *Monte Carlo: concepts, algorithms and applications*. Springer-Verlag, 1996.

K. Gao, D.M. Do, S. Chu, G. Wu, H.A. Kim, and C.A. Featherston. Robust topology optimization of structures under uncertain propagation of imprecise stochastic-based uncertain field. *Thin-Walled Structures*, 175:109238, 2022. doi: 10.1016/j.tws.2022.109238.

A. Genz and B.D. Keister. Fully symmetric interpolatory rules for multiple integrals over infinite regions with Gaussian weight. *Journal of Computational and Applied Mathematics*, 71:229–309, 1996.

H.-O. Georgii. *Stochastik: Einführung in die Wahrscheinlichkeitstheorie und Statistik*. Walter de Gruyter, 2 edition, 2004.

R.G. Ghanem and P.D. Spanos. *Stochastic Finite Elements: A Spectral Approach*. Springer-Verlag New York Inc., 9 edition, 1991.

M.A. Gil, M. López-Díaz, and D.A. Ralescu. Overview on the development of fuzzy random variables. *Fuzzy Sets and Systems*, 157(19):2546–2557, 2006. doi: 10.1016/j.fss.2006.05.002.

M.B. Giles. Multilevel Monte Carlo methods. *Acta Numerica*, 24:259–328, 2015.

M. Götz. *Numerische Entwurfsmethoden unter Berücksichtigung Polymorpher Unschärfe - Aspekte zeitlicher und räumlicher Abhängigkeiten*. PhD thesis, Technische Universität Dresden, 2017.

M. Grigoriu. *Stochastic Calculus: Applications in Science and Engineering*. Birkhäuser Boston, 1 edition, 2002.

M. Hanss. *Applied fuzzy arithmetic: an introduction with engineering applications*. Springer, 2005.

J.C. Helton and F.J. Davis. Latin hypercube sampling and the propagation of uncertainty in analyses of complex systems. *Reliability Engineering and System Safety*, 81(1):23–69, 2003. doi: 10.1016/S0951-8320(03)00058-9.

G.A. Holzapfel. *Nonlinear Solid Mechanics - A Continuum Approach for Engineering*. John Wiley & Sons Ltd, 3 edition, 2000.

S.P. Huang, S.T. Quek, and K.-K. Phoon. Convergence study of the truncated Karhunen–Loève expansion for simulation of stochastic process. *International Journal for Numerical Methods in Engineering*, 52:1029–1043, 2001. doi: 10.1002/nme.255.

M. Imholz, D. Vandepitte, and D. Moens. Derivation of an input interval field decomposition based on expert knowledge using locally defined basis functions. In M. Papadrakakis, V. Papadopoulos, and G. Stefanou, editors, *1st International Conference on Uncertainty Quantification in Computational Sciences and Engineering (UNCECOMP 2015)*, pages 529–547, 2015. doi: 10.7712/120215.4290.583.

P.-P. Jablonski. *Numerische Simulation probabilistischer Schädigungsmodelle mit der Stochastischen Finite Elemente Methode*. PhD thesis, Gottfried Wilhelm Leibniz Universität, 2014.

J.D. Jakeman, M.S. Eldred, and K. Sargsyan. Enhancing l_1-minimization estimates of polynomial chaos expansions using basis selection. *Journal of Computational Physics*, 289:18–34, 2015. doi: 10.1016/j.jcp.2015.02.025.

M. Kaliske and W. Graf. Special Issue: Polymorphic uncertainty modelling for numerical design of structures - Part I & II. *GAMM-Mitteilungen*, 42(1,2), 2019. URL `https://onlinelibrary.wiley.com/toc/15222608/2019/42/1`.

G.J. Klir and M.J. Wierman. *Uncertainty-Based Information - Elements of Generalized Information Theory*. Springer-Verlag, 2 edition, 1999.

F.Y. Kuo, C. Schwab, and I.H. Sloan. Quasi-Monte Carlo finite element methods for a class of elliptic partial differential equations with random coefficients. *SIAM Journal on Numerical Analysis*, 50(6):3351–3374, 2012. doi: 10.1137/110845537.

H. Kwakernaak. Fuzzy random variables - i. definitions and theorems. *Information Sciences*, 15:1–29, 1978.

H. Kwakernaak. Fuzzy random variables - ii. algorithms and examples for the discrete case. *Information Sciences*, 17:253–278, 1979.

O.P. Le Maître and O.M. Knio. *Spectral Methods for Uncertainty Quantification*. Springer Science+Business Media B.V., 2010.

C.F. Li, Y.T. Feng, D.R.J. Owen, D.F. Li, and I.M. Davis. A Fourier-Karhunen-Loève discretization scheme for stationary random material properties in SFEM. *International Journal for Numerical Methods in Engineering*, 73(13):1942–1965, 2008. doi: 10.1002/nme.2160.

J. Li and P. Stinis. A unified framework for mesh refinement in random and physical space. *Journal of Computational Physics*, 323:243–264, 2016. doi: 10.1016/j.jcp.2016.07.027.

Q. Liu and X. Zhang. A Chebyshev polynomial-based Galerkin method for the discretization of spatially varying random properties. *Acta Mechanica*, 228:2063–2081, 2017. doi: 10.1007/s00707-017-1819-2.

G. Manson. Calculating frequency response functions for uncertain systems using complex affine analysis. *Journal of Sound and Vibration*, 288(3):487–521, 2005. doi: 10.1016/j.jsv.2005.07.004.

S. Marelli and B. Sudret. UQLab: A framework for uncertainty quantification in Matlab. In *Vulnerability, Uncertainty and Risk*, pages 2554–2563, 2014. doi: 10.1061/9780784413609.257.

S. Marelli, N. Lüthen, and B. Sudret. UQLab user manual – Polynomial chaos expansions. Technical report, Chair of Risk, Safety and Uncertainty Quantification, ETH Zurich, Switzerland, 2022. Report UQLab-V2.0-104.

M.L. Mika, T.J.R. Hughes, D. Schillinger, P. Wriggers, and R.R. Hiemstra. A matrix-free isogeometric Galerkin method for Karhunen-Loève approximation of random fields using tensor product splines, tensor contraction and interpolation based quadrature. *Computer Methods in Applied Mechanics and Engineering*, 379:113730, 2021. doi: 10.1016/j.cma.2021.113730.

D. Moens and M. Hanss. Non-probabilistic finite element analysis for parametric uncertainty treatment in applied mechanics: Recent advances. *Finite Elements in Analysis and Design*, 47(1):4–16, 2011. doi: 10.1016/j.finel.2010.07.010.

D. Moens and D. Vandepitte. A survey of non-probabilistic uncertainty treatment in finite element analysis. *Computer Methods in Applied Mechanics and Engineering*, 194(12):1527–1555, 2005. doi: 10.1016/j.cma.2004.03.019.

D. Moens and D. Vandepitte. Recent advances in non-probabilistic approaches for non-deterministic dynamic finite element analysis. *Archives of Computational Methods in Engineering*, 13:389–464, 2006. doi: 10.1007/BF02736398.

D. Moens, M. De Munck, W. Desmet, and D. Vandepitte. Numerical dynamic analysis of uncertain mechanical structures based on interval fields. In A.K. Belyaev and R.S. Langley, editors, *IUTAM Symposium on the Vibration Analysis of Structures with Uncertainties*, pages 71–83. Springer Science+Business Media B.V., 2011. doi: 10.1007/978-94-007-0289-9_6.

R.E. Moore, R.B. Kearfott, and M.J. Cloud. *Introduction to interval analysis*. Society for Industrial and applied Mathematics, 10 edition, 2009.

R.L. Muhanna and R.L. Mullen. Uncertainty in mechanics problems - interval based approach. *Journal of Engineering Mechanics*, 127(6):557–566, 2001. doi: 10.1061/(ASCE)0733-9399(2001)127:6(557).

B. Möller. Fuzzy randomness – a contribution to imprecise probability. *ZAMM - Journal of Applied Mathematics and Mechanics / Zeitschrift für Angewandte Mathematik und Mechanik*, 84(10-11):754–764, 2004. doi: 10.1002/zamm.200410153.

B. Möller, W. Graf, and M. Beer. Fuzzy structural analysis using α-level optimization. *Computational Mechanics*, 26:547–565, 2000. doi: 10.1007/s004660000204.

A. Narayan and J.D. Jakeman. Adaptive Leja sparse grid constructions for stochastic collocation and high-dimensional approximation. *Siam Journal on Scientific Computing*, 36(6):A2952–A2983, 2014.

F. Nobile, R. Tempone, and C.G. Webster. An anisotropic sparse grid stochastic collocation method for partial differential equations with random input data. *SIAM Journal on Numerical Analysis*, 46(5):2411–2442, 2008. doi: 10.1137/070680540.

I. Papaioannou. *Non-intrusive finite element reliability analysis methods*. Dissertation, Technische Universität München, Munich, 2012.

B. Peherstorfer, K. Willcox, and M. Gunzburger. Survey of multifidelity methods in uncertainty propagation, inference, and optimization. *SIAM Review*, 60(3):550–591, 2018. doi: 10.1137/16M1082469.

D. Pflüger. *Spatially adaptive sparse grids for high-dimensional problems*. PhD thesis, Fakultät für Informatik, Technische Universität München, 2010.

K.-K. Phoon, S. Huang, and S.T. Quek. Implementation of Karhunen-Loève expansion for simulation using a wavelet-Galerkin scheme. *Probabilistic Engineering Mechanics*, 17:293–303, 07 2002. doi: 10.1016/S0266-8920(02)00013-9.

Z. Qiu, D. Yang, and I. Elishakoff. Probabilistic interval reliability of structural systems. *International Journal of Solids and Structures*, 45(10):2850–2860, 2008. doi: 10.1016/j.ijsolstr.2008.01.005.

S. Rahman. A Galerkin isogeometric method for Karhunen-Loève approximation of random fields. *Computer Methods in Applied Mechanics and Engineering*, 338, 2018. doi: 10.1016/j.cma.2018.04.026.

F.N. Schietzold, A. Schmidt, M.M. Dannert, A. Fau, R.M.N. Fleury, W. Graf, M. Kaliske, C. Könke, T. Lahmer, and U. Nackenhorst. Development of fuzzy probability based random fields for the numerical structural design. *GAMM-Mitteilungen*, 42(1):e201900004, 2019. doi: 10.1002/gamm.201900004.

F.N. Schietzold, W. Graf, and M. Kaliske. Multi-objective optimization of tree trunk axes in glulam beam design considering fuzzy probability-based random fields. *ASCE-ASME Journal of Risk and Uncertainty in Engineering Systems - Part B: Mechanical Engineering*, 7(2):020913, 2021. doi: 10.1115/1.4050370.

A. Schmidt, C. Henning, S. Herbrandt, C. Könke, K. Ickstadt, T. Ricken, and T. Lahmer. Numerical studies of earth structure assessment via the theory of porous media using fuzzy probability based random field material descriptions. *GAMM-Mitteilungen*, 42(1):e201900007, 2019. doi: 10.1002/gamm.201900007.

R. Schöbi. *Surrogate models for uncertainty quantification in the context of imprecise probability modelling.* PhD thesis, ETH Zürich, 2019.

R. Schöbi and B. Sudret. Uncertainty propagation of p-boxes using sparse polynomial chaos expansions. *Journal of Computational Physics*, 339:307–327, 2017. doi: 10.1016/j.jcp.2017.03.021.

G. Shafer. *A mathematical theory of evidence.* Princeton University Press, 1 edition, 1976.

A. Sofi and E. Romeo. A novel interval finite element method based on the improved interval analysis. *Computer Methods in Applied Mechanics and Engineering*, 311:671–697, 2016. doi: 10.1016/j.cma.2016.09.009.

A. Sofi, E. Romeo, O. Barrera, and A. Cocks. An interval finite element method for the analysis of structures with spatially varying uncertainties. *Advances in Engineering Software*, 128: 1–19, 2019. doi: 10.1016/j.advengsoft.2018.11.001.

P.D. Spanos, M. Beer, and J. Red-Horse. Karhunen-loève expansion of stochastic processes with a modified exponential covariance kernel. *Journal of Engineering Mechanics*, 133(7): 773–779, 2007.

G. Stefanou. The stochastic finite element method: Past, present and future. *Computer Methods in Applied Mechanics and Engineering*, 198(9):1031–1051, 2009. doi: 10.1016/j.cma.2008.11.007.

B. Sudret. Polynomial chaos expansions and stochatic finite element methods. In K.-K. Phoon and J. Ching, editors, *Risk and Reliability in Geotechnical Engineering*, pages 265–300. CRC Press, 2015.

B. Sudret and A. Der Kiureghian. Stochastic finite element methods and reliability - a state-of-the-art report. Technical report, Department of Civil & Environmental Engineering, University of California, Berkeley, 2000. Report No. UCB/SEMM-2000/08.

L.M.M. van den Bos, B. Koren, and R.P. Dwight. Non-intrusive uncertainty quantification using reduced cubature rules. *Journal of Computational Physics*, 332:418–445, 2017. doi: 10.1016/j.jcp.2016.12.011.

E. Vanmarcke. *Random Fields: Analysis and Synthesis - revised and expanded new edition.* World Scientific Publishing Co. Pte. Ltd., 2010.

W. Verhaeghe, W. Desmet, D. Vandepitte, and D. Moens. Interval fields to represent uncertainty on the output side of a static FE analysis. *Computer Methods in Applied Mechanics and Engineering*, 260:50–62, 2013. doi: 10.1016/j.cma.2013.03.021.

E. Voelsen, M.M. Dannert, A.A. Basmaji, F. Bensel, and U. Nackenhorst. Sparse polynomial chaos expansion for nonlinear finite element simulations with random material properties. *Proceedings in Applied Mathematics and Mechanics*, accepted, 2023. doi: 10.1002/pamm.202200131.

M. Vořechovský. Simulation of simply cross correlated random fields by series expansion methods. *Structural Safety*, 30(4):337–363, 2008. doi: 10.1016/j.strusafe.2007.05.002.

X. Wan and G.E. Karniadakis. An adaptive multi-element generalized polynomial chaos method for stochastic differential equations. *Journal of Computational Physics*, 209(2):617–642, 2005. doi: 10.1016/j.jcp.2005.03.023.

K. Weichselberger. The theory of interval-probability as a unifying concept for uncertainty. *International Journal of Approximate Reasoning*, 24(2):149–170, 2000. doi: 10.1016/S0888-613X(00)00032-3.

N. Wiener. The homogeneous chaos. *American Journal of Mathematics*, 60(4):897–936, 1938.

D. Xiu. Fast numerical methods for stochastic computations: A review. *Communications in Computational Physics*, 5(2-4):242–272, 2009.

D. Xiu and J.S. Hesthaven. High-order collocation methods for differential equations with random inputs. *SIAM Journal on Scientific Computing*, 27(3):1118–1139, 2005. doi: 10.1137/040615201.

D. Xiu and G.E. Karniadakis. The wiener–askey polynomial chaos for stochastic differential equations. *SIAM Journal on Scientific Computing*, 24(2):619–644, 2002. doi: 10.1137/S1064827501387826.

L.A. Zadeh. Fuzzy sets. *Information and Control*, 8:338–353, 1965.

L.A. Zadeh. Fuzzy sets as a basis for a theory of possibility. *Fuzzy Sets and Systems*, 3(28): 3–28, 1978.

L.A. Zadeh. Fuzzy probabilities. *Information Processing & Management*, 20(3):363–372, 1984.

H. Zhang, R.L. Mullen, and R.L. Muhanna. Finite element structural analysis using imprecise probabilities based on p-box representation. Professional Activities Centre, National University of Singapore, 2010. doi: 10.3850/978-981-08-5118-7_013. 4th International Workshop on Reliable Engineering Computing (REC 2010).

H. Ziegler. A modification of prager's hardening rule. *Quarterly of Applied Mathematics*, 17: 55–65, 1959.

T.T. Zygiridis. A reduced-basis polynomial-chaos approach with a multi-parametric truncation scheme for problems with uncertainties. In T.M. Rassias, editor, *Approximation Theory and Analytic Inequalities*, pages 529–546. Springer International Publishing, 2021. doi: 10.1007/978-3-030-60622-0_26.

Curriculum Vitae

Born in 1990, September 29, Freiburg im Breisgau, Germany

Education

2015	*Peter the Great St. Petersburg Polytechnic University*, Russia
	Research semester abroad as part of the Master studies programme
2014 - 2016	*Leibniz University Hannover*, Germany
	Master studies in Computational Engineering,
	graduating 2016, September 30th, with degree Master of Science (M.Sc.)
2010 - 2014	*Leibniz University Hannover*, Germany
	Bachelor studies in Civil and Environmental Engineering,
	graduating 2014, April 23rd, with degree Bachelor of Science (B.Sc.)
2001 - 2010	*Zinzendorfschulen Königsfeld*, Germany
	High school, graduating June 28th with Abitur

Scientific career

2016 - 2023	*Leibniz University Hannover*, Germany
	Research and teaching assistant at the Institute of Mechanics and Computational Mechanics (IBNM)
2017 - 2020	*German Research Foundation (DFG)*
	Research activity within the priority program SPP 1886 "Polymorphic uncertainty modelling for the numerical design of structures" as a part of the research activities at IBNM

Volunteering and committee work

2019 - 2023	*Faculty Council of the Faculty of Civil Engineering and Geodetic Science* Elected substitute representative of the scientific coworkers for four years (two legislative periods)
2014 - 2015	*Faculty Council of the Faculty of Civil Engineering and Geodetic Science* Elected student representative for one year (one legislative period)
2013 & 2011	*International Building Organisation (IBO)* Volunteer in a three week period project to refurbish a sanatorium for children suffering from bone tuberculosis, Bobrova, Alupka, Ukraine
2012 - 2016	*Student Council of the Faculty of Civil Engineering and Geodetic Science* Elected representative from 04/2013 onwards, before associated member

Awards and scholarships

10/2017	*Victor Rizkallah Foundation* Advancement Award for outstanding scientific achievements at Leibniz University Hannover within the Master Thesis
01/2017	*Victor Rizkallah Foundation* Award in acknowledgement of extraordinary achievements within the Master's degree course Computational Engineering
01/2017	*Ingenieurkammer Niedersachsen* Award to acknowledge extraordinary dedication within the student represetation during their studies
2015	*DAAD scholarship* "Strategic Partnership: Leibniz University Hannover and Peter the Great St. Petersburg Polytechnic University"

Journal publications

^{*)} within this PhD project

^{**)} supervised student works

2022 ^{**)} A.A. Basmaji, A. Fau, J.H. Urrea-Quintero, **M.M. Dannert**, E. Voelsen and U. Nackenhorst, Anisotropic multi-element polynomial chaos expansion for high-dimensional non-linear structural problems, *Probabilistic Engineering Mechanics 70*, 103366, doi: 10.1016/j.probengmech.2022.103366

2022 ^{*)} **M.M. Dannert**, F. Bensel, A. Fau, R.M.N. Fleury and U. Nackenhorst, Investigations on the restrictions of stochastic collocation methods for high dimensional and nonlinear engineering applications, *Probabilistic Engineering Mechanics 69*, 103299, doi: 10.1016/j.probengmech.2022.103299

2022 ^{**)} A.A. Basmaji, **M.M. Dannert** and U. Nackenhorst, Implementation of Karhunen-Loève expansion using discontinuous Legendre polynomial based Galerking approach, *Probabilistic Engineering Mechanics 67*, 103176, doi: 10.1016/j.probengmech.2021.103176

2021 ^{*)} **M.M. Dannert**, M.G.R. Faes, R.M.N. Fleury, A. Fau, U. Nackenhorst and D. Moens, Imprecise random field analysis for non-linear concrete damage analysis, *Mechanical Systems and Signal Processing 150*, 107343, doi: 10.1016/j.ymssp.2020.107343

2019 ^{*)} F.N. Schietzold, A. Schmidt, **M.M. Dannert**, A. Fau, R.M.N. Fleury, W.Graf, M. Kaliske, C. Könke, T. Lahmer and U. Nackenhorst, Developement of fuzzy probability based random fields for the numerical strucutral design, *GAMM-Mitteilungen 42*, e201900004, doi: 10.1002/gamm.201900004

2016 A. Meurer, B. Kriegesmann, **M.M. Dannert** and R. Rolfes, Probabilistic perturbation load approach for designing axially compressed cylindrical shells, *Thin-Walled Structures 107*, 648–656, doi: 10.1016/j.tws.2016.07.021

2016 V. Kuzkin and **M.M. Dannert**, Buckling of a column under a constant speed compression: a dynamic correction to the Euler formula, *Acta Mechanica 227*, 1645–1652, doi: 10.1007/s00707-016-1586-5

Conference contributions

2021   *4th International Conference on Uncertainty Quantification in Computational Sciences and Engineering (UNCECOMP), Athens, Greece (virtual)*
M.M. Dannert, J.L. Häufler and U. Nackenhorst, Limit representations of imprecise random fields, in: M. Papadrakakis, V. Papadopoulos and G, Stefanou (Eds.), Proceedings of the 4th International Conference on Uncertainty Quantification in Computational Sciences and Engineering, 82–99, doi: 10.7712/120221.8024.19110

2021   *14th World Congress on Computational Mechanics (WCCM) & European Congress on Compuational Methods in Applied Sciences and Engineering (EC-COMAS) Congress, Paris, France (virtual)*
M.M. Dannert, E. Voelsen, R.M.N. Fleury, A. Fau and U. Nackenhorst, Efficient random field sampling using sparse polynomial chaos expansion

2019   *29th European Safety and Reliability Conference (ESREL), Hanover, Germany*
M.M. Dannert, R.M.N. Fleury, A. Fau and U. Nackenhorst, Non-linear Finite Element Analysis under Mixed Epistemic and Aleatory Uncertain Random Field Input. In: M. Beer and E. Zio (Eds.) Proceedings of the 29th European Safety and Reliability Conference, 2693–2698, doi: 10.3850/978-981-11-2724-3_0286-cd

2019   *13th International Conference on Application of Statistics and Probability in Civil Engineering (ICASP13), Seoul, South Korea*
M.M. Dannert, A. Fau, R.M.N. Fleury, M. Broggi, U. Nackenhorst and M. Beer, A collocation scheme for deep uncertainty treatment, doi: 10.22725/ICASP13.179

2018   *89th Annual Meeting of the International Association of Applied Mathematics and Mechanics (GAMM), Munich, Germany*
M.M. Dannert, A. Fau, R.M.N. Fleury, M. Broggi, U. Nackenhorst, M. Beer, A probability-box approach on uncertain correlation lengths by stochastic finite element method, Proceedings in Applied Mathematics and Mechanics 18(1), e201800114, doi: 10.1002/pamm.201800114

2017   *12th International Conference on Structural Safety and Reliability (ICOSSAR), Vienna, Austria*
M.M. Dannert, A. Fau, M. Broggi, U. Nackenhorst and M. Beer, A nested collocation algorithm for mixed aleatory and epistemic uncertainties using a probability-box approach, in: C. Bucher, B.R. Ellingwood, D.M. Frangopol (Eds.), Safety, Reliability, Risk, Resilience and Sustainability of Structures and Infrastructure, Proceedings of the 12th International Conference on Structural Safety and Reliability, 820–829

Research and Seminar Reports

Institut für Baumechanik und Numerische Mechanik
Gottfried Wilhelm Leibniz Universität Hannover

Reports that have been published so far:

S 73/1 Seminar über Thermodynamik und Kontinuumsmechanik, Hannover 1973.

F 75/1 "Die Spannungsberechnung im Rahmen der Finite-Element-Methode", R. Ahmad, Dissertation, April 1975.

F 76/1 "Zur Theorie und Anwendung der Stoffgleichungen elastisch-plastisch- viskoser Werkstoffe", H. Mentlein, Dissertation, April 1976.

F 77/1 Seminar über lineare und geometrisch nichtlineare Schalentheorie einschließlich Stabilitätstheorie, Hannover 1978.

F 77/2 "Beitrag zur Berechnung von Gründungsplatten mit Hilfe der Finite- Element-Methode", H. Meyer, Dissertation, Juli 1977.

F 77/3 "Zur Berechnung der Eigenfrequenzen und Eigenschwingungsformen räumlich vorgekrümmter und vorverwundener Stäbe" J. Möhlenkamp, Dissertation, Dezember 1977.

F 77/4 "Zur Theorie und Berechnung geometrisch und physikalisch nichtlinearer Kontinua mit Anwendung der Methode der finiten Elemente", J. Paulun, Dissertation, Dezember 1977.

F 78/1 2. Seminar über Thermodynamik und Kontinuumsmechanik, Hannover 1978.

F 79/1 "Theoretische und numerische Behandlung geometrisch nichtlinearer viskoplastischer Kontinua", K.-D. Klee, Dissertation, Februar 1979.

F 79/2 "Zur Konstruierbarkeit von Variationsfunktionalen für nichtlineare Probleme der Kontinuumsmechanik", J. Siefer, Dissertation, Oktober 1979.

F 80/1 "Theoretische und numerische Behandlung gerader Stäbe mit endlichen Drehungen", M. Kessel, Dissertation, Februar 1980.

F 81/1 "Zur Berechnung von Kontakt- und Stoßproblemen elastischer Körper mit Hilfe der Finite-Element-Methode", P. Wriggers, Dissertation, Januar 1981.95

F 81/2 "Stoffgleichungen für Steinsalze unter mechanischer und thermischer Beanspruchung", J. Olschewski, E. Stein, W. Wagner, D. Wetjen, geänderte Fassung eines Zwischenberichtes zum BMFT-Forschungsvorhaben KWA 1608/5.

F 82/1 "Konvergenz und Fehlerabschätzung bei der Methode der Finiten Elemente", R. Rohrbach, E. Stein, Abschlußbericht eines VW- Forschungsvorhabens, Februar 1982.

F 82/2 "Alternative Spannungsberechnung in Finite-Element- Verschiebungsmodellen", C. Klöhn, Dissertation, November 1982

F 83/1 Seminar über nichtlineare Stabtheorie, Hannover 1983.

F 83/2 "Beiträge zur nichtlinearen Theorie und inkrementellen Finite- Element-Berechnung dünner elastischer Schalen", A. Berg, Dissertation, Juli 1983.

F 83/3 "Elastoplastische Plattenbiegung bei kleinen Verzerrungen und großen Drehungen", J. Paulun, Habilitation, September 1983.

F 83/4 "Geometrisch nichtlineare FE-Berechnung von Faltwerken mit plastisch / viskoplastischem Deformationsverhalten", M. Krog, Dissertation, Dezember 1983.

F 85/1 Verleihung der Ehrendoktorwürde des Fachbereichs Bauingenieur- und Vermessungswesen der Universität Hannover an die Herren Prof. Dr. Drs. h.c. J.H. Argyris, Dr.-Ing. H. Wittmeyer.

F 85/2 "Eine geometrisch nichtlineare Theorie schubelastischer Schalen mit Anwendung auf Finite-Element-Berechnungen von Durchschlag- und Kontaktproblemen", W. Wagner, Dissertation, März 1985.

F 85/3 "Geometrisch/physikalisch nichtlineare Probleme - Struktur und Algorithmen", GAMM-Seminar im Februar 1985 in Hannover.

F 87/1 "Finite-Elemente-Berechnungen ebener Stabtragwerke mit Fließgelenken und großen Verschiebungen", R. Kahn, Dissertation, Oktober 1987.

F 88/1 "Theorie und Numerik schubelastischer Schalen mit endlichen Drehungen unter Verwendung der Biot-Spannungen", F. Gruttmann, Dissertation, Juni 1988.

F 88/2 "Optimale Formgebung von Stabtragwerken mit Nichtlinearitäten in der Zielfunktion und in den Restriktionen unter Verwendung der Finite-Element-Methode", V. Berkhahn, Dissertation, Oktober 1988.

F 88/3 "Beiträge zur Theorie und Numerik großer plastischer und kleiner elastischer Deformationen mit Schädigungseinfluß", R. Lammering, Dissertation, November 1988.

F 88/4 "Konsistente Linearisierungen in der Kontinuumsmechanik und ihrer Anwendung auf die Finite-Elemente-Methode", P. Wriggers, Habilitation, November 1988.96

F 88/5 "Mathematische Formulierung und numerische Methoden für Kontaktprobleme auf der Grundlage von Extremalprinzipien", D. Bischoff, Habilitation, Dezember 1988.

F 88/6 "Zur numerischen Behandlung thermomechanischer Prozesse", C. Miehe, Dissertation, Dezember 1988.

F 89/1 "Zur Stabilität und Konvergenz gemischter finiter Elemente in der linearen Elastizitätstheorie", R. Rolfes, Dissertation, Juni 1989.

F 89/2 "Traglastberechnungen von Faltwerken mit elastoplastischen Deformationen", K.-H. Lambertz, Dissertation, November 1989.

F 89/3 "Transientes Kriechen und Kriechbruch im Steinsalz", U. Heemann, Dissertation, November 1989.

F 89/4 "Materialgesetze zum Verhalten von Betonkonstruktionen bei harten Stößen", E. Stein, P. Wriggers, T. Vu Van & T. Wedemeier, Dezember 1989.

F 89/5 "Lineare Konstruktion und Anwendungen von Begleitmatrizen", C. Carstensen, Dissertation, Dezember 1989.

F 90/1 "Zur Berechnung prismatischer Stahlbetonbalken mit verschiedenen Querschnittformen für allgemeine Beanspruchungen", H.N. Lucero-Cimas, Dissertation, April 1990.

F 90/2 "Zur Behandlung von Stoß- Kontaktproblemen mit Reibung unter Verwendung der Finite-Element-Methode", T. Vu Van, Dissertation, Juni 1990.

F 90/3 "Netzadaption und Mehrgitterverfahren für die numerische Behandlung von Faltwerken", L. Plank, Dissertation, September 1990.

F 90/4 "Beiträge zur Theorie und Numerik finiter inelastischer Deformationen", N. Müller-Hoeppe, Dissertation, Oktober 1990.

F 90/5 "Beiträge zur Theorie und Numerik von Materialien mit innerer Reibung am Beispiel des Werkstoffes Beton", T. Wedemeier, Dissertation, Oktober 1990.

F 91/1 "Zur Behandlung von Stabilitätsproblemen der Elastostatik mit der Methode der Finiten Elemente", W. Wagner, Habilitation, April 1991.

F 91/2 "Mehrgitterverfahren und Netzadaption für lineare und nichtlineare statische Finite-Elemente-Berechnungen von Flächentragwerken", W. Rust, Dissertation, Oktober 1991.

F 91/3 "Finite Elemente Formulierung im Trefftzschen Sinne für dreidimensionale anisotrop-elastische Faserverbundstrukturen", K. Peters, Dissertation, Dezember 1991.

F 92/1 "Einspielen und dessen numerische Behandlung von Flächentragwerken aus ideal plastischem bzw. kinematisch verfestigendem Material", G. Zhang, Dissertation, Februar 1992.97

F 92/2 "Strukturoptimierung stabilitätsgefährdeter Systeme mittels analytischer Gradienten-
ermittlung", A. Becker, Dissertation, April 1992.

F 92/3 "Duale Methoden für nichtlineare Optimierungsprobleme in der Strukturmechanik", R.
Mahnken, Dissertation, April 1992.

F 93/1 "Kanonische Modelle multiplikativer Elasto-Plastizität. Thermodynamische Formulie-
rung und numerische Implementation", C. Miehe, Habilitation, Dezember 1993.

F 93/2 "Theorie und Numerik zur Berechnung und Optimierung von Strukturen aus isotropen,
hyperelastischen Materialien", F.-J. Barthold, Dissertation, Dezember 1993.

F 94/1 "Adaptive Verfeinerung von Finite-Element-Netzen für Stabilitätsprobleme von Flächen-
tragwerken", E. Stein, B. Seifert, W. Rust, Forschungsbericht, Oktober 1994.

F 95/1 "Adaptive Verfahren für die Formoptimierung von Flächentragwerken unter Berück-
sichtigung der CAD-FEM-Kopplung", A. Falk, Dissertation, Juni 1995.

F 96/1 "Theorie und Numerik dünnwandiger Faserverbundstrukturen", F. Gruttmann, Habili-
tation, Januar 1996.

F 96/2 "Zur Theorie und Numerik finiter elastoplastischer Deformationen von Schalenstruk-
turen", B. Seifert, Dissertation, März 1996.

F 96/3 "Theoretische und algorithmische Konzepte zur phänomenologischen Beschreibung an-
isotropen Materialverhaltens", J. Schröder, Dissertation, März 1996.

F 96/4 "Statische und dynamische Berechnungen von Schalen endlicher elastischer Deforma-
tionen mit gemischten finiten Elementen", P. Betsch, Dissertation, März 1996.

F 96/5 "Kopplung von Finiten Elementen und Randelementen für ebene Elastoplastizität mit
Impelementierung auf Parallelrechnern", M. Kreienmeyer, Dissertation, März 1996.

F 96/6 "Theorie und Numerik dimensions- und modeladaptiver Finite- Elemente-Methoden
von Fläschentragwerken", S. Ohnimus, Dissertation, Juni 1996.

F 96/7 "Adaptive Finite Elemente Methoden für MIMD-Parallelrechner zur Behandlung von
Strukturproblemen mit Anwendung auf Stabilitätsprobleme", O. Klaas, Dissertation, Juli
1996.

F 96/8 "Institutsbericht 1971-1996 aus Anlaß des 25-jährigen Dienstjubiläums von Prof. Dr.-
Ing. Dr.-Ing. E.h. Dr. h.c. mult. Erwin Stein", Dezember 1996.

F 97/1 "Modellierung und Numerik duktiler kristalliner Werkstoffe", P. Steinmann, Habilita-
tion, August 1997.

F 97/2 "Formoptimierung in der Strukturdynamik", L. Meyer, Dissertation, September 1997

F 97/3 "Modellbildung und Numerik für Versagensprozesse in Gründungen von Caisonwellen-brechern", M. Lengnick, Dissertation, November 1997.

F 98/1 "Adaptive gemischte finite Elemente in der nichtlinearen Elastostatik und deren Kopplung mit Randelementen", U. Brink, Dissertation, Februar 1998.

F 98/2 "Theoretische und numerische Aspekte zur Parameteridentifikation und Modellierung bei metallischen Werkstoffen", R. Mahnken, Habilitation, Juli 1998.

F 98/3 "Lokalisierung und Stabilität der Deformation wassergesättigter bindiger und granularer Böden", J.M. Panesso, Dissertation, August 1998.

F 98/4 "Theoretische und numerische Methoden in der angewandten Mechanik mit Praxisbeispielen", R. Mahnken (Hrsg.), Festschrift anlässlich der Emeritierung von Prof. Dr.-Ing. Dr.-Ing. E.h. h.c. mult. Erwin Stein, November 1998.

F 99/1 "Eine h-adaptive Finite-Element-Methode für elasto-plastische Schalenproblem in unilateralem Kontakt", C.-S. Han, Dissertation, Juli 1999.

F 00/1 "Ein diskontinuierliches Finite-Element-Modell für Lokalisierungsversagen in metallischen und granularen Materialien", C. Leppin, Dissertation, März 2000.

F 00/2 "Untersuchungen von Strömungen in zeitlich veränderlichen Gebieten mit der Methode der Finiten Elementen", H. Braess, Dissertation, März 2000.

F 00/3 "Theoretische und algorithmische Beiträge zur Berechnung von Faserverbundschalen", J. Tessmer, Dissertation, März 2000.

F 00/4 "Theorie und Finite-Element-Methode für die Schädigungsbeschreibung in Beton und Stahlbeton", D. Tikhomirov, Dissertation, August 2000.

F 01/1 "A C1 - continuous formulation for finite deformation contact", L. Krstulovic-Opara, Dissertation, Januar 2001.

F 01/2 "Strain Localisation Analysis for Fully and Partially Saturated Geomaterials", H. Zhang, Dissertation, Januar 2001.

F 01/3 "Meso-makromechanische Modellierung von Faserverbundwerkstoffen mit Schädigung", C. Döbert, Dissertation, April 2001.

F 01/4 "Thermomechanische Modellierung gummiartiger Polymerstrukturen", S. Reese, Habilitation, April 2001.

F 01/5 "Thermomechanisches Verhalten von Gummimaterialien während der Vulkanisation - Theorie und Numerik", M. Andre, Dissertation, April 2001.

F 01/6 "Adaptive FEM für elastoplastische Deformationen - Algorithmen und Visualisierung", M. Schmidt, Dissertation, Juni 2001.

F 01/7 "Verteilte Algorithmen für h-, p- und d-adaptive Berechnungen in der nichtlinearen Strukturmechanik", R. Niekamp, Dissertation, Juni 2001.99

F 01/8 "Theorie und Numerik zur Berechnung und Optimierung von Strukturen mit elasto-plastischen Deformationen", K. Wiechmann, Dissertation, Juli 2001.

F 01/9 "Direct Computation of Instability Points with Inequality using the Finite Element Method", H. Tschöpe, Dissertation, September 2001.

F 01/10 "Theorie und Numerik residualer Fehlerschätzer für die Finite- Elemente-Methode unter Verwendung äquilibrierter Randspannungen", S. Ohnimus, Habilitation, September 2001.

F 02/1 "Adaptive Algorithmen für thermo-mechanisch gekoppelte Kontaktprobleme", A. Rieger, Dissertation, August 2002.

F 02/2 "Consistent coupling of shell- and beam-models for thermo-elastic problems", K. Chavan, Dissertation, September 2002.

F 03/1 "Error-controlled adaptive finite element methods in large strain hyperelasticity and fracture mechanics", M. Rüter, Dissertation, Mai 2003.

F 03/2 "Formulierung und Simulation der Kontaktvorgänge in der Baugrund- Tragwerks- Interaktion", A. Haraldsson, Dissertation, Juni 2003.

F 03/3 "Concepts for Nonlinear Orthotropic Material Modeling with Applications to Membrane Structures", T. Raible, Dissertation, Juni 2003.

F 04/1 "On Single- and Multi-Material arbitrary Lagrangian-Eulerian Approaches with Application to Micromechanical Problems at Finite Deformations", D. Freßmann, Dissertation, Oktober 2004.

F 04/2 "Computational Homogenization of Microheterogeneous Materials at Finite Strains Including Damage", S. Löhnert, Dissertation, Oktober 2004.

F 05/1 "Numerical Micro-Meso Modeling of Mechanosensation driven Osteonal Remodeling in Cortical Bone", C. Lenz, Dissertation, Juli 2005.

F 05/2 "Mortar Type Methods Applied to Nonlinear Contact Mechanics", K.A. Fischer, Dissertation, Juli 2005.

F 05/3 "Models, Algorithms and Software Concepts for Contact and Fragmentation in Computational Solid Mechanics", C. Hahn, Dissertation, November 2005.

F 06/1 "Computational Homogenization of Concrete", S. Moftah, Dissertation, Januar 2006.

F 06/2 "Reduction Methods in Finite Element Analysis of Nonlinear Structural Dynamics", H. Spiess, Dissertation, Februar 2006.

F 06/3 "Theoretische und algorithmische Konzepte zur Beschreibung des beanspruchungsadaptiven Knochenwachstums", B. Ebbecke, Dissertation, März 2006.100

F 06/4 "Experimentelle Untersuchungen an elastomeren Werkstoffen", M. Dämgen, Dissertation, Dezember 2006.

F 07/1 "Numerische Konzepte zur Behandlung inelastischer Effekte beim reibungsbehafteten Rollkontakt", M. Ziefle, Dissertation, Februar 2007.

F 07/2 "Begleitbuch zur Leibniz-Ausstellung", Hrsg: E. Stein, P. Wriggers, 2007.

F 07/3 "Modellierung und Simulation der hochfrequenten Dynamik rollender Reifen", M. Brinkmeier, Dissertation, Juni 2007.

F 07/4 "Computational Homogenization of micro-structural Damage due to Frost in Hardened Cement Paste", M. Hain, Dissertation, Juli 2007.

F 07/5 "Elektromechanisch gekoppelte Kontaktmodellierung auf Mikroebene", T. Helmich, Dissertation, August 2007.

F 07/6 "Dreidimensionales Diskretes Elemente Modell für Superellipsoide", C. Lillie, Dissertation, Oktober 2007.

F 07/7 "Adaptive Methods for Continuous and Discontinuous Damage Modeling in Fracturing Solids", S.H. Reese, Dissertation, Oktober 2007.

F 08/1 "Student Projects of Micromechanics", Hrsg: U. Nackenhorst, August 2008.

F 09/1 "Theory and Computation of Mono- and Poly- crystalline Cyclic Martensitic Phase Transformations", G. Sagar, Dissertation, August 2009.

F 09/2 "Student projects of Micromechanics", D. Balzani and U. Nackenhorst, Course Volume, Oktober 2009.

F 09/3 "Multiscale Coupling based on the Quasicontinuum Framework, with Application to Contact Problems", W. Shan, Dissertation, November 2009.

F 10/1 "A Multiscale Computational Approach for Microcrack Evolution in Cortical Bone and Related Mechanical Stimulation of Bone Cells", D. Kardas, Dissertation, September 2010.

F 11/1 "Ein Integrales Modellierungskonzept zur numerischen Simulation der Osseointegration und Langzeitstabilität von Endoprothesen", A. Lutz, Dissertation, Oktober 2011.

F 12/1 "Ein physikalisch motiviertes Reifen-Fahrbahnmodell für die Gesamtfahrzeugsimulation", R. Chiarello, Dissertation, Februar 2012.

F 13/1 "Thermomechanical Analysis of Tire Rubber Compounds in Rolling Contact", A. Suwannachit, Dissertation, September 2012.

F 13/2 "Towards a Finite Element Model for Fluid Flow in the Human Hip Joint", K. Fietz, Dissertation, September 2013.101

F 14/1 "Micro-Mechanically Based Damage Analysis of Ultra High Performance Fibre Reinforced Concrete Structures with Uncertainties", A. Hürkamp, Dissertation, Dezember 2013.

F 14/2 "Numerical Solution of High-Dimensional Fokker-Planck Equations with Discontinuous Galerkin Methods", F. Loerke, Dissertation, Dezember 2013.

F 14/3 "Numerische Simulation probabilistischer Schädigungsmodelle mit der Stochastischen Finite Elemente Methode", P.-P. Jablonski, Dissertation, September 2014.

F 15/1 "On a Finite Element Approach for the Solution of a Mechanically Stimulated Biochemical Fracture Healing Model", A. Sapotnick, Dissertation, November 2015.

F 15/2 "Simulation of Elastic-Plastic Material Behaviour with Uncertain Material Parameters. A Spectral Stochastic Finite Element Method Approach", S. Fink, Dissertation, November 2015.

F 15/3 "A Fully Micro-mechanically Motivated Material Law for Filled Elastomer", O. Stegen, Dissertation, Februar 2016.

F 16/1 "A modified adaptive harmony search algorithm approach on structural identification and damage detection", M. Jahjouh, Dissertation, Januar 2016,

F17/1 "Computation Simulation of Piezo-electrically Stimulated Bone Adaption Surrounding Activated Teeth Implants", A. Shirazibeheshtiha, Dissertation, Januar 2017.

F 17/2 "A Constitutive Contact Model for Homogenized Tread-Road Interaction in Rolling Resistance Computations", R. Bayer, Dissertation, Februar 2017.

F 17/3 "A Posteriori Error Estimates for Advanced Galerkin Methods", M.O. Rüter, Habilitation, November 2017.

F 17/4 "Probabilistische Finite Element Modellierung des mechanischem Materialverhaltens von Salzgestein", M. Grehn, Dissertation, Dezember 2017.

F 18/1 "Modelling and numerical simulation for the prediction of the fatigue strength of airsprings", N.K. Jha, Dissertation, März 2018.

F 18/2 "A model reduction approach in space and time for fatigue damage simulation", M. Bhattacharya, Dissertation, Mai 2018.

F 18/3 "Numerical investigation on hydrogen embrittlement of metallic pipeline structures", M. Möhle, Dissertation, Mai 2018.

F 18/4 "Institute Seminar 2018", U. Nackenhorst, Holle, August 2018.

F 18/5 "A stochastic fatigue model for casted aluminium structures", G. Narayanan, Dissertation, August 2018.

F 20/01 "A Micro-mechanically Motivated Approach for Modelling the Oxidative Aging Process of Elastomers", D. Beurle, Dissertation, December 2019.

F 20/02 "A Semi-incremental Model Order Reduction Approach for Fatigue Damage Computations", S. Alameddin, Dissertation, January 2020.

F 20/03 "A Coupled ALE Lagrangian Approach for the Simulation of Treaded Tires", T.A. Palanichamy, Dissertation, August 2020.

F 21/01 "A parametric modeling concept for predicting biomechanical compatibility in total hip arthroplasty", M. Bittens, Dissertation, July 2021.

F 21/02 "Stochastic Modelling and Numerical Simulation of Fatigue Damage", W. Zhang, Dissertation, July 2021.

F 22/01 "Support Vektor Regression für Anwendungen im Bereich der Elasto-Plastizität", S. Funk, Dissertation, April 2022.

F 22/02 "Anisotropic Damage Modelling of Concrete at Meso-scale", M. Hammad, Dissertation, October 2022.